O-17 NMR STUDIES OF SOME SILICATE CRYSTALS AND GLASSES

Erdem Kamil YILDIRIM

A thesis submitted to the University of Warwick for admission to the degree of Doctor of Philosophy

Department of Physics

March 2000

List of Contents

List of Tables

List of Figures

Acknowledgements

I would like to thank the Higher Educational Council of Turkey and Kirikkale University for providing the financial assistance, and the Department of Physics for providing the facilities that made this work possible. I would like to thank Michael B. Henderson at the University of Manchester for making the sodalites and kalsilite and Julian Bent for making tin-silicate glasses. I also thank Dr. Diane Holland for her help during this study.

I would like to thank to thank present and old members of the NMR group namely, Dr. Andy Howes, Dr. Mark Smith, Dr. Kelly Moran, Dr Kevin Pike, Dr Rosli Hussin, Dr. Thomas Reimer.

A number of people helped me during this study but I would like to express my gratitude to a few close friends, for being there and providing every possible assistance they can. I also thank my parents, and especially my wife for their continuous support during this study.

Finally I would like to thank my supervisor Prof. Ray Dupree for his excellent guidance and interest which made this study very good experience.

Declaration

The work for this thesis was carried out in the Department of Physics at the University of Warwick from October 1995 to September 1999. This thesis is the result of my own independent research except where referenced and has not been previously submitted for any other degree.

Part of this work was presented at the Rocky Mountain Conference in 1998 as a poster entitled "A study of the relationship between structure and ^{17}O electric field gradient parameters in some aluminosilicates" E.K.Yildirim, S. Kitchin, C.M.B.Henderson, D.M. Hamilton, and R. Dupree. A paper with this title is also being submitted to Solid State NMR.

It is anticipated that further parts of this thesis will be published in the future.

Erdem K. YILDIRIM

Abstract

Crystalline and glassy silicates were investigated by means of ^{17}O NMR. The dependence of the measured efg on the Si-O-Al bond angle was investigated in some crystalline aluminosilicate sodalites and kalsilite. The results show that C_Q increases with increasing bond angle while η decreases with increasing bond angle and they both follow a similar function to that found for the Si-O-Si bond angle. The cluster calculations also confirm that the dependence of C_Q and η on the Si-O-Al bond angle is similar to that of one Si-O-Si linkage. The chemical shift decreases as the bond angle increases. However this dependence does not seem to be monotonic.

The structural role of Al in aluminosilicate glasses was studied by means of ^{17}O 3Q MAS NMR in sodium aluminosilicate glasses with Si/Al= 3,1.5,1,0.7. 3Q MAS NMR results showed the presence of Si-O-Si species as well as Si-O-Al species in glasses with Si/Al>1. The 3Q MAS NMR spectrum of glass with Si/Al=0.7 displayed the presence of Al-O-Al linkage as well as Si-O-Al. These results showed that as the Si/Al ratio decreases from 3 to 0.7 Si-O-Si linkage is replaced by Al-O-Al linkage as a result of addition of Al into the structure.

The structural role of Sn in tin-silicate glasses was also studied mainly by means of ^{17}O MAS NMR. The model developed from the ^{17}O MAS NMR spectra of these glasses showed the possible coexistence of two and three coordinated oxygen atoms in the structure. Therefore some of the Sn has to be in three coordinated to oxygen for charge balancing. The ^{17}O MAS NMR spectra of a partially crystallised sample showed three distinct sites which are assigned as Sn-O-Sn, Si-O-Sn, and Si-O-Si on the basis of their chemical shift. The C_Q values obtained from the simulations of these peaks supports this assignment. The ^{29}Si MAS NMR of the same sample showed two crystalline and a glassy peaks which are fitted to two crystalline and two glassy sites. The possible composition of this sample was calculated and found to be $SiSn_8O_{10}$.

Chapter 1

Introduction

Nuclear Magnetic Resonance (NMR) is based on the fact that transitions can be induced between magnetic spin energy levels of certain atomic nuclei in a magnetic field. It provides information about processes at the atomic level. One of the most important aspects of NMR is that the frequency measured in the NMR spectrum of an atomic nucleus in a particular chemical or structural environment is a very sensitive probe that of environment.

Much of the development of high resolution NMR was restricted to the liquid state in the early years due to the effect of nuclear magnetic interactions which may cause excessive line broadening in solids. Soon after the discovery of NMR, chemical shift, spin-spin coupling and relaxation processes were observed in the liquid state. Development of solid state NMR was slow due to the relatively static nature of the structure of solids, which prevented the observation of high resolution NMR spectra. However, in the early 1970's and later years, development of mainly three experimental techniques , magic angle sample spinning (MAS), high power dipolar coupling, and appropriate multi pulse sequences, made it possible to obtain high resolution NMR spectra and resulted in rapid development of solid state NMR. In principle the high resolution NMR spectra of solid samples, obtained using these techniques, resemble those of liquids and may provide structural information on solid materials at the molecular level. Further development of solid state NMR for nuclei with I>1/2 was possible with the development of more complex spinning experiments such as dynamic angle spinning (DAS), double rotation (DOR) and multiple quantum magic angle spinning (MQ-MAS) techniques in recent years. In particular the MQ MAS technique

is very promising since it does not need any special apparatus or complex mechanical settings as in the case of DAS and DOR. It will be discussed in chapter 2, as well as the basic principles of NMR.

This study involves investigation of some crystalline and glassy silicates namely aluminosilicates and tin-silicates, using NMR in order to obtain structural information on these materials. NMR is an ideal tool for structural investigation of glasses since in these systems there is no long range order so that diffraction techniques such as x-ray diffraction spectroscopy can give limited information on them. Since NMR depends only on the local , short range order, it can provide very valuable structural information about glasses. It is also essentially a quantitative technique with the signal intensity being proportional to the number of nuclei in a particular environment in a sample. Aluminosilicates are quite important materials for geology and earth science, since they are found in important rock forming minerals and man made glasses. Their industrial importance is due to utilization of them as catalysts and absorbers. Tin is not a common constituent of glasses. However it is found at high concentrations in the surface of the float glasses. Due to the difficulty of making tin-silicate glasses there has not been very much work on them. Therefore information on the structural role of tin in the tin-silicates is quite valuable. Fundamentals of glass structure including information on aluminosilicates and tin-silicates are given in chapter-3.

As high resolution solid state NMR became more widespread the range of nuclei studied expanded from ^{1}H and ^{13}C to others such as ^{23}Na, ^{27}Al, ^{29}Si, and ^{17}O. This study involves mainly ^{17}O NMR since it is one of the few direct probes of oxygen environments in aluminosilicates and tin-silicates. Furthermore ^{17}O NMR has the ability to distinguish bridging from non-bridging oxygens as well as bridging oxygens in Si-O-

Si, Si-O-Al, Al-O-Al, Si-O-Sn, and Sn-O-Sn linkages. The difference between ^{17}O NMR spectra of the glass and the crystal is that glass spectra are broad and featureless while crystal spectra have well defined second order quadrupole patterns for the crystals. Since it is a quadrupolar nucleus it is possible to obtain quadrupolar coupling parameters which are a measure of the electric field gradient (efg) tensor at the oxygen nucleus. Knowledge of the efg tensor can be related to the local distribution of electrons and arrangement of charge on neighbouring atoms or ions, thus providing insight into the character of the chemical bonds. Although the dependence of Si-O-Si bond angle on the quadrupolar parameters has been investigated by many researchers, the dependence of the quadrupolar parameters on Si-O-Al bond angle has not been investigated in aluminosilicates. This study investigates this relation in aluminosilicate crystals in chapter 5 by means of ^{17}O NMR.

Structural models for aluminosilicate glasses are based on the presence of a three dimensional network of SiO_4 and AlO_4 tetrahedra and direct linkage between two Al through oxygen is forbidden. However in the case of excess Al over Si, i.e Si/Al<1 the structural role of Al causes some controversy, since most researchers claim it is in octahedral coordination while some researcher claims it forms triclusters. Chapter 6 investigates the structural role of Al in sodium aluminosilicate glasses by means of ^{17}O MQ MAS NMR. The structural role of Sn in tin-silicates is also of interest and discussed in chapter 7.

Aims

- Preparation of ^{17}O enriched samples of some crystalline and glass aluminosilicates and of tin-silicate glasses.
- To obtain ^{17}O quadrupolar parameters for some crystalline aluminosilicates to determine the dependence of Si-O-Al bond angle on these parameters.
- To prepare peraluminous glasses and to obtain information on the incorporation of excess Al in the structure by using NMR, particularly the ^{17}O NMR.
- To determine ^{17}O quadrupolar parameters in these glasses and to use these parameters to obtain information on Si-O-Al bond angles.
- To investigate the possible presence of three coordinated oxygen in tin-silicate glasses.
- General investigation of a crystalline tin-silicate which was formed from the glass.

Chapter 2
Background Theory

2.1 Introduction

The basic principle of NMR lies in the measurement of the energy separation of the ground state nuclear spin energy levels in an applied field. The first NMR signals were observed independently by two different groups of physicists in 1945. Bloch and his colleagues detected a signal from the protons of water [1], while Purcell and his colleagues observed a signal from the protons of paraffin [2]. Although the first NMR signals were observed in 1945, useful chemical applications started after the discovery of shift effects, the Chemical shift [3] and Knight shift [4] in 1949 and 1950 respectively. The first commercial Fourier Transform NMR spectrometers were introduced in the early seventies, after the power of one pulse experiment was understood [5].

NMR spectra of liquids are in general much narrower than those of solids because molecular motion in the liquids causes averaging of many interactions which are orientation-dependent. Although their motional averaging causes considerable loss of information for solutions, it gives spectra of high-resolution. Extension of NMR to the solid state was slow since the relatively static nature of the structure results in the anisotropic interactions (dipolar, chemical shift anisotropy, and quadrupolar) broadening the NMR spectral lines, masking the small differences in the isotropic chemical shift. It was suggested that this broadening could be reduced by physically imposing motion on the powdered solid. The technique is called Magic Angle Spinning (MAS) [6], and involves the spinning of the sample at an angle of 54°.44′ to the external magnetic field. It is now routine to obtain high-resolution spectra for solids

by MAS, and more complex spinning experiments such as dynamic angle spinning (DAS), double rotation (DOR) [7-9] and multiple quantum magic angle spinning (MQ-MAS) techniques [10]

Solid state NMR is a powerful tool for investigation of amorphous materials, since conventional diffraction techniques cannot give detailed information on these materials due to the lack of long range order. However this lack of long range order has less effect on an NMR spectrum which depends mostly on the local, short range order. NMR is also essentially a quantitative technique with the signal intensity being proportional to the number of nuclei in a particular environment in the sample, giving an additional advantage over the traditional infra-red or X-ray fluorescence coordination determination techniques.

Theoretical background about NMR can be found in numerous texts and a few are listed in the references [11][12][13].

2.2 The Principles Of Nuclear Magnetic Resonance

Almost all elements in the periodic table have at least one isotope which possess nuclear spin angular momentum, P, and therefore magnetic moment, μ. These two quantities are related through the expression

$$\mu = \gamma P \qquad (2.1)$$

where γ, the gyromagnetic ratio, is a constant characteristic of the particular nucleus. The NMR phenomenon arises as a result of interaction between μ of a nucleus, and the applied static magnetic field, B_0.

According to quantum theory, angular momentum and nuclear magnetic moment are quantized and only certain orientations of magnetic moment are allowed. The allowed values or eigenvalues of the angular momentum in the z direction of a cartesian coordinate system are measured in units of ħ and are defined by the relation;

$$P_z = \hbar m_I \tag{2.2}$$

where m_I is the magnetic quantum number, and related to the spin quantum number with the relation

$$m_I = I, I-1, I-2, \ldots, -I \tag{2.3}$$

Therefore the total number of possible eigenstates or energy levels is given by (2I+1).

In the presence of magnetic field B_0, magnetic moments are aligned with the direction of B_0, and experience a torque, which is the vector product of the magnetic moment and the magnetic field and, according to Newton's laws of motion, this torque is equal to the rate of change of the angular momentum.

$$\frac{dP}{dt} = \tau = \mu \times B_0 \tag{2.4}$$

the direction of this torque is perpendicular to μ and B_0, thus forcing μ to precess around B_0. By substituting equation (2.1) into equation (2.4) we obtain the equation of motion.

$$\frac{d\mu}{dt} = \gamma \mu \times B_0 \tag{2.5}$$

which describes precession of the μ around B_0 at a frequency of ω_0. Figure 2.1 illustrates such a precession.

$$\omega_0 = -\gamma B_0 \tag{2.6}$$

which correspond to the frequency

$$\nu_0 = \frac{\gamma}{2\pi} B_0 \tag{2.7}$$

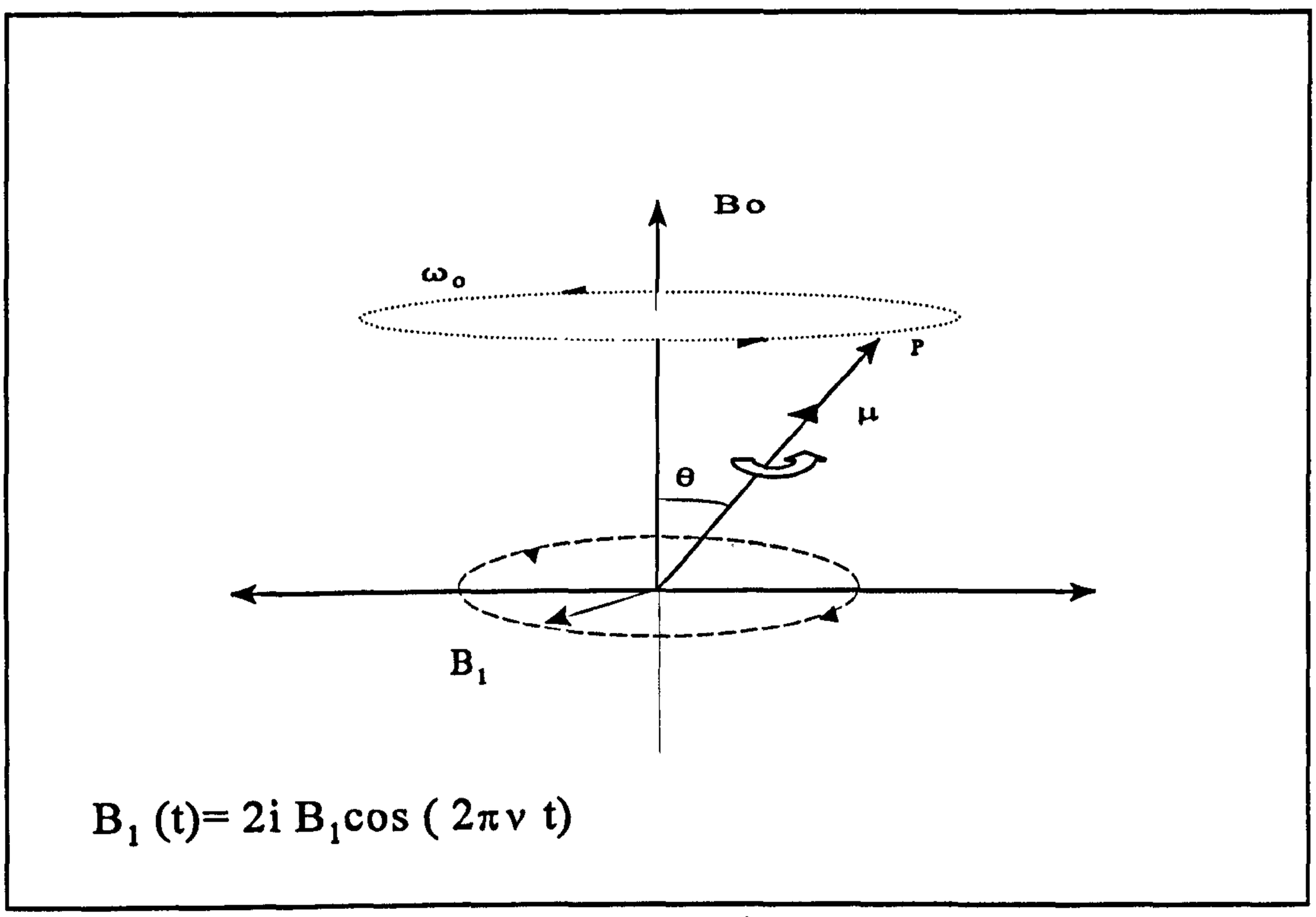

Figure 2.1. Schematic representation of magnetic moment precessing around the B_0. If a B_1 field with a frequency equal to the Larmor frequency is applied at right angles to the B_0, the transition is triggered by the absorption of energy into the nuclear spin system.

In the absence of an external magnetic field, the energy levels of an atomic system are said to be degenerate, i.e, they all have the same energy. This degeneracy is removed by the external magnetic field as a result of the interaction between nuclear moment, μ, and B_0 called the Zeeman interaction. When a nucleus (such as proton I=1/2) is

placed in the static magnetic field, this interaction is given by (B_0 is assumed to be in the z direction)

$$H = -\mu . B_0 = -\gamma \hbar B_0 I_z \tag{2.8}$$

The energy of a m^{th} state is given by;

$$E_m = -\gamma \hbar B_0 m_z \tag{2.9}$$

The energy levels are separated by an energy gap, ΔE.

$$\Delta E = 2\mu_z B_0 = \gamma \hbar B_0 \tag{2.10}$$

Therefore splitting of the energy levels occurs in the presence of an intense magnetic field. Figure 2.2 shows the energy separation between nuclear spin states for I=3/2.

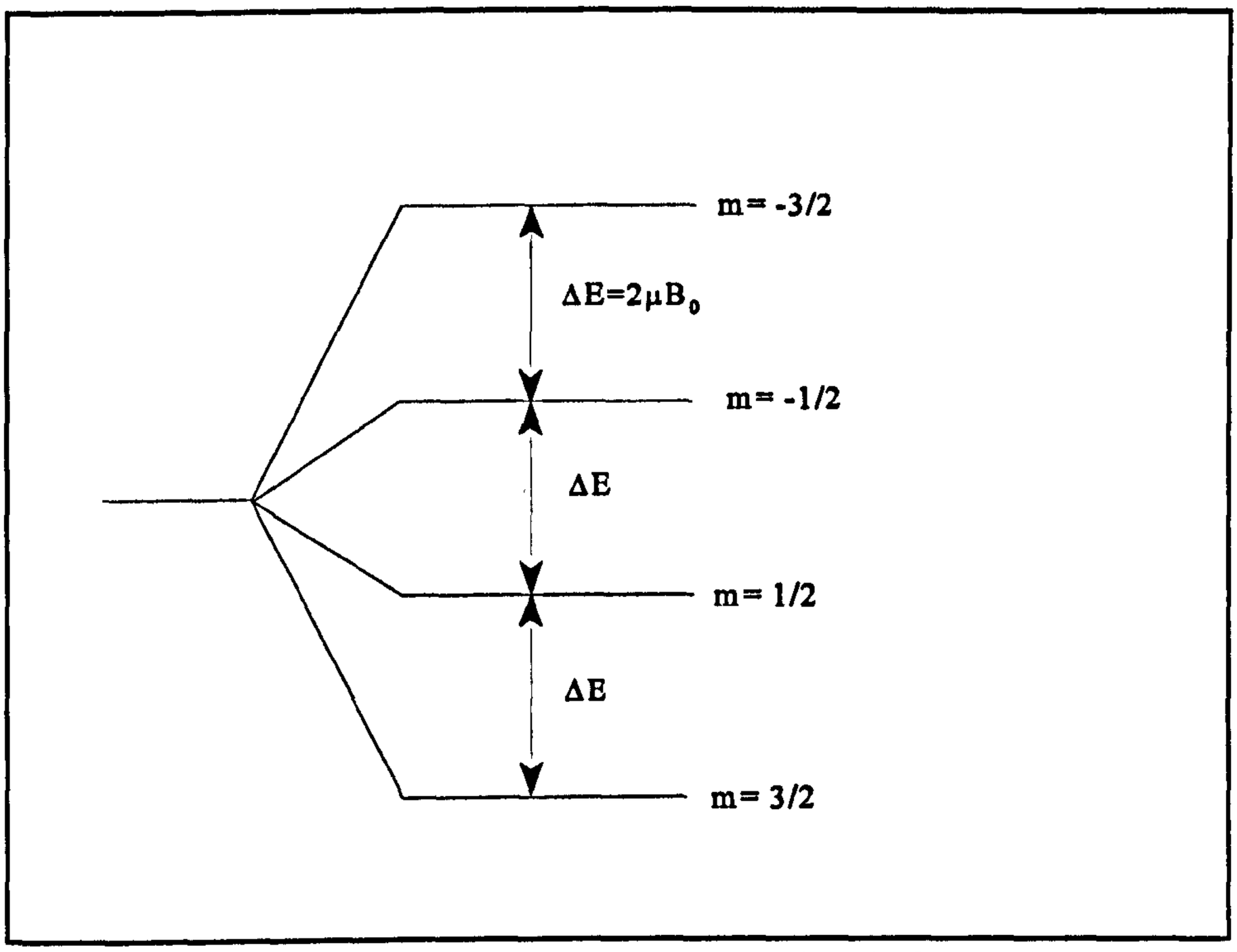

Figure 2.2. Zeeman splitting of nuclear energy levels for I=3/2

The energy difference between the states is determined by the B_0, i.e., the larger the B_0, the larger the energy difference. In an NMR experiment the energy ΔE must be absorbed in order to excite a nucleus in the energy level E_m to the next upper level E_{m-1}.

NMR is based on the transition between different nuclear Zeeman levels of a particular nucleus. The frequency of these transitions are given by equation 2.6 and 2.7, where ν_o is the resonance frequency in Hertz and ω_o is the resonant frequency in radians/second. This frequency describes the resonance condition and it is known as the Larmor frequency. The energy difference for a transition between the states can be provided by an external oscillating radio frequency field B_1, perpendicular to B_0, with a frequency of ν_0 as shown in figure 2.1.

In both solids and liquids magnetic nuclei are distributed between their energy states. For a large number of nuclei (with I=1/2), the distribution of the nuclei of higher (m=-1/2) and lower (m=1/2) energy states, in thermal equilibrium, is given by the Boltzman relation,

$$\frac{N_-}{N_+}=\exp\left(\frac{-\Delta E}{kT}\right)=\exp\left(\frac{-\gamma h B_0}{2\pi kT}\right) \qquad (2.11)$$

where N_- and N_+ are the numbers of nuclei in the ground and excited state, respectively and k is the Boltzman constant, T is the absolute temperature.

In solid state NMR the Zeeman interaction is not the only interaction present. There are also some other anisotropic interactions, such as magnetic dipole, chemical shift and quadrupolar interactions which affect the NMR lineshape and the frequency. These interactions are particularly important, since they provide valuable information about the local environment in glasses and inorganic solids.

2.3 Magnetic Dipole Interaction

The dipole-dipole interaction is one of the broadening mechanisms, which is always present in a solid where there is very little motion of the atoms, and affects the lineshape of an NMR spectrum. The magnetic dipole interaction arises from the coupling of a nuclear spin with the local field of its neighbouring spins. Therefore this interaction represents the effect of the neighbouring nuclear magnetic moments on the nucleus of interest. This interaction is in the same form as for two classical magnetic dipoles separated by a distance r, shown in figure 2.3a, and can be written as,

$$H_d = \frac{\hbar^2}{2} \sum_{i<j} \frac{\gamma_i \gamma_j}{r_{ij}^3} (3\cos^2\theta_{ij} - 1)(I_i . I_j - 3I_{iz} I_{jz}) \qquad (2.12)$$

where 'r_{ij}' is the distance between two neighbouring nuclei and θ is the angle between the internuclear vector and the magnetic field.

This interaction may arise from three different interactions which are homonuclear dipolar coupling, interaction between like spins; heteronuclear dipolar coupling interaction between unlike spin; interaction between the nucleus and unpaired electron spins. Figure 2.3b shows the powder pattern observed in a polycrystalline sample for an isolated spin pair. The observed nucleus will experience each energy state of neighbouring spin as a perturbation in the local magnetic field. The effect of this interaction is proportional to $\gamma_i \gamma_j$, for unlike spin and therefore especially strong for a nuclide with a high γ. The overall affect of this interaction on an NMR spectrum is to broaden the line. Since the magnetic dipolar interaction varies as $(3\cos^2\theta\text{-}1)$ it is possible to remove this interaction by using MAS

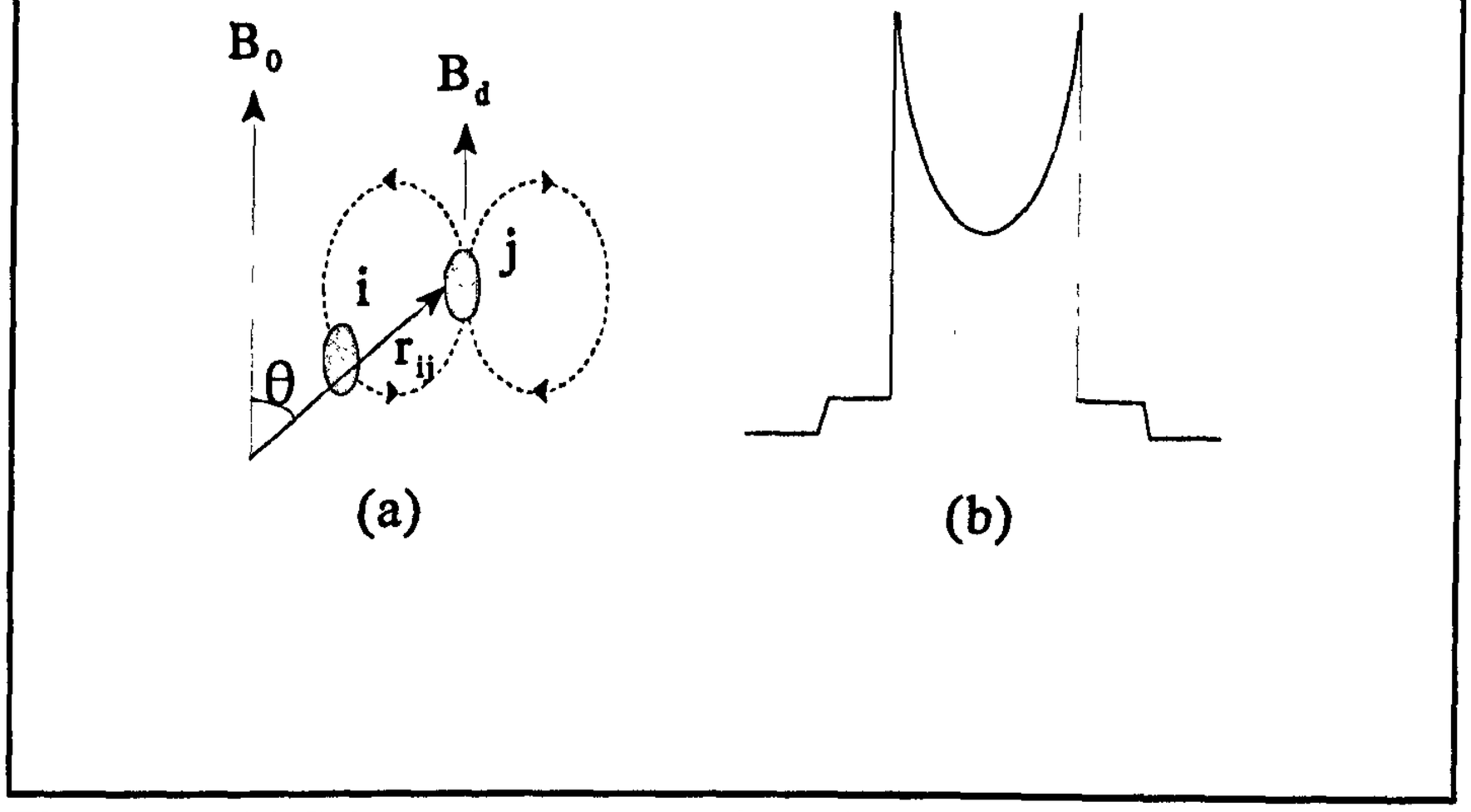

Figure 2.3 (a) Schematic representation of two neighbouring nuclei i and j separated by internuclear vector r_{ij}, (b) the dipolar lineshape for isolated pair of spin 1/2 with a small amount of broadening from neighbouring spins.

2.4 Chemical Shift Interaction

The chemical shift interaction arises from the magnetic shielding of the nucleus caused by the electrons circulating around the nucleus. The Hamiltonian describing the effect of the chemical shift interaction is,

$$H_{cs}=\hbar\gamma I.\sigma.B \qquad (2.13)$$

where σ is known as the shielding tensor called chemical shift which varies with the position of the nucleus in the molecule. As a result of this shielding the magnetic field at the nucleus is given by,

$$B=B_0(1-\sigma) \qquad (2.14)$$

and the resonance frequency of the nucleus becomes

$$\omega = \gamma B_0 (1 - \sigma) \tag{2.15}$$

which leads to a shift in the resonance frequency. Therefore for a particular nucleus, the NMR signal has different frequencies for different chemical environments.

One can choose a coordinate system, the principle axis system (PAS), where this tensor is diagonal and σ_{xx}, σ_{yy} and σ_{zz} are the only non zero components. In general σ is given by

$$\sigma = \sigma_{isot} + 1/2\Delta(3\cos^2\theta - 1 + \eta_{cs}\sin^2\theta\cos^2\phi) \tag{2.16}$$

where

$$\sigma_{isot} = 1/3(\sigma_{xx} + \sigma_{yy} + \sigma_{zz}) \tag{2.17}$$

$$\eta_{cs} = (\sigma_{xx} - \sigma_{yy})/(\sigma_{zz} - \sigma_{isot}) \tag{2.18}$$

$$\Delta = \sigma_{zz} - \sigma_{isot} \tag{2.19}$$

and θ, ϕ are the angles which rotate the laboratory frame into the PAS.

The shielding tensor σ consist of two terms which are diamagnetic σ_d and paramagnetic σ_p terms.

$$\sigma = \sigma_d + \sigma_p \tag{2.20}$$

The paramagnetic term is strongly dependent on the local symmetry of the electronic charge about the nucleus and is zero for a spherically symmetric distribution. The diamagnetic term arises from circulation of electrons around the nucleus. This

circulation produces a magnetic field which opposes the external magnetic field, B_0.

In liquids only the isotropic part of the chemical shift is obtained due to rapid molecular motion, leading to the well resolved sharp NMR spectral resonance lines. However in the solid state, due to lack of rapid molecular motion, spectral lines are subject to broadening. For a single crystal, in a fixed orientation to the magnetic field, a single sharp resonance line is observed for each magnetic orientation of a particular nucleus to the field direction, and position of the lines is dependent on the orientation of the crystal. In a powdered glassy or polycrystalline material where molecules are orientated in all possible directions with respect to the magnetic field, the observed line will be the superposition of lines resulting from crystallites lying at different directions with respect to the magnetic field. Figure 2.4 shows the resulting lineshape called the powder pattern.

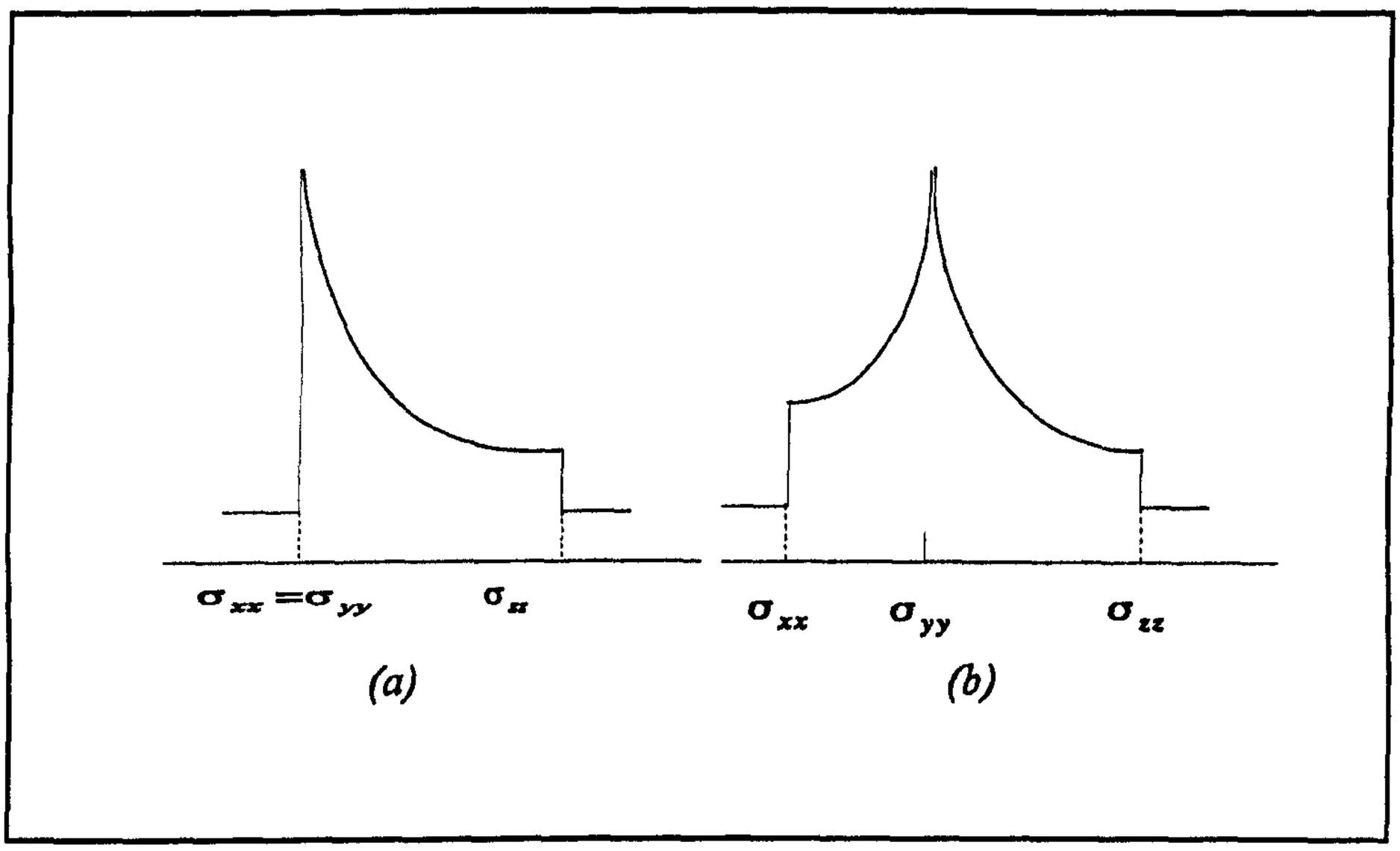

Figure 2.4 (a) Powder pattern lineshape for an axially symmetric chemical shift tensor ($\sigma_{xx}=\sigma_{yy}\neq\sigma_{zz}$) (b) Powder pattern lineshape for an arbitrary symmetry chemical shift tensor.

The contribution to the line width due to chemical shift anisotropy depends on the nucleus and on the symmetry of its surroundings, it is small for light elements, up to 30 ppm for ^{1}H, 140 ppm for ^{29}Si in crystalline silicates and up to ~10000 ppm for some heavy atoms ^{59}Co, ^{185}Pt [14]. The broadening due to chemical shift anisotropy is inhomogeneous, and can be removed effectively by MAS, resulting in a well resolved spectrum figure 2.5.

In general, values of σ_{iso} cannot be calculated accurately from first principles for complex structures. However , an initio calculations on small molecular clusters that are the major structural features of silicates have recently shown great potential in quantifying at least relative effects of parameters such as coordination numbers, bond angles, and distances, etc. [15][16].

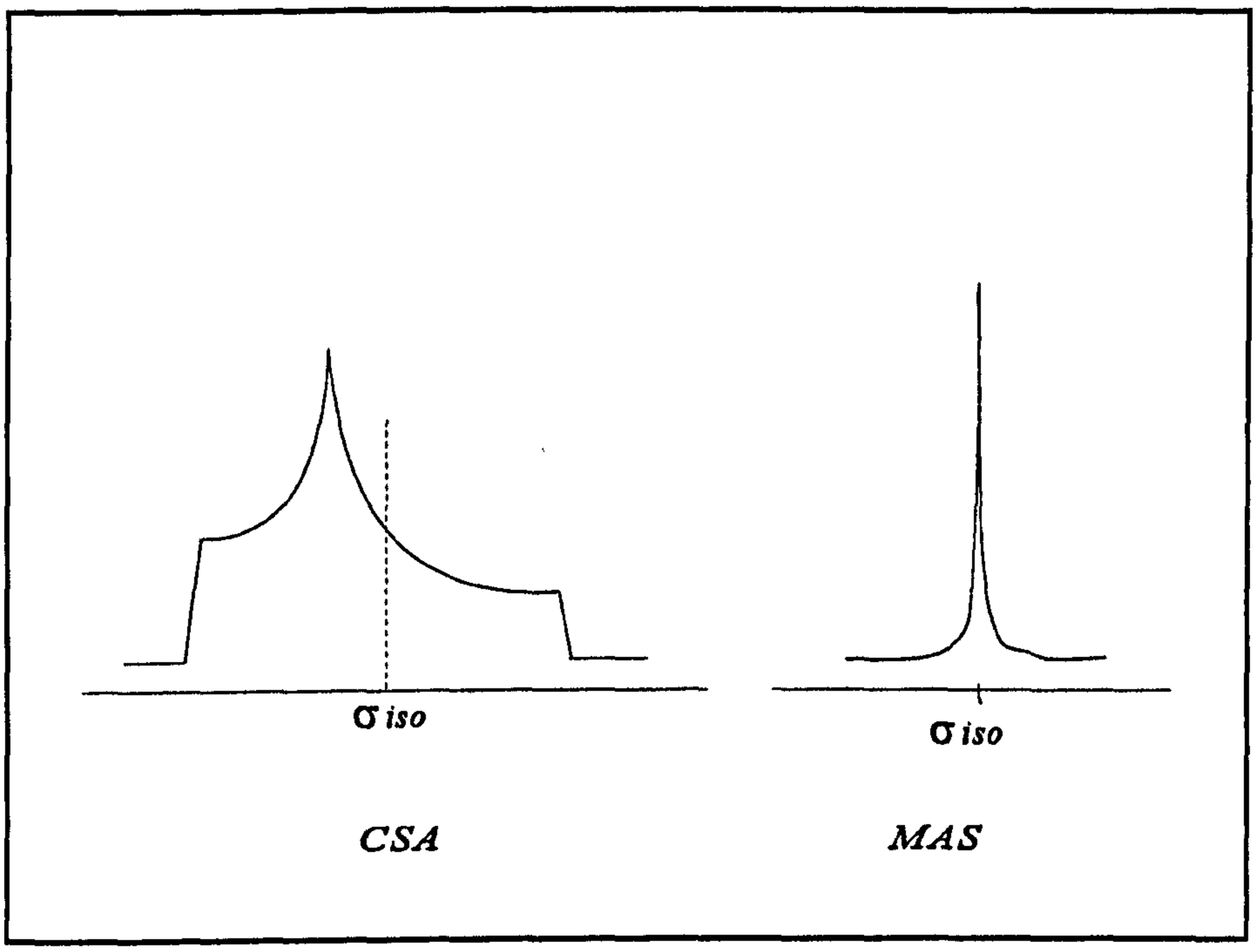

Figure 2.5 Removal of broadening caused by CSA under MAS.

2.5 The Nuclear Quadrupole Interaction

Nuclei with spin quantum number I>1/2 have an electric quadrupole moment (eQ) as well as a magnetic moment because of the deviation from a spherical charge distribution of the nucleus. The quadrupolar effect arises due to interaction between the quadrupole moment of the nucleus and the electric field gradient produced by the surrounding electrons. The electric field gradients can originate from electrons in the chemical bonds of the atom and charges on neighbouring atoms or ions. However a major contribution to the electric field gradient ,efg, comes from bonding electrons, since closed shells of electrons do not generate an electric field gradient. Therefore quadrupolar nuclei are quite sensitive probes for chemical bonding and local atomic arrangement, because of the interaction with the efg which depends on the nature of chemical bonds and the arrangement of ions around the atoms [17]. The electric field gradient tensor $V_{\alpha\beta}$ is described in its principal axis as

$$\frac{\partial^2 V}{(\partial\alpha\partial\beta)} \equiv V_{\alpha\beta} \tag{2.21}$$

where $V_{\alpha\beta}$ is diagonal; i.e., $V_{\alpha\beta} = 0$ if $\alpha \neq \beta$, and $V_{zz}>V_{xx}>V_{yy}$, and in this system

$$\frac{\partial^2 V}{\partial z^2} = V_{zz} = eq \tag{2.22}$$

is known as the field gradient. In the presence of a magnetic field B_0, the total Hamiltonian can be written by neglecting anisotropic chemical shift and scalar spin-spin couplings [10],

$$H = H_Z + H_Q \tag{2.23}$$

$$H=-\gamma\hbar B_0 I+\frac{e^2qQ}{4I(2I-1)}[3I_z^2-I(I+1)+\frac{\eta}{2}(I_+^2+I_-^2)] \qquad (2.24)$$

where eQ is the quadrupole moment of the nucleus and I_z is the z component of the quantum spin vector,

$$I_\pm=I_x\mp I_y \qquad (2.25)$$

η is the asymmetry parameter which describes the deviation from axial symmetry and is defined by

$$\eta=\frac{V_{xx}-V_{yy}}{V_{zz}} \qquad (0\le\eta\le1) \qquad (2.26)$$

In general it is conventional to define the size of the quadrupolar interaction in terms of

$$C_Q=\frac{e^2qQ}{h} \qquad (2.28) \qquad \text{and} \qquad \nu_Q=\frac{3e^2qQ}{2I(2I-1)h} \qquad (2.29)$$

C_Q is the quadrupole coupling constant and it is a measure of the magnitude of EFG for a given nuclide, or sometimes the field gradient (in MHz), and ν_Q the quadrupolar frequency. For a quadrupolar nucleus in a magnetic field there are mainly two cases: $H_z \gg H_Q$ or $H_z \ll H_Q$. The latter situation (very strong quadrupolar interaction) leads to NQR (nuclear quadrupolar resonance), and the former case is the subject of NMR

The quadrupole interaction shifts the energy levels in the presence of an external magnetic field. This shift depends on the quadrupole moment of the nucleus, eQ, and the orientation of the B_0 field with respect to the principal axes of the electric field gradients present at the nuclear site. In the case of glass or polycrystalline powder all orientations are possible and the observed NMR lineshape is made up of responses for all possible orientations (powder pattern). If the applied magnetic field is much larger than the quadrupole interaction, ($H_z >> H_Q$), then the quadrupolar interaction is considered to be a perturbation and the total energy of the m^{th} level of such a quadrupole interaction is given by standard perturbation theory for axial symmetry ($\eta=0$) [10-12][18][19].

$$E_m = E_m^0 + E_m^1 + E_m^2 \tag{2.30}$$

$$E_m^0 = -h\nu_o \tag{2.31}$$

where

$$E_m^0 = \frac{3hC_Q}{8I(2I-1)}(3\cos^2\theta - 1)(m^2 - a/3) \tag{2.32}$$

where a=I(I+1)

$$E_m^2 = \frac{-9hC_Q^2 m}{128\nu_0 I^2(2I-1)^2}(\sin^2\theta(8m^2 - 4a + 1) + \sin^4\theta(-2m^2 - 2a + 1)) \tag{2.33}$$

The first order approximation considers only E_m^1 which causes a splitting of the unperturbed Larmor frequency into 2I components of frequencies υ_m^1 as shown in figure 2.6. These energy levels are shifted from ν_0 by ν_m^1 in first order.

$$\nu_m^1 = -\frac{3C_Q}{4I(2I-1)}(3\cos^2\theta - 1)(m - 1/2) \qquad (2.34)$$

As can be seen from figure 2.6 and equation.34, the central transition (1/2↔ -1/2) is not affected by the quadrupolar interaction to the first order. However the satellite transitions (-1/2↔-3/2, and 3/2↔ -1/2) can be sufficiently broad that they become difficult or impossible to observe with conventional pulse techniques, figure 2.7.

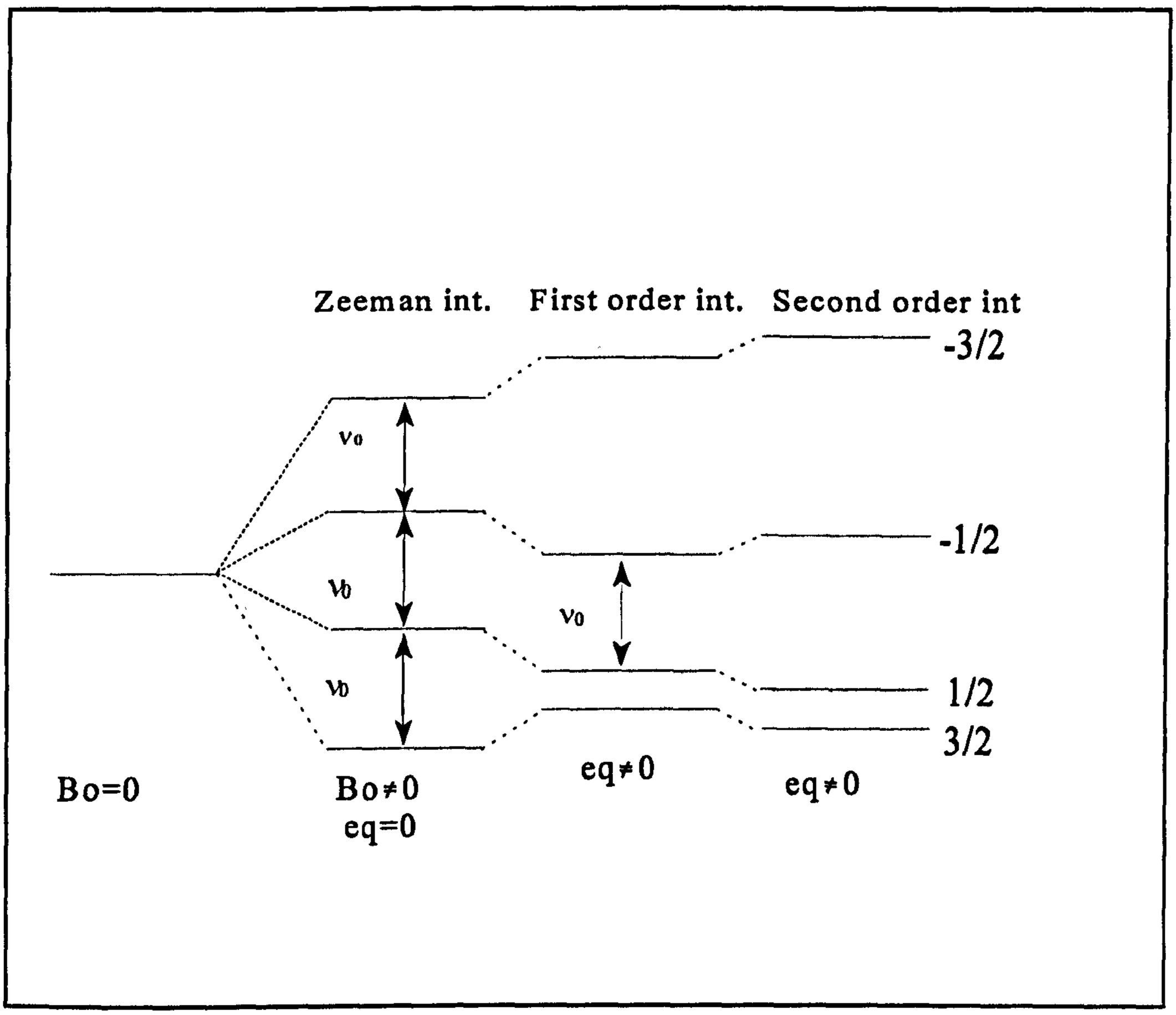

Figure 2.6 Energy level for an I=3/2 spin showing the effects of the quadrupolar interaction to first and second order.

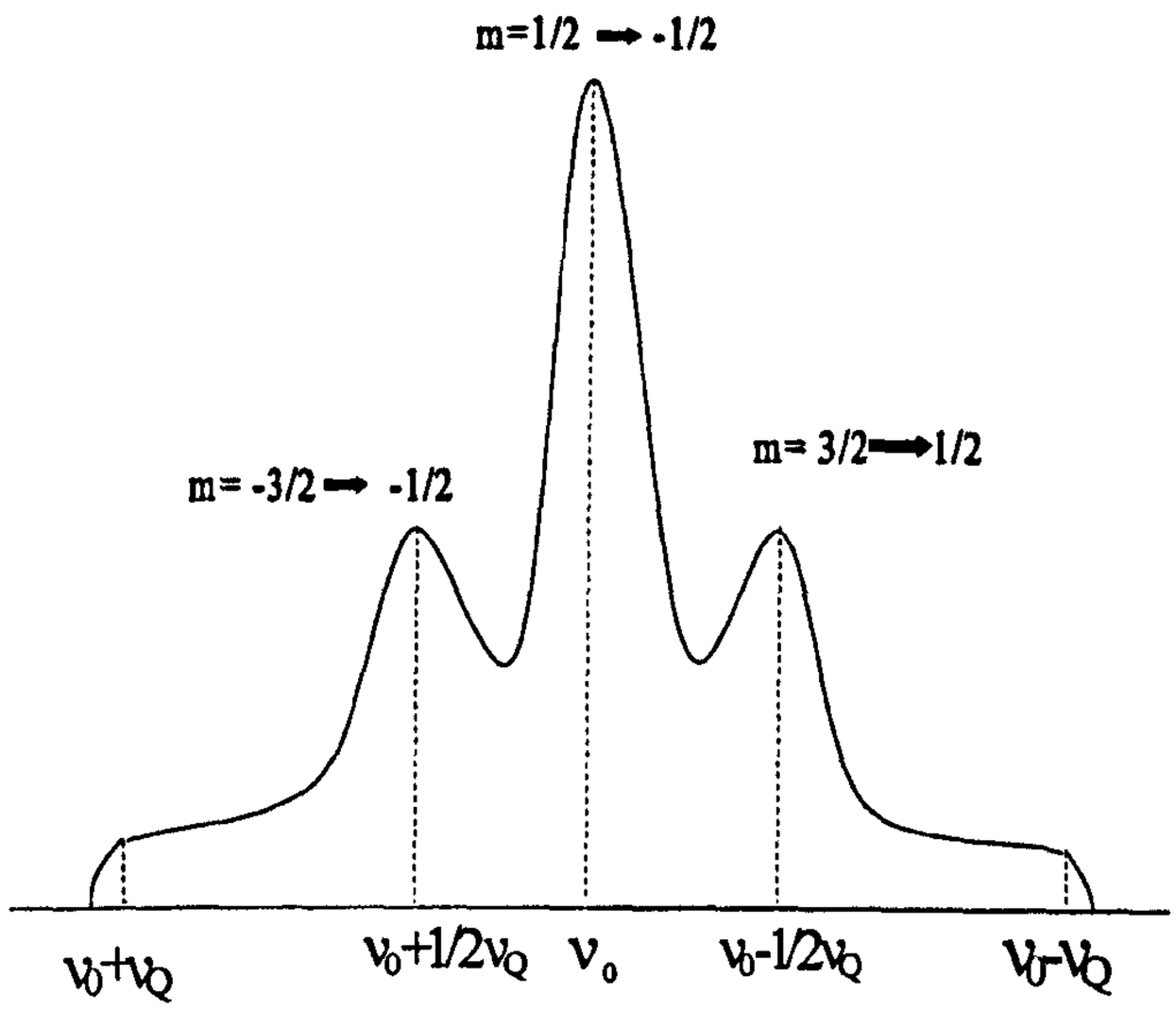

Figure 2.7 First order quadrupolar powder pattern for I=3/2 showing the satellite -3/2→-1/2 etc. transitions. $\eta=0$, $\nu_Q=(½)e^2qQ/h$.

Although the central transition is not affected by the first order interaction, the second order interaction, equation 2.35, affects the spectrum and shifts the central transition with respect to the Larmor frequency. Figure 2.8 shows the typical second order asymmetric lineshape of the central transition from a powdered material without dipolar interaction. The satellite transitions will be spread out over a very large frequency region such that they cannot be observed without special efforts, such as high spectrometer sensitivity and a broad sweep range. The second order shift for the central (1/2↔ -1/2) transitions, $\nu_{1/2}^2$, given below produces the lineshape of figure 2.8.

$$\nu_{1/2}^2 = \frac{-9C_Q^2}{64\nu_0 I^2(2I-1)^2}(a-3/4)(1-\cos^2\theta)(9\cos^2\theta-1) \qquad (2.35)$$

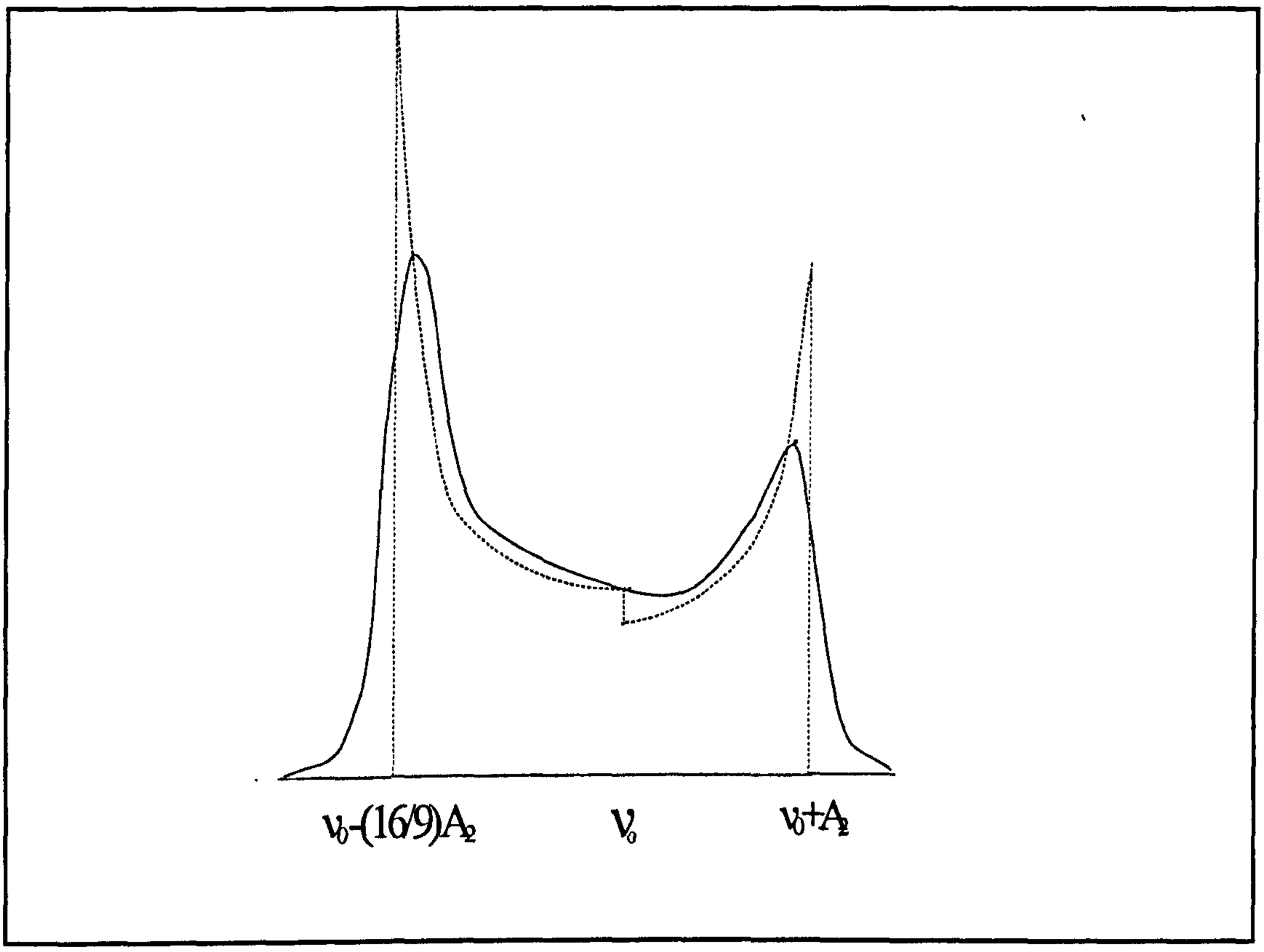

Figure 2.8 Second order quadrupole broadened lineshape for the central (1/2↔ -1/2) transition. $\eta=0, A_2=(9\nu_Q^2/144\nu_0)[\ I(I+1)-3/4]$

2.6 High Resolution NMR Spectra of Solids

Generally all interactions discussed above are termed as line broadening interactions in solid state NMR and, as stated earlier, prevent the observation of possible chemically different sites in a powdered sample because of the broad powder pattern. Therefore, obtaining high resolution NMR spectra from powdered samples has been a challenge for researchers. There are a number of techniques to remove these

interactions and obtain high resolution solid state NMR spectra, such as MAS, VAS, DAS, DOR, MQ-MAS, and only the most widely used technique MAS and one of the new developed techniques MQ-MAS will be briefly discussed here.

2.6.1 Magic Angle Spinning (MAS)

Introduction of a time dependence of the interactions in powders results in removal of the anisotropic parts of the internal Hamiltonian causing significant narrowing of the spectral lines of powders, as in the liquids and such a time average can be imposed by mechanical rotation of the entire solid sample (rotor) about a single axis, so-called Magic Angle Spinning (MAS),shown in figure 2.9. This technique involves the spinning of the sample at an angle of 54.44° with respect to the external static magnetic field B_o [5].

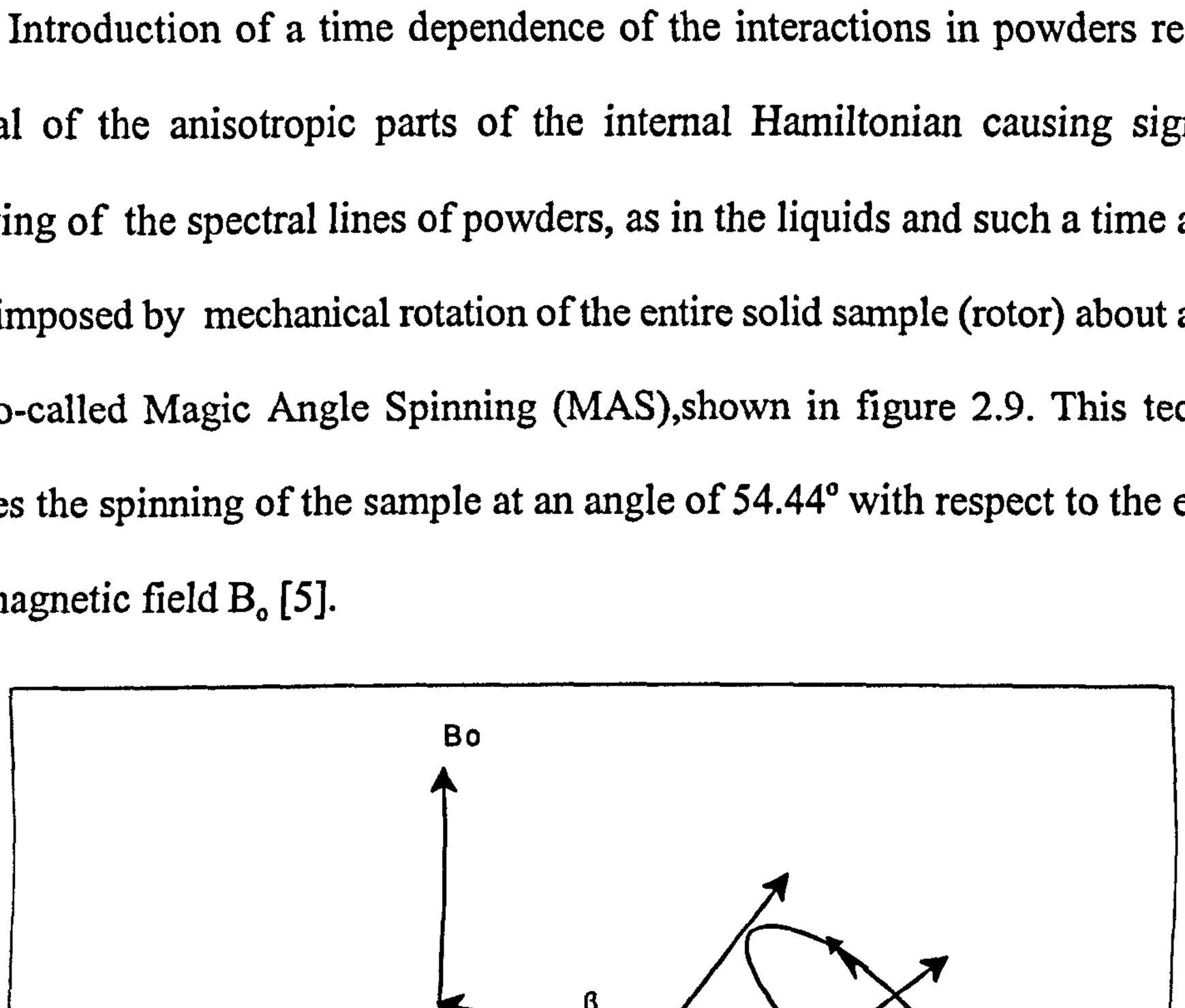

Figure 2.9 Schematic representation of MAS.

The all line broadening interactions briefly discussed above have an orientation dependence, to first order, containing the factor $(3\cos^2\theta-1)$ where θ is the angle between the external magnetic field, B_o and the largest component of the tensor describing the interaction or, a vector r describing the relevant interaction in the case of chemical shift and quadrupole interactions, r is the z component of their principal axis system while in the case of the dipole-dipole interactions, r is the vector between two nuclei (internuclear vector r_{ij}). Rapid sample spinning removes the time dependent term [20]. A given internuclear vector is indicated to have an angle, λ, with respect to the axis of the rotor. When the spinning occurs around the axis of the rotor, the angle θ, will vary between $\beta-\lambda$ and $\beta+\lambda$, where β is the angle between axis of the rotor and B_0. Clearly the average NMR interaction will depend on $\langle 3\cos^2\theta-1\rangle$ which is given by

$$<3\cos^2\theta-1>=1/2(3\cos^2\beta-1)(3\cos^2\lambda-1) \qquad (2.36)$$

when the angle β is 54.44° the average $\langle 3\cos^2\theta-1\rangle$ is zero for all initial values of θ and the effects in the spectrum of all first order anisotropic interactions are entirely removed, providing the spinning speed is fast enough, giving sharp lines and high resolution NMR. At the expense of the loss of information that is contained in these orientation dependent parameters, sometimes enormous narrowing of the NMR spectrum is obtained.

The spinning speed of the rotor is the important part of this technique since to obtain a high resolution NMR spectrum the spinning speed should be greater than the line width of the static spectrum. Currently spinning speeds of 5 to 15 kHz are fairly routine. MAS has artifacts called spinning side bands which occur exactly at the spinning speed. For a quadrupolar nucleus, a separate set of side bands may be observed

for each pair of satellite transitions. MAS cannot completely remove the second order quadrupole interaction leaving, sometimes, broad and complex line shapes for nuclei such as ^{17}O, ^{23}Na, ^{27}Al, shown in figure 2.10. However calculations of the central lineshape under MAS conditions [21][22] show that significant narrowing occurs even though the second order effect cannot be removed totally. Therefore it is possible to obtain relatively high resolution NMR spectra from a quadrupolar nucleus with moderate C_Q by using MAS.

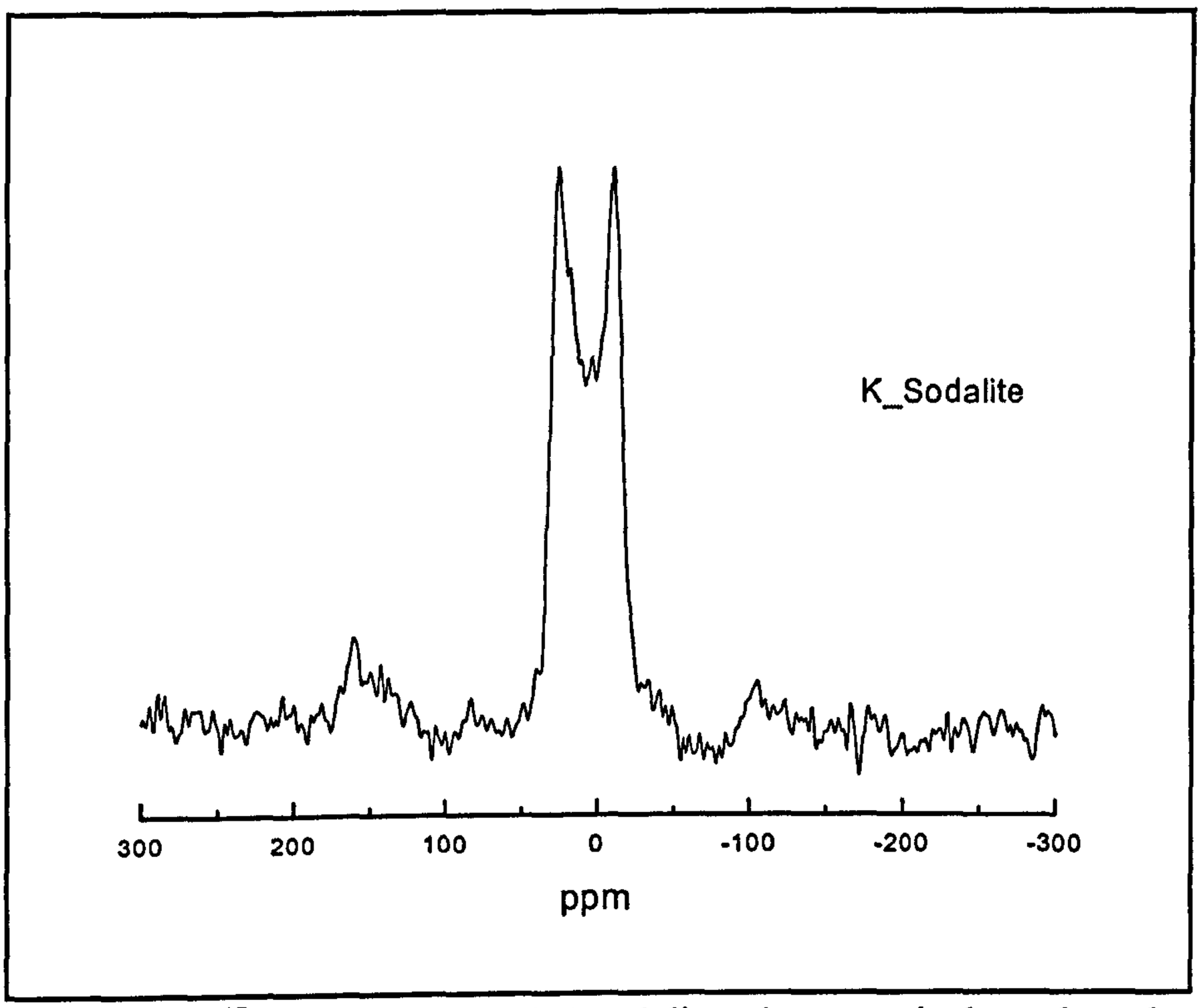

Figure 2.10 ^{17}O MAS NMR of K-sodalite, shows typical quadrupolar lineshape.

However recently developed techniques such as Double rotation (DOR), Dynamic angle spinning (DAS) [7-9] have the capability of removing second order quadrupolar effects resulting in high resolution NMR spectra. Another promising technique for obtaining high resolution NMR spectra from a quadrupolar nucleus is

Multiple Quantum NMR (MQ NMR) [10][23][24] which will be discussed below.

2.6.2 Multiple Quantum MAS NMR (MQ MAS NMR)

Although MAS has been very important in the development of solid state NMR applications, it is not capable of removing the quadrupolar effects. In general MAS only manages to reduce second-order quadrupolar broadenings by a factor of ~3. The development of a theoretical framework , involving an expansion of second order effects in terms of zero, second and fourth rank spherical tensor components [25][26], made possible DAS and DOR [7-9]. However technological problems limit DOR while DAS encounters problems in strongly dipolar coupled systems.

An alternative method was proposed by Frydman et.al.[10]. He proposed a two-dimensional multi quantum method, similar in several aspects to DAS, now called multiple-quantum MAS NMR, (MQ MAS-NMR). This technique is technically much easier than DAS since it only involves spinning the sample at MAS conditions. It enhances the resolution of the spectra for quadrupolar nuclei and is based on the correlation of <m , -m> multiple quantum transition to the central transition <1/2 , -1/2>. As explained earlier, in a magnetic field, energy levels of the sample are split (figure 2.6). In this case the dominant interaction is the Zeeman interaction

$$H_z = -\nu_L I_z \qquad (2.37)$$

and it is perturbed by a smaller quadrupolar interaction.

$$H_Q = \nu_Q(\theta,\varphi)\{3I_z^2 - I(I+1)\} \qquad (2.38)$$

Therefore the Larmor frequency ν_L should be much greater than the quadrupolar frequency ν_Q which is given as

$$\nu_Q(\theta,\varphi)=[e^2qQ/h(3\cos^2\theta-1+\eta\sin^2\theta cos2\varphi)]/[4I(2I-1)] \quad (2.39)$$

where θ and φ are the angles, describing the orientation of the external field B_0 within the PAS of the quadrupolar tensor.

The I^2_z dependence of the quadrupolar Hamiltonian makes it possible to avoid first order quadrupole broadening on any <m , -m> transition, and implies that all NMR transitions between states differing in their I_z value ($\pm1/2\leftrightarrow\pm3/2$,$\pm3/2\leftrightarrow\pm5/2$ etc.) will be affected by anisotropic first order quadrupole effects. In addition to that the second order quadrupole effect also broadens these transition. The evolution for a m↔-m spin coherence after excitation can be described by a multirank expansion of its phase ϕ [27].

$$\phi(m,\beta,t)=2mt\nu^{CS}+\nu_0^Q C_0^I(m)+\nu_2^Q(\theta,\varphi)C_2^I(m)P_2(\cos\beta)t+\nu_4^Q(\theta,\varphi)C_4^I(m)P_4(\cos\beta)t \quad (2.40)$$

where

$$C_0^I(m)=2m[I(I+1)-3m^2]$$

$$C_2^I(m)=2m[8I(I+1)-12m^2-3]$$

$$C_4^I=2m[18I(I+1)-34m^2-5]$$

are zero second and fourth rank coefficients depending on the spin number and order of the transition.

$$P_2(\cos\beta)=\frac{(3\cos^2\beta-1)}{2} \tag{2.41}$$

$$P_4(\cos\beta)=\frac{(35\cos^4\beta-30\cos^2\beta+3)}{8} \tag{2.42}$$

are second and fourth order Legendre polynomials and

$$\nu_0^Q=[(e^2qQ/h)^2(3+\eta^2)]/[10\nu_L[2I(2I-1)]^2] \tag{2.43}$$

is the isotropic or zero rank quadrupolar shift. $\nu_2^{\circ}(\theta,\varphi)$ and $\nu_4^{\circ}(\theta,\varphi)$ are second and fourth rank angular dependent frequencies responsible for the observed line broadening [27]. In order to refocus anisotropic interaction to obtain high resolution spectra second and fourth order Legendre polynomials should be removed. However there are no common roots between $P_2(\cos\beta)$ and $P_4(\cos\beta)$ so no single axis can simultaneously remove the second and fourth rank quadrupolar anisotropies. The DAS method removes the anisotropy by spinning the sample at two angles consecutively for times t_1 and t_2. By choosing the appropriate angles and the ratio of times the refocussing condition is met.

$$P_2(\cos\beta_1)t_1+P_2(\cos\beta_2)t_2=0 \tag{2.44}$$

$$P_4(\cos\beta_1)t_1+P_4(\cos\beta_2)t_2=0 \tag{2.45}$$

as a result at the time t_1+t_2 the signal is free from anisotropic broadening

It is possible to propose an alternative method to DAS in a completely analogous manner. The MQMAS method uses the change in coherence order to remove anisotropies. In addition, this technique involves MAS which removes second rank

quadrupolar shift as well as dipolar and chemical shift interactions. Therefore MAS provides the condition.

$$P_2(\cos\beta_{mas})=0 \tag{2.46}$$

The remaining fourth rank quadrupolar shift is cancelled by choosing two different coherence orders $(-m_i \leftrightarrow m_i)_{i=1,2}$ and spins are allowed to evolve under the effects of these two transitions. Coefficients of these coherences fulfill the second order averaging condition.

$$C_4^I(m_1)t_1+C_4^I(m_2)t_2=0 \tag{2.47}$$

Therefore allowing the spins to evolve at the coherence levels m_1 and m_2 for t_1 and t_2 times respectively leads to a zero coefficient for the fourth rank quadrupolar shift at the time t_1+t_2.

Although the selection rules restricts the $m_2 \leftrightarrow -m_2$ transition to the central transition $-1/2 \leftrightarrow 1/2$ one can use phase cycling to chose the desired multiple quantum coherence during t_1. Therefore the evolution phases ϕ_1 and ϕ_2 correlated in 2D MQMAS can be written as

$$\phi_1=\nu_1 t_1=[2m_1\nu^{cs}+C_0^I(m_1)\nu_0^Q+C_4^I(m_1)P_4(\cos\beta_m)\nu_4^Q(\theta,\varphi)]t_1 \tag{2.48}$$

$$\phi_2=\nu_2 t_2=[\nu^{cs}+C_0^I(1/2)\nu_0^Q+C_4^I(1/2)P_4(\cos\beta_m)\nu_4^Q(\theta,\varphi)]t_2 \tag{2.49}$$

and consequently the signal (an echo) forms at

$$t_2=[C_4^I(m_1)/C_4^I(1/2)]t_1 \qquad (2.50)$$

The ratio of t_2 to t_1 is called the MQMAS ratio (R) and R=19/12 for I=5/2 with p=3 quantum coherence.

There are a number of pulse sequences used to obtain 2DMQMAS spectra [28]. The most basic pulse scheme is the two pulse sequence (shown in figure 2.11) where the MQ transition is excited by a single, high power rf pulse which excites many transitions in the quadrupolar spin system. After the first pulse MQ coherence is allowed to evolve for a time t_1 after which a second pulse is applied. The second pulse converts the MQ coherence into a p= -1 coherence, which is observed during t_2, since MQ transitions can not be detected directly. After the second pulse an echo forms at a time t_2 (equation 2.50) as a diagonal ridge as shown figure 2.12. Since these two pulses are non-selective they excite all coherences, in order to chose the coherence of interest, the pulse sequence is cycled through the appropriate phases as an rf phase shift ϕ degrees seen as a phase shift of $m\phi$ degrees for a m-quantum coherence [29]. Figure 2.13 shows the resonance as ridges lying along the R after 2D Fourier transformation. It is possible to obtain the isotropic spectrum by projecting the whole spectrum on a line through the origin perpendicular to the R (MQMAS ratio).

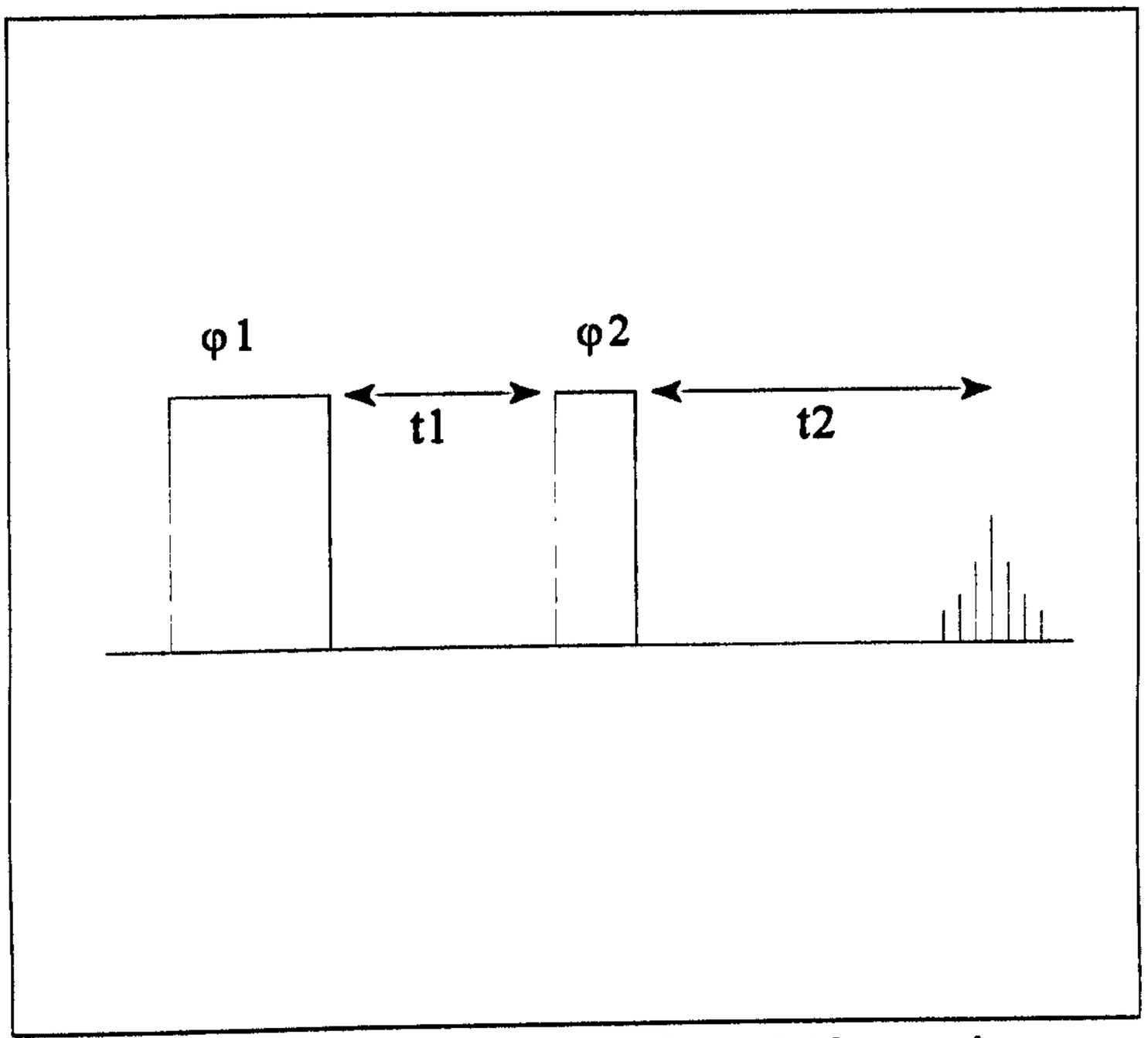

Figure 2.11 Two pulse sequence for an MQ experiment

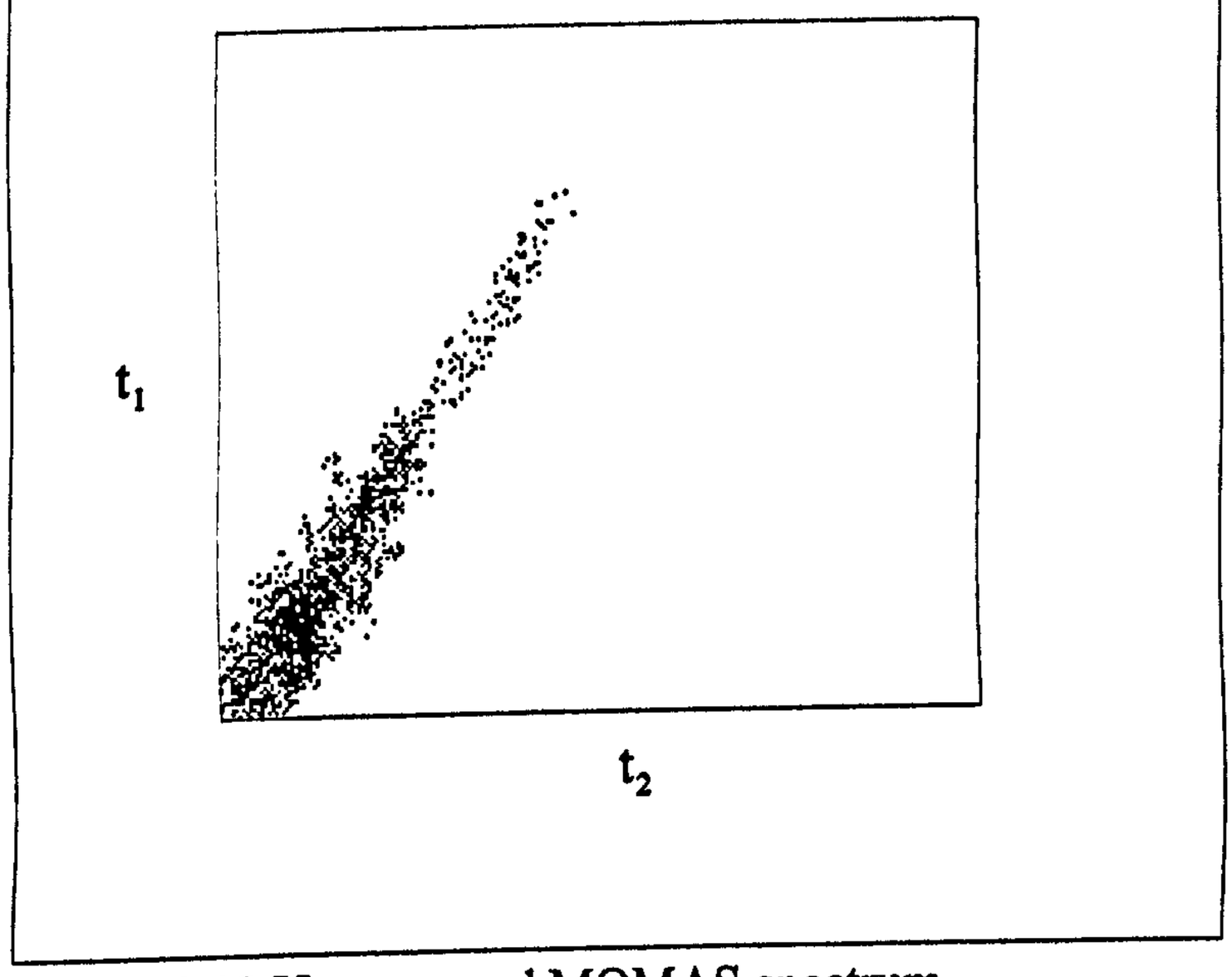

Figure 2.12 Unprocessed MQMAS spectrum

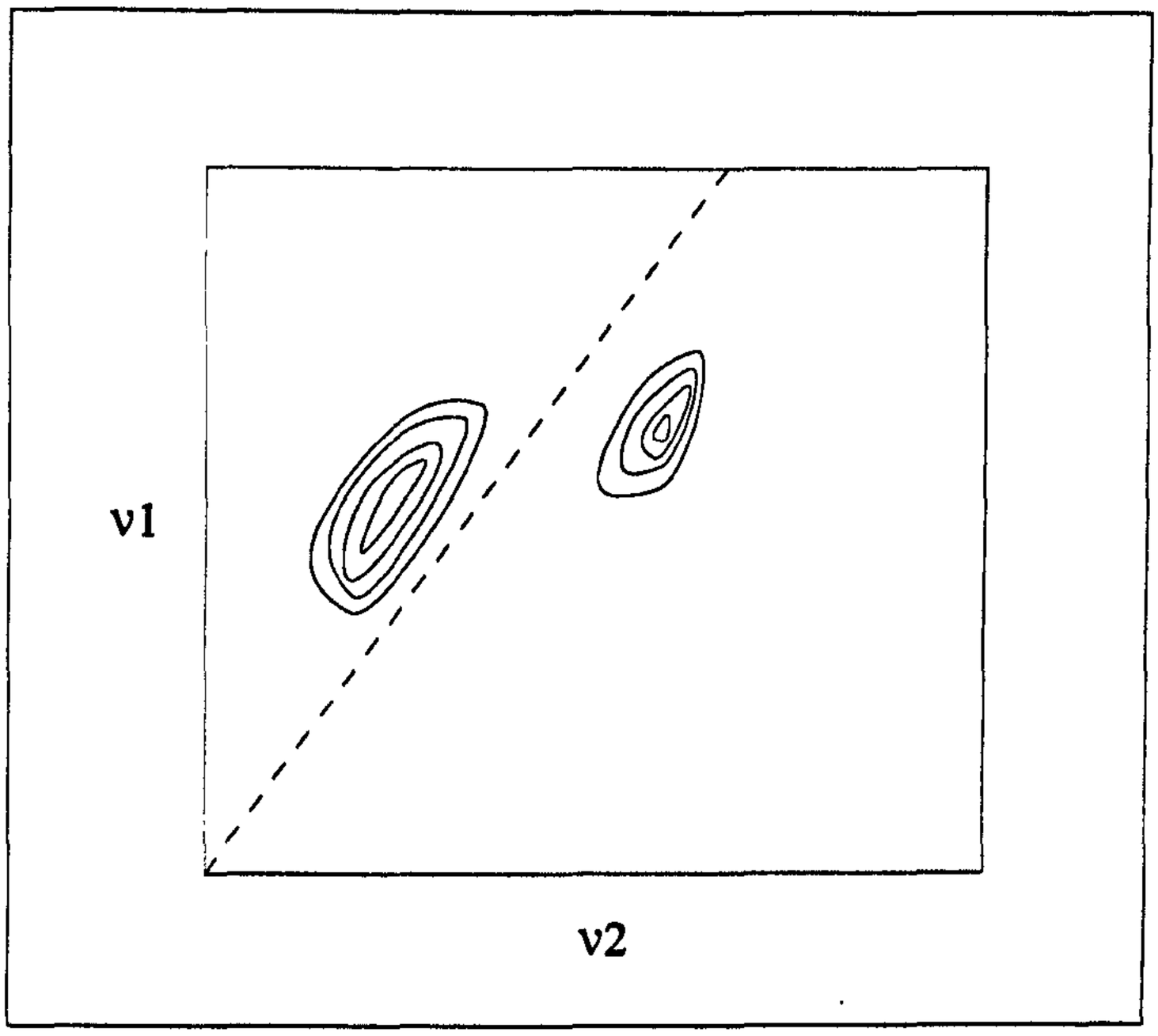

Figure 2.13 MQMAS spectrum after Fourier transformation in both dimensions.

2.6.2-1 Processing of MQMAS Data

In a 2D MQMAS experiment data are acquired as rows of FIDs each of which corresponds to a different time interval (t_1) between pulses. The intensity of the signal decreases for each FID as the t_1 time interval increases, eventually leading to a negligible signal. At the end of the experiment the spectrum obtained in time vs time domain as shown in figure 2.12, is Fourier transformed in both dimensions to produce a frequency vs frequency spectrum, figure 2.13. Although it is not essential, one can apply shearing to obtain isotropic spectra in the ν_1 (isotropic dimension) as shown in figure 2.14. This makes the extraction of information and extraction of 1D slices easier. Shearing projects the points which lie on the same slope, equal to the anisotropy axis, onto a line parallel to the ν_2 (anisotropic dimension). It is applied between the Fourier transforms and given as

$$S'(t_1', \nu_2') = \exp(-iR\nu_2 t_1) S(t_1, \nu_2) \tag{2.51}$$

where $S(t_1, \nu_2)$ is the signal Fourier transformed with respect to t_2 As a result of the processing, ν_2 frequency is now correlated with a purely isotropic frequency,

$$\nu_1' = \nu_1 + \nu_2 R \tag{2.52}$$

causing the resonances to appear in a 3Q MAS experiment for spin I=5/2 at

$$\nu_1' = [17\nu^{cs} - 80\nu_0^Q]/12 \tag{2.53}$$

$$\nu_2 = \nu^{cs} + 8\nu_0^Q - 56\nu_4^Q \tag{2.54}$$

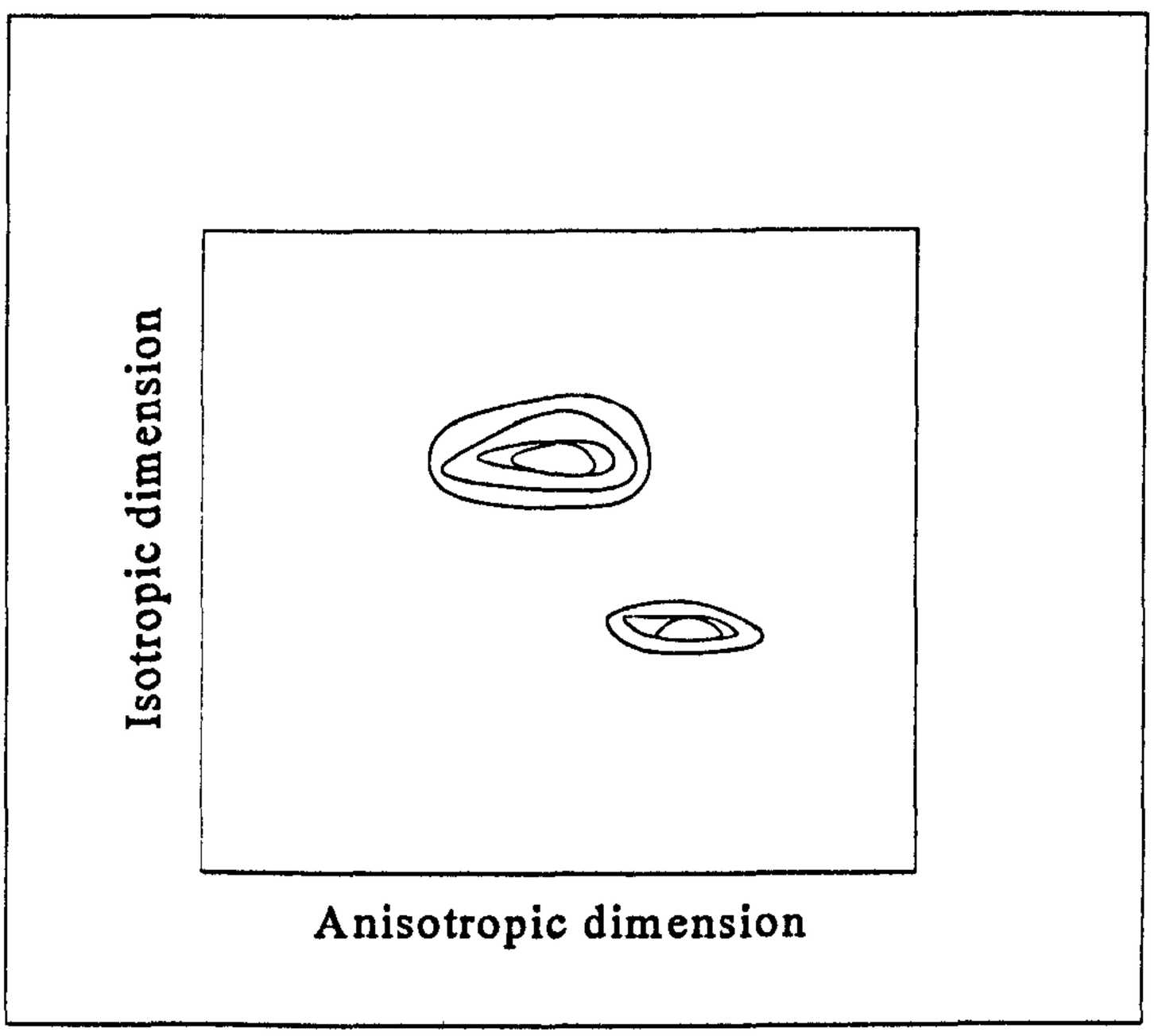

Figure 2.14 MQMAS spectrum after shearing

This spectrum contains a purely isotropic component along the ν_1 dimension whereas the ν_2 dimension contains the quadrupolar powder pattern. Therefore the isotropic spectrum can easily be obtained by projection of the entire 2D spectrum on the ν_1 axis

while MAS spectrum, can be obtained by projection of entire spectrum on the ν_2 axis. The next major point in processing MQMAS spectra is setting the reference. In the first dimension (anisotropic dimension) setting the reference is done by using a reference solution (water in our case) and zero point is set as in the same way in a 1D experiment. However the zero point in the second dimension (isotropic dimension) cannot be set experimentally. The carrier frequency is located in the centre of both dimensions. The shift at the carrier frequency in the second dimension (isotropic dimension) is the same shift at the carrier frequency in the first dimension (anisotropic dimension) as shown in figure 2.15.

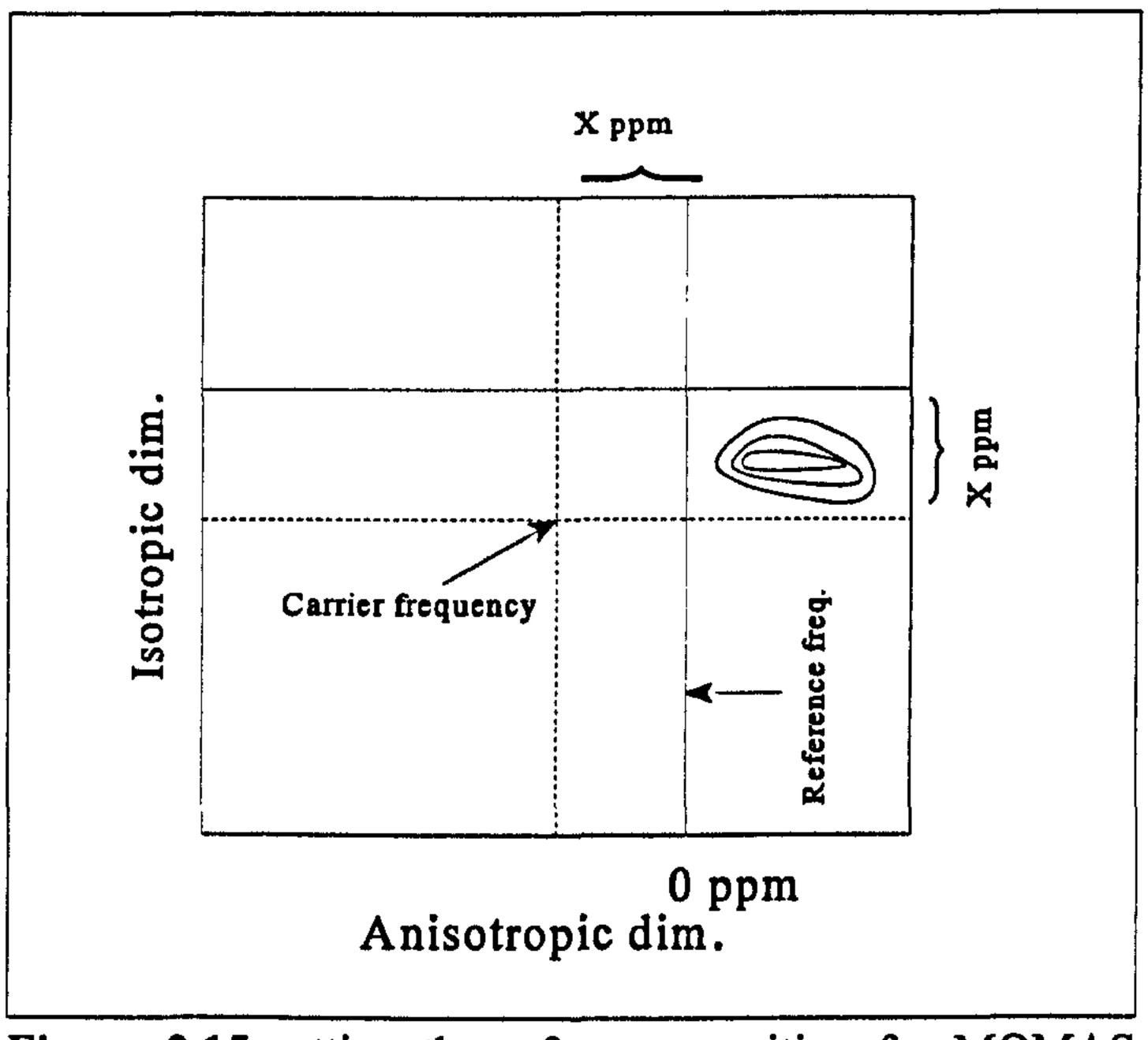

Figure 2.15 setting the reference position for MQMAS spectra

This is valid for data obtained with or without delayed acquisition or processed with or without shearing [28]. The zero point in the isotropic dimension is therefore set according to the following equation.

$$0.5+(scalingfactor)\frac{(carrierfrequency-referencefrequency)}{spectralwidthofisotropicdimension} \qquad (2.55)$$

where the scaling factor is 17/31 for a 3Q MAS experiment.This in turn gives the high resolution isotropic spectra of quadrupolar nuclei in powdered samples [21,22][30][31].

References

[1] F. Bloch, W.W. Hansen and M.P. Pickard, Phys. Rev. 69 (1946) 127.

[2] E.M. Purchell, H.C. Torrey and R.V. Pound, Phys. Rev. 69 (1946) 37.

[3] W.G. Procter and F.C. Yu, Phys. Rev. 77 (1950) 717.

[4] W.D. Knight, Phys. Rev., 76 (1949)1259.

[5] R.R. Ernst and W.A. Anderson, Rev. Sci. Instr. 37 (1966) 93.

[6] E.R. Andrew, Inter. Rev. Phys. Chem., 1 (1981) 195.

[7] A. Samoson, E. Lipmaa, A. Pines, Mol. Phys., 65(1988)1013.

[8] K.T. Muller, Y. Wu, B.F. Chmelka, J.F. Stebbins, A. Pines, J. Am. Chem. Soc., 113(1991)32

[9] I. Farnan, P.J. Grandinetti, J.H. Baltisberger, J. F. Stebbins, U. Werner, M. Eastman, A. Pines, Nature 358(1992)31.

[10] L. Frydman, J.S. Horwood, J. Am. Chem. Soc., 117(1995)5367.

[11] A. Abragam, Principles of Nuclear Magnetism, Oxford Uni. Press, 1985.

[12] C.P. Slichter, Principles of Magnetic Resonance, Springer-Verlag, 3rd. edition 1990.

[13] R.K. Harris, Nuclear Magnetic Resonance Spectroscopy, Longman Scientific and Technical, 1986.

[14] R. Dupree, "Line Broadening in Solids", in Nuclear Magnetic Resonance in Modern Technology, G. E. Maciel (ed.), Kluwer Academic Publishers (1994) 87-103.

[15] J.A. Tossel, J Non-Cryst Solids, 120 (1990), 13-19.

[16] J.A. Tossel, Phys Chem Minerals, 19 (1992), 338-342

[17] J. Wong, C.A. Angell, Glass Structure by Spectroscopy, Marcell Dekker, Inc., New York, 1976.

[18] C.P. Poole, H.A. Farach, Theory of Magnetic Resonance, (1987), Willey.

[19] M. Cohen, F. Reif, Solid State Phys., 5(1981)195.

[20] M.E. Smith, A High Resolution Multinuclear Resonance Study of Ceramic Phases, PhD. Thesis university of Warwick,(1987)

[21] H.S. Behrens, B. Schnabel, Physica.114B(1981)185-190.

[22] D. Muller, Ann. Phys., 39(1982)451-460.

[23] C. Fernandez, J.P. Amoureux, Solid State NMR, 1995.

[24] D. Massiot, B. Touzo, D. Trumeau, J.P. Coutures, Solid State NMR, (1995).

[25] A. Llor, J.Virlet, Chem. Phys. Lett., 152(1988)248.

[26] E.W. Wooten, K.T. Muller, A. Pines, Acc. Chem. Res., 25(1992)209.

[27] A. Medek, J.S. Harwood, L. Frydman, J. Am. Soc., 117(1995)12779-12787.

[28] M.E Smith, E.R.H. van Eck, Progress in NMR Spectroscopy, 34(1999)159-201.

[29] R.R. Ernst, G. Bodenhausen, A. Wokaun, Principles of NMR in One and Two Dimensions, Clarendon Press, Oxford, 1987.

[30] C. Fernandez, J.P. Amoureux, Chem. Phys. Lett. (1995).

[31] G. Wu, D. Rovnyak, R.G. Griffin, J. Am. Chem. Soc., 118(1996)9326-9332.

Chapter 3

Fundamentals of Glass Structure

3.1 Introduction

One of the definitions of a glass concentrates on the conventional method of preparation. Glass generally is defined as a product of melting which forms a solid, amorphous material on solidification of the melt without crystallization or devitrification [1-3]. The conventional method involves cooling from the liquid state, without crystallization occurring, until the viscosity becomes so great that the structure of the liquid becomes fixed. The term amorphous can be used as the condensed phase lacks long range order according to diffraction criteria. Since it is possible to form an amorphous solid by means other than cooling the melt, such as vapour deposition, chemical or electro deposition, shock treatment, sol-gel etc, more general definition is needed. The other definition concentrates on the structure of a glass: "a glass is an amorphous solid completely lacking in long range periodic atomic structure and exhibiting a region of glass transformation behaviour" [4-9]. The glass transformation is a region in the cooling period of the melt in which the temperature lies between the limits where the enthalpy is that of the liquid and that of the frozen solid. Figure 3.1 shows the volume as a function of temperature characteristics for crystals, liquid and glass. There are two types of pathways that a liquid, which might originate from a crystal or a glass, could follow on cooling. It may crystallize at or below the melting temperature, T_m, or it may undercool sufficiently without crystallization to form a glass. The liquid volume decreases steadily along the line (a-b). If the cooling rate is sufficiently slow, the melt will crystallize at T_m, along with a rapid decrease in the

volume (b-c). On further cooling crystalline material contacts along (c-d). If however the cooling rate is fast enough, crystallization can be avoided at T_m. On further cooling the decrease in volume of the new supercooled liquid continues with the slope (b-e). When the melt reaches a certain temperature (T_g) the slope of the curve changes gradually to (e-f) and continues with a line whose slope is nearly equal to that of the corresponding curve for the crystalline material. In this region the increase in viscosity is so great that the atoms can no longer completely rearrange to the equilibrium liquid structure and atomic arrangement that is present becomes effectively frozen in, and, on further cooling, the material acquires the rigid, elastic properties of a crystalline solid but without the regular three dimensional periodicity of a crystal structure. This change in properties or behaviour, from a supercooled liquid to a glass, takes place at a temperature or range of temperatures called the *glass transition temperature* T_g.

All the definitions shares two common characteristics. First, no glass has a long range, periodic atomic arrangement and, even more importantly, every glass exhibits the time-dependent glass transformation, T_g. In the glass-transition interval, viscosity increases from 10^8 to 10^{13} Poise.

The difference between a glass and a crystal is best displayed by X-ray diffraction where glass exhibits diffuse broad peaks instead of sharp Bragg peaks produced by crystalline materials. Because of the complexity and disorder of the glass structure, information from x-ray diffraction cannot be used to deduce a complete geometric structure as in the case of crystalline materials.

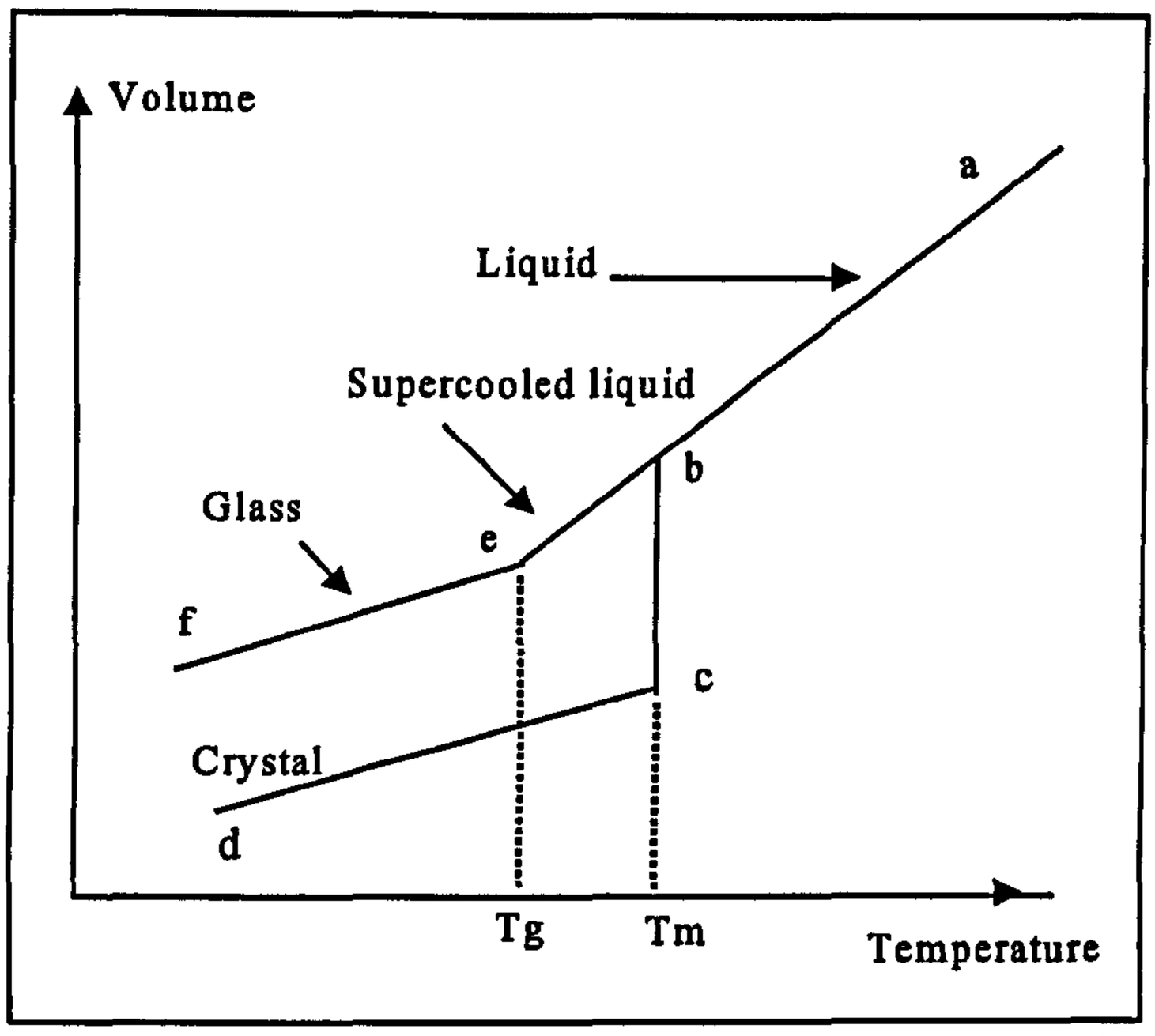

Figure 3.1 Schematic illustration of the change in the volume with temperature as the liquid is cooled, showing the difference in behaviour between glass and crystalline solids

3.2 Structural Theories of Glass

Apart from quartz (SiO_2) , GeO_2 and B_2O_3 glasses, almost all glasses are multi component and chemically very complex. Therefore the structures are very complicated. There are a number of structural theories of glass formation and the first ones were based on the structures of silicate crystals.

Goldschmidt in 1926 [10] proposed a theory based on his observations. He suggested that oxides of the general formula R_nO_m form glasses most easily when the ionic radius ratio of the cation to the oxygen ion lies in the range between 0.2 and 0.4. The radius ratios in this range tend to produce cations surrounded by four oxygen ions in the form of tetrahedra. In 1932 Goldschmidt's proposal was extended by Zachariasen [11]. He first found that Goldschmidt's theory was not satisfactory and tried to put forward a new approach which is as follows. He observed that mechanical properties

of glass and the corresponding crystal are similar, so that the rules applied to the crystal structure also apply to the corresponding glasses. According to his model, glasses have three dimensional networks or arrays, without symmetry or periodicity, in which no unit of the structure is repeated in regular intervals, i.e.; the structure must be distorted. The distortions can be obtained by variations in bond angles, bond lengths and rotation of structural units around their axes. He suggested that the energy contents of glass and crystal should be similar and therefore the coordination number of the cation of the glass-forming oxide must be close to that observed in the crystal. In other words, the local structural units in the glass and in the crystal are practically identical. Then he considered conditions for constructing a random network as shown in figure 3.2. Zachariasen thus proposed some empirical laws for glass formation, which were confirmed later by x-ray diffraction studies by Warren [12-14]. These rules are known as the '*random network model*' and it is the most widely used model for glass structures. The rules are as follows;

1. An oxygen atom is linked to at most two cations.

2. The coordination number of the cation must be small (≤ 4).

3. The oxygen polyhedra, formed by oxygen atoms around the cation, must share corners only and not edges or faces.

4. The polyhedra link up to form a continuous three dimensional network.

The implications of these rules are illustrated in figure 3.2 which shows two dimensional [SiO_4] tetrahedron linkage in crystalline and amorphous SiO_2. The fourth oxygen situated either above or below the plane of the drawing. The random network model has its limitations since it was developed for glasses quenched from metastable

melts at relatively slow cooling rates [15] and containing not less than 50 mol% glass formers [16]. Mackenzie [17] showed that the rules for the random network model are applicable to all types of non-crystalline oxides prepared by routes other than melt cooling. It should be noted that the random network theory is largely applicable to oxide glasses only.

In addition to the random network theory there are a number of other theories which attempt to explain the glass structure: Smekal [18] suggested another theory of glass formation, based on the nature of the bonds in the material. He proposed that only melts which contain bonds half ionic and half covalent can form a glass. Stanworth [19] further developed the mixed bond concept by using Pauling's partial ionic character model. Lebedev's crystallite theory [20] suggested that the structure of glasses can be regarded as an accumulation of microcrystalline entities, with these crystallite regions connected by amorphous regions. In the end, Lebedev [21] himself modified his original interpretation of the crystallite theory by deemphasizing the term 'crystallite'. In his opinion, disordered as well as ordered regions in the form of defined chemical compounds are present in a glass. However in general there is almost no evidence to support the existence of crystalline behaviour in most of the glasses.

Despite all efforts it is not easy to suggest a complete theory which has ability to describe all glass structures at once, since a wide range of elements and bonding types are involved in amorphous materials. Such a complete model should be able to explain all data available. Shelby [4] suggests that any structural model which can only explain some of the existing data and ignores the rest, is not complete, and for a complete structural model for glasses some factors of the structure must be explained

by the model. These factors are as follows.

1. Coordination number of cations.

2. Bond angle distribution and rotations

3. Connectivity of network units

4. Dimensionality of the network

5. Intermediate range order

6. Morphology

7. Field strength, bond strength, site specific bonding

8. Nature of free volume

9. Impurities, defects.

The starting point for any model for glass structure is to identify the coordination number of network forming cations. The network structure consists of buildings blocks which are the most basic element of any model for the structure of glasses and gives the coordination number of cations which occupy sites in the network. These blocks are well defined and have order at a level of several atoms or ions which extends over a very short distance so that it is called '*short range order*'. As stated earlier, a glass does not have long range order and its structure has a random character which is introduced by bond angle distribution and rotations so that the building blocks are remain connected. Another step in a model for glass structure is connectivity which can be considered as the number and arrangement of '*bridging (BO) and nonbridging bonds (NBO)*' which connect every building block.

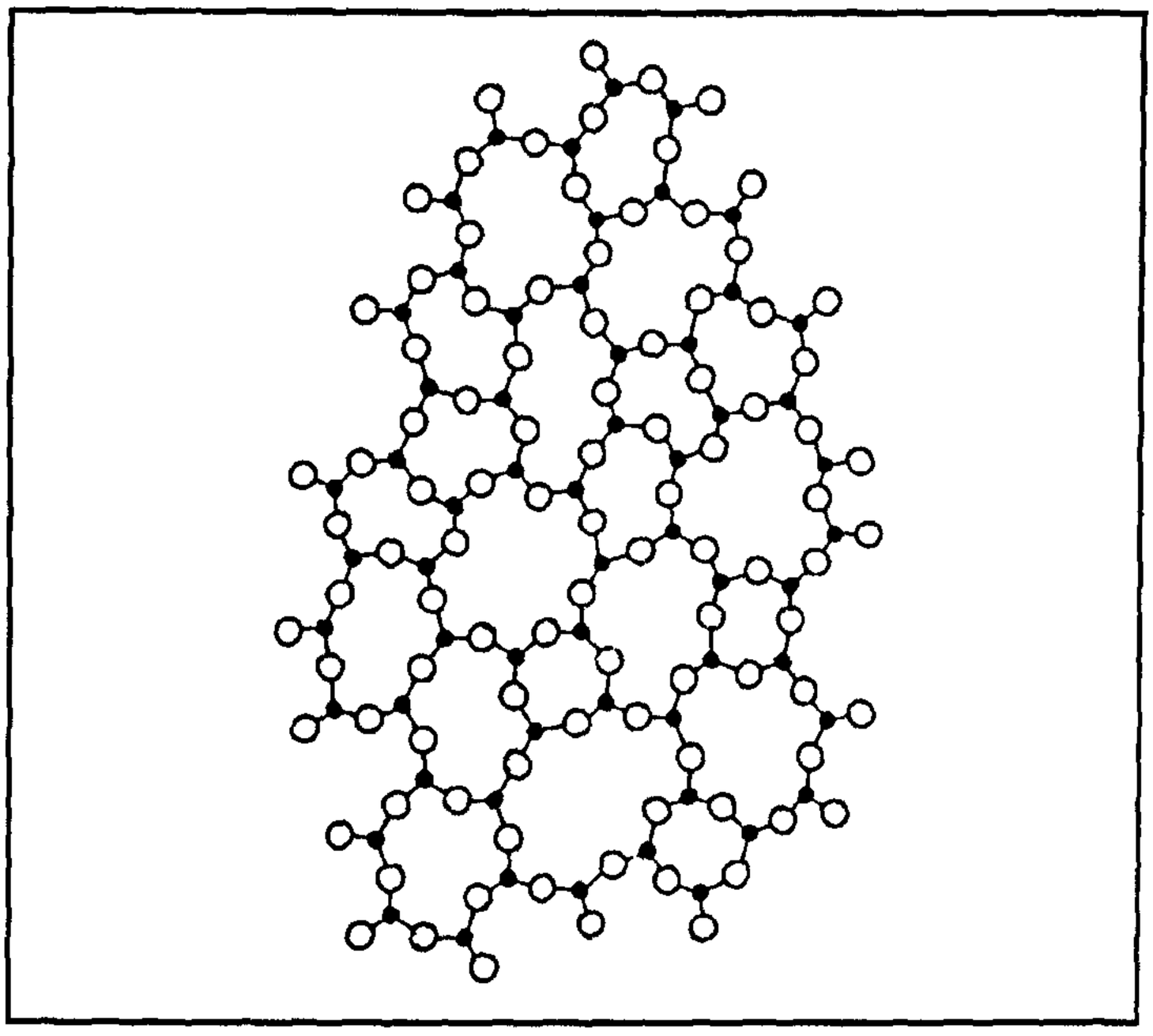

(a)

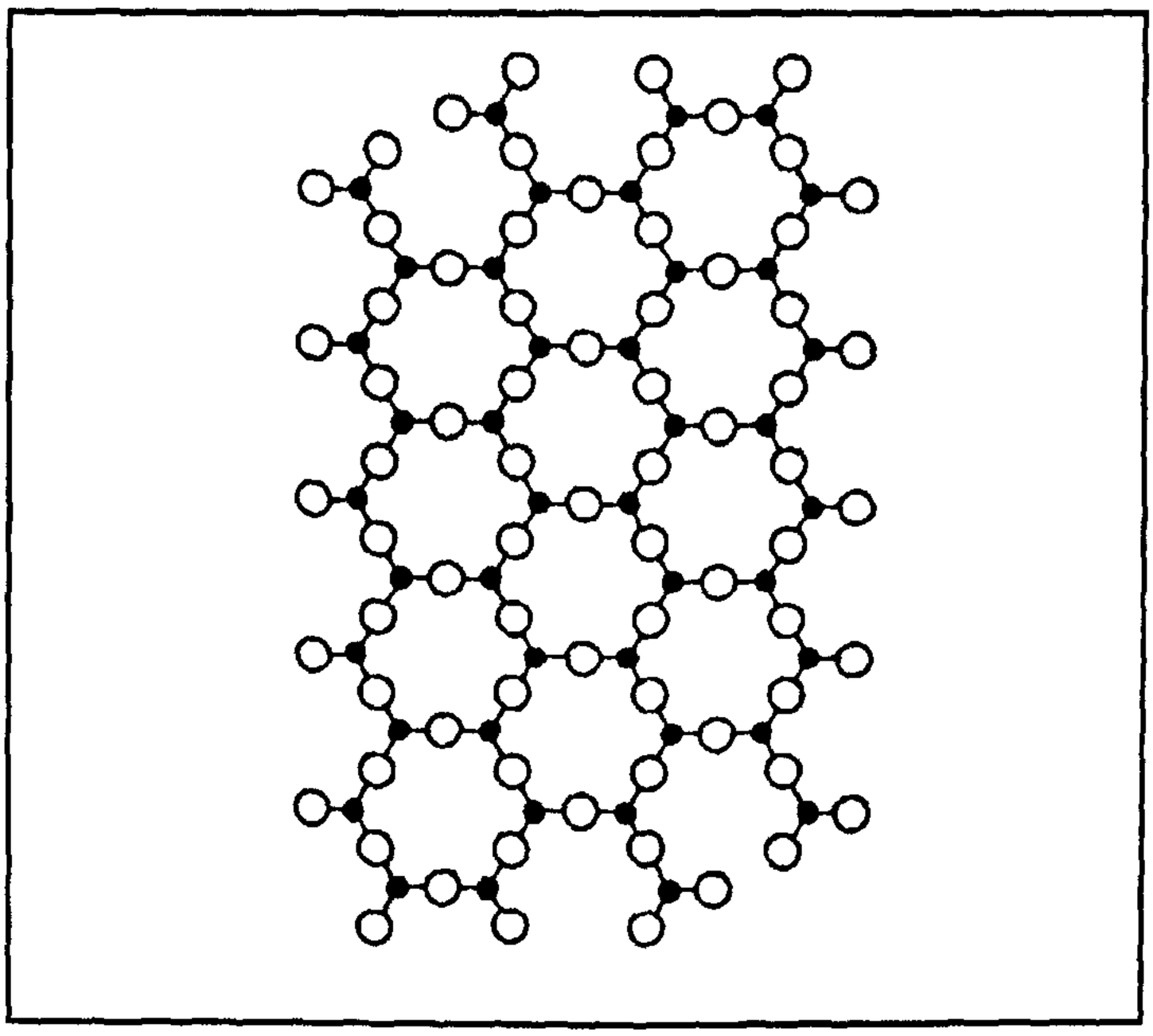

(b)

Figure 3.2 Schematic representation of [SiO_4] linkages in (a) glassy or amorphous state, (b) crystalline state [21].

3.2.1 Oxide Glasses

Almost every model for oxide glasses starts with vitreous silica and alkali silicate glasses. In order to describe the concentration of bridging oxygens per tetrahedron in these glasses the Q^n notation is used, where n (n is between 0 and 4) represents the number of bridging oxygens. A tetrahedron fully linked into the network by four bridging oxygen atoms is described as a Q^4 unit, while a tetrahedron with no bridging oxygens is described as Q^0 as shown in figure 3.3.

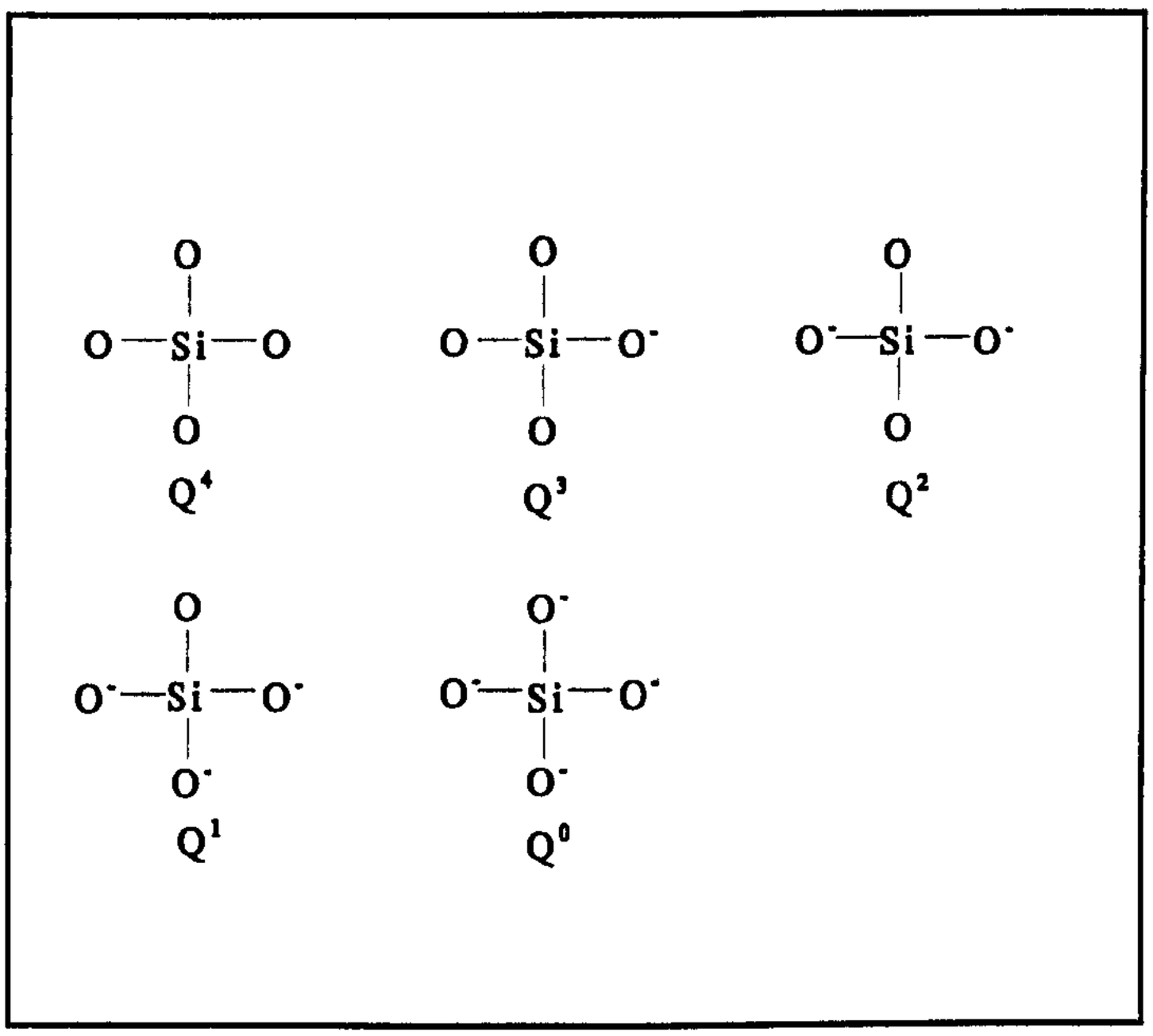

Figure 3.3 Schematic representation of the different Q^n species. O^- is non-bridging oxygen atom.

The distribution of different bond types i.e., the quantities of different Q^n species in a glass determines its structural properties. The distribution can be divided into three [22]

a) *binary distribution(constrained random)*:NBO repel each other leading to maximum dilution which in turn gives successive formation of lower Q^n types, and a homogenous distribution of no more than 2Q types result.

b) *statistical distribution:* the distribution of NBO is determined only by composition and statistics and this model has no limit on the number of Q^n species present for any composition.

c) *cluster*: NBO cluster, eventually leading to phase separation.

According to Stanworth [19] oxides, which are the most important glass formers, can be classified into three groups on the basis of electronegativity of the cation:

(1) *network formers* in which cations form bonds with oxygen with fractional ionic character. These are good glass producers e.g. SiO_2, GeO_2, P_2O_5, B_2O_3 and they can form glasses directly on cooling to form a continuous, rigid 3-dimensional structure, with a cation coordination number of generally 3 or 4

(2) *modifiers*: this class of oxides only modifies the network structure created by network forming oxides. Cations in the oxides have very low electronegativities, and therefore form highly ionic bonds to the oxygen e.g. alkali Li_2O, Na_2O, or alkaline earth oxides CaO, MgO. If they are introduced into a glass they break up the network and modify the structure. Figure 3.4 shows the structure of sodium silicate glass and the effect of the addition of Na_2O into the glass as a network modifying ion which causes some structural changes. Extra oxygen atoms, introduced into the glass by Na_2O, increase the O/Si ratio and as a result some of the oxygen atoms do not bond to two silicon atoms. Bonds are broken and two types of oxygen '*bridging and non-bridging oxygens*' exist in the glass network. Bridging oxygen atom (BO) is covalently bonded to two silicon atoms, and gives a Si-O-Si unit, while non-bridging oxygen (NBO) atom, covalently bonded to one silicon and ionically bonded to one sodium atom, gives a $Si\text{-}O^-\text{-}Na^+$ unit. The overall effect of introducing Na_2O molecules into the silica network is a weakening of the glass structure. The schematic diagram shown in figure 3.4 indicates

that the introduction of one molecule of Na_2O produces two nonbridging oxygen atoms. Other modifying oxides (Li_2O, K_2O etc.), play the same role as Na_2O when introduced into a glass structure.

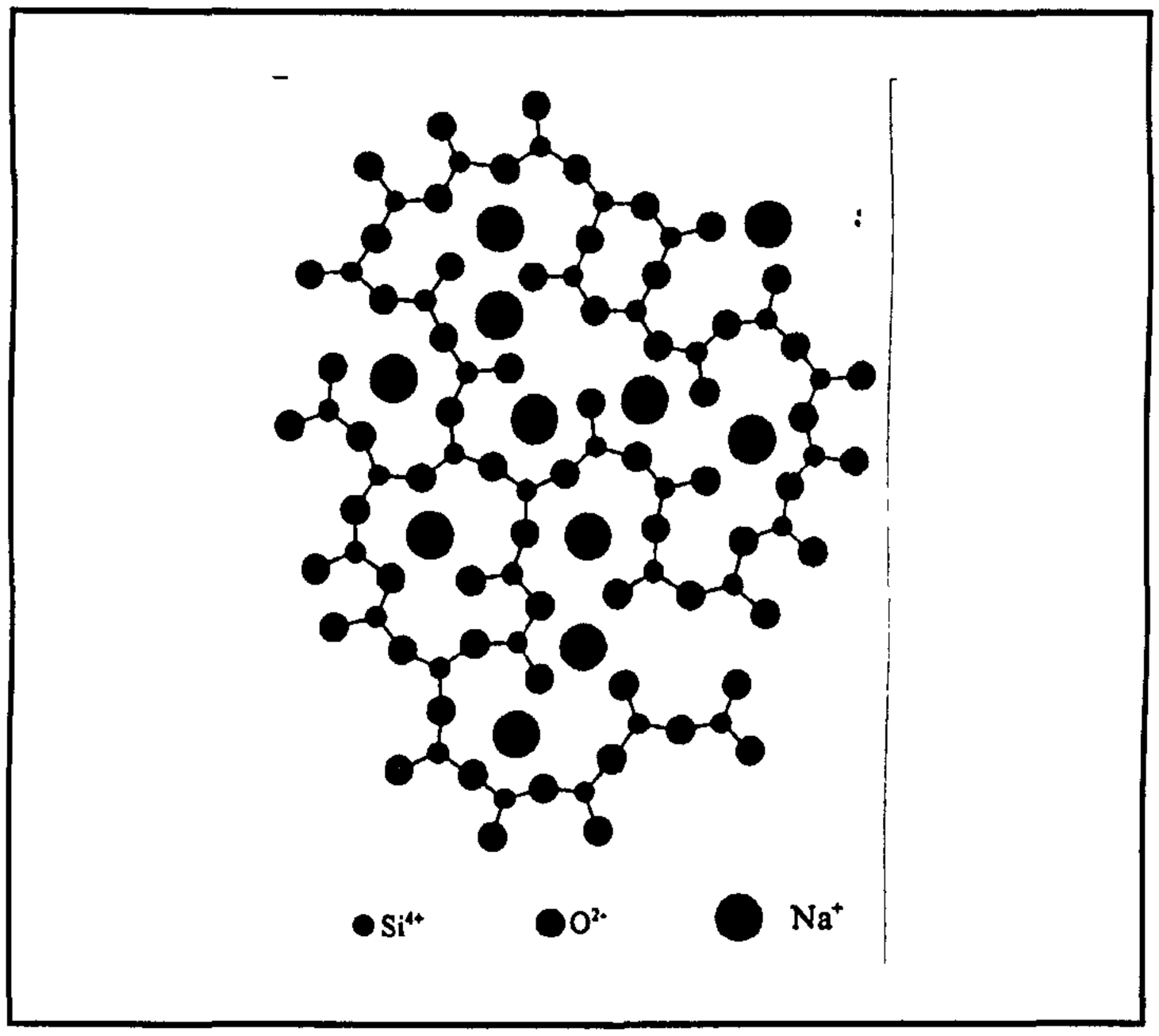

Figure 3.4 A two dimensional arrangement of atoms (or ions) in a sodium silicate glass [21]. When Na_2O is introduced into the glass structure, the large sodium ions are located in the larger cavities.

(3) *intermediates*: in these oxides the cation is slightly more ionic (lower electronegativity) and they cannot form glasses by themselves. They are capable of replacing cations in the network e.g Al_2O_3, TiO_2. They either reinforce the network (coordination number 4) or loosen the network (coordination number 6-8). The effect of an intermediate oxide such as Al_2O_3 is illustrated in figure 3.5. It strengthens the network by removing the non-bridging oxygens, which are introduced into the glass with the modifying ion. Aluminum ions, in crystals, can be found four or six coordinated with oxygen giving rise to $(AlO_4)^-$ or octahedral $(AlO_6)^{3-}$ groups. The

tetrahedral group can replace the (SiO_4) tetrahedra and gives the arrangement in figure 3.5. Repolymerization occurs through the Si-O-Al linkages resulting in a glass of greater stability. Other intermediate oxides like BeO and PbO also play a role similar to that of Al_2O_3 in silicate glasses.

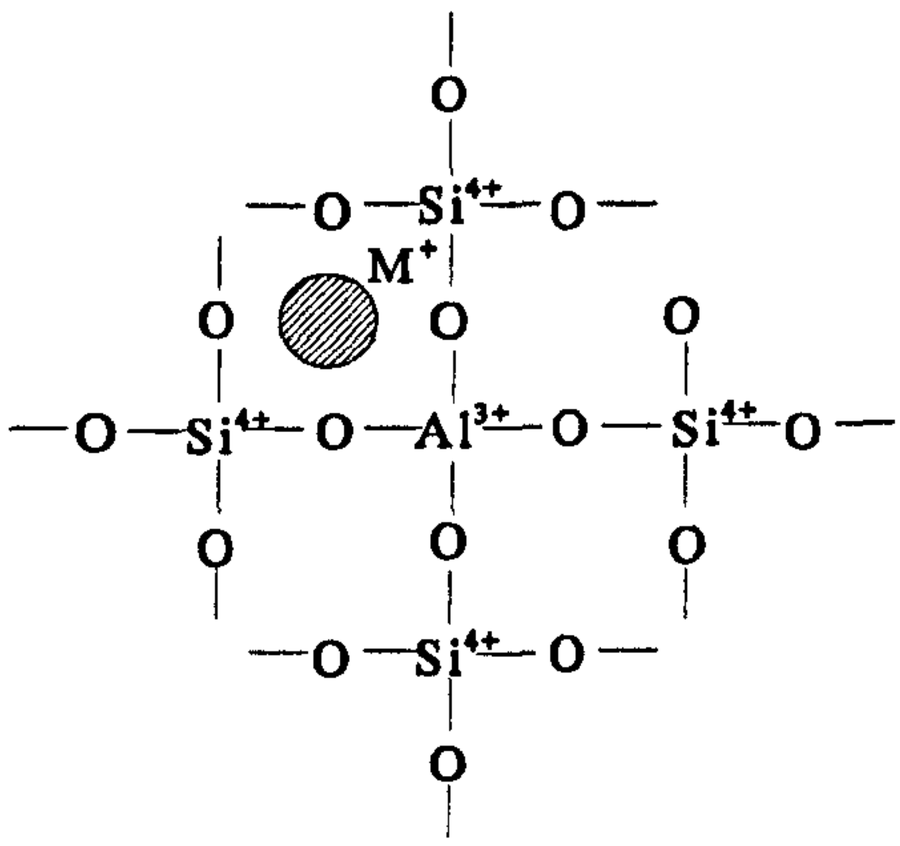

Figure 3.5 Schematic representation of the introduction of an intermediate oxide (Al_2O_3) in a silicate network. For charge neutrality, the sodium ion is located near the $[AlO_4]^-$ tetrahedron.

In the binary model, the number of Q^n species is limited to two in a single composition Q^n and Q^{n-1}. The value of n depends upon the composition. Thus for a fully polymerized glass such as SiO_2 only Q^4 units are present. In the statistical model, the distribution of nonbridging oxygens per silicon is determined from probability and composition.

3.3 Application of NMR to Glass Structure

Although Nuclear Magnetic Resonance Spectroscopy (NMR) has become the most widely used tool for the characterization of organic molecules in liquid solution,

its application to the crystalline and then to glassy materials began after the development of high-field superconducting magnets, pulsed Fourier transform methods and application of the magic angle spinning (MAS) technique [23]. Since then, NMR has made great contributions towards developing the understanding of glass structure and properties.

In general, structural information which has been successfully explored by NMR includes; (i) quantification of short-range order and intermediate range order (coordination number, distribution of BO and NBO, etc.), (ii) distribution functions for topological parameters (bonding and bond angle distribution). Most of the early NMR studies on glasses were primarily concerned with determination of nearest neighbour environments by using magic angle spinning (MAS) NMR lineshapes. Dupree and Holland [22] gave a review of the structural determination for several glass systems and ceramics by MAS NMR. Structural studies on minerals and glasses using NMR have also been reviewed by Stebbins [24] and Kirkpatrick [25]. A more comprehensive review of MAS NMR of glasses has been given by Eckert [26].

3.3.1 O-17 NMR

As Farnan et. al. [30] states that "since oxygen is the most abundant element and is a constituent of silicate crystals and most amorphous materials and many other inorganic compounds, the possibilities of carrying out oxygen NMR in the solid state have particular attractions. However most of the studies on the silicate glasses are concentrated on the cation and its coordination. Oxygen is the connecting atom between locally ordered SiO_4 tetrahedra as well as between silicon and network modifying cations which are also thought to have locally ordered environments. Therefore the

intermediate range disorder in these glasses will be reflected by these oxygen atoms which makes oxygen NMR a direct and sensitive way to characterize these interconnections". However the ^{17}O NMR studies are hindered by experimental limitations. Since it is a quadrupolar nucleus (I>1/2), it has a quadrupole moment which interacts with the electric field gradient at the nucleus. This in turn causes line broadening in ^{17}O NMR spectrum which limits the resolution. Line broadenings caused by a distribution of oxygen environments contains information on disorder in the glass but this information is masked by the anisotropic quadrupolar interaction, which is only partially removed by magic angle spinning (MAS). Recently developed two-dimensional NMR techniques, such as multiple quantum magic angle NMR (MQMAS NMR) [27], and dynamic angle spinning [28-30] can provide high resolution ^{17}O NMR spectra, since these techniques are capable of removing the quadrupolar interaction as discussed earlier in chapter 2.

3.4 Materials Studied

3.4.1 Aluminosilicates

The atomic arrangements of aluminosilicates have been studied extensively because they are found in important rock-forming minerals, which form from rapidly cooling magmas [31] and also many man-made glasses have aluminosilicate compositions. This property makes them important for geology and earth science. Aluminosilicates have also some industrial importance since some of them, such as zeolites, are used as catalysts and absorbers. The role of aluminium is generally accepted as intermediate in most of the aluminosilicates. In these glasses aluminium occurs in the aluminium-oxygen tetrahedra which substitute directly into the network for silicon-oxygen tetrahedra and form bridging oxygens. However in order to maintain

local charge neutrality an appropriate cation must be present in the vicinity of aluminium-oxygen tetrahedron, which has four bridging oxygen atoms and therefore excess negative charge of -1. As a result of this it is possible to visualize the aluminium-oxygen tetrahedron as a large anion with an effective charge of -1 distributed over the entire anion. The presence of an aluminium-oxygen tetrahedron $(AlO_4)^-$ will modify the local structure in many ways [31],

a) it replaces the Si-O non-bridging oxygens by Si-O-Al

b) electronic charge is transferred from non-bridging oxygens to the $(AlO_4)^-$ groups resulting in preferential location of modifier cations near these groups.

c) and it increases the number of possible Si environments as well as oxygens by substituting Si by Al.

The conventional view of glass structure suggests the following argument: for a fully linked tetrahedron 2 oxygen atoms are needed for each tetrahedron. However aluminium oxide only provides 1.5 oxygen for each aluminium-oxygen tetrahedron so that the extra oxygen atoms needed are provided by the alkali or alkaline earth oxides. The oxygen atoms provided by the alkali or alkaline earth oxides are used in formation of aluminium-oxygen tetrahedra. Thus there are no oxygen atoms available for the formation of NBO's. Each added aluminium removes one NBO from the structure as shown in figure 3.1. When the total concentration of modifier oxides is equal to that of alumina, the structure should be a fully polymerized network of Q^4 units, with no NBO present [31-35]. However this simple model for alkali/alkaline earth aluminosilicate is not applicable to those glasses containing more alumina than total modifier oxide [4]. In such glasses, peraluminous glasses, the structural role of aluminium with insufficient metal cations for electrical charge balance of Al^{3+} in tetrahedral coordination is not as

clear as both structural data and data on physical properties of peraluminous melts are conflicting. The two most common models proposed for the structure of such glasses are,

a) Excess aluminium ions occur in octahedral coordination, with three BO and three NBO in each octahedron [34-36].

b) Lacey [37] from geometrical and energetic considerations suggested that in aluminosilicate glasses and melts with insufficient alkali or alkaline earths for electrical charge balance, the aluminium remains in tetrahedral coordination in a tricluster geometry in which three coordinated oxygen connects the corners of three tetrahedra of aluminium-oxygen and silicon- oxygen. If the tricluster contains one aluminium-oxygen and two silicon-oxygen tetrahedra, the overall unit will be charge balanced whereas if it contains two aluminium-oxygen and one silicon-oxygen tetrahedra the unit will need an associated modifier cation to compensate the -1 charge of the cluster.

Although there are some problems and uncertainties in the structure of peraluminous aluminosilicate, the structure of peralkaline aluminosilicates, where alumina to modifier oxide concentration is less than one, is better understood. Engelhardt [38] and Kirkpatrick [39] concluded form the ^{29}Si and ^{27}Al NMR data that in a depolymerized peralkaline aluminosilicate glass, aluminium sits in a fully polymerized structural unit, i.e.,Q^4 unit. This information is also consistent with Raman spectra of K-aluminosilicate and Na-Ca-aluminosilicate glasses [40-42]. Brown [43] also suggested earlier that the aluminium in aluminosilicate crystals tends to associate with a tetrahedral site nearest the smallest intertetrahedral angle. The unit with the smallest intertetrahedral angle is the fully polymerized, three dimensional network unit (Q^4).

In aluminosilicate glasses distribution of aluminium-oxygen tetrahedra is in a manner that the aluminium-oxygen tetrahedron tends to connect to four silicon-oxygen tetrahedra, i.e., aluminium-oxygen tetrahedra avoid direct links to other such tetrahedra. This arrangement is called aluminium avoidance or Loweinstein's rule [43].

3.4.2 Tin-Silicates

Although tin is not a common constituent of glasses it is found at high concentrations in the surface of float glasses and it is thought to be the cause of the surface deformation of these glasses with heat treatment [44]. Although compositional modification does not extend far into the surface, the physical and chemical behaviour differ from the upper surface. Float glass has many components in its structure and tin is more stable in the tetravalent state and, by analogy with Si and Ge, tin is expected to be act as an intermediate in tin-silicate glasses. The divalent state is readily oxidized to the tetravalent and by analogy with Pb, the structural behaviour is more complex, such as modifier at low tin concentration and intermediate at high concentrations. These are very complex structures and interpretation of them is very difficult. Thus understanding of the structural role of tin in the silicate glasses and its effect on the properties is quite important.

Due to the difficulty of making $SnO\text{-}SiO_2$ glasses they have not attracted as much attention as the $PbO\text{-}SiO_2$ system. This difficulty arises from disproportionation of SnO. Therefore most of the early studies on the $SnO\text{-}SiO_2$ system were concentrated on the preparation of glass. Keysselitz et.al. [45] first reported that it was possible to make these glasses by heating compressed pellets of mixtures of stannous oxalate and silica. Carbó Nóver et.al. studied the crystallization and decomposition of $SnO\text{-}SiO_2$

glasses and concluded that glasses containing more than 62 wt% (42 mol%) crystallize at temperatures higher than 600°C to produce a new metastable stannous metasilicate ($SnSiO_3$) crystalline phase [46]. There is more in the literature on preparation of these glasses [47-49].

As mentioned above tin has two stable valencies, tetravalent and divalent states. Divalent tin in the form of SnO has been shown to fulfill various structural roles as either modifier or intermediate, depending on the type of glass system and composition. On the other hand tetravalent tin in the form of SnO_2 is only a minor component in any glass system due to its low solubility rate especially in alkali free glass. However the solubility of SnO_2 can be increased by adding alkali oxide into the glass melt although the amount that can be dissolved does not exceed the alkali content of the glass. It has been also shown that the SnO (Sn^{2+}) is the main species compared to the SnO_2 (Sn^{4+}) [50-51]. Therefore the divalent tin is a major component while tetravalent tin is minor in any glass system. This must be due to the fact that the two valence states of the tin play different structural roles in the structure of the glass, and these different roles must be as a result of the structural difference between SnO and SnO_2.

The SnO_2 with Sn^{4+} crystallizes with the rutile like structure which is a body centred tetragonal, and can be regarded as an ionic crystal [52]. Sn^{4+} ions are located at the corners and at the centre of the cell ,while oxygen ions are located at nonregular interstitial sites, causing distortion of the cell from cubic to tetragonal. Fig 3.6 shows the unit cell of rutile like SnO_2. In this structure tin is in an octahedron of oxygen ions and the electron density distribution close to the tin is approximately spherical [53]. Volf [54] has classified the oxides with bond strength bigger than 0.8 and the coordination number bigger than 4, as oxides that show poor solubility. Sn^{4+} with bond

strength of 1.01 and coordination number of 6, posses strong competition for silicon in polymerization. Therefore it forms a six coordinated oxygen polyhedron, with high bond strength and different geometry than the SiO_4 group so that it is more difficult to link to the polyconic network silicon of tetrahedra.

The SnO with Sn^{2+} has a complex tetragonal crystal structure, similar to PbO, and contains asymmetrical units. Figure 3.7 shows the crystal structure of SnO. In the crystal structure the valence forces extend more to one direction, and as a result of this the asymmetrical building units consist of a Sn atom located at the top of a square pyramid bonded with its four oxygen neighbours placed at the corners of the base of the pyramid. Figure 3.7a shows the bonding arrangement of tin atom to the four oxygen atoms where 5s electrons that do not take part in bonding are located just above the tetragonal pyramid and occupy a mixed ($s\text{-}p_z$) orbital [53]. Therefore these asymmetrical building block of $(SnO_4)^{6-}$ form a layered structure as shown in figure 3.7c. This is because four O^{2-} ions easily repel the polarisable shell of Sn^{2+}, especially its two outermost (inert $5s^2$) electrons. The SnO structure and its structural role in glass is complex.

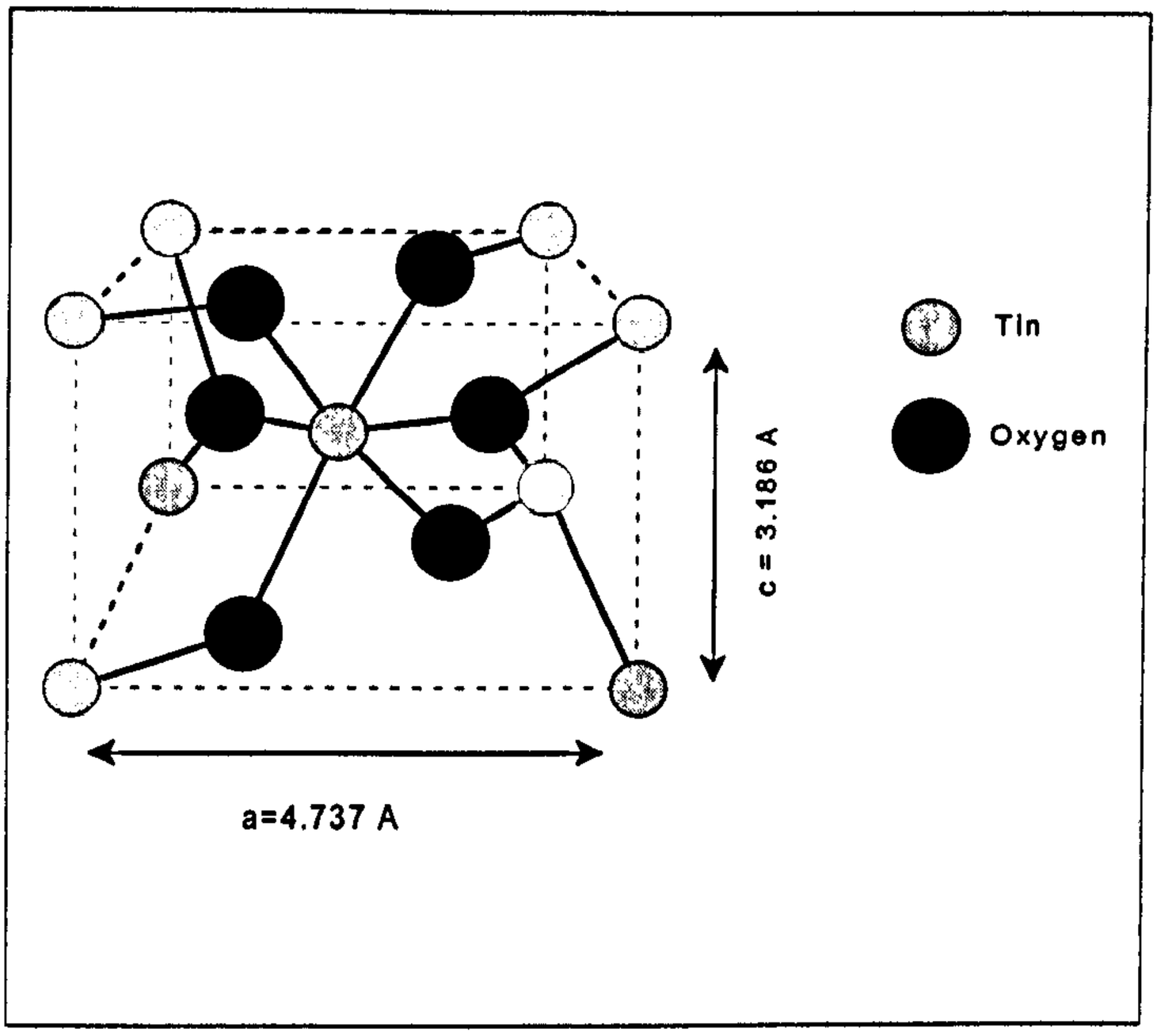

Figure 3.6. Unit cell of rutile like structure of SnO_2 [53].

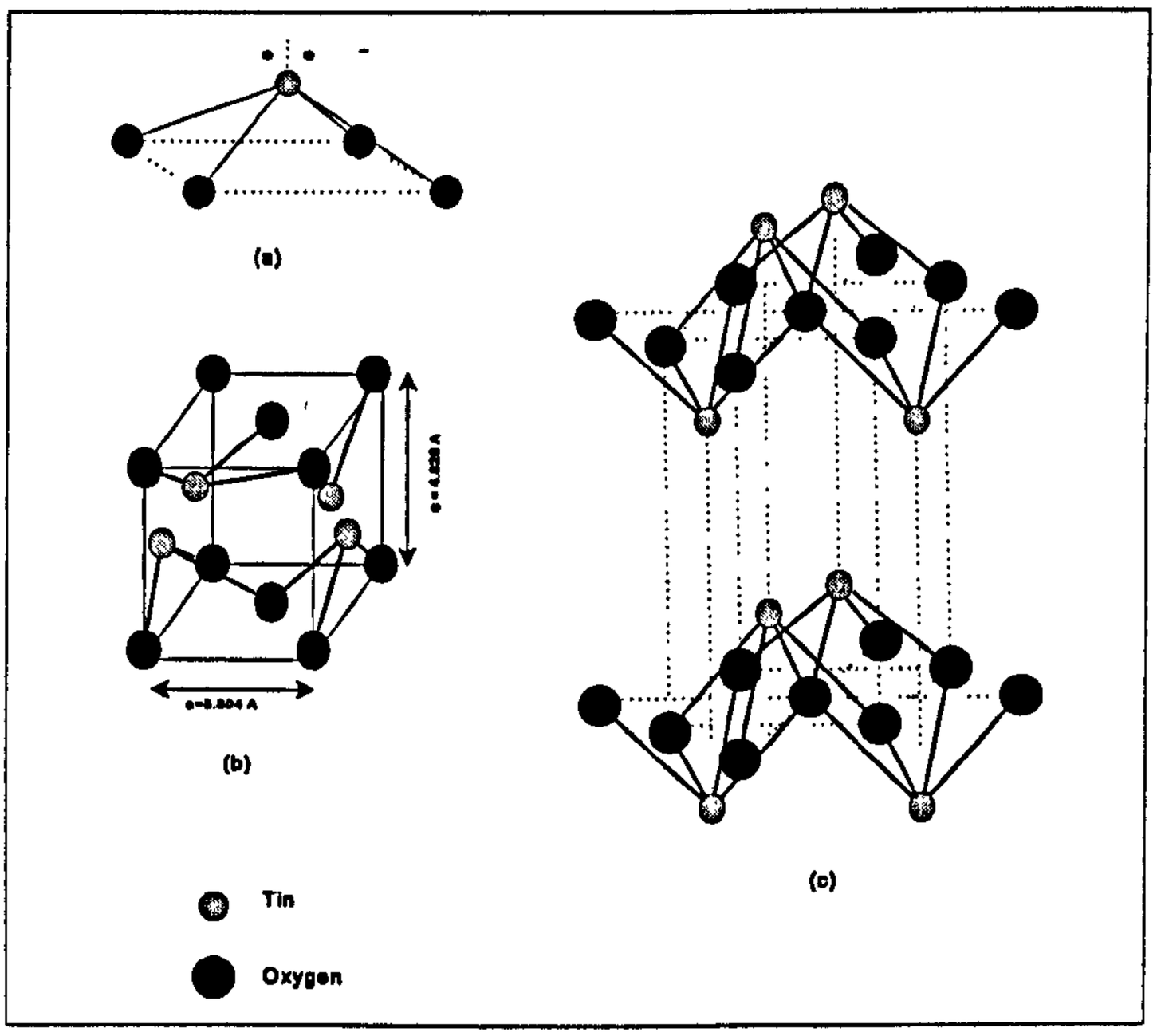

Figure 3.7 The crystal structure of SnO (a) the arrangements of bonds from a tin atom to a oxygen atoms. Two dots represents the inert pair of electrons, (b) unit cell of SnO, the tetragonal layered structure [56-57]

References

[1] G.O. Jones, "Glass", Chapman & Hall , 1971.

[2] P.W. McMillan, in "Glass-ceramics", Academic Press, London, 1979.

[3] M.B. Volf, "Chemical Approach to Glass, Glass Science and Technology 7", Elsevier, Amsterdam, 1984.

[4] J.E. Shelby, Introduction to Glass Science and Technology, The Royal Society of Chemistry, 1997.

[5] S.R. Elliot, Physics of Amorphous Materials, Longman, London, 1983.

[6] R. Zallen, The Physics of Amorphous Solids, John Wiley, New York, 1986.

[7] J. Wong and C.A. Angell, "Glass structure by spectroscopy", Marcell Dekker, Inc. New York, 1976.

[8] A. Paul, "Chemistry of Glasses", Chapman & Hall, 1982.

[9] H. Rawson, "Properties and Application of Glass", Elsevier, Amsterdam, 1980.

[10 V.M. Goldschmidt, Skrifter Norske Videnskaps Akad (Oslo) Math-Naturwiss K1 8(1926)7.

[11] W.H. Zachariasen, J. Am. Ceram. Soc. 54 (1932) 3841.

[12] B.E. Warren, Phys. Rev. 45 (1934) 657.

[13] B.E. Warren, J. Am. Ceram. Soc. 17 (1934) 249.

[14] B.E. Warren, J. Appl. Phys. 8 (1937) 645.

[15] A.C. Wright, J. Non-Cryst. Solids, 123,(1990), 129

[16] J.D. Mackenzie,'Modern Aspects of the Vitreous State' Butterworths, London, 1960.

[17] J.D. Mackenzie, J. Non-Cryst. Solids, 95-96, (1987) 441.

[18] Smekal, J. Soc. Glass Technol.,35 (1951) 411.

[19] Stanworth, 'Physical Properties of Glass', Oxford University Press, London, 1950.

[20] AA Lebedev, Trudy Cossud Opt. Inst. 2:57 (1921)

[21] W. Vogel, "Glass Chemistry", Springer-Verlag, 2nd edition, 1994.

[22] R. Dupree and D. Holland, in "Glasses and Glass-Ceramics", ed. M. H. Lewis, Chapman Hall, London, 1989.

[23] C.M. Schramm, B.V. De Jong, V.E. Parziali, J. Am. Chem. Soc., 106 (1984) 4396.

[24] L.F. Gladden, T.A. Carpenter and S.R. Elliott, Phil. Mag. B53 (1986) L81.

[25] A.R. Grimmer, M. Magi, M. Hahnert, H. Stade, A. Samoson, W. Weiker and E. Lippmaa, Phys. and Chem. of Glasses 25 (1984) 105.

[26] W.R. Taylor, Proc. Ind. Acad. Sci. 99 (1990) 99.

[23] E. Lippmaa,M. Magi, A.Samosen, G. Engelhardt, J. Am. Chem. Soc. 103 (1980)4992-4996.

[24] J.F. Stebbins, in Spectroscopic Methods in Minerology and Geology, ed. F.C. Hawthorne. (1988). Reviews in Minerology vol. 18, Mineral Soc. of America.

[25] R.J. Kirkpatrick, in Spectroscopic Methods in Minerology and Geology, ed. F.C. Hawthorne. (1988). Reviews in Minerology vol. 18, Mineral Soc. of America.

[26] H. Eckert, Prog. in NMR Spectroscopy 24 (1992) 159.

[27] L. Frydman, J.S. Horwood, Journal of American Chem. Soc., 117,(1995),5267.]

[28] A. Samason, E. Lipmaa, A. Pines, Mol. Phys., 65 (1988) 1013.

[29] A. Llor, J. Virlet, Chem. Phys. Lett., 152 (1988)248.

[30] I. Farnan, P.J. Grandinetti, J.H. Baltisberger, J.F. Stebbins, U. Werner, M. Eastmen,A. Pines, Nature, 358(1992)31.

[31] B.O. Mysen, Structure and properties of silicate melts, Elsvier, Amsterdam,1988.

[32] J.F. Stebbins, in Structure , Dynamics and Properties of Silicate Melts, eds J.F. Stebbins, P.F. McMillian& D.B. Dingwell, Minerological Soc. Of America, Washington

[33] A. Navrotsky, Physics and Chemistry of Earth Materials, Chembridge Univ. Press, 1994.

[34] A. Leonard, S. Suziki, J.J. Fripiat, C. De Kimpe, J. Phys. Chem. 68 (1964) 2608-2617.

[35] T. Hanada, N. Soga, J. Am. Ceram. Soc., 65 (1982) C84-C86.

[36] Morikawa, S.I. Miwa, M. Miyake, F. Marumo, T. Sata, J. Am. Ceram. Soc., 65(1982)78-81.

[37] E.D. Lacy, Acta Crystall., 18 (1963)141-150.

[38] G. Engelhardt, M. Nofz, K. Forkel, F.G. Wishmann, M. Magi, A. Samason, E. Lipmaa, Phys. Chem. Of Glasses, 26(1985)157-165.

[39] R.J. Kirkpatrick, R. Oestrike, C.A. Weiss, K.A. Smith, E. Oldfield, Am. Miner., 71(1986)705-711.

[40] F. Domine, B. Priou, Am. Miner., 71(1986)38-50.

[41] B.O. Mysen, D. Virgo, I. Kushiro, Am. Miner., 66(1981)678-701.

[42] B.O. Mysen, F.J. Ryerso, D. Virgo, Am. Miner., 66(1981)106-117.

[43] G.E. Brown, G.V. Gibbs, P.H. Ribbe, 54(1969)1044-1061.

[44] A. Pilkington, Proc. Roy. Soc. London A314(1969)1.

[45] B. Keysselitz, E.J. Kohlmeyer, Mettal Erz., 30(1933)172.

[46] J. Carbó Nóver & Williamson, J. Phys. Chem. Glasses, 8(4)(1967)164-168.

[47] H. Spandau, E.J. Kohlmeyer, Z. Anorg. Allg., 254(1947)65.

[48] J. Carbó Nóver, J. Williamson, Phys. Chem. Glasses, 8(4) (1967) 164.

[49] T. Ishikawa, S. Akagi, Phys. Chem. Glasses, 19(5) (1978) 108.

[50] N.I. Min'ko, B.F. Kislitsyn,S.A. Fabrikant, L.K. Konik, Steklo I Keramika, 4(1973)19.

[51] N.I. Min'ko, Izv. Akad. Nauk SSSR, Neorg. Matter, 9(10)(1973)1816.

[52] A.F. Wells, Structural Inorganic Chemistry, 1962, Clarendon Press, Oxford.

[53] C. Cossement, J. Darville, J-M. Gilles, J.B. Nagy, C. Fernandez, J.P. Amoureux, magnetic Resonance in Chemistry, 30(1992)263.

[54] M.B. Volf, Chemical Approach to Glass, Glass Science and Technology 7, 1984, Amsterdam.

Chapter-4

Experimental Methods and Techniques

4.1 Introduction to Pulsed Fourier Transform (FT) NMR

The development of FT NMR spectroscopy started with the introduction of the pulse technique in 1950 by Hahn [1]. Lowe and Norberg [2] showed that the response of the spin system to the RF pulse, a decaying signal with respect to time known as the free induction decay (FID), is the Fourier transform corresponding to the steady-state (continuous wave, CW). In other words, the information contained by the FID in the time domain is the same information contained by the CW in the frequency domain. This was demonstrated by sweeping the field and using a box-car integrator [3] and by computing the Fourier transform (FT) of the FID after a single pulse[4]. The FT pulse technique has become widely used for high resolution applications since it has advantages over the CW technique such as time efficiency especially for multi line spectra [4].

A schematic representation of a modern NMR spectrometer is shown in figure 4.1 [5][6]. In a modern NMR experiment a large static magnetic field is applied to the sample resulting in a net macroscopic nuclear magnetization. Larger magnetic fields improve both sensitivity and the resolution by increasing the chemical shift dispersion and also by reducing the second order quadrupolar broadening. The magnetic field over the sample should be homogenous and should not drift over the timescale of the experiment. Therefore superconducting cryomagnets are ideal magnets to use with an NMR system.

In a pulsed NMR experiment the manipulation of the magnetization is done by a sequence of RF-pulses applied at the Larmor frequency of the nucleus. Therefore the RF

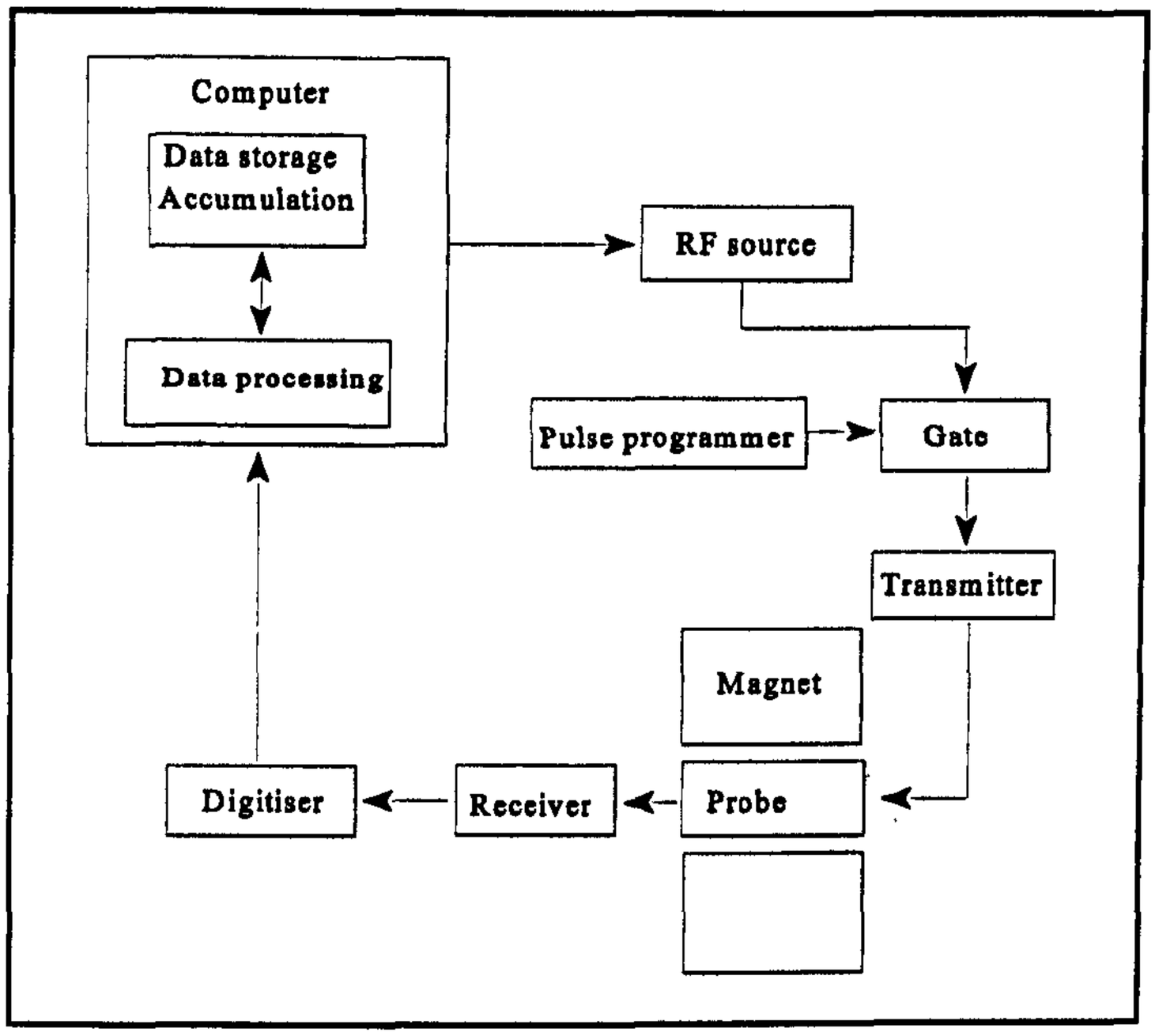

Figure 4.1 Schematic representation of a pulse FT-NMR spectrometer

source should be able to produce stable frequencies over a wide range, since the field strength is fixed. The RF-source is linked to the pulse programmer via a gate, to produce the required length of pulses. The pulse programmer should be flexible to allow the production of complex pulse programs. These pulses drive the RF transmitter which produces long rectangular pulses which are typically 0.5 to 40 μs in length with an amplification of up to 1 kW. The transmitter applies the RF-pulses into the probe where the sample is held, inside the magnet. The probe has a tunable electrical circuit, shown in figure 4.2, with a coil (NMR coil) which is capable of standing the transmitter pulse (~kV) and converts the processing nuclear magnetization into a voltage of ~μV for detection by the receiver. The probe is tuned to the resonance frequency of the nuclei of interest by adjusting the variable capacitor and is matched to the transmitter and receiver by adjusting the variable inductance. The NMR coil produces the oscillating magnetic field (B_1) which

is dependent on the quality factor ($Q=2\pi L/R$) of the coil, (i.e. the design of the tunable circuit) and the power supplied by the transmitter. Large values of Q produce large values of B_1 and therefore a more sensitive NMR coil.

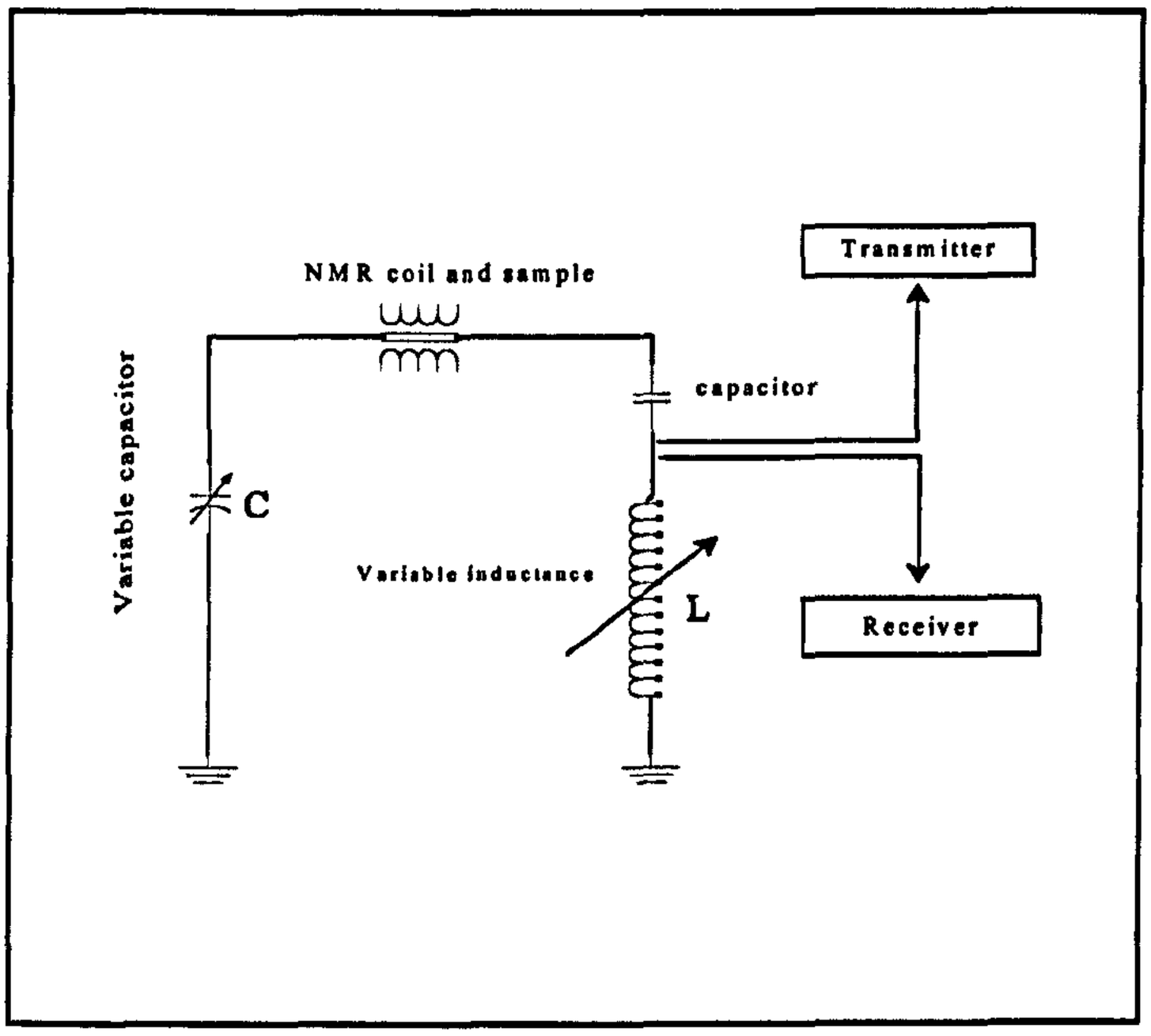

Figure 4.2 Tuning circuit of NMR probe

The B_1 alternating magnetic field, produced in the NMR coil in the presence of the large static magnetic field, is given by,

$$B_1 = B_1(I_x \cos\omega t + I_y \sin\omega t) \qquad (4.1)$$

where ω is the frequency of the B_1 field and is equal or close to the Larmor frequency of the nuclei of interest. The B_1 field tips the thermal equilibrium magnetization, M_z from the z axis by an angle θ which is given by

$$\theta = \gamma B_1 t_p \qquad 4.2$$

where γ is the gyromagnetic ratio of a nucleus and t_p is the pulse width. Figure 4.3 illustrates the behaviour of the magnetization vector M after the B_1 rf field is applied. The tip angle of interest ,θ, can be set by varying either γB_1 or t_p. One of the most common tip angles used in an NMR experiment is θ=90 (π/2) which tips the total magnetization into the x-y plane of rotating frame. In this position the signal has the maximum intensity as shown in figure 4.3. Another common tip angle in an NMR experiment is the θ=180 (π) which tips the total magnetization into the (-z) direction. The resulting transverse magnetization produced by the B_1 induces a small voltage in the coil which is amplified by the preamplifier before going into the receiver via a number of filters.

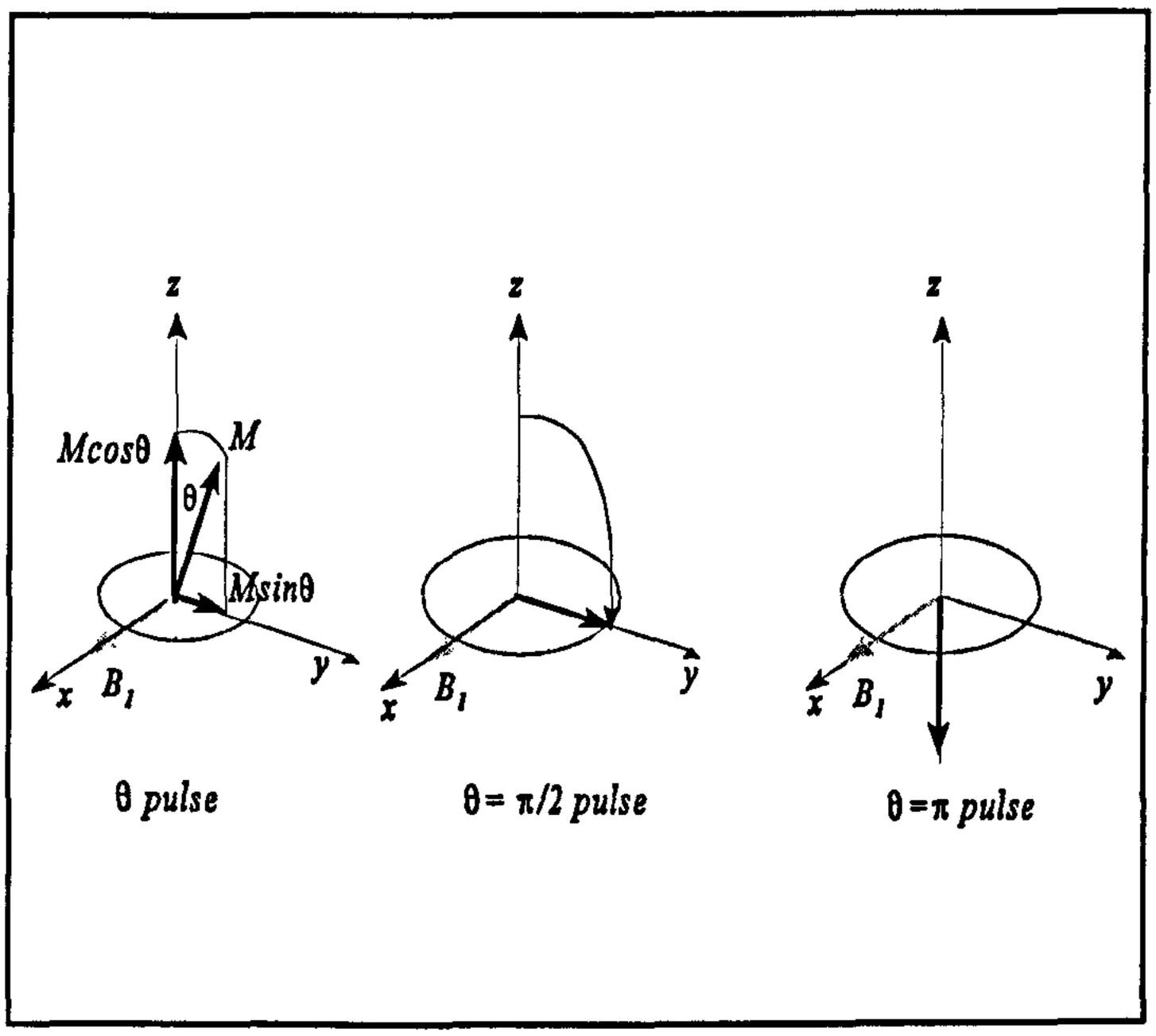

Figure 4.3 The position of the magnetization vector M after the B_1 rf field applied in the x-direction in the rotating coordinate system.

The receiver should recover quickly from any overload produced by the RF-pulse. The first part of the signal (FID) can be corrupted due to ringdown (decay of the RF-pulse) and mechanical oscillation of the probe induced by the RF-pulse [7]. The time immediately

after the pulse where the signal is corrupted by these effects is called the dead time of the probe. The amplified signal is detected by the phase sensitive detectors (PSD) which distinguishes the frequencies higher and lower than the irradiation frequency, by observing in phase and out of phase components of the signal. In general most of the spectrometers use two PSD's which in turn improves the signal-to-noise (S/N) by $2^{1/2}$ compared to usage of a single PSD [5]. The resulting signal is converted into digital form and stored for later manipulation by computer. The maximum observable spectral width is dependent on the digitisation rate.

The Fourier transform of a sine wave with a frequency of ν_0 in a rectangular envelope of duration t_p shows that the irradiation as a function of frequency is related to ν_0 and t_p by,

$$F \propto sinc[\pi(\nu - \nu_0)t_p] \qquad 4.3$$

Figure 4.4 shows the frequency and time domains of an RF pulse with a frequency of ν_0 and duration of t_p. In order to make sure that all lines or parts of lines are irradiated uniformly in the region of interest the spectral range of interest should be at the centre of this sinc-function. In practice as the length of the pulse determines the tip angle, short but intense RF-pulses are needed in solid state NMR.

4.2 The NMR Probes and Spinners

There are a variety of commercial and home made probes which cover a wide range of frequencies allowing multinuclear operation. These probes are static, single and double bearing single coil probes which are capable of performing high resolution NMR experiments in solids and liquids [8][9]. The single and double bearing (DB) probes can

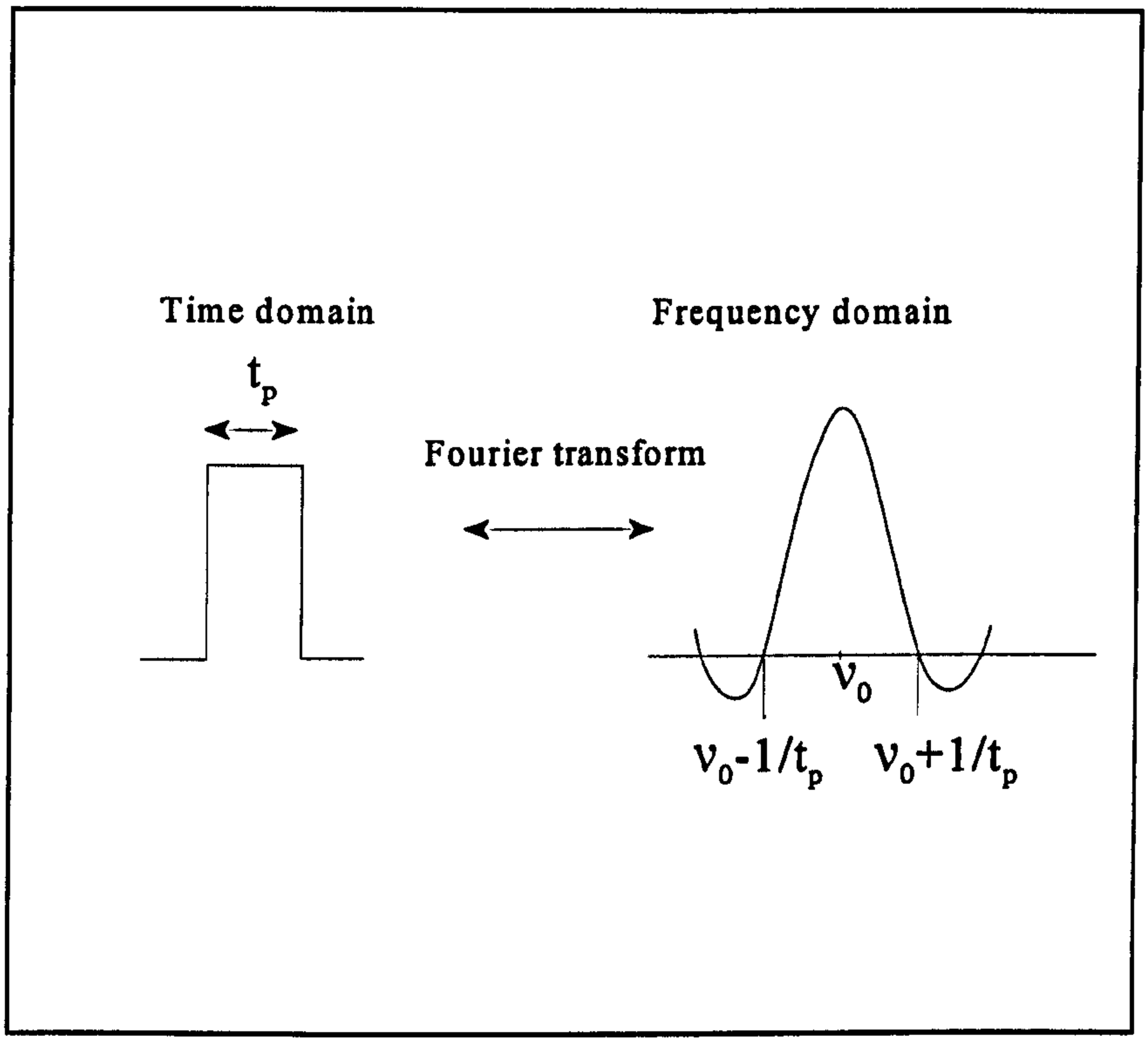

Figure 4.4 The relationship between time and frequency domains of an RF-pulse.

be used to perform static and sample spinning experiments and they are capable of decoupling and cross-polarization. 4mm high speed Bruker and Chemagnetics probes were used in this study. The Bruker double bearing probe uses 4mm spinners which are made of silicon nitride, alumina or zirconia. The Chemagnetics 4mm probe is a double resonance 200 to 600 MHz MAS probe which is capable of spinning at maximum 18 kHz in the temperature range of -150 to 250°C. This probe uses Chemagnetics zirconia pencil rotor and Kel-F, teflon or boron nitride caps and sample spacers. Figure 4.5 shows the Chemagnetics 4mm spinner.

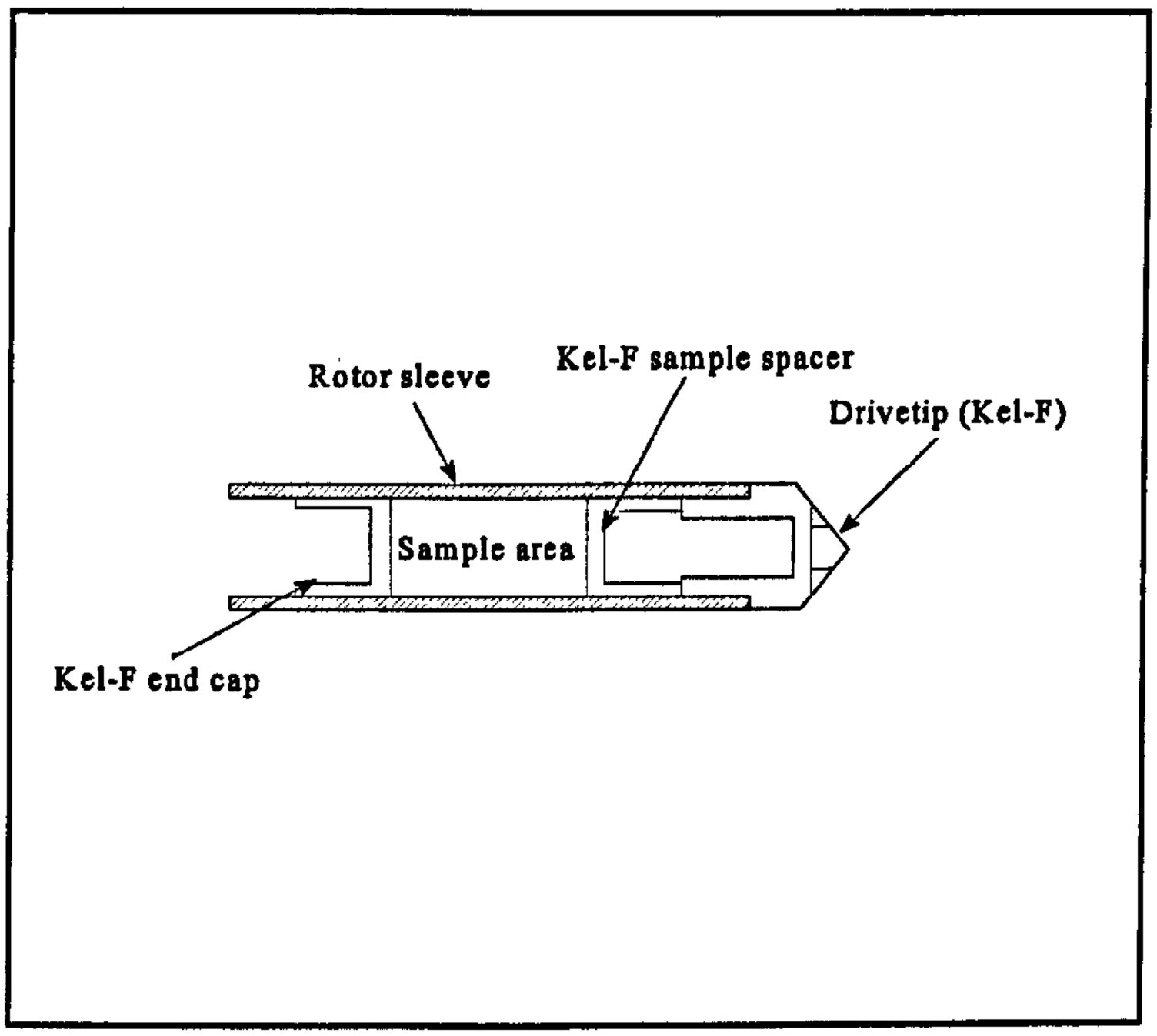

Figure 4.5 Schematic representation of Chemagnetics 4mm zirconia pencil rotor

4.3 Pulse programs

Two different pulse programs were used for the MAS experiments to obtain NMR spectra, one of which is a simple single pulse and spin-echo pulse sequence [10]. Figure 4.6 shows the single ($\pi/2$) pulse sequence and its effect on the macroscopic magnetization. The delay after the pulse and before acquisition is to protect the receiver. The net macroscopic magnetization along the z axis of the laboratory system is tipped by the B_1 field along the x axis of the rotating frame. After application of a $\pi/2$ pulse, the resulting transverse magnetization which produces the NMR signal begins to spread out and the net macroscopic magnetization returns to the equilibrium due to spin- lattice relaxation (transverse relaxation). The spin echo pulse sequence used is shown in figure 4.7 where the first pulse is a $\pi/2$ pulse and the second pulse is a π. Phase cycling was used with this

experiment to reduce the effect of ringdown and other artifacts such as base line errors [11]. The second pulse (π) in this experiment refocuses the individual nuclear spins, which are fanned out after the $\pi/2$ pulse as shown in figure 4.6, into the -y direction. The second pulse is applied after a certain delay period, τ, and the refocussing along the -y direction occurs after a further τ delay. The resulting transverse magnetization produces the NMR signal called the spin-echo. Figure 4.7 shows the spin-echo pulse sequence.

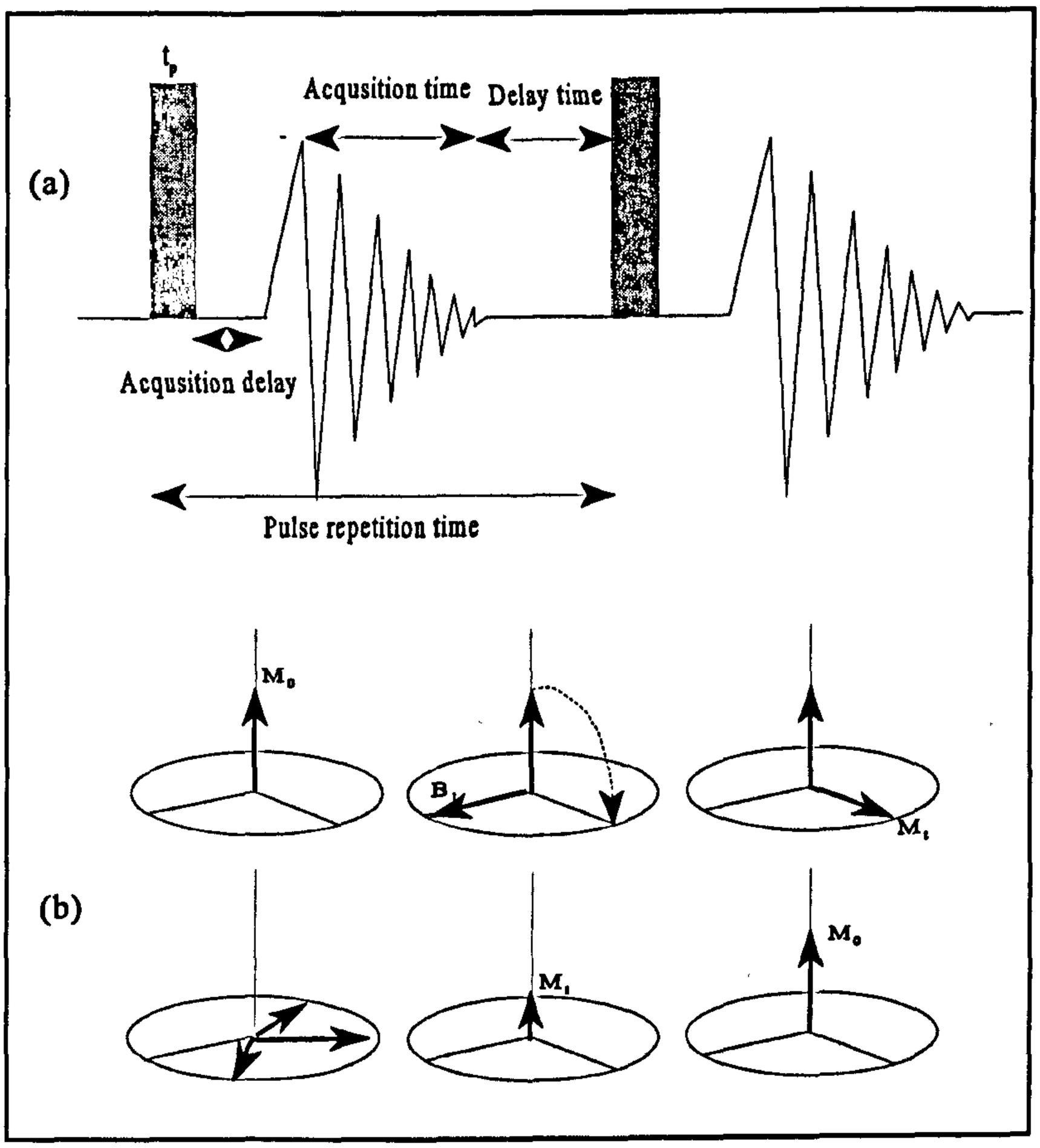

Figure 4.6 (a) Schematic representation of a single pulse sequence, (b) The effect of a single $\pi/2$ pule on the macroscopic magnetization.

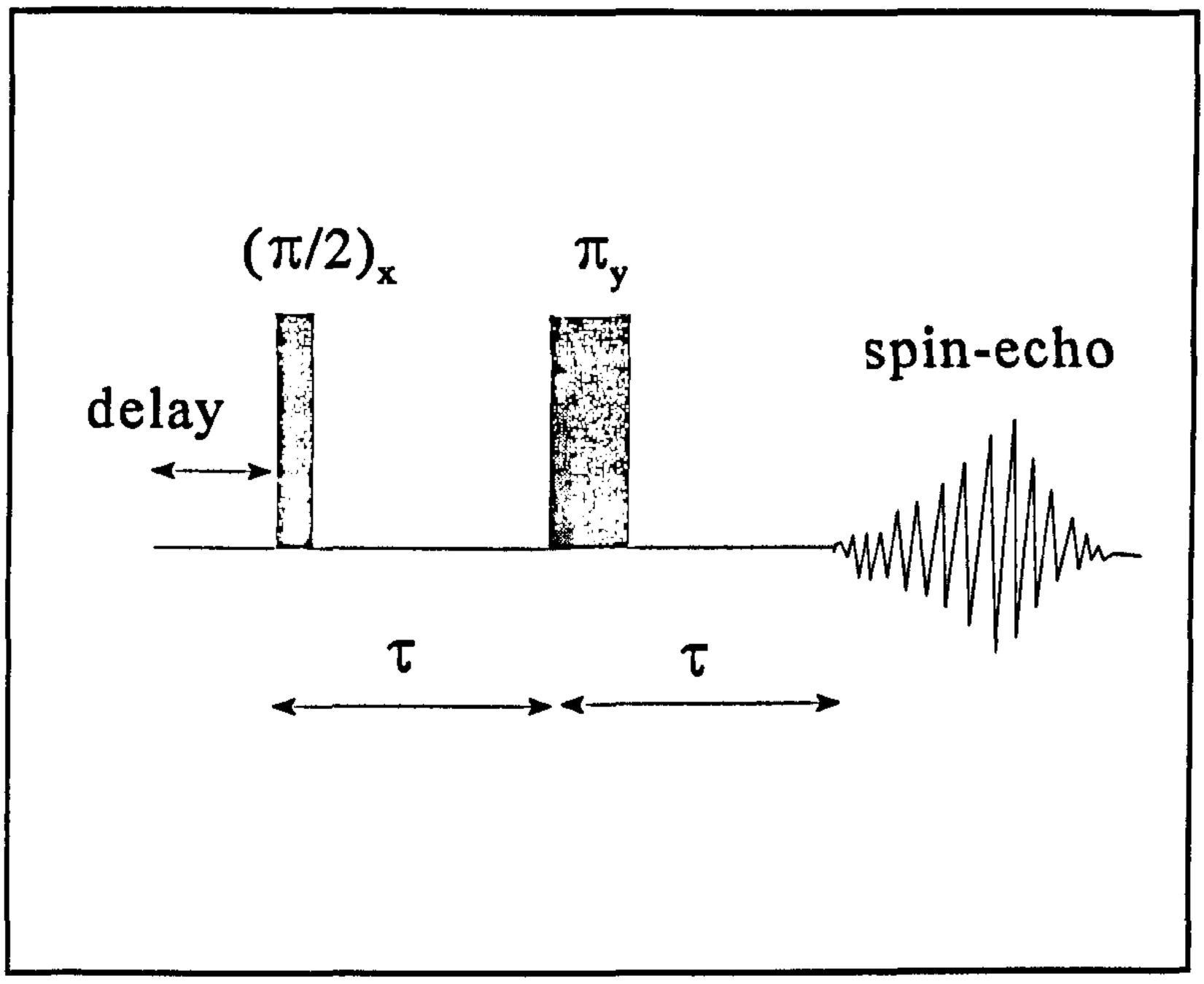

Figure 4.7 Spin-echo pulse sequence where τ is the delay time between pulses .

The MQ MAS experiments were performed by using a split-t1 pulse sequence [12]. Figure 4.8 shows the pulse sequence and the coherence transfer pathway for this experiment. The term coherence in its most basic form, is the route by which the signal reaches the receiver, and it is preferred since the signals are quantum mechanical coherence between two spin states. A transition between two spin states can be related to a coherence. The first pulse excites the triple quantum coherence (p=+3) and the second pulse converts this into the single quantum coherence (p=+1). Then the third pulse transfers the coherence into p= -1 for the detection of the signal.

In split-t_1 MQMAS (MQ=3Q) experiments for spin I=5/2, the evolution time t_1 is split between the single and triple quantum evolution times in the ratio of 19/12 which is the MQMAS ratio for spin I=5/2. The whole echo forms at the centre of $t_2=(19/12)t_1$ for all values of t_1.

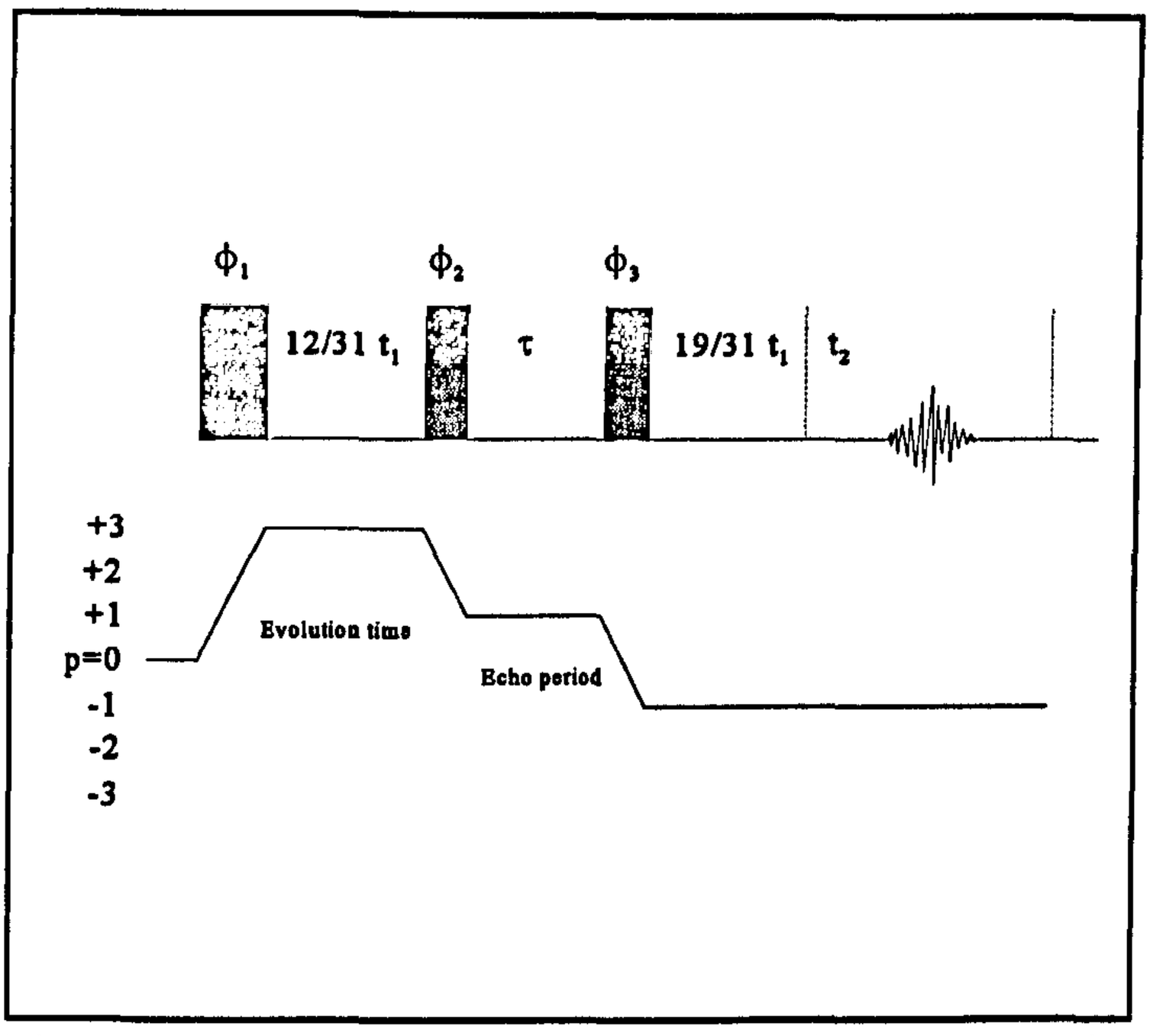

Figure 4.8 The pulse program and coherence transfer pathway diagram for the optimum phase modulated split-t_1 experiment for spin I=5/2 nuclei. [12]

One of the key factors in an NMR experiment is the calibration of pulse widths, since the observation of a maximum signal depends on the optimum pulse length which changes with the power level. The calibration of pulses is especially important in the case of MQMAS experiments. All three pulses must be adjusted to obtain the maximum signal.

4.4 Data Acquisition

Data acquisition can be divided into two major steps. The first step is to set up the necessary conditions for the experiment and second step is collecting the signal. Setting up the experiment consists of a few steps which are briefly as follows. The preamplifier box is changed to match the carrier frequency for the required nucleus for the Bruker MSL-360 spectrometer which has a superconducting magnet with a fixed B_0 field. The desired pulse

program is read into the computer. After that the acquisition parameters such as pulse length which is important for the MQ MAS experiment, pulse delay between pulses, spectral width (SW) (in two dimensions for the MQ MAS), dwell time are entered for the nucleus of interest. These values are different from one nucleus to another and they also may be different from one sample to another for the same nucleus. The delay time between pulses is dependent on the T_1 relaxation time and it differs for each sample. Approximately $5T_1$ between pulses gives unsaturated data, although the delay time can be made shorter by choosing an appropriate flip angle, θ, for nuclei having a long T_1. Therefore S/N can be optimized in an MAS experiment [4][13]. The table 4.1 shows some of the experimental parameters used in MAS and MQ MAS experiments. One can write such a standard file and save on the computer so that this standard file can be used for the other experiments providing that the probe, pre-amplifier and the power level are tuned properly. Detailed information on setting up the experimental parameters can be found elsewhere [7][14]. After setting up the necessary parameters a solution-state spectrum is run since the chemical shift (CS) or the peak position of the spectrum is measured relative to standard materials for all NMR active nuclei. This is called the spectrum reference (SR) which is the distance in Hz between the centre of the spectral width and the resonance position of the single line produced by the nuclei of interest in the liquid. As the resonance frequency depends on the B_0 field the measurement of the SR is necessary for every NMR experiment because the B_0 field decays in time. A list of references used in this study is given in table 4.2, and a more detailed list can be found in ref[15].

***Table 4.1** Experimental parameters for MAS and MQMAS experiments*

MAS			
Nuclei	*pulse width (μs)*	*pulse delay(s)*	*number of pulses*
^{17}O	*1*	*1-2*	*3600-5000*
^{29}Si	*0.8-1*	*30-60*	*320-1200*
^{27}Al	*0.3-0.5*	*0.5-1*	*300*

MQMAS				
Nuclei	*excitation pulse(μs)*	*echo pulse(μs)*	*detection pulse(μs)*	*pulse delay (s)*
^{17}O	*2.5-3.5*	*0.6-1.3*	*0.7-1.3*	*1-2*

***Table.4.2** List of the references and their Larmor frequencies for the two spectrometers used in this study.*

Nuclei	Reference material	Larmor frequency (MHz)	
		8.45T	14.4T
^{17}O	H_2O	48.8	81.3
^{29}Si	TMS	71.5	119
^{27}Al	$AlCl_3$	93.8	156.3

In the second step of the acquisition the data were collected once the parameters mentioned above were set up properly. This process is fully automatic and started when the acquisition command was entered by the operator. The collected signal (FID) was digitized by the analogue to digital converter (ADC) and saved in the computer memory. Finally the resulting FID was saved on the disc with proper file name and could be recalled from the memory at any time for processing.

In the case of MQMAS experiments, in addition to the above parameters, the sweep width in second dimension (SW2), related to that dwell time in second dimension (DW2)

and the number of slices in the second dimension (acquisition length in the second dimension Al2) were also set up. The number of scans (NS) was set to integer multiples of 96 since the split-t_1 experiment has 96 phase cycling steps. The echo time was set to integer multiples of 1/(spinning speed) to reduce artifacts and it should be long enough to obtain the whole echo.

4.5 Data processing and manipulation

After collection of the FID, the time domain signal is processed to obtain a conventional absorption spectrum to allow interpretation. Sophisticated software provided by the spectrometer computer allows rapid manipulations which are mainly Fourier transformation, smoothing of the spectra, phase correction, and baseline correction for the MAS experiments. These operations must be performed with care to ensure that the final spectrum is a true representation of the time domain signal in the frequency domain. A typical processing sequence would be as follows:

a) In a single pulse experiment the first few points of the digitised FID may be corrupted due to probe dead time or the pulse leaking from the transmitter to the receiver. Therefore these first few points are removed (left shift). In a spin echo experiment the middle of the echo is found and from this point the Fourier transform is performed

b) The FID is smoothed by multiplying an exponential function, Lorentzian or a Gaussian which improves the signal to noise ratio but reduces the resolution. This process is called line broadening since the line is broadened by this process [7]. Incorrect usage of line broadening causes the distortion of the true line shape and prevents the interpretation of the spectra. Therefore it is best to use as little line broadening as possible[16].

c) The FID then undergoes a Fourier transform to obtain the frequency domain spectrum.

d) The resulting spectrum after Fourier transform is a mixture of the absorption and dispersion signals. The first order phase is independent of the frequency and is due to misadjustment of the phase of the detector. The second order phase is dependent on the frequency. These phases are corrected to obtain the true absorption line shape and it is done by eye, by observing peak symmetry and baseline.

e) The base line also may be distorted due to probe dead time. In that case baseline correction is performed.

In the case of processing MQMAS data , which is obtained using split-t1 pulse sequence, the above procedure is followed in the first dimension. Briefly apodazation, Fourier transform, first order and zero order phase corrections are applied. Since in the split-t1 experiment subsequent FIDs appears at the same place, which is determined by the tau evolution time divided by the acquisition time in virtual time scale, the apodization is applied on the tau echo time in the first dimension (MAS or anisotropic dimension). The first order phase correction is carried out until the complex part of the signal goes to zero in the MAS direction.. Next step is to transpose the spectrum to the second dimension (isotropic dimension) where the first point of the data is multiplied by 0.5 in the case of complex-complex Fourier transform and then another Fourier transform is applied with respect to t_1. The resulting spectrum is then transposed back to the first dimension to display the spectrum in a conventional way where the MAS (anisotropic) dimension appears on the x-axis and the isotropic dimension appears on the y-axis.

4.6 O-17 Enrichment of the Samples

All samples used in this study are enriched to 10-25% in ^{17}O. The enrichment of the crystalline aluminosilicate will be discussed in chapter 5. The enrichment of the aluminosilicate and tin-silicate glasses will be explained here.

For the aluminosilicate glasses enriched $Si^{17}O_2$, $Al_2{}^{17}O_3$ and $Na_2C^{17}O_3$ were used. $Si^{17}O_2$ was prepared by direct synthesis in a 250 ml flask under nitrogen flow, using hydrolysis of $SiCl_4$ with isotropically enriched $H_2{}^{17}O$. The addition of the $H_2{}^{17}O$ into the $SiCl_4$ was carried out very slowly in an ice bath to slow down the reaction. The reaction proceeds smoothly in diethyl ether $(C_2H_5)_2O$ without oxygen scrambling according to the equation[17],

$$SiCl_{4(liq)} + 2H_2{}^{17}O_{(liq)} \rightarrow Si^{17}O_{2(liq)} + 4HCl_{gas}$$

Then the flask was left under constant nitrogen flow overnight to evaporate the diethyl-ether. The resulting white powder was rinsed in distilled water and boiled dry. After that it was heated at 200°C under vacuum for about 24 hours to remove the remaining HCl $(C_2H_5)_2O$ and $SiCl_4$. However further heat treatment up to 600°C was necessary to remove the carbon in the powder, whose colour changed from white to brown if carbon was present.

$Al_2{}^{17}O_3$ was prepared in a similar manner to that of $Si^{17}O_2$ by using aluminium-sec butoxide $[Al(OC_4H_9)_3]$ and $H_2{}^{17}O$ under constant nitrogen atmosphere. The appropriate amount of aluminum-sec butoxide was dissolved in isopropanol $[(CH_3)_2CHOH]$ for

smoother reaction according to the equation below,

$$2Al(OC_4H_9)_3 + 3H_2^{17}O \rightarrow Al_2^{17}O_3 + 6CH_9OH$$

Aluminium-sec butoxide was mixed with isopropanol and $H_2{}^{17}O$ was added in small portions to the mixture under nitrogen atmosphere. The mixture was vigorously stirred throughout the process. Once the addition of the $H_2{}^{17}O$ was finished the mixture was left in the glove box under nitrogen for about two days to evaporate unwanted products of the process. To remove the remaining carbons and protons some of the resulting white powder was heated up to 200°C under nitrogen flow. However heating the powder at 200℃ was not enough to obtain the $Al_2{}^{17}O_3$ phase. This lead to more silica enriched aluminosilicate samples than we expected. Then this white powder was heated up to 600°C which proved to be enough for removal of the remaining carbon and protons and produced the $Al_2{}^{17}O_3$ phase.

$Na_2C^{17}O_3$ was prepared in a teflon bottle which is capable of standing the heat up to 150°C. The appropriate amount of the Na_2CO_3 was mixed with the 1 gr of $H_2{}^{17}O$ and sealed in the teflon bottle which was placed in a drying oven and left at 120°C for about 4 days. The reaction follows the equation below.

$$Na_2CO_3 + H_2^{17}O \rightarrow Na_2{}^{17}O + CO_2$$

All products at the end of these processes were checked by using ^{17}O MAS NMR in order to make sure the enrichment was successful. ^{29}Si, ^{27}Al MAS NMR experiments were also performed on these products to see we have the right phase.

References

[1] E.L. Hahn, Phys. Rev., 80 (1950) 580

[2] I.J. Lowe, R.E. Norberg, Phys. Rev., 107(1957)46.

[3] W.G Clark, Rev. Sci. Inst., 35(1964)316.

[4] R.R. Ernst, W.A. Anderson, Rev. Sci. Inst., 37(1966)93.

[5] Aspect 300 MSL software manual, Bruker Manual,1986.

[6] MSL System Description, Bruker 1986.

[7] E. Fukushima, S.B.W. Roeder, Experimental Pulse NMR, !981, Addison-Wesley.

[8] NMR probe head series MAS-DB, Bruker manual,1985.

[9] Users Manual for Solid State Probes, Doty Sci. Instruments, Colombia, USA, 1986

[10] H. Eckert, Progress in NMR Spectroscopy, 24(1992) 159.

[11] A Handbook of Nuclear Magnetic Resonance, Freeman (Longman) 1988.

[12] S.P. Brown, S. Wimperis, J. Mag. Reson., 124,(1997)279-285.

[13] R. Dupree, M.E. Smith, J. Mag. Reson., 75(1987)153.

[14] M.L. Martin, J.J. Delpuech, G.J. Martin, Practical NMR Spectroscopy, Heyden and Son Ltd, London 1980.

[15] R.K. Harris, Nuclear Magnetic Resonance Spectroscopy, Longman Scientific and Technical,1986.

[16] L.F. Gladden, TA Carpenter, J. Klinowski, S.R. Elliot, J. Mag. Resn., 66(1986) 93.

[17] A.E. Geissberger, P.J Bray, J. Non Crys. Solids, 54(1983)121-137.

CHAPTER 5

The Relationship Between O-17 NMR Quadrupolar Parameters and The Si-O-Al Bond Angle in Aluminosilicates

5.1 INTRODUCTION

Aluminosilicates are one of the most common materials found in important rock forming minerals, ceramics and glasses. They are used as catalysts and absorbers and have attracted much attention. Information on their structure helps in the understanding of their properties and in the development of new usage areas.

The relationship between the intertetrahedral bond angle T-O-T' (T,T'= Si, Al) and the NMR parameters of different nuclei (^{29}Si, ^{27}Al,) have been extensively investigated for these materials. The majority of the work concentrates on the relationship between the ^{29}Si NMR chemical shift and the bond angle. Ramdas et.al.[1], developed a simple relationship between ^{29}Si chemical shift and the total of the four Si...T bond lengths involving the central Si atom in Si(nAl) units and claimed that by using this simple correlation the average value of T-O-T angle for each kind of silicon in an aluminosilicate of unknown structure (including amorphous material) can be reliably estimated from ^{29}Si MAS NMR alone. Newsam also tried to explain the variation in ^{29}Si chemical shift data with five different functions of Si-O-T (T=Si, Al) for aluminosilicates[2]. From the ^{29}Si NMR chemical shifts of the Na-A and Na-X zeolites Thomas et.al. [3], suggested the existence of an effect of Si-O-T (T=Si, Al) angle θ, on the magnitude of ^{29}Si chemical shift. Later studies by Jarman [4] on zeolites Zk-4 and TMA sodalite, and by Grimmer et al.[5], on the mineral zunyite provide

further support for this hypothesis. Weller et.al. [6], found a simple linear correlation between ^{29}Si chemical shift and the Si-O-Al bond angle in aluminosilicate sodalites with a Si/Al ratio of 1. The same kind of linear correlation between ^{27}Al chemical shift and Si-O-Al bond angle was also observed in these sodalites [7].

Although oxygen is the most abundant atom in these materials, it has received very little attention by means of ^{17}O NMR, because of the (historical) difficulties associated with doing ^{17}O solid-state NMR, such as the low natural abundance of ^{17}O (0.037%) and the line broadening effect of the quadrupolar interaction. It connects the SiO_4 and AlO_4 tetrahedra thus ^{17}O NMR is a sensitive and direct way to investigate these interconnections. However, relatively little is known of the relationship between ^{17}O NMR parameters and structure when compared to the more commonly used spin 1/2 probes such as ^{13}C, ^{29}Si , or ^{31}P

The quadrupolar coupling constant, $C_Q=e^2qQ/h$, and the associated asymmetry parameter, η, are of interest because they reflect the electric field gradient at the nuclear site and therefore provide valuable information about the local symmetry of local structure, since these parameters are extremely sensitive to the local environments. The electric field gradient of oxygen is directly influenced by highly variable T-O-T (T=Si,Al) bond angle and by the T atoms so that different linkage types such as Si-O-Si, Si-O-Al, Al-O-Al, Al-O-P, and terminal oxygen atoms (Si-O) have been found to show distinctive ^{17}O NMR parameters [8][9][10][11][12].

Tossel and co-workers have shown that ab initio quantum chemical calculations can be a powerful tool for researchers trying to relate measured ^{17}O NMR parameters to structural features[13][14][15]. Indeed, the Tossell group's ab initio calculations predicted trends in ^{17}O quadrupolar coupling parameters with Si-O-Si bond angle that

have been experimentally verified using ^{17}O DAS in $K_2Si_4O_9$ by Farnan et.al. [16]. They proposed a semiempirical formula to explain the dependence of the oxygen efg on the bridging angle, Si-O-Si given by,

$$C_Q = C_{Q180}\frac{2\cos\theta}{\cos\theta - 1} \tag{5.1}$$

where θ is the Si-O-Si angle and C_{Q180} is the efg value at the Si-0-Si angle of 180° found to be 6.06 MHz. Grandinetti et.al [17][18] also proposed a semiemprical correlation (equation 5.2) between Si-O-Si bond angles (θ) and ^{17}O quadrupolar parameters using a Townes-Dailey analysis[19]. He later tested his proposal with experimental observation of five distinctly resolved ^{17}O sites in the SiO_2 polymorph coesite

$$C_Q = C_{Q180}\left[\frac{3\cos\theta - 1}{2\cos\theta - 1}\right]^2 \tag{5.2}$$

with C_{Q180} of 6.06 MHz

The asymmetry parameter (η) of the EFG is another quadrupolar parameter whose relation with the bond angle has been investigated. Sternberg [20] from primarily a geometric starting point for a symmetric AX_2 bond, found that the asymmetry parameter

$$\eta = -\frac{3(\cos\theta + 1)}{3\cos\theta - 1} \tag{5.3}$$

Grandinetti et.al.[18] also derived the same formulae to describe the correlation between the Si-O-Si angle and the asymmetry parameter,η, using the Townes-Dailey model.

As outlined above most of the work has been done on the correlation between Si-O-Si bond angle and the one of the NMR parameters, such as chemical shift or quadrupolar coupling constant. However there seems to be very little work done on the effect of Si-O-Al bond angle (figure 5.1) on NMR parameters in these materials. Finding the relationship between Si-O-Al bond angle and the ^{17}O NMR quadrupole parameters in crystalline aluminosilicates, would be very useful for identifying and distinguishing the multiple oxygen sites in materials (including glasses) whose structure are unknown or partially known.

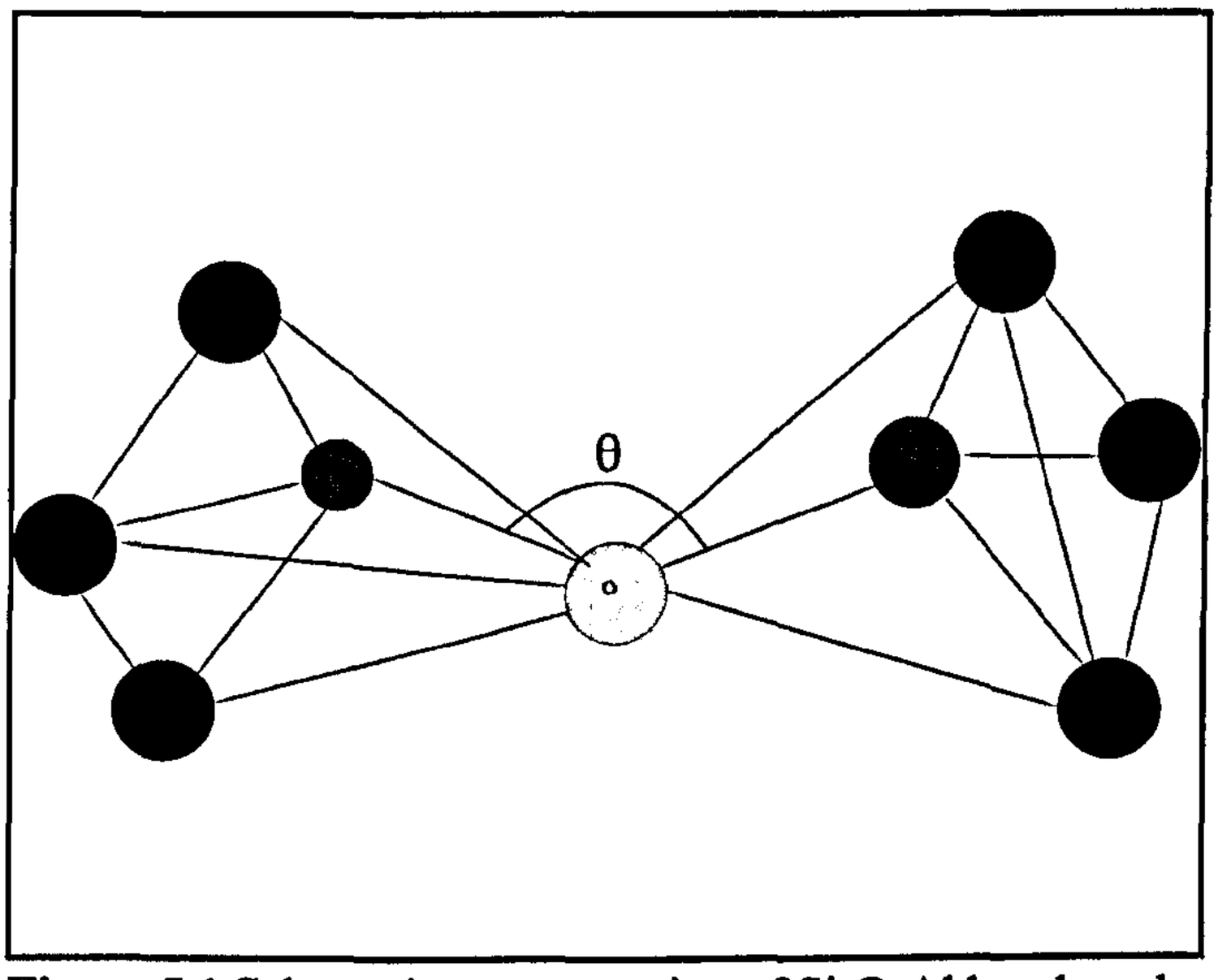

Figure 5.1 Schematic representation of Si-O-Al bond angle.

As the quadrupole coupling constant reflects the electric field gradients around quadrupolar nuclei, it may have great potential as a parameter that can be related to the local electronic/geometric structural environments of such nuclei. Therefore it is likely to be of similar importance to the chemical shift parameter for description and identification in structural studies.

We therefore chose four aluminosilicate sodalites, LiCl, Li-NaCl NaCl, KCl and kalsilite as model compounds as they all have a Si/Al ratio of 1 and cover a wide range of bond angles. Furthermore they should have only Si-O-Al bonds. The sodalites have all one oxygen site which makes obtaining and interpreting the spectrum easy, while kalsilite has two oxygen sites one of which is three times more abundant than the other site.

Aluminosilicate sodalites have an ordered framework which consists of AlO_4 and SiO_4 tetrahedra. Their cubic symmetry is the result of the close packing of interconnected sixfold rings of (Al, Si)O_4 tetrahedra which are stacked parallel to {111} in an ABCABC...type of sequence [21]. The structure is further characterized by (Al, Si)O_4 rings of four tetrahedra parallel to {100}. The overall linkage of (Al, Si)O_4 tetrahedra results in a cubo octahedral cavity. These six membered rings result in continuous channels allowing for interframework ions [22]. In these channels they can contain anionic species such as Cl^-, SO_4^{2-}. Their general formula is $M_8[AlSiO_4]_6X_2$, where M may be sodium, lithium, silver or more rarely other monovalent or divalent cations and X represents one divalent or two monovalent anions. The sodalite structure can be viewed as made from sodalite cages to fill the space completely. Fig 5.2 shows the sodalite cage structure. In an ideal sodalite the anion is located at the centre of the sodalite cage and tetrahedrally coordinated to the four cations whereas the cations are located in front of the six rings in the sodalite cage and are coordinated to three framework oxygen atoms and to the anion. In these materials the exchange of cations occurs readily, thus allowing the synthesis of sodalites of a variety of compositions. This is due to the flexibility of aluminosilicate framework, through changes in the Si-O-Al bond angle which allows a wide ranges of ion sizes to be incorporated into the

cavities. Although the size of the ions mainly influences the Si-O-Al angle [3,4][23] distortion of tetrahedra have also been reported [24]. The sodalite type framework structure is also found in beryllosilicate $(Be_6Si_6O_{24})^{12}$ [25], borate$(B_{12}O_{24})^{12}$[26], aluminate $(Al_{12}O_{24})^{12}$ [27], and Ga and Ge substituted analogues of the aluminosilicate sodalites [28]. The sodalite cage is also used as a building unit in many zeolites [29], and many complicated structures of compounds such as α-Mn, Sb_2Tl_7, tetrahedrite can be related to that of sodalites [30]. Henderson et.al. [31], synthesized many of the sodalites and Taylor et.al. [32], developed a computer model for the crystal structure of sodalite which was replaced later by the distance least squares (DLS) modelling technique of Dempsey et.al. [33].

Kalsilite is a framework topology consisting of corner linked single six membered $(Al, Si)O_4$ tetrahedra containing interstices, filled with K^+ ions. Its framework topology is based on stuffed derivatives of tridymite [34]. Figure 5.3 shows the schematic representation of kalsilite. The ideal trydimite structure requires an unusual T-O-T bond angle of 180° at the oxygen atom lying on the triad axis where T is the tetrahedral cation. However this can only be achieved averaging over different O atom positions, but determination of true atomic distributions is not straightforward. Some insights into how the average T-O-T angles vary with temperature are provided by variations in the lattice parameters by Capobianco and Carpenter[35]. They calculated the $T\text{-}O_1\text{-}T$ and $T\text{-}O_2\text{-}T$ angles 143.5° and 154.1° respectively by using the lattice parameters and the Al-O and Si-O distances. Although it has two chemically different oxygen sites the $T\text{-}O_1\text{-}T$ is three times more abundant than the other oxygen site. Table-5.1 gives the aluminosilicate sodalites and kalsilite and their Si-O-Al bond angles used in this study.

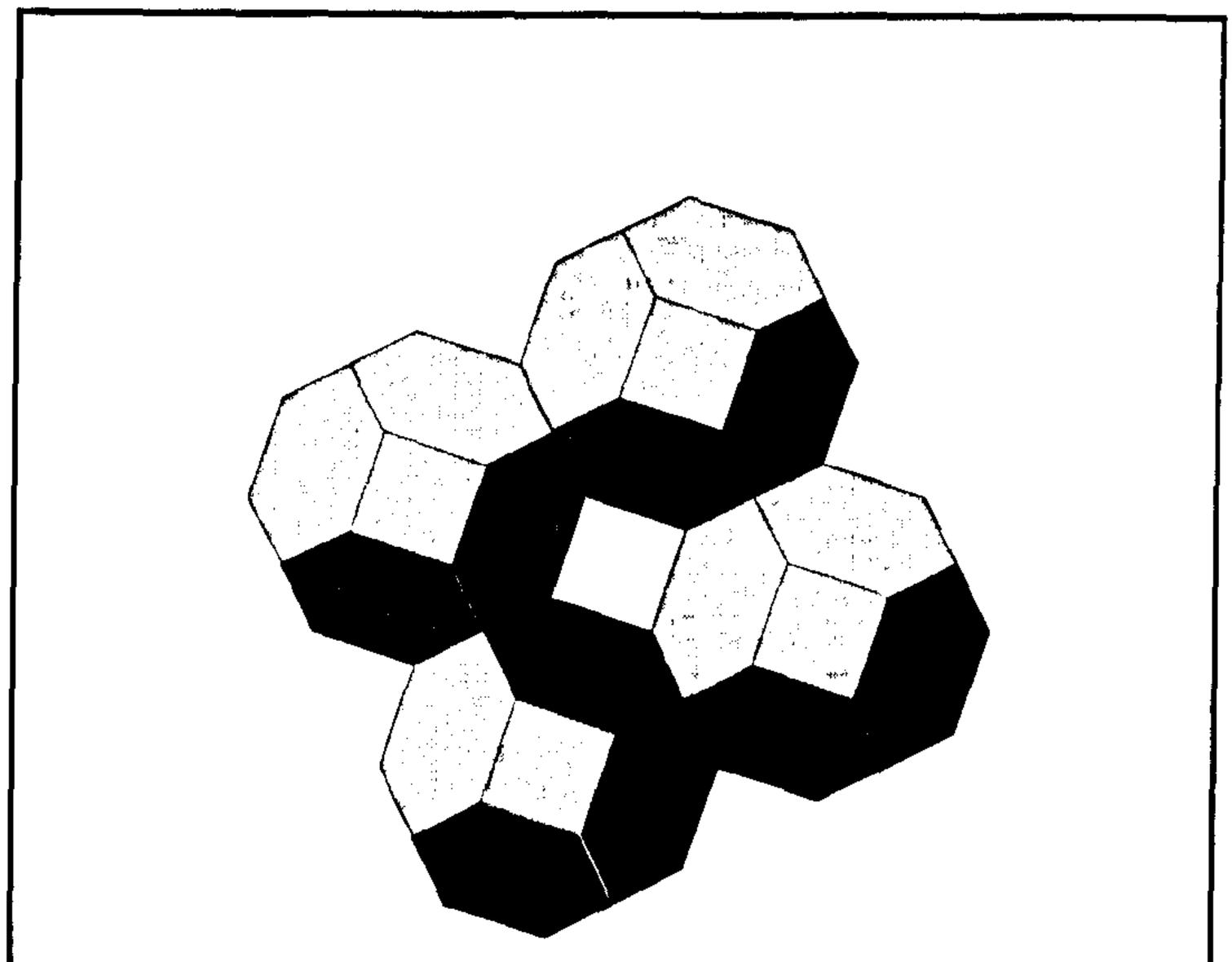

(a)

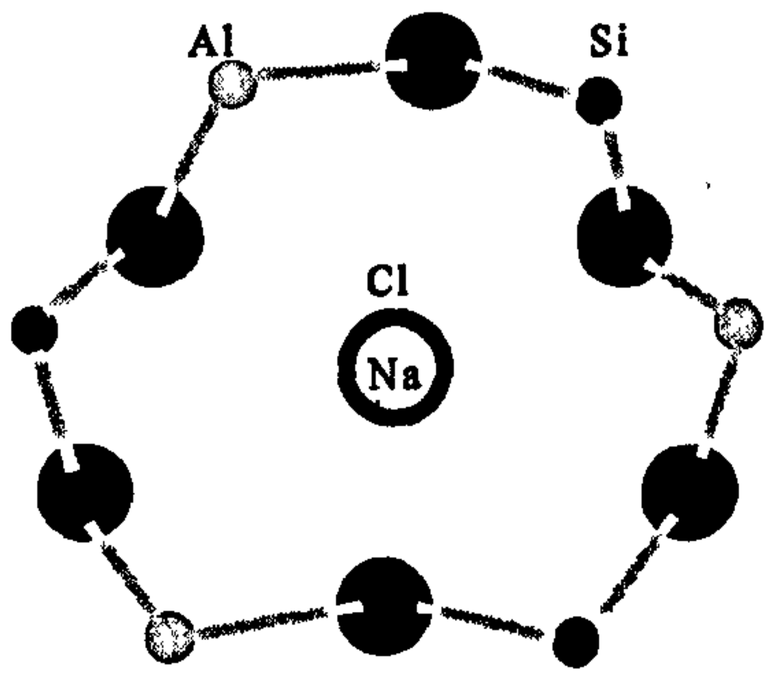

(b)

Figure 5.2 (a) Schematic representation of sodalite cage (b) The atomic arrangement around the Na

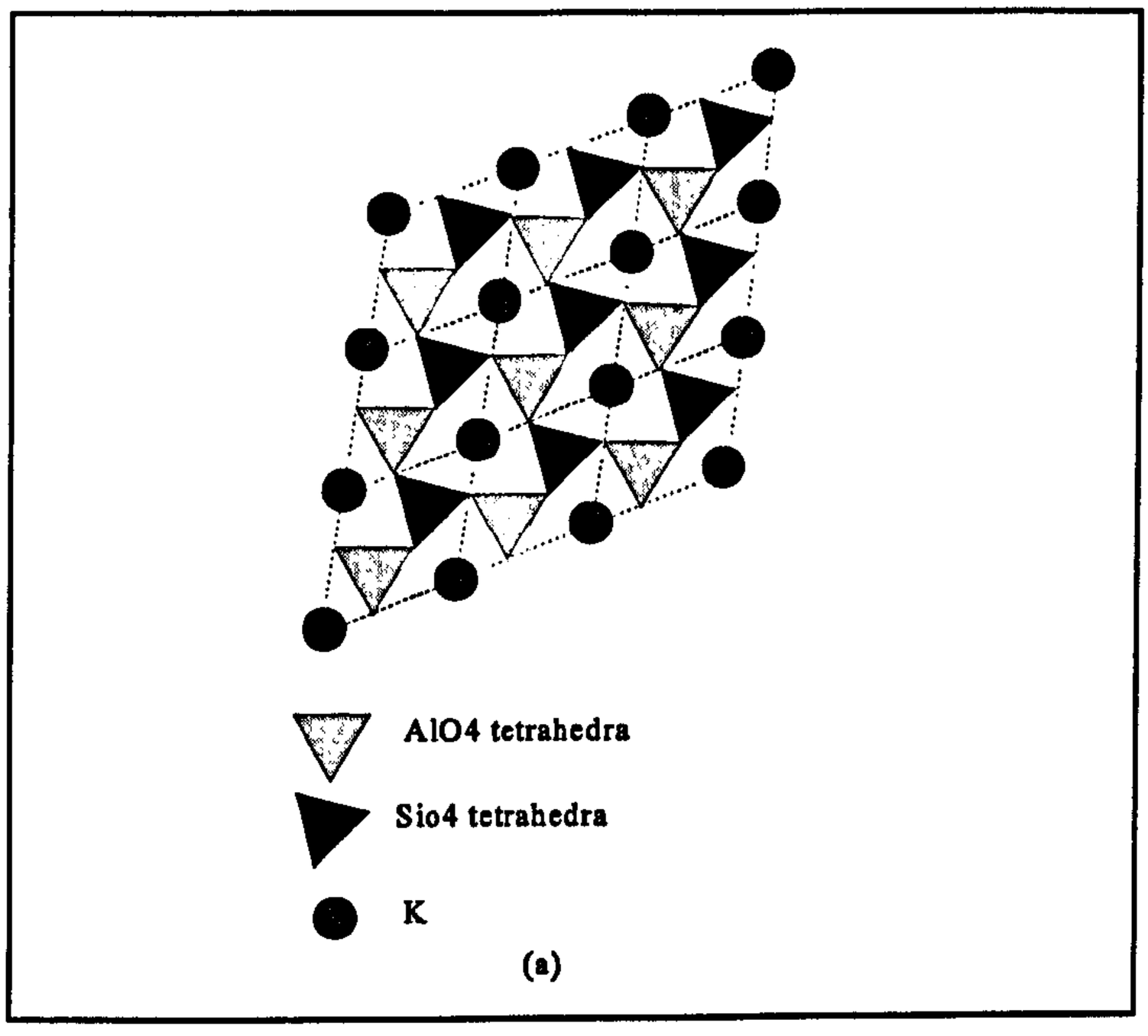

Figure 5.3 (a)Schematic representation of Kalsilite (b) the atomic arrangement around the K-atom

Table-5.1 The crystalline aluminosilicate model compounds chosen for this study (sodalites and kalsilite) and their Si-O-Al bond angle which are obtained from ref [3]and [32] [34].

Material	Si-O-Al Bond Angle
$Li_8Al_6Si_6O_{24}Cl_2$	124.6
$(Li_{4.6}\text{-}Na_{3.4})Al_6Si_6O_{24}Cl_2$	129.1
$Na_8Al_6Si_6O_{24}Cl_2$	138.1
$KAlSiO_4$(Kalsilite)	143.5, 154.1
$(K_{6.8}Na_{1.2})Al_6Si_6O_{24}Cl_2$	152.7

5.2 Experimental Procedures

These samples were prepared by Henderson at the University of Manchester. In order to produce the ^{17}O enriched aluminosilicates that we investigated in this study, many samples of end member NaCl sodalite ($Na_8Al_6Si_6O_{24}Cl_2$) were synthesized from a mixture of NaCl (in excess) and a gel of nepheline ($NaAlSiO_4$) composition prepared by the method of Hamilton et.al.[36]. ^{17}O enrichment was done by adding 1 ml of ^{17}O enriched water into the about 1.5-2.5 gms of the solid mixture. Then this mixture was loaded into a gold capsule whose diameter was about 1 cm and the length was about 7cms. The ends of the capsule were sealed by using arc-welding. These capsules then were heated in a cold-seal pressure vessel at 600°C and 1 kbar water vapour pressure for times varying from 5 to 11 days. At the end of this process, excess NaCl was dissolved and the sample dried. All the samples were well crystalline, phase-pure NaCl-sodalite having a cell parameter of 8.878(1) Å. NaCl-sodalite was used for preparation of Li- and K-Cl-sodalites by using ion exchange in the appropriate alkali chloride melt at about 50°C above its melting temperature for about 1 hour. Then the sample was washed free of excess alkali chloride. Cell parameters of LiCl and KCl sodalites are 8.447(2) Å and

9.223(2) Å, respectively. From the data obtained by Henderson et.al.[31] these cell parameters indicate that the LiCl sample has an end-member composition ($Li_8Al_6Si_6O_{24}Cl_2$) and the K-sample has the composition ($K_{6.8}Na_{1.2}Al_6Si_6O_{24}Cl_2$). An attempt to replace some of the K with Rb by ion exchange in RbCl melt was unsuccessful as the sample broke down to another phase. An intermediate Li-NaCl sodalite sample was also prepared by ion exchanging a synthetic NaCl-sodalite in a mixed alkali (Li-Na)Cl melt. About 90 mol.% NaCl-10 mol.% LiCl was enough to give a satisfactory intermediate composition sodalite solid solution after 30 minutes exchange. The sample was annealed at 850°C for about 30 minutes, and X-ray powder diffraction revealed that the it was a well crystalline synthetic sodalite. Therefore Li-Na distribution should be homogeneous in the cavity cation sites of this phase, and its cell parameter of 8.640(1) Å gives the composition of $(Li_{4.6}Na_{3.4})Al_6Si_6O_{24}Cl_2$.

Oxygen-17 NMR spectra of these sodalites were obtained using the Bruker MSL spectrometer operating at 8.45 T, corresponding to an ^{17}O frequency of 48.8 MHz. Since our aim was to obtain the ^{17}O NMR quadrupole parameter we obtained only ^{17}O MAS NMR spectra using the 4mm Bruker MAS probe. Typically 10kHz spinning speed was used as the line widths of these are not very broad. Chemical shifts were reported in ppm (parts per million) from an external reference sample of tap water ($H_2{}^{17}O$, natural abundance).

The nuclear quadrupole coupling constant, C_Q, and the asymmetry parameter, η, and the isotropic chemical shift, δ_i, were obtained by computer line-shape simulation of the experimental spectra. For the line-shape simulations two software packages, PASC POWDER on the Bruker Aspect 3000 [37] and Qmas 1/2 model of the Win-Fit module included in the Bruker Win-NMR program for PC's were used [38].

5.3 Results and discussion

Figures 5.4, 5.5 and 5.6 show the ^{17}O MAS NMR spectra and simulations of the aluminosilicate sodalites and kalsilite investigated in this work. As mentioned above, all sodalites have only one oxygen site in their structure except kalsilite, which has two chemically different oxygen sites in its structure. However there is no sign of the second oxygen site from the ^{17}O MAS NMR spectra of kalsilite. The sodalite spectra are quite well defined. Since the efg at the nucleus of interest determines the width of the spectrum, and η determines the shape of the spectra, line-shape simulation of the ^{17}O MAS NMR spectra obtained from of all samples were done over a range of C_Q and η values to find the best fit as shown in figures 5.4, 5.5 and 5.6. C_Q, η and chemical shift, δ_i, values obtained from the simulations are given in table 5.2 along with C $_Q$and η values of Na-LSX aluminosilicate obtained by Pingel et.al.[39] in table 5.3. They investigated the correlation between ^{17}O chemical shift and Si-O-Al bond angle in zeolites by means of MQ MAS and DOR NMR at the high field of 17.6 T so that they aimed to determine the Si-O-Al angles in those materials, which are not accessible for X ray structure determination and they obtained the C_Q and η by simulating the isotropic projections of 2D MQ MAS spectra.

Pingel et al., [39], on the basis of chemical shift vs. angle, assigned O-2 with Si-O-Al angle of 141.5, and O-3, with Si-O-Al angle of 136.3, with C_Q values of 3.3 MHz, and 3.4 MHz respectively. Although they claim that the chemical shift decreases linearly with increasing bond angle and sites can be assigned according to their chemical shifts, our results do not agree with this. Figure 5.7 shows the chemical shift as a function of Si-O-Al bond angle obtained in this study and ref [39]

The chemical shift decreases with increasing bond angle but this relation is not monotonic so that it can not be used to determine the unknown sites alone. We reassigned these C_Q values as 3.3 MHz to the O-3 and 3.4 MHz to the 0-2 site, on the basis that C_Q increases with increasing bond angle as shown in figure 5.8a and 5.8b.

According to the table 5.2 the quadrupole coupling constant, C_Q, increases with increasing Si-O-Al angle, and the asymmetry parameter, η, decreases with increasing Si-O-Al angle, as expected from equation 5.1 and 5.2. Figure 5.8a presents the ^{17}O quadrupole coupling constant as a function of Si-O-Al angle. Filled circles represent the data

Table 5.2 *^{17}O quadrupole parameters and Si-O-Al angles obtained from line-shape simulations for the aluminosilicate sodalites and kalsilite.*

Sample	C_Q (MHz ± 0.3)	η ± 0.05	Si-Ô-Al	δ(ppm±1)
Li-SODALITE	3.05	0.62	124.6	66
Li-Na-SODALITE	3.3	0.45	129.1	48
Na-SODALITE	3.55	0.23	138.1	54
KALSILITE	3.61	0.2	143.5, 154.1	46
K-SODALITE	3.88	0.02	152.7	41

Table-5.3 *^{17}O quadrupole parameters of four different oxygen sites of Na-LSX [39].*

Na-LSX	C_Q (MHz)	η	Si-Ô-Al	δ (ppm)
O_1	3.2	0.4	132.5	50.3
O_2	3.4	0.3	136.3	41.7
O_3	3.3	0.3	141.5	45
O_4	3.6	0.15	146.8	36.

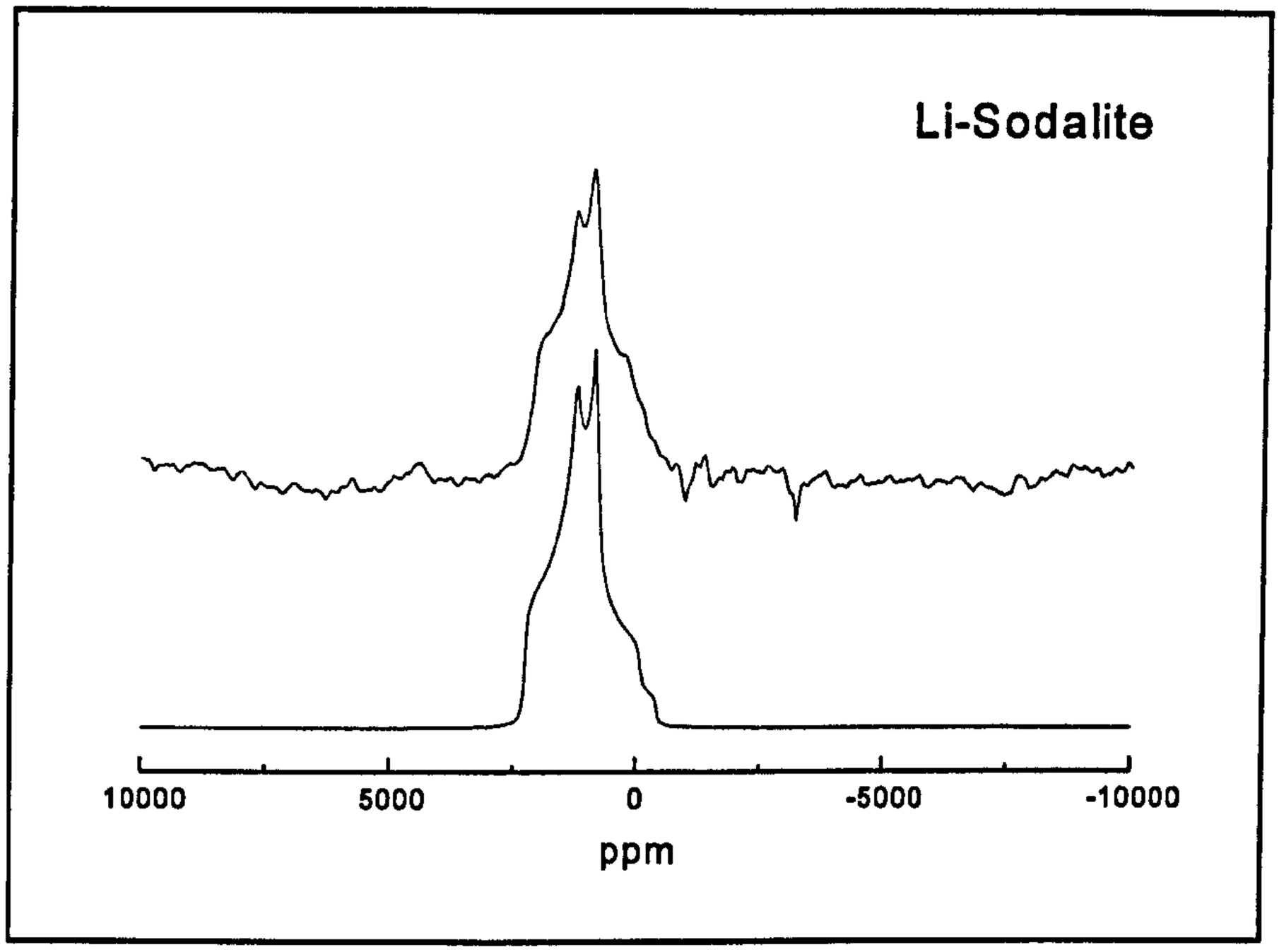

(a)

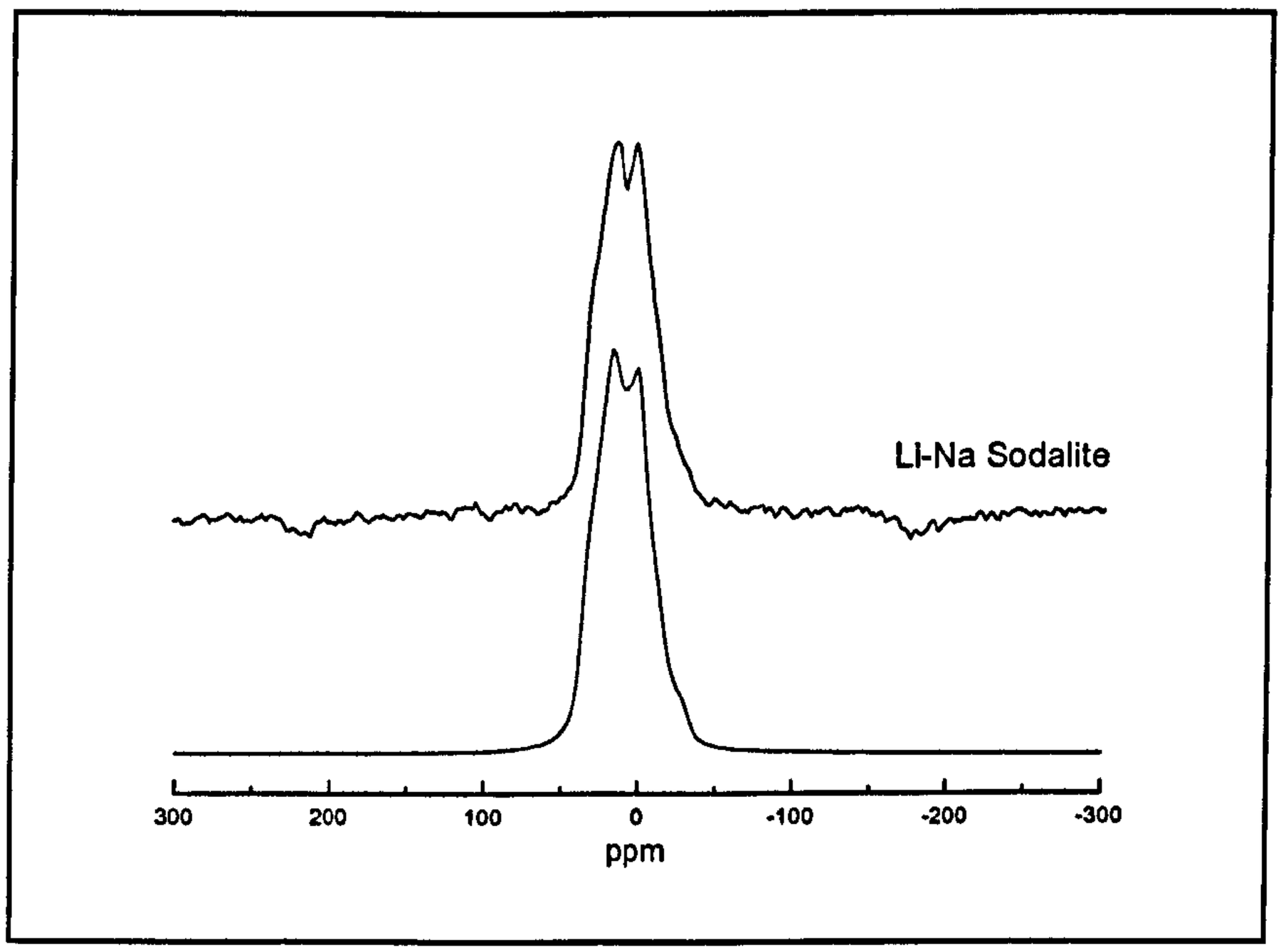

(b)

Figure-5.4 ^{17}O NMR MAS spectrum and simulation of, (a)$Li_8Al_6Si_6O_{24}Cl_2$, (b) $(Li_{4.6}Na_{3.4})Al_6Si_6O_{24}Cl_2$.

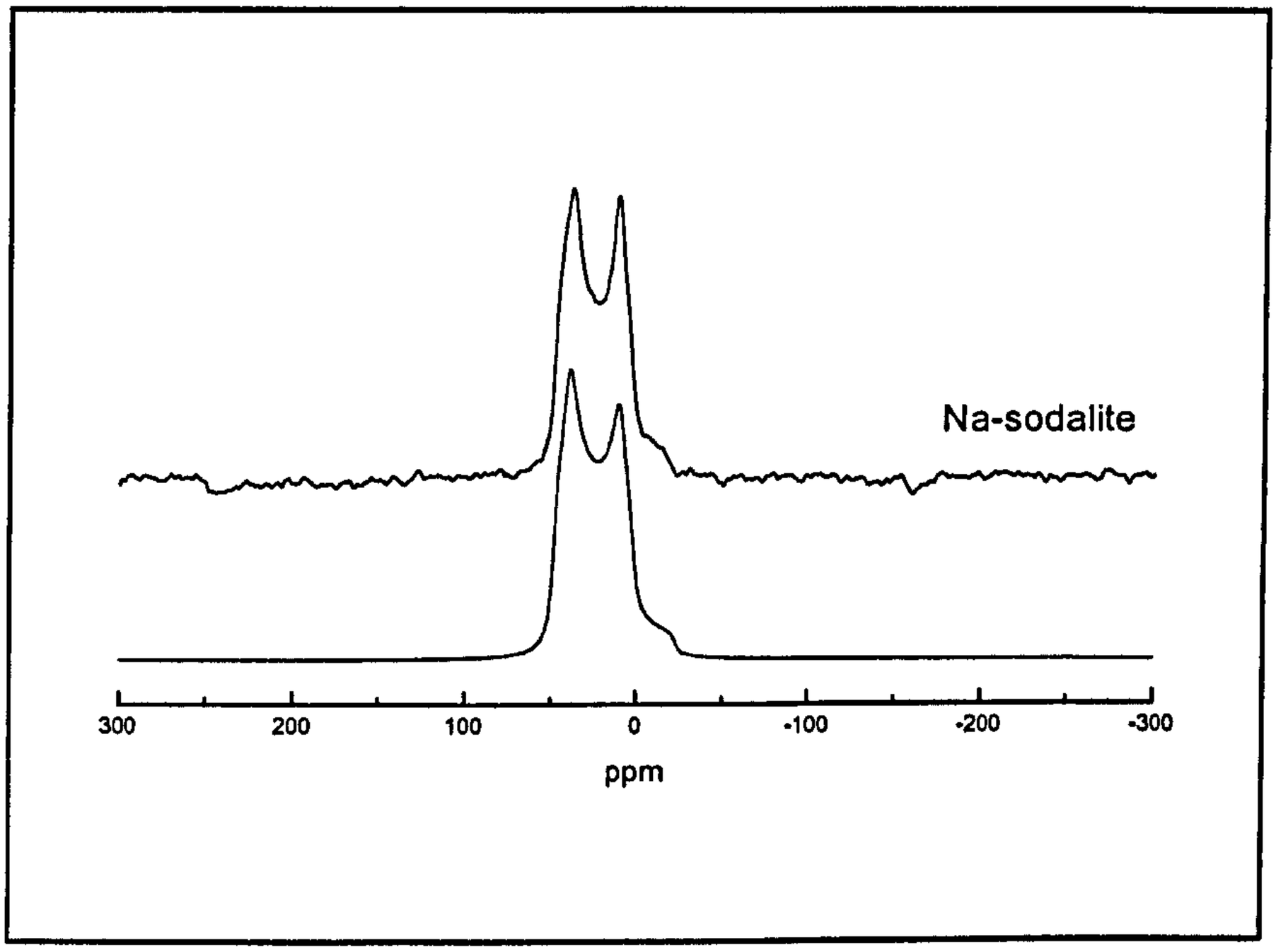

(a)

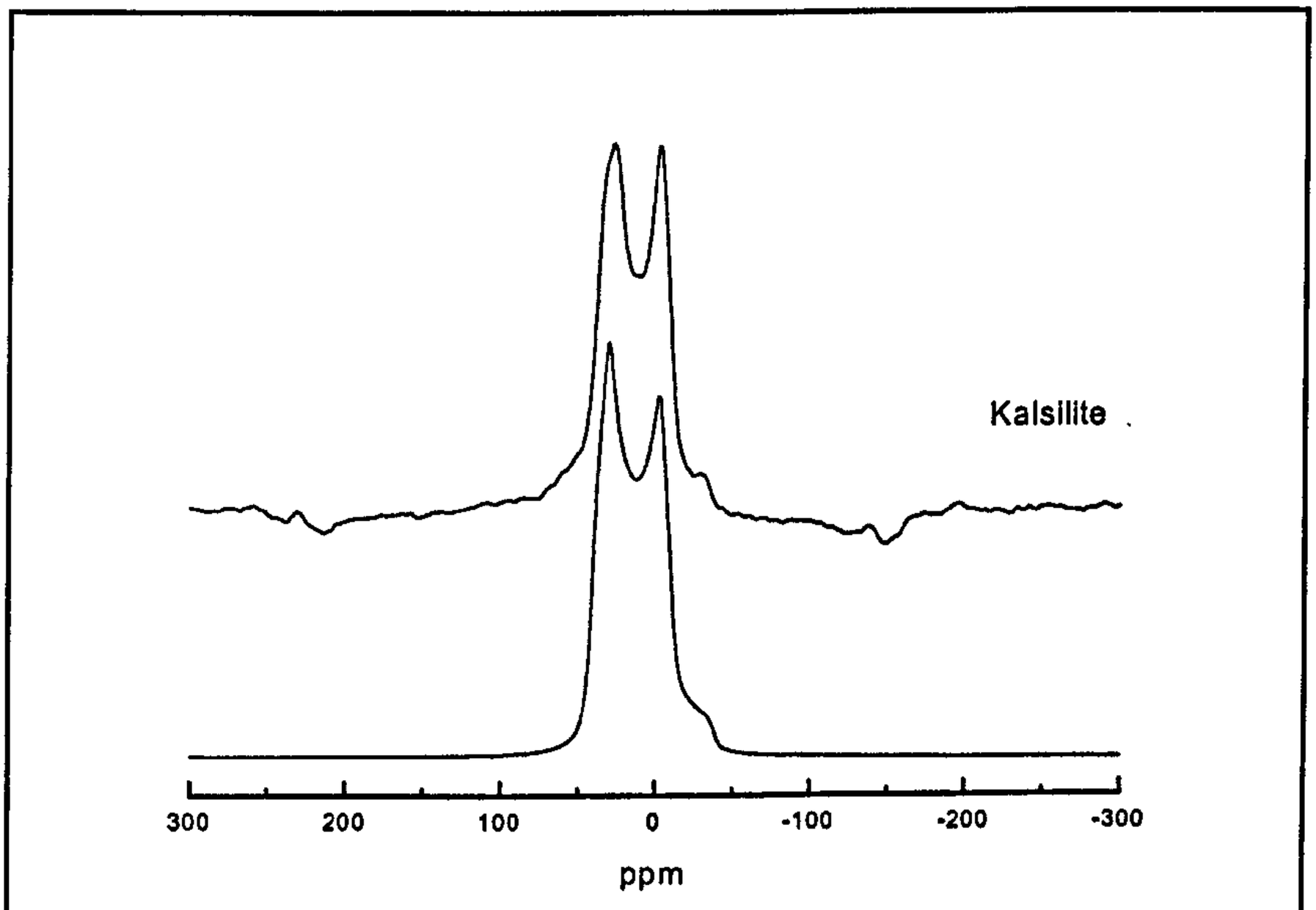

(b)

Figure 5.5. ^{17}O NMR MAS spectrum and simulation of, (a) $Na_8Al_6Si_6O_{24}Cl_2$, (b) Kalsilite $KAlSiO_4$.

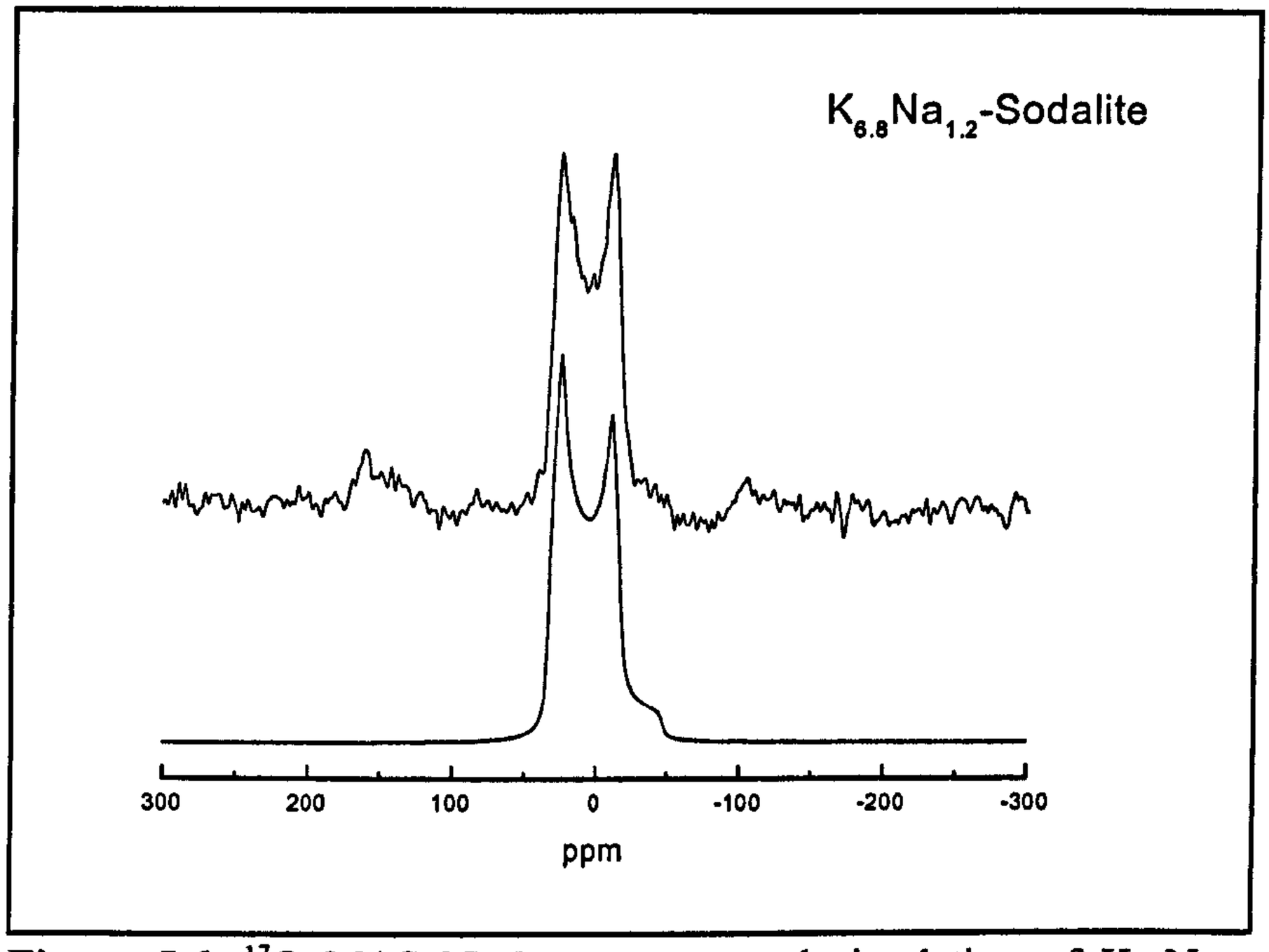

Figure 5.6. ^{17}O MAS NMR spectrum and simulation of $K_{6.8}Na_{1.2}$ sodalite: $K_{6.8}Na_{1.2}Al_6Si_6O_{24}Cl_2$.

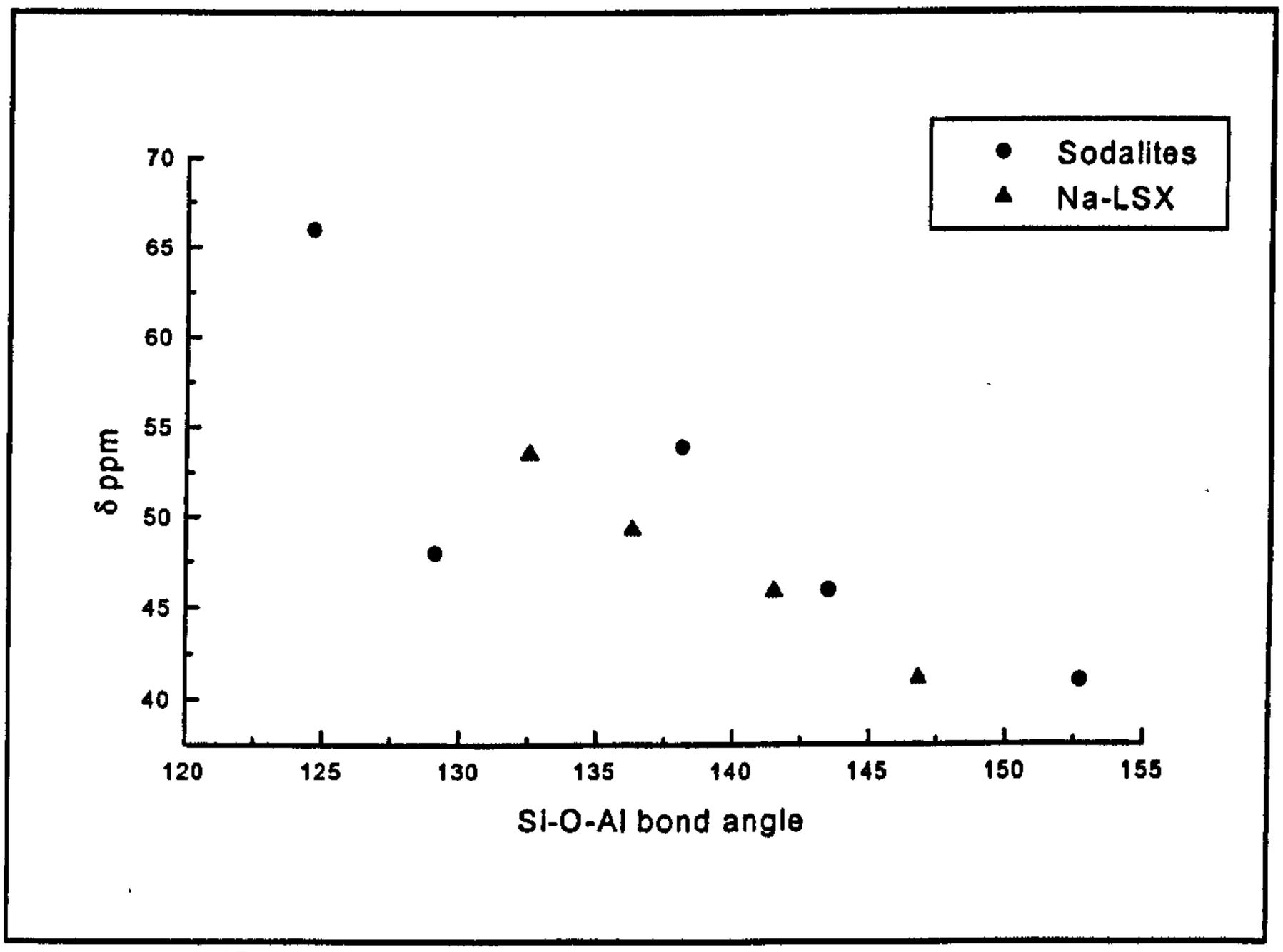

Figure 5.7 ^{17}O NMR chemical shifts against Si-O-Al bond angle in sodalites and Na-LSX.

obtained during this study from the aluminosilicate sodalites and kalsilite, while the triangles represent the data obtained from ref [39] for the purpose of comparison. In both cases the quadrupole coupling constant increases with increasing Si-O-Al angle, as in the case of Si-O-Si angle. We fitted our data to equation 5.1 (Figure 5.8a) and equation 5.2 (Figure 5.8b) in order to test both correlations for the Si-O-Al angle. Although both equations were proposed for the symmetric linkage of Si-O-Si, it seems that the relationship between C_Q and asymmetric Si-O-Al angle also closely follows the same equations with a smaller C_{Q180}=4.13 MHz and C_{Q180}=4.17 MHz for equation 5.2 and equation 5.1 respectively. However equation 5.2 seems to represent the data better than equation 5.1. We also fitted the Na-LSX data from ref [39] to both equations which fit the data very closely giving C_{Q180}=3.92 MHz, and C_{Q180}= 3.90 MHz for equation 5.1 and equation 5.2 respectively, shown in figures 5.8a and 5.8b.

The asymmetry parameter of the efg obtained from the line-shape simulations is also plotted against Si-O-Al angle along with the asymmetry parameters from ref [39] shown in figure 5.9. η decreases with increasing Si-O-Al angle as in the case of Si-O-Si. Our data, shown as black circles in the figure, seem to follow the equation 5.3 giving a reasonable fit at large angles but systematically greater than equation 5.3 for $\theta \leq 135°$. The data of Na-LSX, shown with triangles, also follow equation 5.3, with some scatter. Although equation 5.3 was derived for a symmetric linkage of T-O-T, it appears also to describe the relationship between, η, and the asymmetric linkage of Si-O-Al quite well at large angles.

In order to obtain more information whether all these equation obtained for the symmetric linkage of T-O-T are also applicable to the asymmetric linkage of Si-O-Al, cluster calculations were performed using, Gaussian 94, on a model cluster of $(OH)_3Si$-

O-Al(OH)$_3$ by Prof. Dupree [40]. Figures 5.10a and 5.10b show the dependence of the predicted ^{17}O C_Q and η, data for the bridging oxygen in the (OH) Si-O-Al(OH) $_3$ molecule as a function of Si-O-Al angle. In these calculation we did not take account of the effect of the cation atom whose presence could have a significant effect on the magnitude on the C_Q depending on its location [17]. However we are interested in the angular dependence of the C_Q and this effect should not change this dependence. An increase in the magnitude of C_Q and decrease of η with increasing Si-O-Al angle is observed similar to the data presented above. The calculated values of C_Q also fitted to equation 5.1 and equation 5.2 shown in figure 5.10a. Both equation 5.1 and equation 5.2 give a reasonable fit to the data with C_{Q180}=4.19 MHz and C_{Q180}= 4.17 MHz respectively, similar to the experimentally obtained C_{Q180} of 4.13 MHz for the same equation. Figure 5.10b shows the calculated asymmetry parameters which are in good agreement with the equation 5.3. However the calculated asymmetry parameters are smaller than the experimental values at low angles.

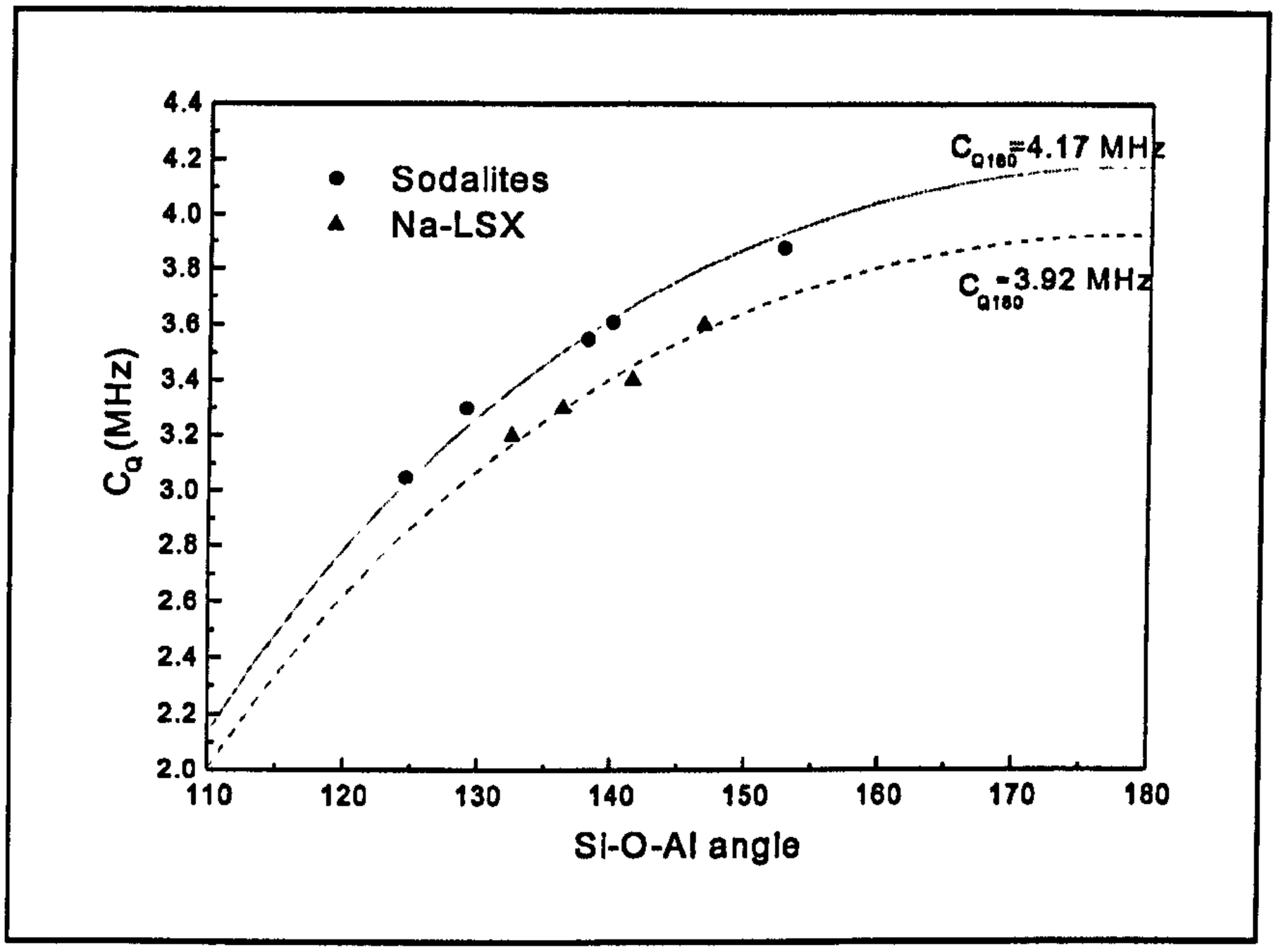

(a)

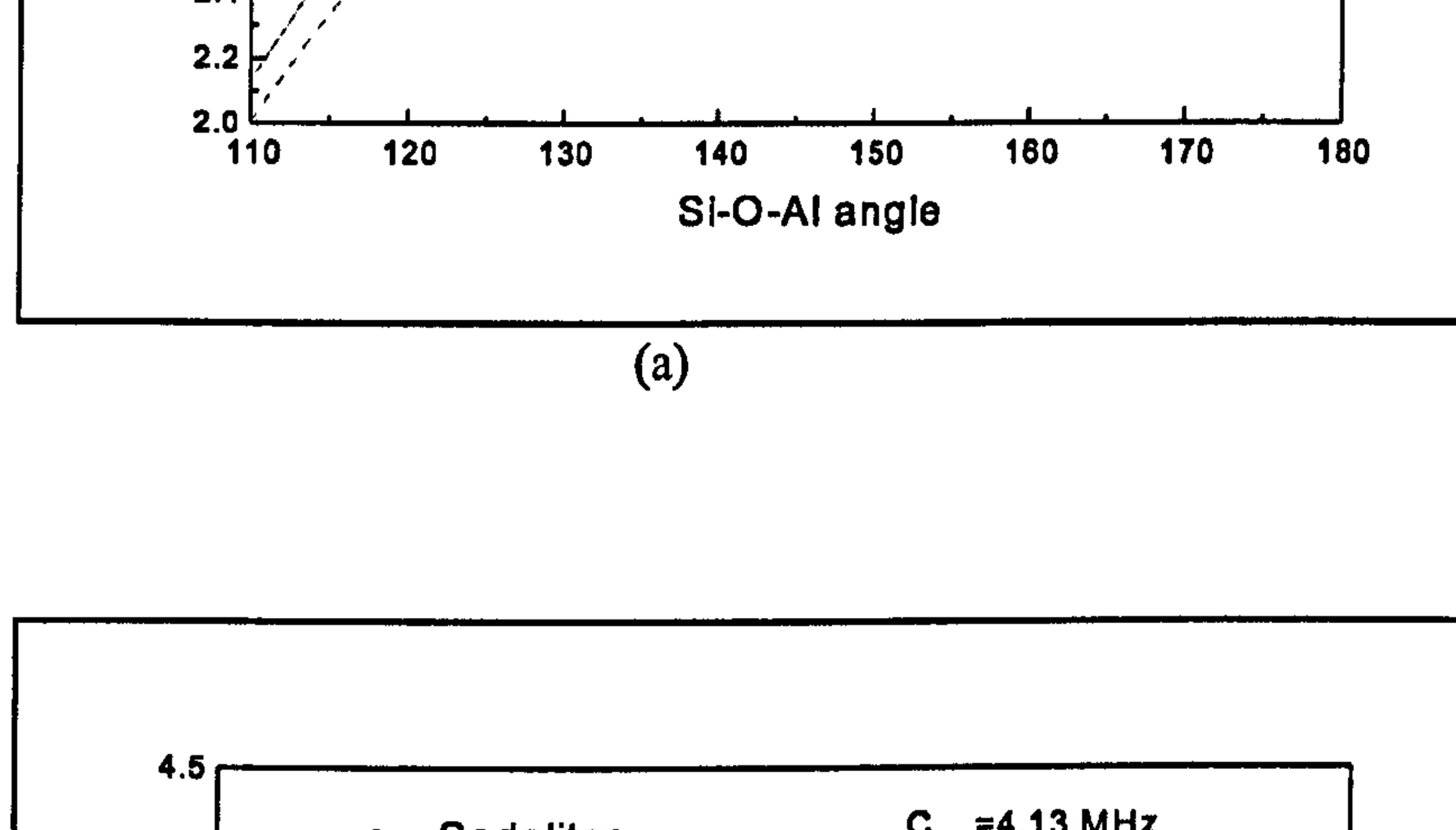

(b)

Figure 5.8 The angular dependence of ^{17}O quadrupole coupling constant with Si-O-Al bond angle; a)C_Q vs Si-O-Al angle for sodalites and kalsilites (filled circles), and Na-LSX [36] (triangle) fitted to equation 5.1; b) same data fitted with equation 5.2.

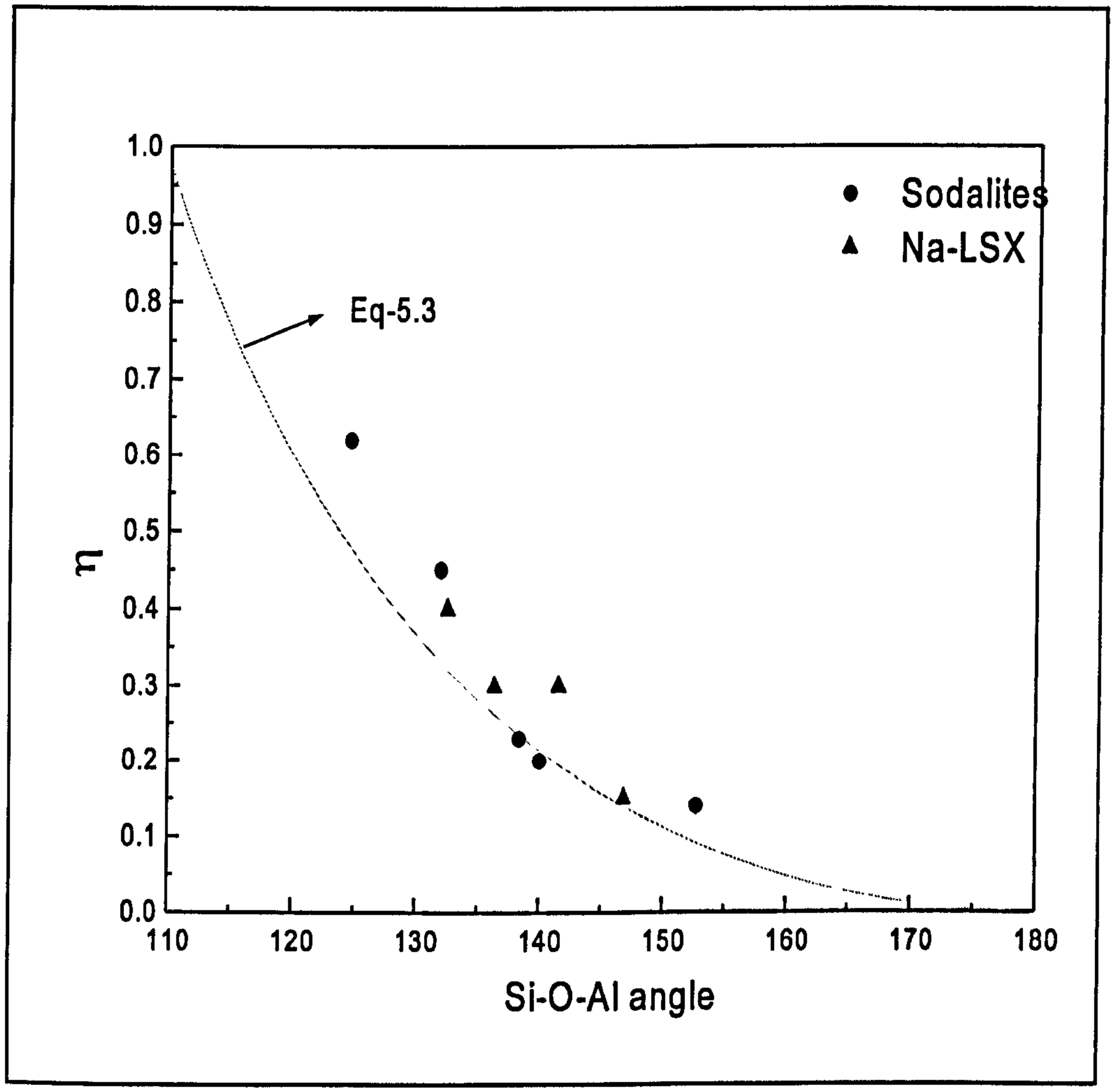

Figure 5.9. Asymmetry parameters of sodalite-kalsilite (filled circles) and Na-LSX (triangle) as a function of Si-O-Al angle. The solid line represents the equation 5.3.

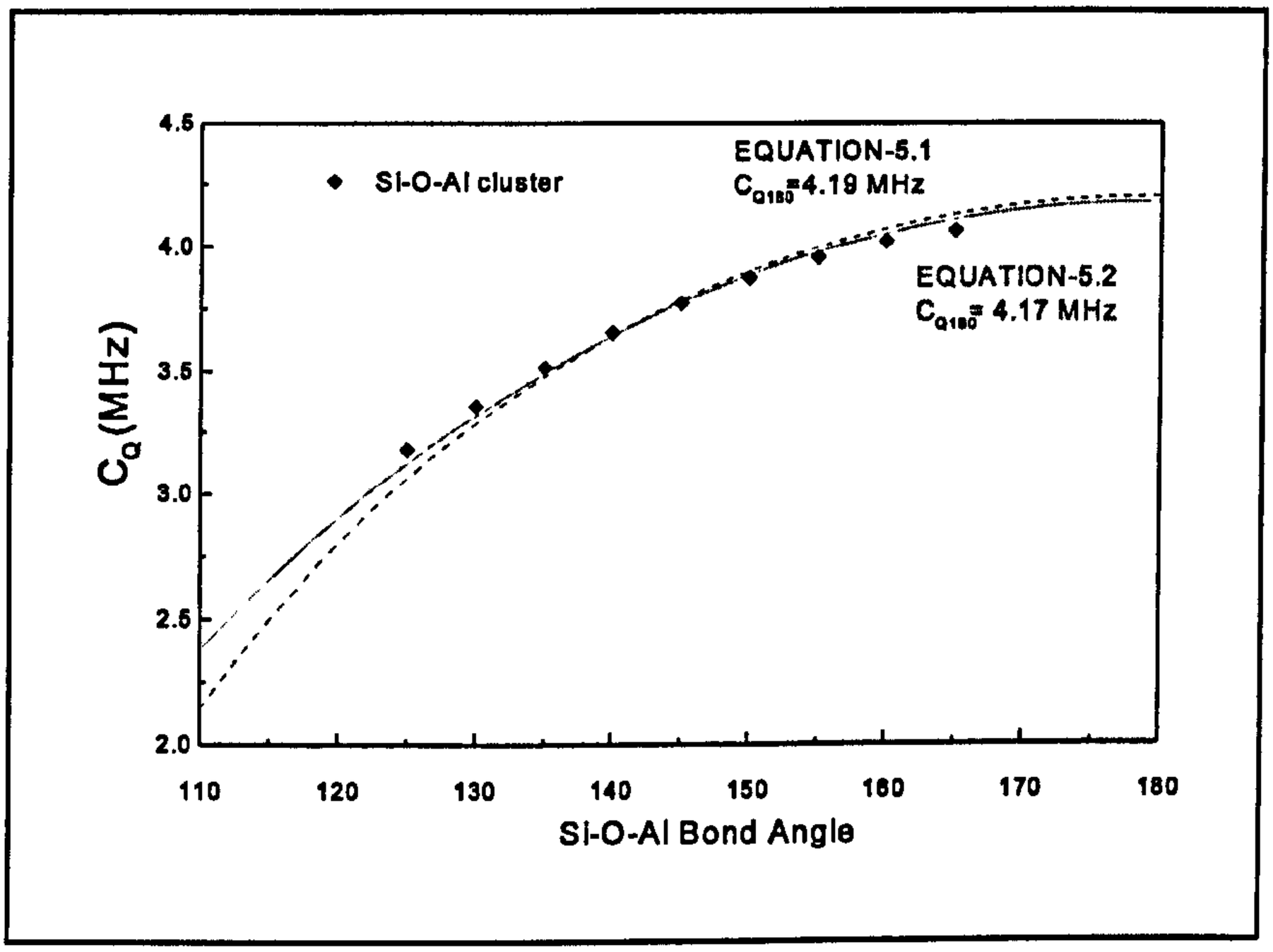

(a)

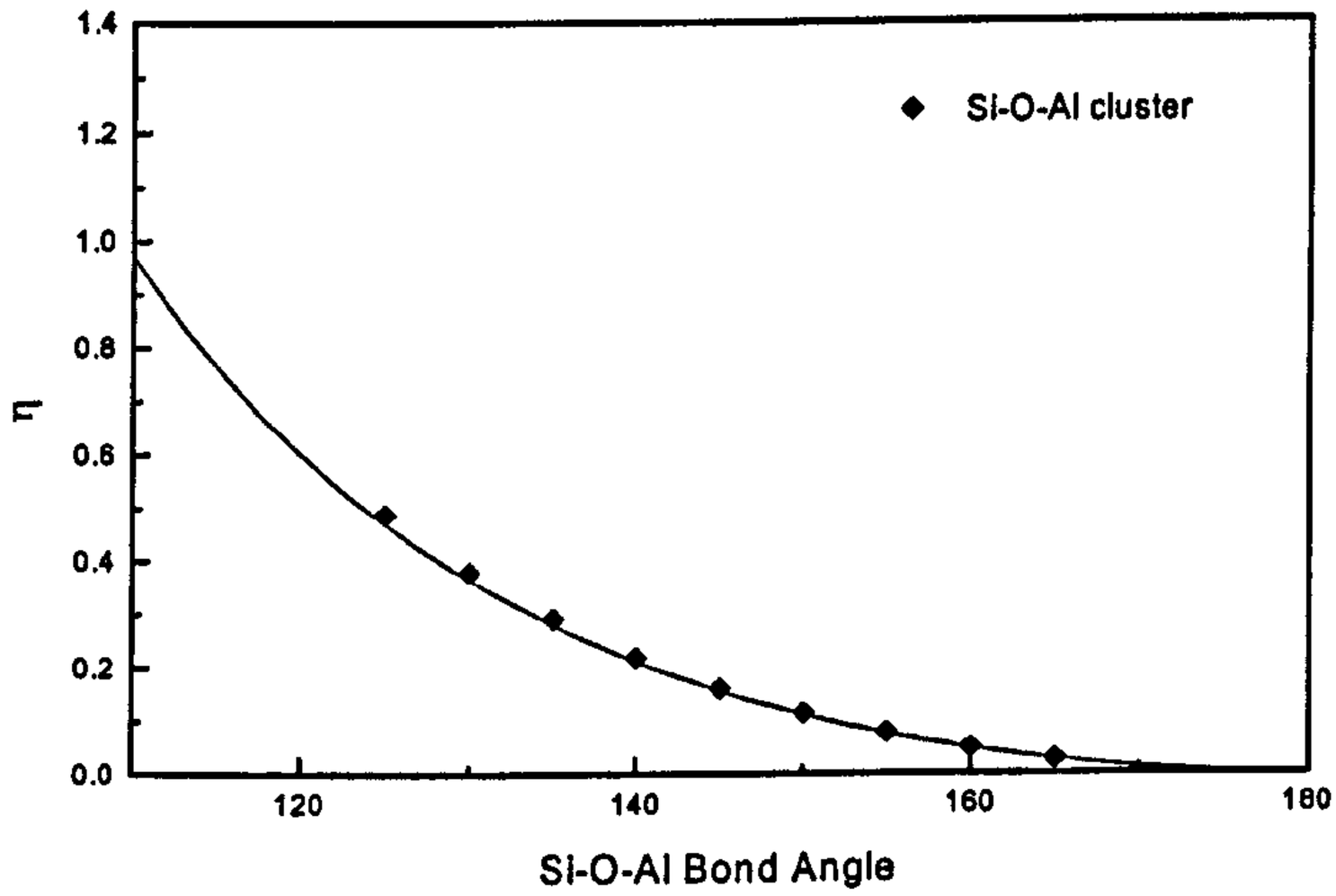

(b)

Figure 5.10. Cluster calculation of model $(OH)_3Si\text{-}O\text{-}Al(OH)_3$, a) calculated C_Q as a function of Si-O-Al angle. The dashed line represents the equation 5.1 and solid line represents the equation 5.2; b) calculated η as a function of Si-O-Al angle and the solid line represents equation 5.3.

5.4 Conclusion

The dependence of ^{17}O quadrupole coupling constant C_Q on the bond angle of Si-O-Al is functionally similar to that found for the Si-O-Si symmetric bond. In fact it very closely follows the correlation derived for Si-O-Si bonds (equation 5.2) but with a smaller C_{Q180}=4.13 MHz as expected when Al replace Si. The behaviour of the asymmetry parameter, of ^{17}O with Si-O-Al bond angles is also similar to that found for Si-O-Si bonds although it increased more rapidly at small angles. The cluster calculations modelled the behaviour of the field gradient quite well although the calculated asymmetry parameters were smaller than experimental values at low bond angles. Although the shift increases as the Si-O-Al angle decreases the variation does not seem to be monotonic.

We believe that it is possible to use ^{17}O NMR as a structural tool to distinguish and identify the multiple oxygen sites in materials whose structure is known or partially known. The result we presented here clearly shows a correlation between quadrupole coupling parameters of ^{17}O and Si-O-Al bond angle in aluminosilicates, and this correlation may be used for finding the bond angles and related structural parameters by simply simulating the ^{17}O NMR spectrum and obtaining the C_Q, and η.

References

[1] S. Ramdas, J. Klinowski, Nature,1984, Vol: 308,521-523.

[2] J.M. Newsome, J. Phys. Chem., 1987,91,1259-1261.

[3] J.M. Thomas, C.A. Fyfe, S. Ramdas, J. Klinowski, G.C. Gobbi, J. Phys. Chem., 1982, 86, 3061-3064

[4] R.H. Jarman, JCS Chem. Commun., 1983,512-513.

[5] A.R. Grimer, F. Von Lampe, M. Tarmek, E. Lipmaa, Chem.Phys. Lett., 1983,97,185-187

[6] M.T. Weller, G. Wong, J. Chem. Soc., 1988, 1103-1104.

[7] H.S. Jacobsen, P. Norby, H. Bildose, H.J. Jacobsen, Zeolites, 1989,9,491.

[8] A.E. Geissberger, P.J. Bray, J. Non-Cryst. Solids, 54 (1983),121

[9] S. Schramm, R.J. Kirkpatrick, E. Oldfield, J. Am. Chem. Soc. 105 (1983) 2483.

[10] H.K.C. Timken, S.E Schramm, R.J. Kirkpatrick, E. Oldfield, J. Phys. Chem. 91 (1987) 1054.

[11] T.H. Walter, G.I. Turmer, E. Oldfield, J. Mag. Reson. 76 (1988) 106.

[12] K.T. Mueller, J.H. Baltisberger, I.E.W. Wooten, A.Pines, J. Phys. Chem. 96 (1992) 7001.

[13] J.A. Tossell, P. Lazzeretti, Chem. Phys. Lett., 1987, 112, 205.

[14] J.A. Tossell, P. Lazzeretti, Phys. Chem. Miner., 1988, 15, 564.

[15] C.G. Lindsay, J.A. Tossell, Phys. Chem. Miner., 1991, 18, 191.

[16] I. Farnan, P.J. Grandinetti, J.H. Baltisberger, J.F. Stebbins, U. Werner, M.A. Eastman, A. Pines, Nature, 1992, 358, 31.

[17] K.E Vermillin, P. Florian, P.J. Grandinetti, J. Chem. Phys. 108 (1988) 7274.

[18] P.J. Grandinetti, J.H. Baltisberger, I. Farnan, J.F. Stebbins, U. Werner, A. Pines, J. Phys. Chem. 99 (1995) 12341.

[19] C.H. Townes, B.P. Dailey, J. Chem. Phys. 17 (1949) 782.

[20] U. Sternberg, Solid State Nuclear Mag. Reson., 2 (1993)181.

[21] I. Hassan, H.D. Grundy, Acta Cryst., 1984, B40, 6-13.

[22] R. Barrer, D.E.W. Vaughan, J. Chem. Solids, 1971, 32, 731-743

[23] G. Engelhardt, S. Luger, C. Buhl, J. Felsche, J. Zeolites, 9 (1989) 182.

[24] W. Depmeier, Acta. Crystallogr., B40,(1984),185.

[25] L. Pauling, Z. Kristallogr., 1930,74, 213-225.

[26] P. Smith, S. Garcia-Blanco, L. Rivoir, Z. Kristallogr., 1961, 115, 460-463

[27] W. Depmeir, J. Appl. Cryst., 1979, 12, 623-626.

[28] S.D. McLaughlan, D.J. Marshall, Phys. Lett. A, 1970, 32, 343-344.

[29] W.M. Meier, Zeolite Structures In Molecular Sieves, London: Society of Chemistry for Industry, pp. 10-27.

[30] H. Nyman, B.G. Hyde, Acta Cryst., 1981, A37, 11-17.

[31] C.M.B. Handerson, D.Taylor, Spectrochim.Acta. Part A, 1977, 33, 283-290.

[32] D.Taylor, C.M.B. Henderson, Phys. Chem. Miner., 1978, 2, 325-336.

[33] M.J. Dempsey, D. Taylor, Phys. Chem. Miner.1980,6, 197-208.

[34] A.J. Perotta, S.M. Smith, J.V. Smith, Min. Mag. 35 (1965)588-595.

[35] C. Capobianco, M. Carpenter, American Min., 74(1989)797-811.

[36] D.L. Hamilton, C.M.B. Henderson, Min. Mag., 36 (1968) 832-838.

[37] Aspect 3000 MSL software Manual, Bruker Manual 1986.

[38] Win_NMR, Software Manual, Bruker 1997.

[39] U.T. Pingel, J.P. Amoureux, T. Anupold, F Bauer, H. Ernst, C. Fernandez, D. Freude, A. Samoson, Chem. Phys. Lett., in press.

[40] Private connection from Prof. Ray Dupree, University of Warwick, Department of Physics.

Chapter 6

O-17 Multiple Quantum Magic Angle Nuclear Magnetic Resonance Study of Aluminosilicate Glasses

6.1 Introduction

Aluminium containing oxide crystals and glasses are abundant in nature as well as being among the most commonly used technological materials. Understanding the structures of these materials is thus fundamental to many problems in earth and in materials sciences. In that respect, there is a long standing interest in understanding the structure of aluminosilicate glasses in relation to their material properties. The structure of aluminosilicate glasses with the general formula of $MO\text{-}Al_2O_3\text{-}SiO_2$ is more complicated. The network of aluminosilicate glasses consist of SiO_4 tetrahedra and AlO_4 tetrahedra which may replace the SiO_4 leading to a wide variety of structural subunits. A detailed structural model for aluminosilicate glasses describes them in terms of $Q^n(mAl)$ building units similar to that of silicates. The charge balance of this unit is provided by an alkali or alkaline earth metal cation [1]. This model defines a total set of 15 different $Q^n(mAl)$ units, where n=0-4 and m=0-n, shown in table 6.1[2]. However in an aluminosilicate glass only three of these fifteen units are expected to form as main building units. The types and the molar fractions of the $Q^n(mAl)$ units can be determined from the overall chemical composition of the sample by assuming; a) that only $Q^n(mAl)$, $Q^{n+1}(mAl)$ and $Q^{n-1}(mAl)$ units, i.e. at maximum two NBO oxygen, can be present in a given glass, b) tetrahedral Al is substituted in the most polymerized Q^n unit , i.e. with the lowest number of NBO oxygen, c) in the composition range $MO \geq Al_2O_3 \leq 0.5SiO_2$ all Al is tetrahedrally bound in the aluminosilicate network and follows Lowenstein's

rule which states that Al-O-Al linkages are prohibited and the Si/Al ratio reaches 1 at best [3], d) excess Al forms neutral species and does not act as a network modifier. Mysen et al. do not agree with the last part of this model since they claim Al^{3+} acts as a network modifier when Al^{3+} is in excess over the charge balancing alkaline earth cations (e.g., Ca^{2+}) from the Raman studies of sodium, calcium and magnesium aluminosilicacate glasses [4][5][6].

The classical view of the aluminosilicates tells us that for a fully linked network, 2 oxygen atoms are needed for each tetrahedron and aluminum oxide provides only 1.5 oxygen for each tetrahedron. The remaining oxygens are provided by the alkali or alkaline earth oxides which are used for formation of AlO_4 tetrahedra. Furthermore the alkali or alkaline earth cation provides the necessary charge balance to compensate the excess negative charge of aluminium oxide. Since each added aluminium removes one NBO (nonbridging oxygen), when the total concentration of modifier oxides is equal to that of alumina, the structure should be fully polymerized and no NBO's should be present. Although the physical properties suggest the validity of this structural model, spectroscopic observations have not always supported it [7][8] and this classical approach is no longer valid when the amount of alumina exceeds the total modifier oxides in a glass. Such glasses are called peraluminous glasses. The structural role of Al^{3+} in these glasses where there is insufficient metal cations available for electrical charge balance is subject to some controversy. It was suggested by Day et al., that the excess aluminium in aluminosilicate glasses and melts with Al/Si>1 occurs in octahedral coordination [9][10][11]. Lacy [12] considered the coordination of aluminium in detail

***Table 6.1** Fifteen Qⁿ(mAl) units and their structural representation in aluminosilicates [2].*

Q unit	Structure	Q unit	Structure
Q^0	O OSiO O	$Q^3(2Al)$	O SiOSiO Al O Al
Q^1	O OSiO Si O	$Q^3(3Al)$	O AlOSiO Al O Al
$Q^1(1Al)$	O OSiO Al O	Q^4	Si O SiOSiO Si O Si
Q^2	O SiOSiO Si O	$Q^4(1Al)$	Si O SiOSiO Al O Si
$Q^2(1Al)$	O SiOSiO Al O	$Q^4(2Al)$	Si O AlOSiO Al O Si
$Q^2(2Al)$	O AlOSiO Al O	$Q^4(3Al)$	Si O AlOSiO Al O Al
Q^3	O SiOSiO Si O Si	$Q^4(4Al)$	Al O AlOSiO Al O Al
$Q^3(1Al)$	O SiOSiO Al O Si		

and his argument is as follows: in a glass of $NaAlSi_3O_8$ composition the alkali cation will occupy the interstices of the network so that each of their oxygen neighbours is shared between two tetrahedral units. The univalent cations provide the charge balance. In a typical binary soda-silica glass the sodium ions act as network modifier cations, breaking the network. Around each sodium ion, there are a proportion of nonbridging oxygens which are directly linked to the molar proportion of the alkali, and also there is a proportion of oxygens each shared between two tetrahedral groups. If it is assumed that aluminium occurs as an interstitial species it should have a variable number of accidental oxygen neighbours. The number of the oxygens could be four, five or six, since the screening would be very poor for three oxygens and more than six oxygen can not be gathered touching an aluminum atom. Such a small highly charged ion with an oversize oxygen cage would constitute an unstable configuration of high free energy. Therefore for the glass composition above, aluminium cannot act as an interstitial cation in a manner exactly comparable to that of sodium. Furthermore he suggested some hypothetical structures and showed the invalidity of those structures. Then he instead suggested a tricluster model for such glasses where three coordinated oxygens connecting three tetrahedra which may be one AlO_4 tetrahedron and two SiO_4 tetrahedra or two AlO_4 tetrahedra and one SiO_4 tetrahedron. However this model contradicts with Lowenstein's aluminum avoidance rule which states Al-O-Al linkages are prohibited and Si/Al ratio reaches 1 at best [3]. Later in 1966, Riebling et al [13], concluded from the viscosity and density data of alkali aluminosilicate melts that, although excess aluminium in glasses and melts with Al/Na>1 must form AlO_6, not every aluminum

atom occurs in octahedral environment.

For a binary silicate liquid (e.g., $CaSiO_3$ or Na_2SiO_3) the viscosity increases as the network modifier oxide (CaO or Na_2O) is replaced by Al_2O_3 and reaches a maximum when Na_2O/Al_2O_3=1 (or CaO/Al_2O_3=1) [11]. According to the conventional model of aluminosilicate structure [14][15], this viscosity increase arises from a gradual conversion of NBO to BO which in turn requires that all of the aluminium remain in tetrahedra, and each oxygen atom of the tetrahedra is bonded to only one other tetrahedral cation. Therefore for a glasses of tectosilicate composition, where the charge of the modifier cation equals to the number of aluminum atoms (as in $NaAlSi_3O_8$ or $CaAl_2Si_2O_8$), only BOs are present [9][10]. Stebbins et al. disagree with the classical view according to findings from the ^{17}O 3QMAS NMR measurements of $CaAl_2Si_2O_8$. They claim that considerable amount of NBO can be present in a tectosilicate glass [16] and suggest the formation of triclusters as shown in figure 6.1. and thus Al-O-Al linkages.

In general the formation of triclusters in aluminosilicates is found to be not very likely by many researchers on the basis of numerous quantum chemical studies which have found that the combination of an Al-O-Al corner sharing tetrahedral linkage and a Si-O-Si linkage to be higher in energy than two Si-O-Al linkages [17][18] which indicates the instability of Al-O-Al linkages [13]. However, these computational results are not in good agreement with the observations, since many crystalline framework silicates show considerable Al, Si disorder at high temperatures and must contain appreciable numbers of Al-O-Al linkages [19].

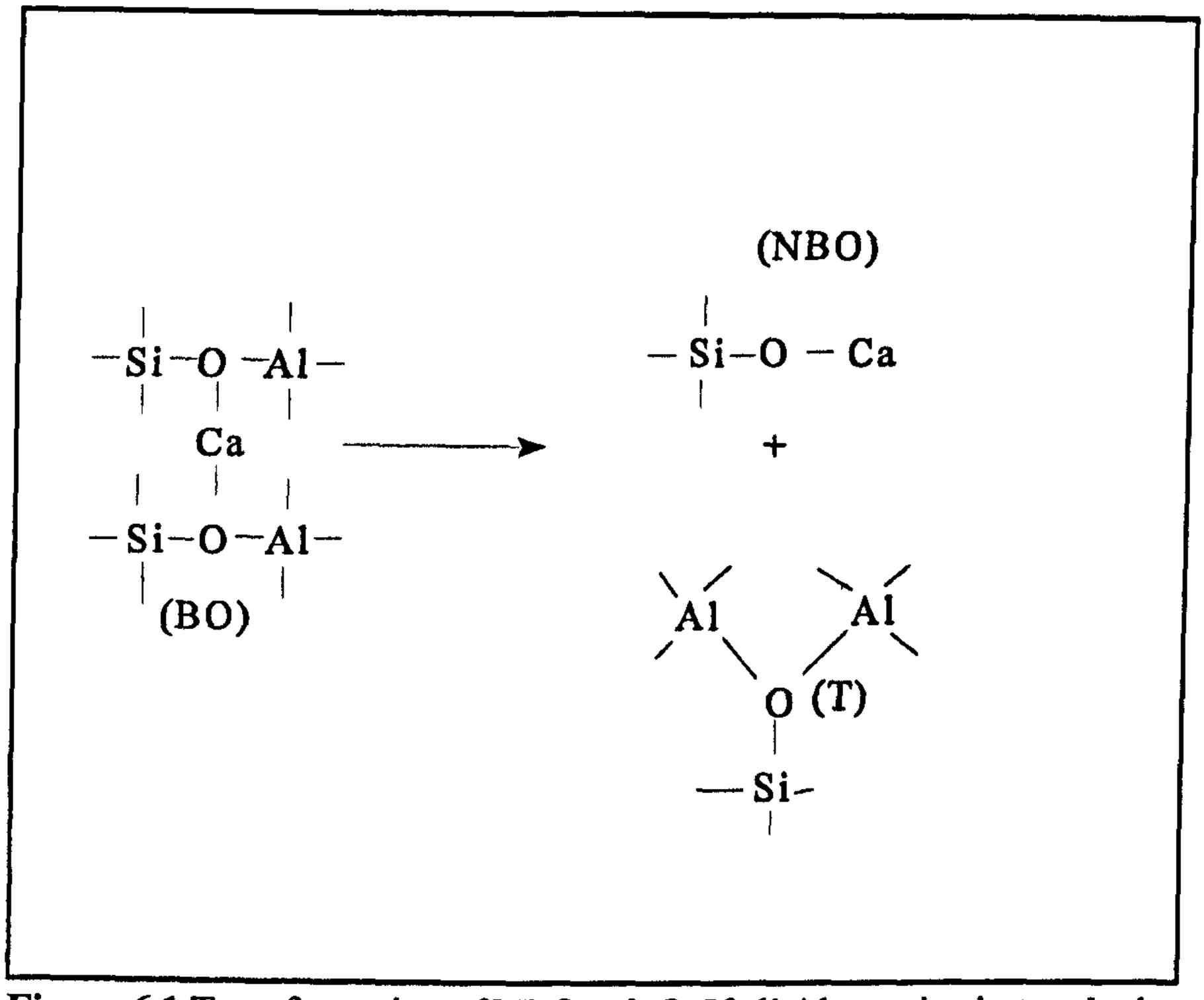

Figure 6.1 Transformation of NBO to BO. If all Al remains in tetrahedra the new structural unit formed is considered to be tricluster, or if AlO_5 or AlO_6 sites are formed, the tricluster oxygen (T) may itself behave as an NBO [14].

Tossel also investigated the molecular basis of the Al avoidance rule by performing ab initio self consistent field molecular orbital calculations on two different isomers of the molecular anion $Si_2Al_2O_4H_8^{2-}$, in which the Si and Al atoms are either alternating, i.e., ...Si-O-Al-O-Si-O-Al..., or paired, i.e., Si-O-Si-O-Al-O-Al..., around the four membered ring [14]. He concluded that the formation of alternating Si, Al structures are more likely than the formation of paired structures, by only a modest amount of energy, so that paired structures, e.g., Al-O-Al linkages, are possible in high temperature disordered materials.

As well as other experimental techniques (e.g, EXAFS, Raman spectroscopy, XRD...) aluminosilicates have also been investigated by means of mainly ^{29}Si and ^{27}Al

MAS NMR [20][21][22][23] and these investigations revealed that the aluminum is tetrahedrally coordinated in compositions at around M/Al=1 where M=Li, Na, K, Ca and therefore Lowenstein's rule was obeyed. Engelhardt et al [24], from the ^{29}Si and ^{27}Al MAS NMR of aluminosilicate glasses with composition $CaO.Al_2O_3.SiO_2$ concluded; a) that one to three main types of Q_n^m building units may be present in the glass network, b) that the coexisting Q_n^m units differ by only one Si-O-T (T=Si,Al) and the tetrahedrally coordinated aluminum is preferentially bound to the most polymerized Q_n^m units present in the glass, c) if the composition is $CaO=Al_2O_3 \leq SiO_2$ the structure is a fully polymerized three dimensional network, and increase of the CaO content over the Al_2O_3 results in depolymerization of the glass network, d) for glasses with composition, $CaO \geq Al_2O_3 \leq 0.5SiO_2$ all aluminum is in tetrahedral coordination, in compositions with $CaO \leq Al_2O_3$ or $Al_2O_3 > 0.5SiO_2$ aluminum is present as neutral extra-network Al species (i.e., not bound to the tetrahedral aluminosilicate network of the glass) in the form of $Al^{3+}(AlO_2^-)$ or triclusters.

As already stated, although oxygen is the most abundant element in the aluminosilicates, the NMR study of ^{17}O has not attracted much attention due to its low natural abundance and its spin quantum number I=5/2, which means it has quadrupolar interaction, the effect of which is described in chapter 3. It has been shown that ^{17}O NMR is a promising method for studying the structure and bonding in these materials [25][26][27]. Especially ^{17}O NMR studies shows that bridging oxygens (which connect two tetrahedra e.g., Si-O-Al, Si-O-Si) and nonbridging oxygens have distinctly different chemical shifts and quadrupolar coupling constants [28][29]. However lack of resolution of ^{17}O MAS NMR spectra due to broadening caused by the quadrupolar interaction,

prevented observation and detection of different types of bridging oxygens in detail in aluminosilicates until recently. The development of MQMAS, DAS and DOR techniques provided very detailed high resolution NMR spectra as demonstrated by recent work on zeolites and on glasses [30][31][32]. On the other hand it is still difficult to observe minor amounts of Al-O-Al linkages and lack of data on this kind of site in crystalline model compounds caused great difficulty for the characterization of these sites. Tossel have predicted the NMR parameters for different linkages in the aluminosilicates by using ab initio calculations, given in table 6.2, [19].As table 6.2 shows, Si-O-Si has the biggest quadrupolar coupling constant, while Al-O-Al exhibits the smallest quadrupolar coupling constant. The quadrupolar coupling constant of Si-O-Al is always intermediate between Si-O-Si and Al-O-Al.

The purpose of this study is to probe the structure of aluminosilicate glasses by means of ^{17}O NMR spectroscopy and to use multiple quantum NMR as well as MAS to be able to obtain high resolution spectra which may reveal the possible Si-O-Al, Si-O-Si, Al-O-Al species in these glasses. ^{29}Si and ^{27}Al NMR were also performed to obtain more information on these glasses.

6.2 Experimental Procedures

We have investigated a range of sodium aluminosilicate glasses with different Si/Al (R) ratio. Since we performed ^{17}O MAS MQ NMR on these samples as well as ordinary MAS, samples were isotropically enriched in ^{17}O in the range of 20-25%.

Table 6.2 *Calculated values of the magnitude of q and NQCC at the oxygen nucleus in a series of four membered ring molecules [19].*

Molecule	bridging bond	q (au)	NQCC (MHz)
$Si_4O_4H_8$	Si-O-Si	0.945	4.96
$Al_4O_4H_8^{4-}$	Al-O-Al	0.516	2.71
$Si_2Al_2O_4H_8^{2-}$	Si-O-Al	0.746	3.91
$Si_2Al_2O_4H_8^{2-}$	Si-O-Si	0.935	4.91
Si...Si...Al...Al...	Si-O-Al	0.727	3.82
	Al-O-Al	0.512	2.68
$Si_2Al_2O_4H_{12}^{2+}$	Si-(OH)-Al	1.476	7.75
$Si_2Al_2O_4H_{12}^{2+}$	Si-(OH)-Si	1.616	8.48
...Si...Si...Al...Al	Si-(OH)-Al	1.435	7.53
$Si_2Al_2O_4H_8Na_4^{2+}$	Si(ONa)-Al	0.699	3.67
$Si_2Al_2O_4H_8Na_4^{2+}$	Si-(ONa)-Si	0.882	4.63
...Si...Si...Al...Al...	Si-(ONa)-Al	0.726	3.81
	Al-(ONa)-Al	0.447	2.34

The enrichment procedure was explained in chapter-4. In order to prepare enriched glasses $Si^{17}O_2$, $Na_2C^{17}O_3$, and $Al_2{}^{17}O_3$ were mixed in appropriate amounts and ground with a pestle and mortar. Then the mixture was placed into a platinum tube which was then sealed at both ends by torch or arc welding, to prevent the oxygen exchange. The sealed platinum tube was then placed into the high temperature melting furnace and was heated up to 1610-1650°C. In order to obtain homogeneous melts the platinum tube was left at that temperature for three hours. Then the tube was taken out from the furnace and placed into water to obtain fast cooling. Samples were glassy by appearance and by X-ray. After grinding, the samples were ready for NMR investigations.

6.3 Results and Discussion

6.3.1 Si-29 MAS NMR

As mentioned above we have investigated four sodium aluminosilicate glasses with different Si/Al ratio (R). In order to characterize and confirm their compositions we have performed ^{29}Si NMR on these glasses in the field of 8.45T. ^{29}Si MAS NMR spectra of three glasses are given in figure 6.2. They are featureless, broad lines as one expects from a glass and also they are slightly asymmetric. The first sodium aluminosilicate glass (glass-1) with composition R=3, has a peak at about -97ppm with line width at half maximum about 18ppm. The peak of the second glass sample (glass-2) where R=1.5, appears at about -89 ppm and the spectrum width decreases compared to the first glass by about 2ppm to 16ppm. Unfortunately we were not able to do ^{29}Si MAS NMR on the third glass (glass-3) due to loss of the whole sample after a crash of the rotor while it was spinning at 5 kHz. One of the main problems encountered with making these glasses was that the end product was a very small amount. This is due to the small amount of enriched $Si^{17}O_2$ we were able to produce (about 1g) and the cost of producing large amounts of enriched $Si^{17}O_2$, $Na_2{}^{17}O$, and $Al_2{}^{17}O_3$. Finally the fourth glass (glass-4), where R=0.7, has a peak at about 82ppm with a width at half maximum about 6ppm. These chemical shift values and the spectrum widths are in good agreement with Stebbins et al. [33] for glasses of these compositions. Therefore we were able to confirm the nominal composition of these glasses as well as Q^n(mAl) species in these glasses. However the width at half maxima of the spectrum of glass-4 differs from that of the corresponding glass investigated by Stebbins [33] since it is smaller. The chemical shifts and the widths of the ^{29}Si NMR spectra are given in table 6.3.

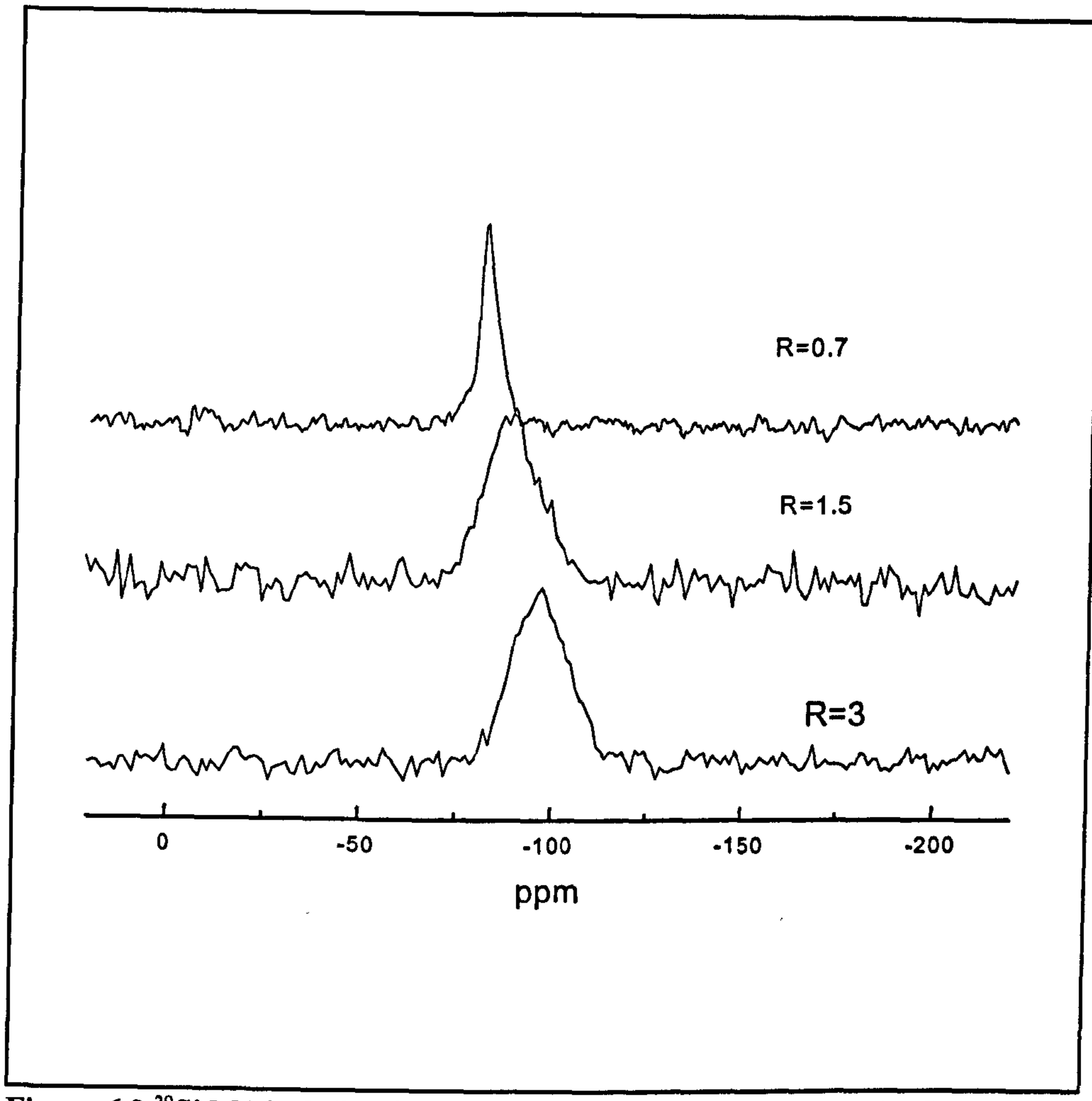

Figure 6.2 ^{29}Si MAS NMR of glasses investigated in this study in the field of 8.45 T.

Table 6.3 ^{29}Si NMR parameters of aluminosilicate glasses investigated in this study.

Sample	Chemical shift (±1ppm)	width (±1ppm)	Composition	$Q^n(mAl)$[2]
Glass-1	-97	18.0	Na_2O-Al_2O_3-$6SiO_2$	$Q^4(1Al)$
Glass-2	-89	16.0	Na_2O-Al_2O_3-$3SiO_2$	$Q^4(3Al)$
Glass-3			Na_2O-Al_2O_3-$2SiO_2$	
Glass-4	-82	6.0	Na_2O-Al_2O_3-$1.4SiO_2$	$Q^4(4Al)$

It is clear that as R(Si/Al) ratio decreases the ^{29}Si peak shifts towards higher frequency (more positive shifts) due to replacement of silicon atoms by aluminum atoms. Each replacement of silicon atom with an aluminum atom results in about 5 ppm shift [2]. The widths of the spectra also decrease from about 18ppm to about 6 ppm as the R(Si/Al) decreases. This may be due to that as the R decreases the number of aluminums around the silicon increases resulting in a decrease in the number of possible different $Q^n(mAl)$ species in the glass. Therefore for the glass-4, where R=0.7, only $Q^4(4Al)$ units are present which in turn gives the norrow peak.

6.3.2 Al-27 MAS NMR

We have performed ^{27}Al MAS NMR on the four sodium aluminosilicate glasses in an external field of 14.4T using a Chemagnetics 4mm probe. Samples were spun at about 15 kHz. Figure 6.3 shows the ^{27}Al MAS NMR spectra of four glasses which are broad and with no structure. The chemical shifts are in the approximate range of 54-66 ppm which is typical of tetrahedrally coordinated AlO_4 groups. There are no signs of second site in the first three glasses. However glass-4 with $Al_2O_3/NaO>1$ composition a further weak signal was observed at chemical shift about 6ppm which indicates the presence of a small amount of six coordinated AlO_6 octahedra in this glass. Engelhardt et al., observed a similar spectrum in calcium aluminosilicate glasses with $Al_2O_3/CaO>1$ [1]. The line width of the spectrum seems to decrease as the R(Si/Al) ratio decreases although the widths of glass-3 with R=1 and glass-4 with R=0.7 are quite similar. This may indicate a decrease of the second order quadruple broadening. Table 6.4 shows the ^{27}Al MAS NMR parameters of the aluminosilicate glasses we

investigated.

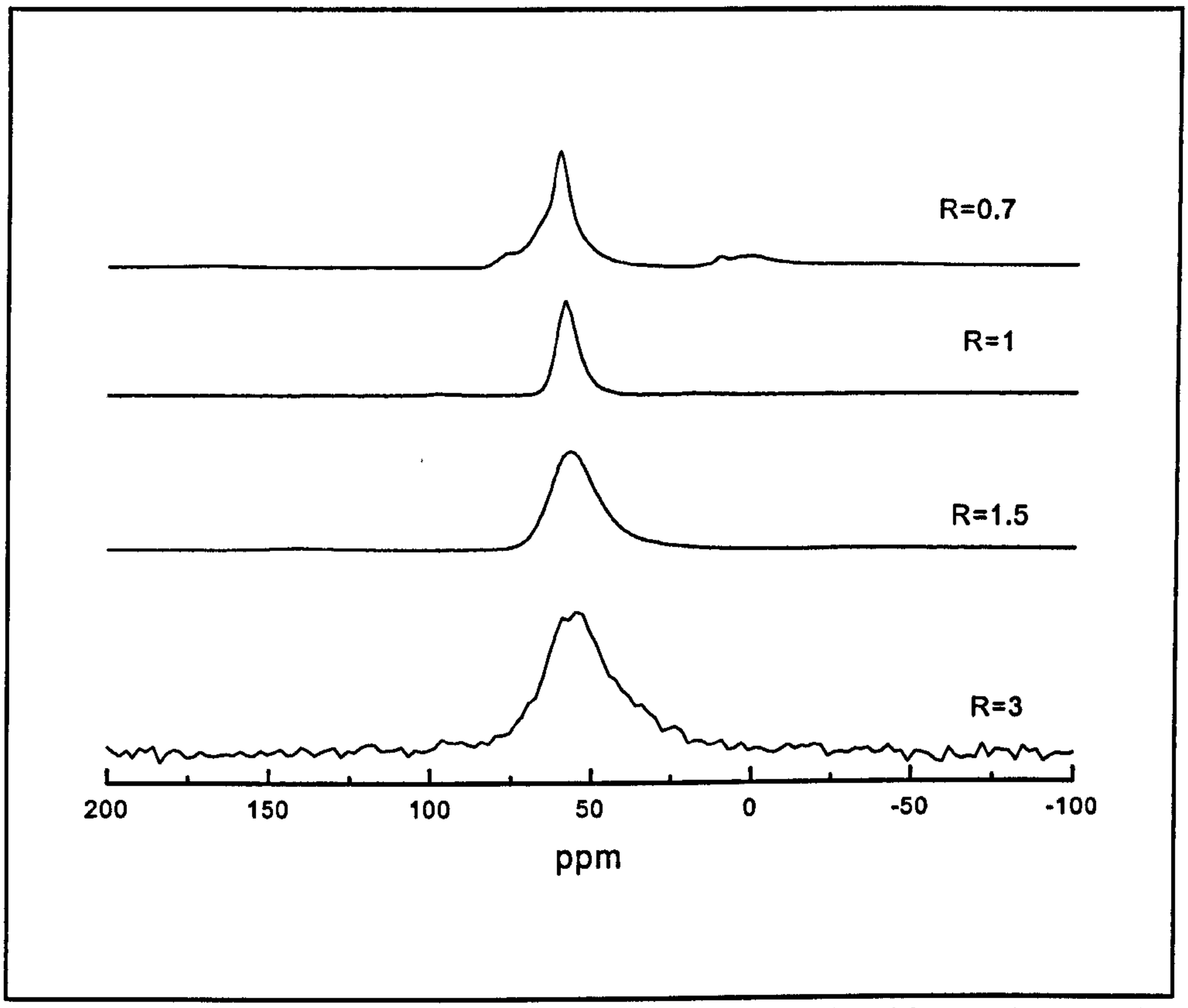

Figure 6.3 ^{27}Al MAS NMR spectrum of sodium aluminosilicate glasses with different Si/Al (R) ratio investigated in this study.

Table 6.4 *^{27}Al NMR parameters of aluminosilicate glasses investigated in this study*

Sample	Composition	Peak position(ppm±1)	Width (ppm±1)
Glass-1 (R=3)	Na_2O-Al_2O_3-6SiO_2	54	24
Glass-2 (R=1.5)	Na_2O-Al_2O_3-3SiO_2	56	16
Glass-3 (R=1)	Na_2O-Al_2O_3-2SiO_2	57	10
Glass-4 (R=0.7)	Na_2O-Al_2O_3-1.4SiO_2	66	10

6.3.3 O-17 NMR

Although it is possible to obtain information from ^{29}Si and ^{27}Al NMR, undoubtably the most informative nucleus would be ^{17}O in the oxygen containing materials and particularly aluminosilicates. Its large chemical shift range and relatively small quadrupole moment mean that it has attractive NMR attributes. High resolution ^{17}O NMR has the potential to distinguish different types of bridging oxygen sites in framework aluminosilicates. Therefore we have performed ^{17}O MAS NMR as well as ^{17}O 3Q MAS NMR on the sodium aluminosilicate glasses to obtain high resolution.

MAS experiments were performed at two fields, 8.45T and 14.4T, spinning at about 10 kHz and 15-20 kHz respectively and the spectra are shown in figure 6.4 and 6.5. These spectra are broad and featureless and slightly asymmetric. There is little indication of possible Si-O-Al, Si-O-Si, Al-O-Al sites being present in these glasses. The chemical shift range is between 20-40 ppm.

Two dimensional 3Q MAS NMR experiments were performed by using the 'split t1' [34] pulse program which was explained in detail in chapter 4. The reason the 'split t1' pulse program was used is that the resulting 2D spectrum does not require shearing which may distort the lineshape [34].

Figure 6.6 shows the two dimensional 3Q MAS spectrum of glass-1 with composition of $Na_2O.Al_2O_3.6SiO_2$. The spectrum clearly shows two resolved peaks at about 22ppm and 32ppm in the MAS direction. The major peak at 22ppm is in similar position to Si-O-Al peaks previously reported in 3Q MAS studies of $NaAlSi_3O_8$ glass [30] and 3Q MAS studies of $NaAlO_2$ glass [32]. The second peak is also in a similar position to that reported in the ref [30] for the Si-O-Si site.

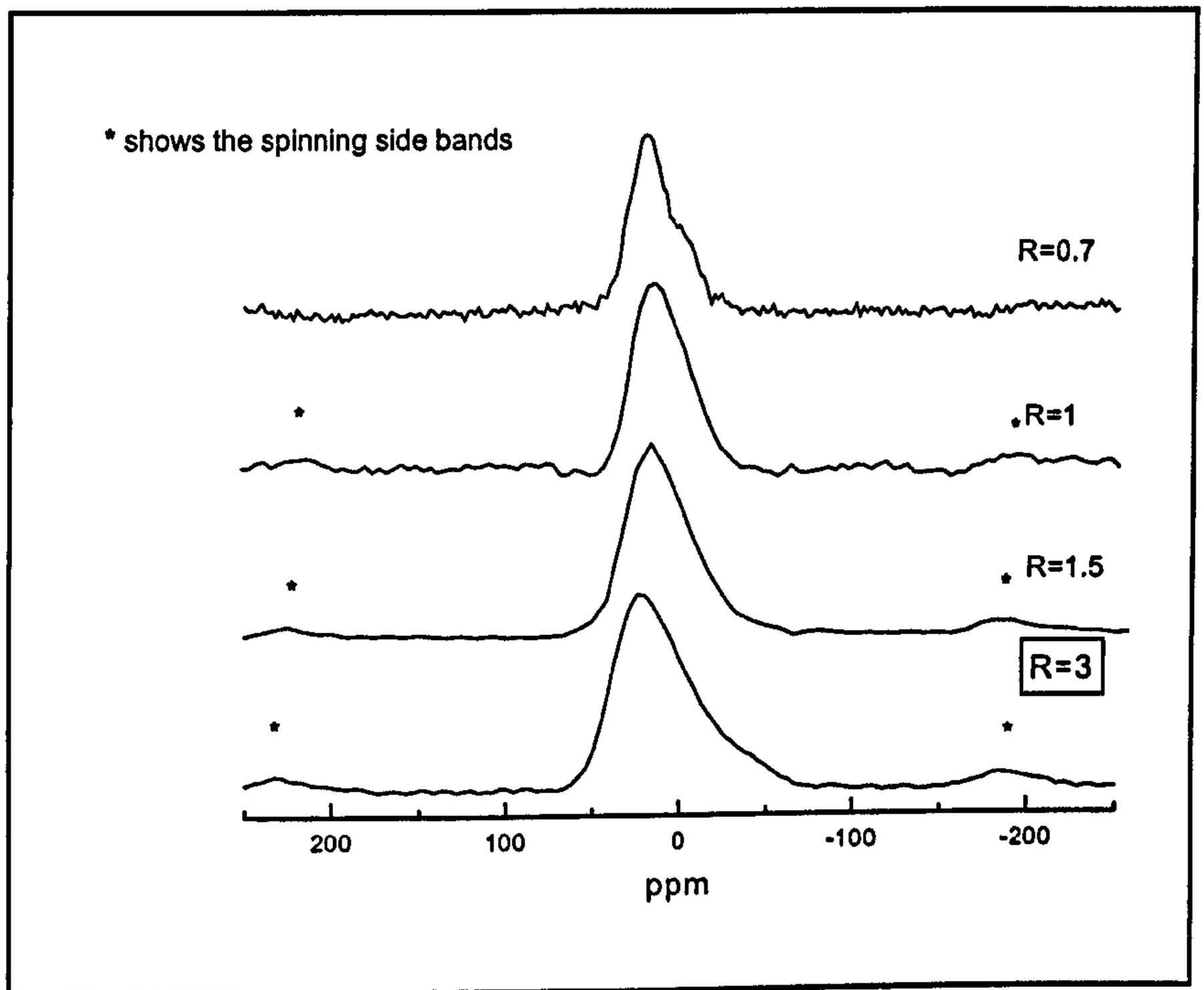

Figure 6.4 ^{17}O MAS NMR spectra of sodium aluminosilicate glasses, in the field of 8.45 T.

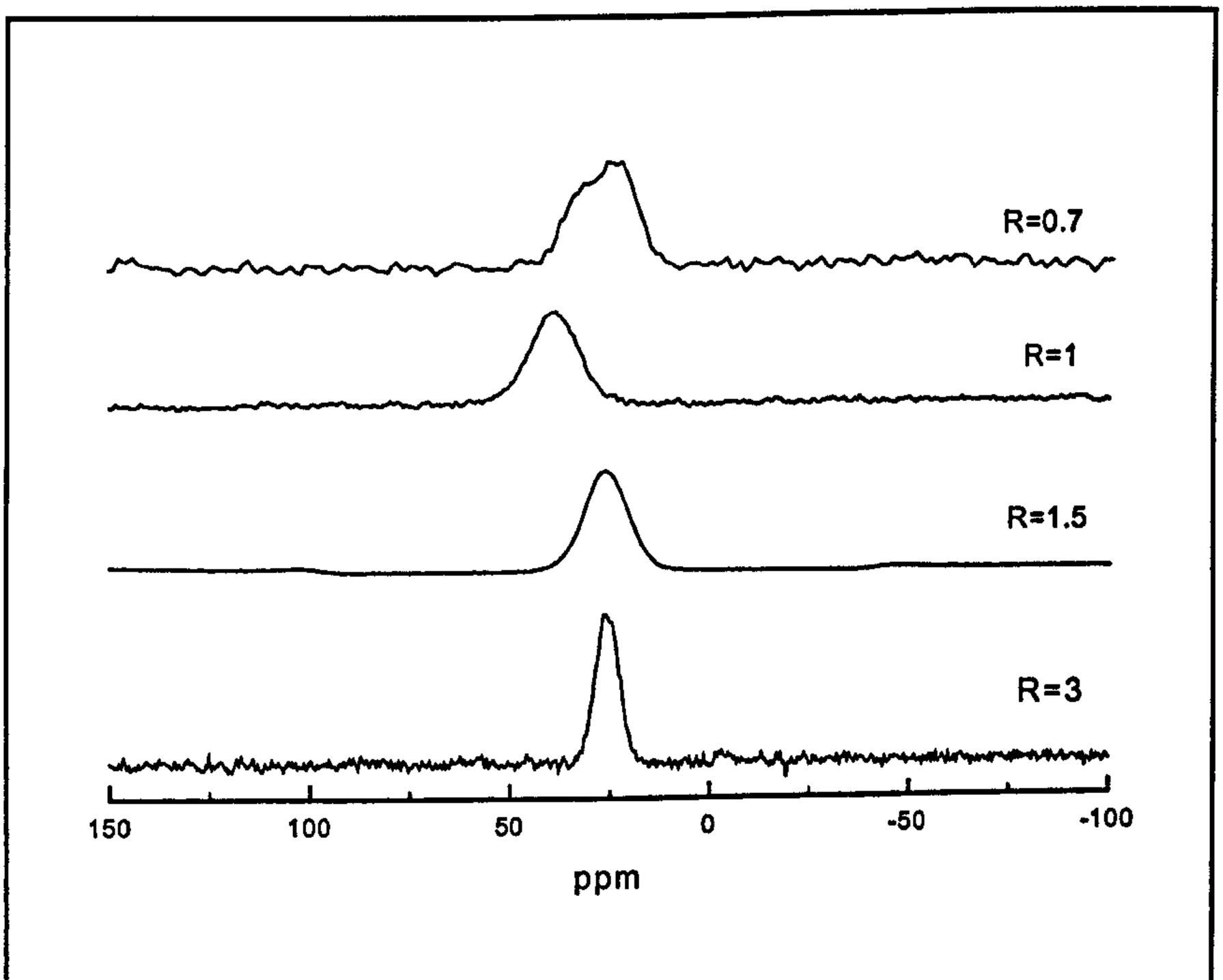

Figure 6.5. ^{17}O MAS NMR spectra of sodium aluminosilicate glasses in the field of 14.4T

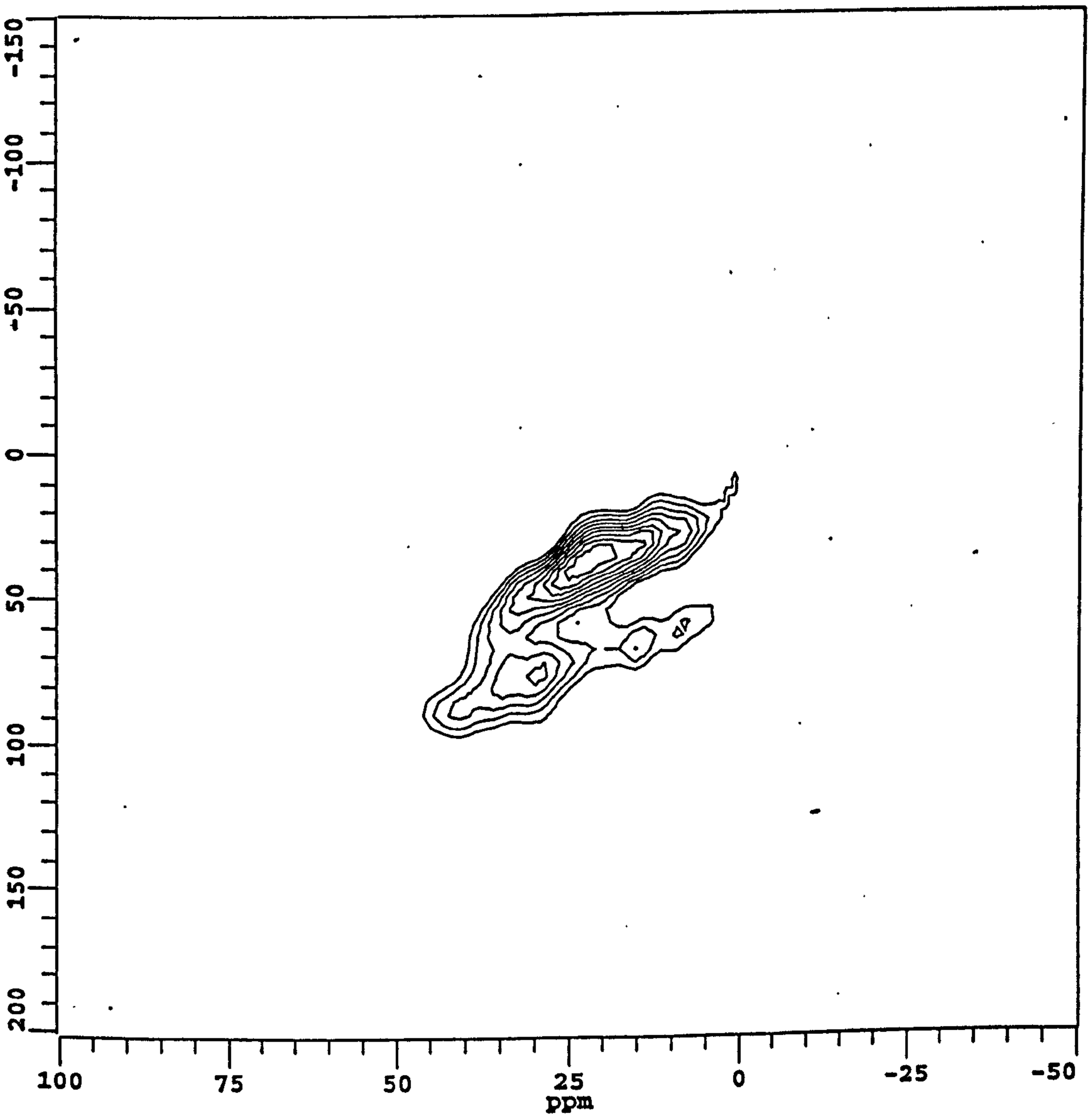

Figure 6.6 ^{17}O 3Q MAS NMR spectrum of glass-1 with R=3.

The shape of the peak, a narrow ridge aligned along a slope of 1, suggests the presence of a range of chemical shift distribution in the sample. In order to obtain quadrupolar parameters for both peaks, we simulated individual slices from each peak, shown in figure 6.7a and 6.7b. The values of quadrupolar parameters obtained from these simulations are given in table 6.5.

Table 6.5 *^{17}O quadrupolar parameters of two sites in the glass-1 obtained from the 3Q MAS NMR experiment.*

Site	C_Q (±0.3MHz)	η (±0.1)	δ(±3 ppm)
Si-O-Al	3.35	0.3	26
Si-O-Si	5.11	0.7	57

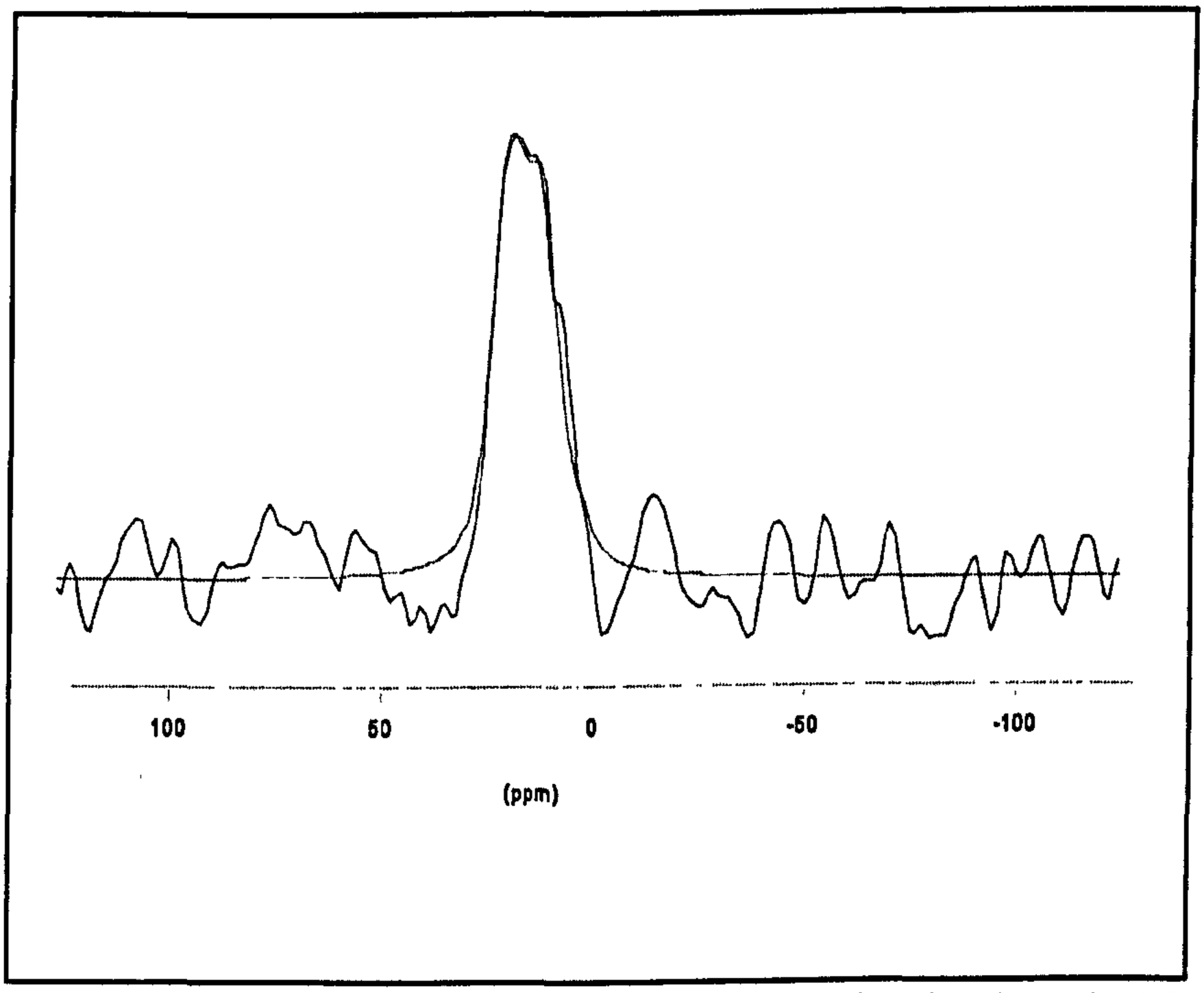

Figure 6.7a A slice of Si-O-Al site along the MAS direction from the 3Q MAS spectrum of glass-1 (R=3) and its simulation.

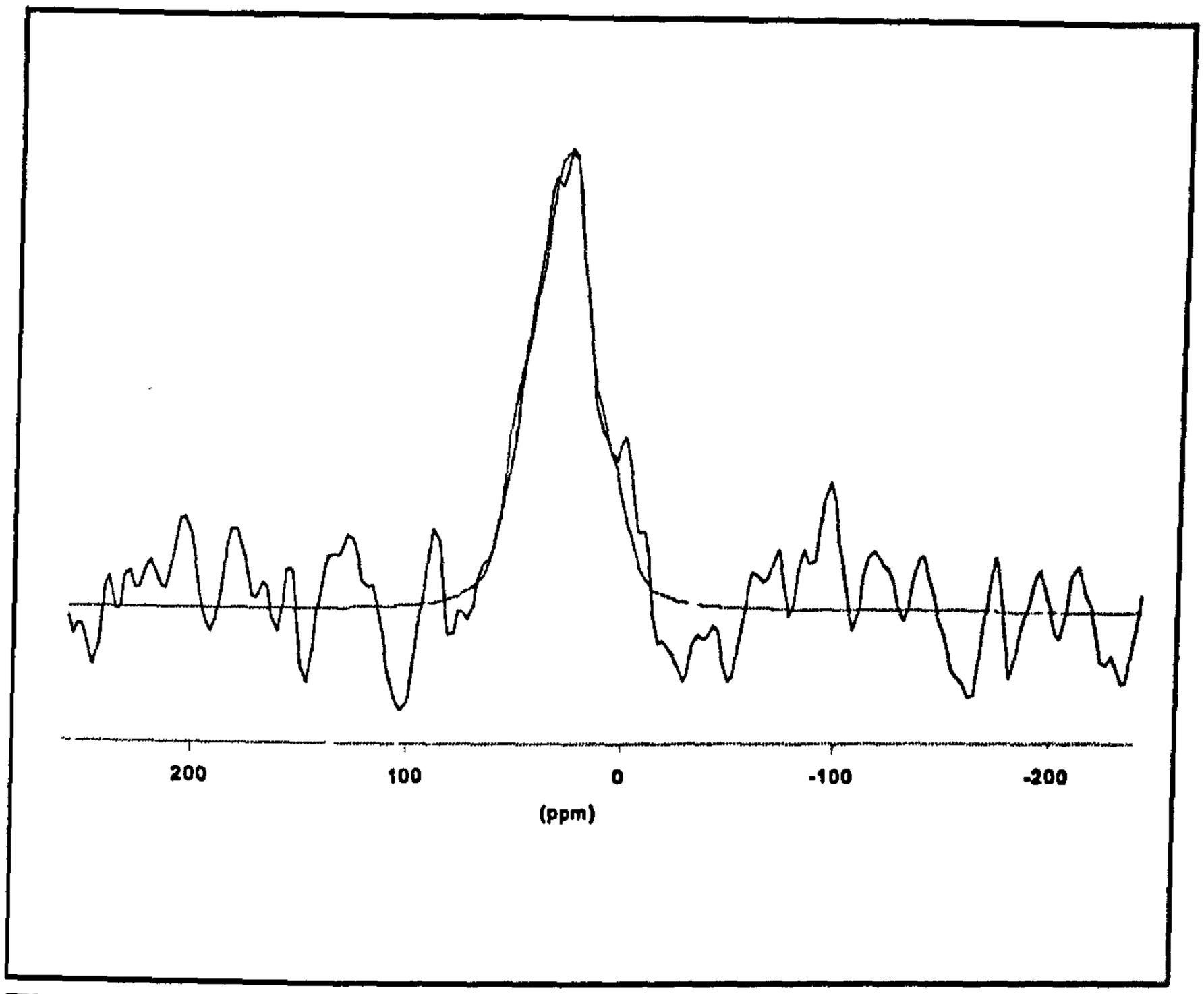

Figure 6.7b A slice of Si-O-Si site along the MAS direction form the 3Q MAS spectrum of glass-1 (R=3) and its simulation.

The 3Q MAS NMR spectrum of glass-2 also exhibits two resolved peaks similar to that observed for the glass-1, shown in figure 6.8. The first peak at about 25 ppm in the MAS dimension is attributed to the Si-O-Al site and the second peak at about 30ppm in the MAS dimension is attributed to the Si-O-Si site. Although the intensities from the MQ MAS NMR spectra can not be used quantitatively, the second peak, Si-O-Si, seems to decrease in intensity with decreasing Si/Al ratio from 3 to 1.5. The two peaks also lie along a slope of 1 which indicates the distribution of chemical shifts in the sample. The simulation of an individual slice was also carried out, shown in figure 6.9. The simulation for the second peak cannot be performed due to lack of any shape of the peak as a result of poor signal to noise. The quadrupolar parameters obtained from this simulation are C_Q=3.47 ±0.3 MHz, η=0.5±0.1 and the chemical shift (δ) is about 32ppm.

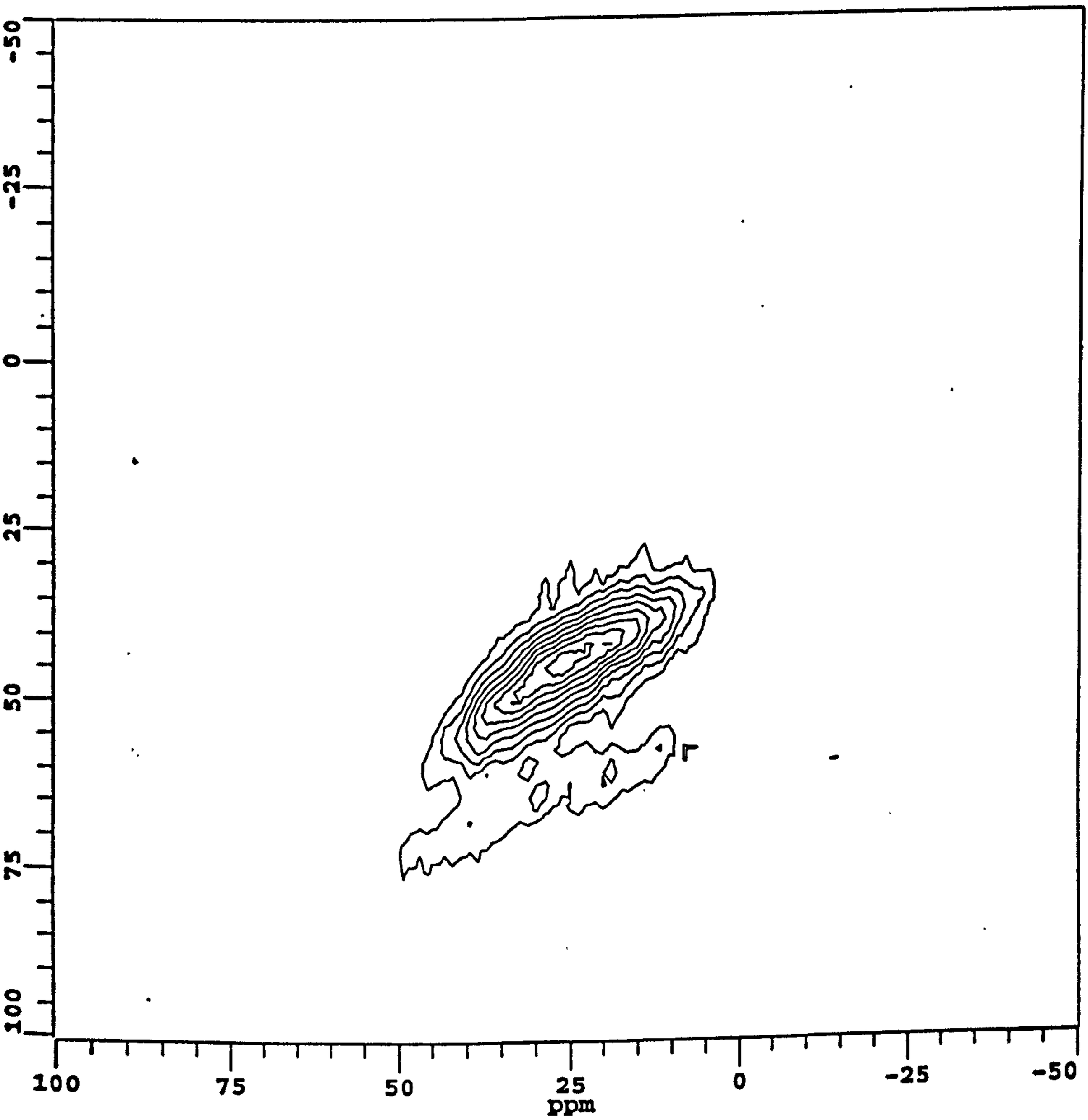

Figure 6.8 ^{17}O 3Q MAS NMR spectrum of glass-2 with R=1.5

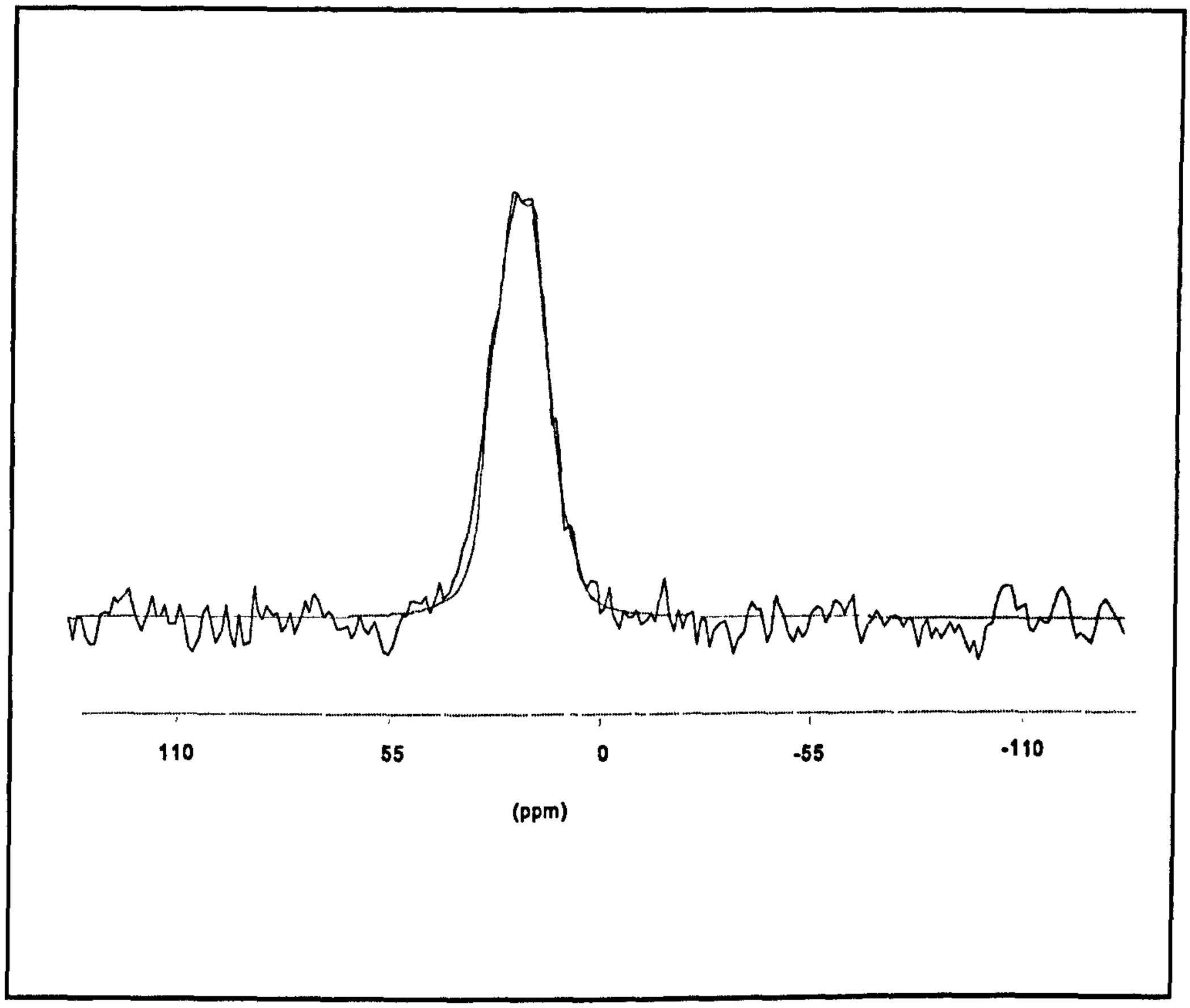

Figure 6.9 A slice of Si-O-Al along MAS direction from the 3Q MAS spectrum of glass-2 (R=1.5) and its simulation.

Figure 6.10 shows the 3Q MAS spectrum of glass-3 which shows only a single peak as expected from its stoichiometry. As its Si/Al ratio is 1 we would not expect to observe any Si-O-Si or Al-O-Al sites in this glass. The single peak appears at about 27ppm in the MAS direction and can be attributed to the Si-O-Al site. The simulation of a slice of this peak gives similar quadrupolar parameters to that obtained for the Si-O-Al site of the first two glasses which are C_Q=3.37 ±0.3 MHz, η=0.4±0.1 and δ= 32ppm, shown in figure 6.11.

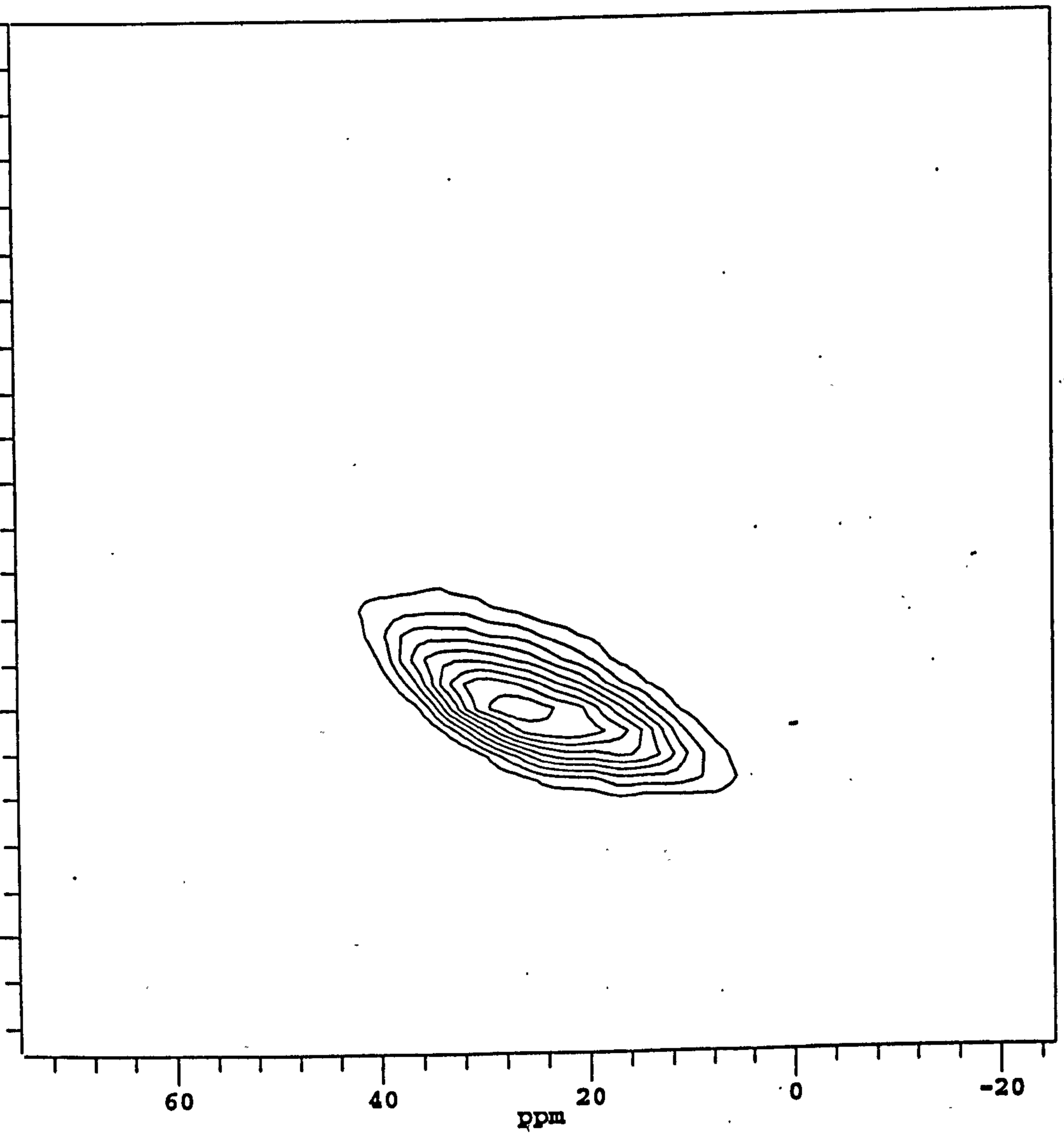

Figure 6.10 ^{17}O 3Q MAS spectrum of glass-3

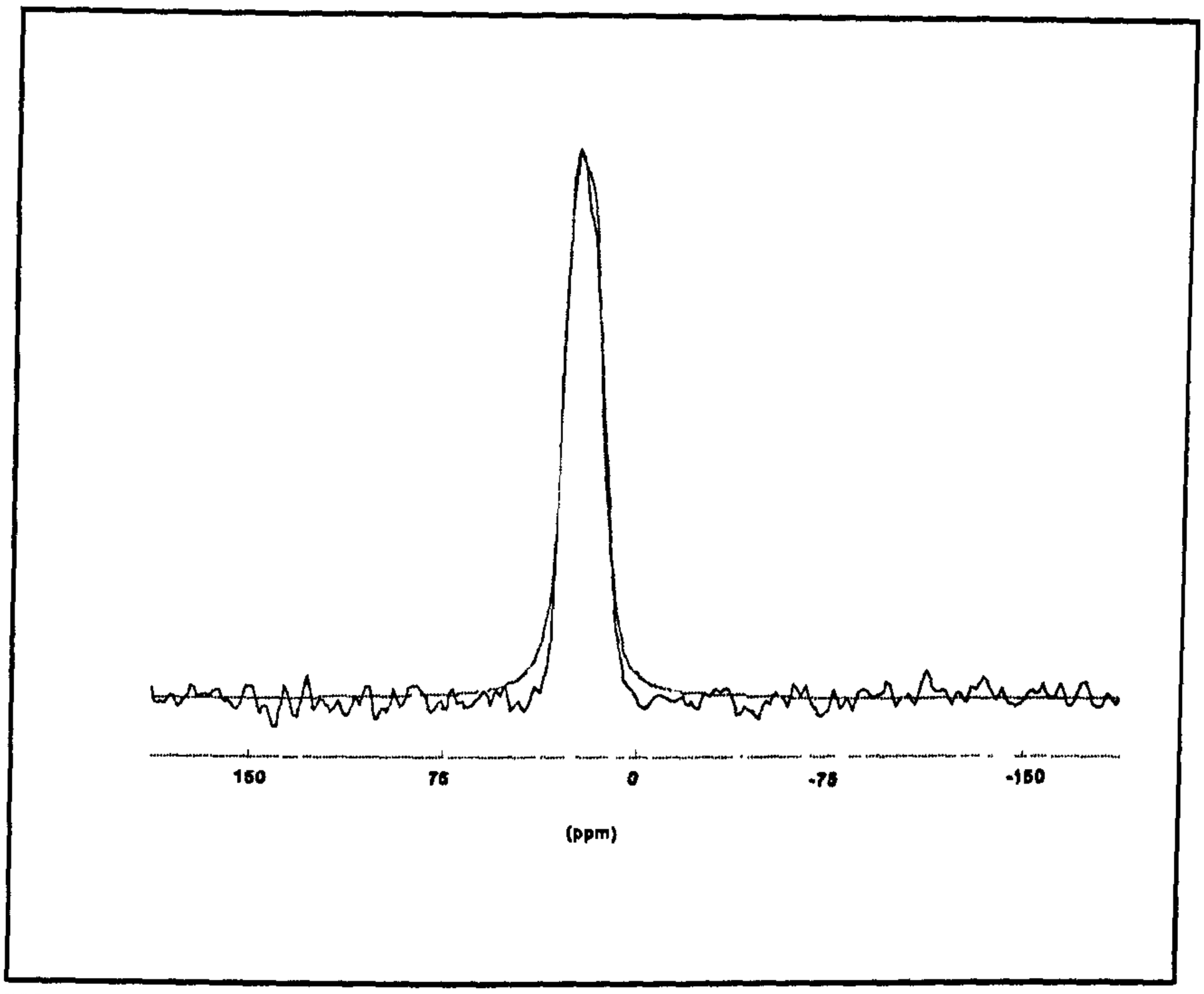

Figure 6.11 A slice of Si-O-Al site along MAS direction from the 3Q MAS spectrum of glass-3 and its simulation.

The most interesting 3Q MAS spectrum was obtained from the last glass sample with the Si/Al ratio of 0.7. The XRD inspection of this sample shows the presence of a small amount of a crystalline sodium aluminate. As already mentioned and shown in figure 6.3 the ^{27}Al spectrum of this sample indicates the presence of small amount of octahedral aluminum in the sample. The 3Q MAS spectrum of this sample, shown in figure 6.12, has two well resolved peaks and the main peak at 28ppm, has a typical quadrupolar line shape and it is quite wide. This peak can be attributed as Si-O-Al site from its position which is similar to those observed earlier. The second peak appears at about 17ppm in the MAS dimension which is similar to that observed for the Al-O-Al site in $NaAlO_2$ glass by Stebbins [32]. This peak also lies along the slope of 1 indicating the presence of a chemical shift distribution in the sample.

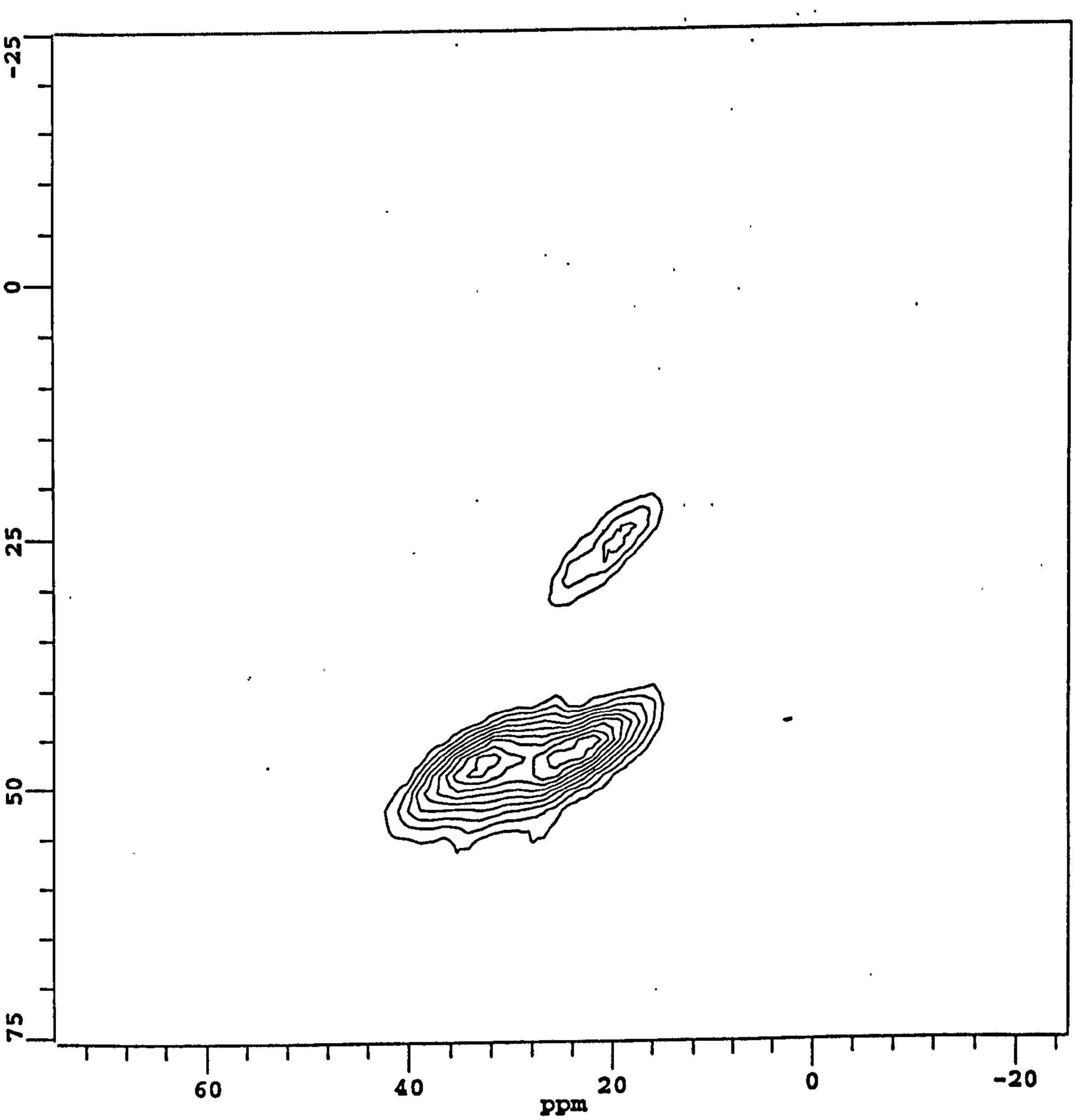

Figure 6.12 ^{17}O 3Q MAS spectrum of glass-4 with R=0.7

In order to find out the distribution of quadrupolar coupling constants for the Si-O-Al site a few slices were taken and simulations were performed on them as well as on a slice from the Al-O-Al site. Figure 6.13a shows one of those slices and its simulation taken from the Si-O-Al site and figure 6.13b-shows a slice and its simulation from the Al-O-Al site. The results of the simulations are given in table 6.5. The changes in the quadrupolar coupling constant at the Si-O-Al site is very small since it decreases from 3.16 MHz to 3.02 MHz which indicates the small distribution of Si-O-Al bond angles in the sample. We have also calculated the corresponding bond angles from the figure 5.7 and they are given in table 6.6. The results show the decrease in bond angle from 126° to 123° with decreasing quadrupolar coupling constant. The quadrupolar coupling constants obtained from the simulations for the Si-O-Al, Si-O-Si and Al-O-Al species in all four glasses are in good agreement with the values calculated by Tossel [19]. The increase in asymmetry parameter for each site with decreasing bond angle is consistent with figure 5.9, although the bond angle values calculated from this figure are 2° greater than values obtained from figure 5.7. The intensity of the slices (signal is visible at slice 119 and goes to zero at 131) goes through a maximum at the angle of 125°. Although the MQ MAS NMR is not quantitative, the ratio of total Al-O-Al species to the Si-O-Al species is about 0.175/1.

Table 6.6 ^{17}O quadrupolar parameters of two sites in glass-4 obtained from the 3Q MAS NMR experiment.

Site	C_Q (±0.3MHz)	η (±0.1)	δ (±3ppm)	Si-O-Al bond angle	Intensity
Si-O-Al slice123	3.16	0.39	42	126°	0.3
Si-O-Al slice125	3.13	0.42	39	125°	0.7
Si-O-Al slice128	3.02	0.46	31	123°	0.4
Al-O-Al	2.45	0.55	26		0.7

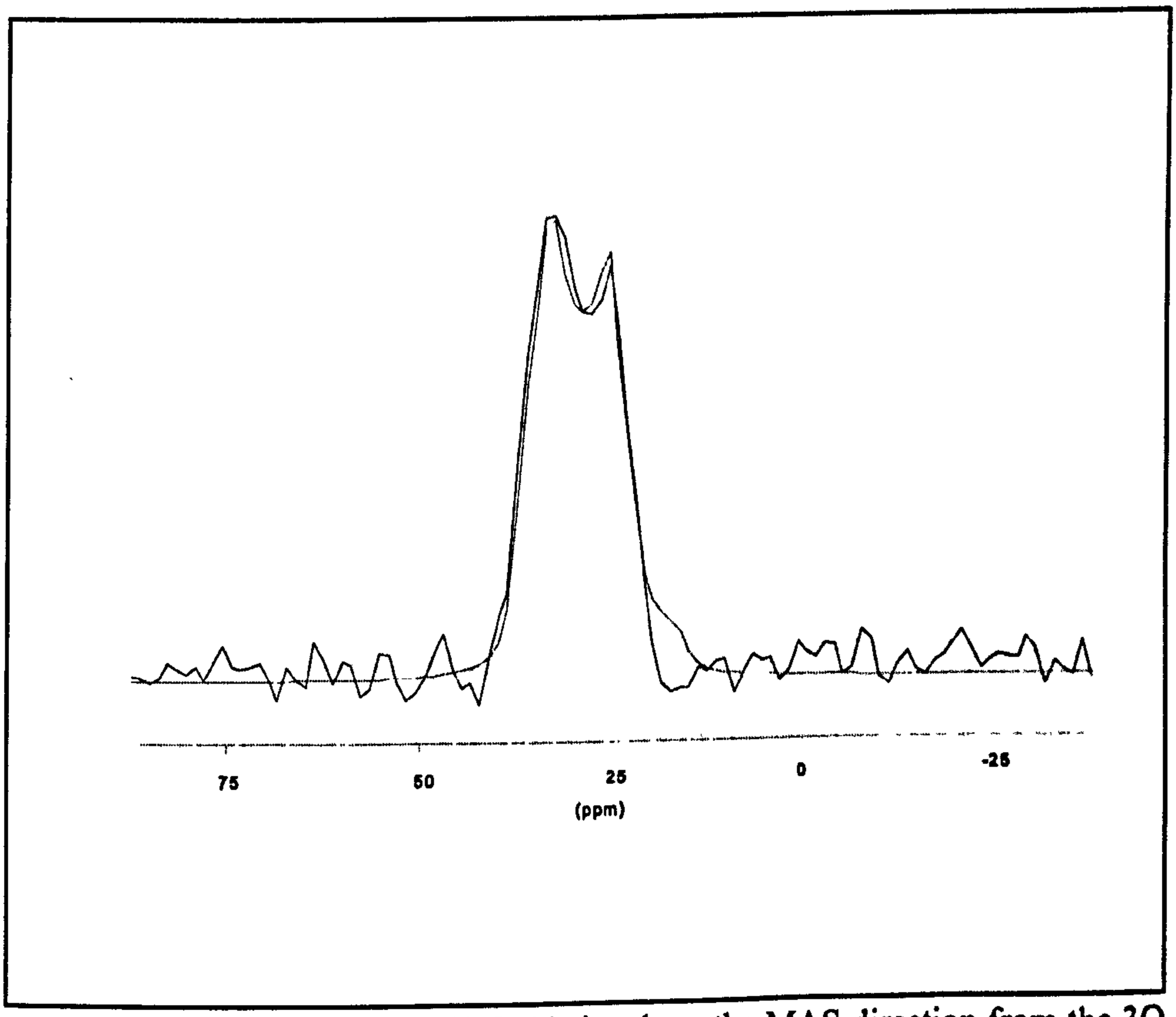

Figure 6.13a Slice 125 of the Si-O-Al site along the MAS direction from the 3Q MAS spectrum of glass-4 (R=0.7) and its simulation.

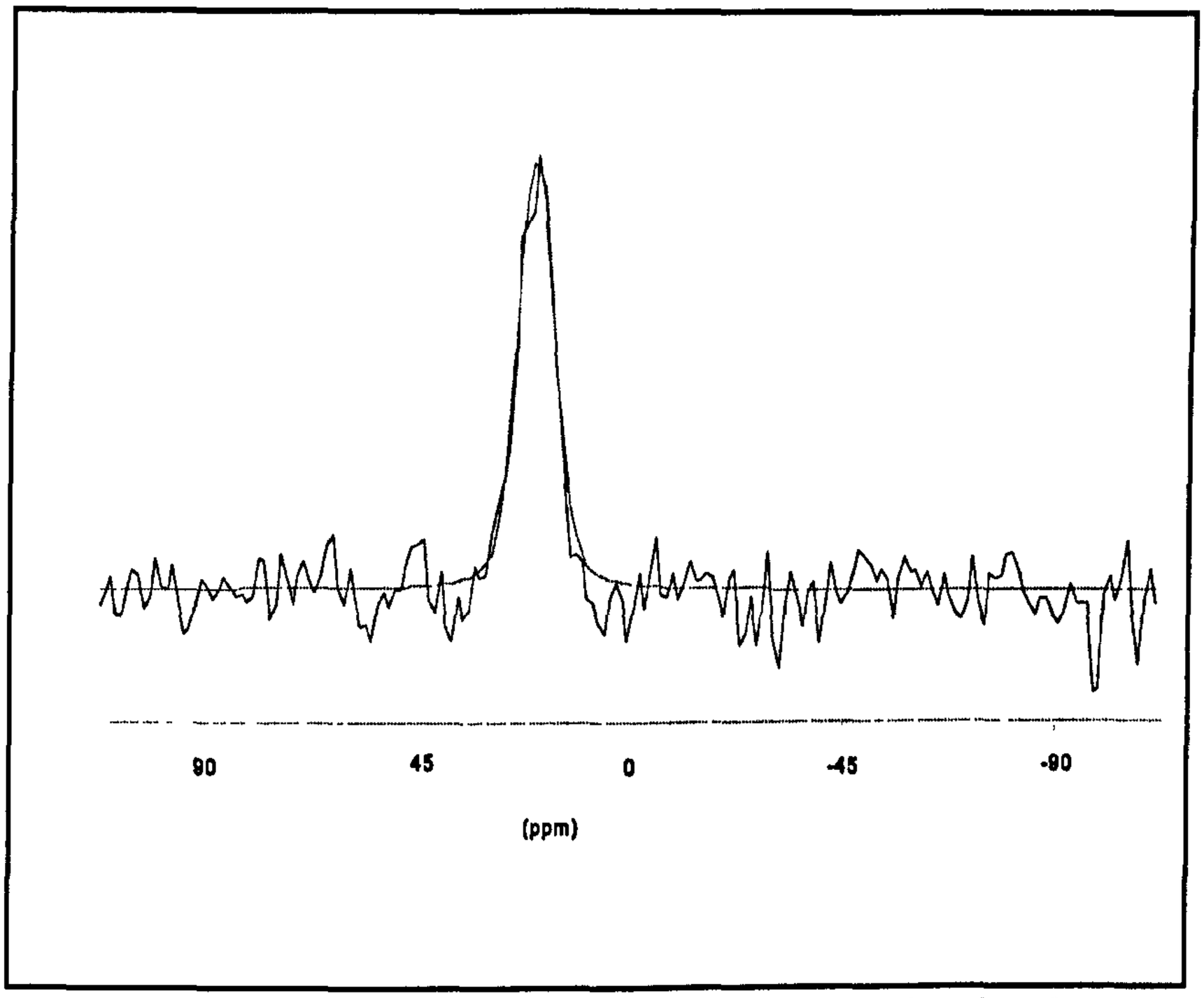

Figure 6.13b A slice of Al-O-Al site along the MAS direction from the 3Q MAS spectrum of glass-4 (R=0.7) and its simulation.

6.4 Conclusion

^{29}Si MAS spectra do not give much information on the degree of order in these samples. However the shift in their peak position as the Si/Al ratio decreases from 3 to 0.7 indicates the replacement of silicon atoms by aluminum atoms.

^{27}Al MAS NMR gives a featureless glassy spectrum for all three samples with $Al_2O_3 \leq Na_2O$ with no indication of a second site. For the glass-4 the ^{27}Al MAS spectrum confirms the presence of a small amount of octahedral aluminum in the sample.

The most valuable information was obtained from ^{17}O NMR. The MAS spectra in both fields do not give much information since they are broad and featureless due to second order quadrupolar line broadening. However 3Q MAS experiments provided very valuable information since the spectra yield the presence of different species , Si-

O-Al, Si-O-Si, Al-O-Al, in these glasses. The peak of these species and the quadrupolar coupling constants obtained from the simulations are in good agreement with the calculated data which is a good indication that quadrupolar coupling constants may be used to distinguish different species in glasses. The presence of Al-O-Al species in glass-4 with Si/Al ratio of 0.7 may be indication of OAl_3 or OAl_2Si triclusters. We believe that this site originates from the glass in the sample since the signal in the 3Q MAS spectrum lies along the chemical shift axis. If this site originated from the small amount of a crystal in the sample the signal would appear parallel to the MAS dimension. Another indication that this signal is from the glass, is the intensity of this site is ~15% which is much greater than the amount of crystal material. The distribution of quadrupolar coupling constant at the Si-O-Al site of glass-4 enables us to find the distribution of Si-O-Al bond angles in that site by using figure 5.7. The MQ MAS experiments also show that this technique is very valuable to obtain high resolution NMR spectra.

Reference

[1] G. Engelhardt, M. Nofz, K. Forkel, F.C. Fishmann, M. Magi, A. Samoson, E. Lipmaa, Phys. Chem. Glasses, 26(1985)157.

[2] G. Engelhardt, D. Michael, High Resolution Solid State NMR of Silicates and Zeolites, Jhon Wiley & Sons Ltd, Norwich.

[3] W. Lowenstein, Am. Mineral, 39(1954)92.

[4] B.O. Mysen, D. Virgo, F.A. Seifert, Rev. Geophys. Space Phys., 20(1982)353.

[5] B.O. Mysen, D. Virgo, J. Kushiro, Am. Miner., 66(1981)678.

[6] F. Seifert, B.O. Mysen, D. Virgo, Am. Miner., 67(1982)696

[7] R. Bruckner, H.U. Chun, H. Goretzki, M. Sammet, J. Non-Cryst. Solids, 42(1980)49.

[8] B.M.J. Smets, T.P.A. Lommen, Phys. Chem. Glasses, 22(1981)158.

[9] D.E Day and G.E. Rindone, J. Am. Chem. Soc., 45(1962)489.

[10] D.E Day and G.E. Rindone, J. Am. Chem. Soc., 45(1962)496.

[11] D.E Day and G.E. Rindone, J. Am. Chem. Soc., 45(1962)579.

[12] E.D. Lacy, Phys. Chem. Glasses, 4(1963)234.

[13] E.F. Riebling, J. Chem. Phys., 44(1966)2857-2865.

[14] B.O. Mysen, Structure and Properties of Silicate Melts, Elsevier (1988) Amsterdam.

[15] A. Navrotsky, Physics and Chemistry of Earth Materials, Chambridge University Press, 1994.

[16] J.F. Stebbins, Z. Xu, Nature, 390(1997)60.

[17] E.C. Hass, P.G. Mezey, P.J. Plath, J. Molecular Structure, 76(1981)389-399.

[18] A. Navrotsky, K.L. Geisinger, P. McMillan, G.V. Gibbs, Phys. Chem. Minerals, 11(1985)284-298.

[19] J.A. Tossel, American Minerologist, 78(1993)911-920.

[20] J.B. Murdock, J.F. Stebbins, I.S.E Carmichael, Am. Mineral., 70(1985)332.

[21] R.J. Kirkpatrick, R. Oestrike, Jr. C.A. Weiss, K.A. Smith, E. Oldfield, Am. Mineral. 71(1986)705.

[22] B.H.W.S. DeJong, C.M. Schramm, V.E. Parziale, Geochim. Cosmochim. Acta, 47(1983)1223.

[23] E. Lipmaa, A. Samoson, M. Magi, J. Am. Chem. Soc., 108(1986)1730.

[24] G. Engelhardt, M. Nofz, F.G. Wihsmann, M. Magi, A. Samoson, E. Lipmaa, Phys. Chem. Glasses, 26(1985)157.

[25] S. Schramm, R.J. Kirkpatrick, E. Oldfield, J. Am. Chem. Soc., 105(1983)2483-2485.

[26] G.L. Turner, S.E. Chung, E. Oldfield, J. Mag. Reson., 64(1985)316-324.

[27] K.T. Mueller, J.H. Baltisberger, E.W. Wooten, A. Pines, J. Phys. Chem., 96(1992)7001-7004.

[28] H.K.C. Timken, G.L. Turner, J.P. Gilson, L.B. Welsh, E. Oldfield, J. Am. Chem soc., 108(1986)7231-7235.

[29] T.H. Walter, G.L. Turner, E. Oldfield, J. Mag. Reson., 76(1986)106-120.

[30] P.J. Dirken, S.C. Kohn, M.E. Smith, E.R.H. van Eck, Chem. Phys. Lett., 266(1997)568-574.

[31] Z. Xu, J.F. Stebbins, Solid State Nuclear Magnetic Resonance, 11(1998)243-251.

[32] J.F. Stebbins, K.L. Sung, J.V. Ogelsby, American Minerologist, (1998).

[33] S.K. Lee, J.F. Stebbins, American Minerologist, 84(1999)937-945.

[34] S.P Brown, S. Wimperis, J. Mag. Reson., 124(1997)153.

Chapter-7
Tin Silicates

7.1 Introduction

Tin is a major constituent in the surface of float glasses as well as in coatings applied to float glass. Therefore understanding the structural role of tin in tin silicate glasses is quite important. However it has not attracted much attention due to the difficulty of making bulk SnO-SiO_2 glasses because of the disproportionation of SnO.

The first studies of this system concentrated on the preparation of the glass and reported that it was possible to make the glass by heating compressed pellets of mixtures of stannous oxalate and silica [1]. Later this technique was improved by heating mixtures of SnO+SiO2 in alumina crucibles [2] and it was also found that the glasses readily decomposed to metallic Sn, SnO_2 and quartz on heat treatment.

The crystallization and decomposition of SnO-SiO_2 glasses with composition 28 to 59 mol% SnO were studied by Carbo Nover and Williamson [3]. They prepared these glasses by the method first described by Keysselitz & Kohlmeyer and found that glasses containing > 42 mol% SnO partially crystallise and form a metastable crystalline phase (said to be $SnSiO_3$). This phase decomposes to metallic Sn, SnO_2 and SiO_2 at and above 700°C.

Ishikawa et al. also investigated SnO-SiO_2 glasses, containing SnO in the range of 32-57 mol%, by means of X ray radial distribution and infrared absorption measurements [4] and data showed that the structure of the glasses resembles that of crystalline metastable $SnSiO_3$ with increasing tin content thus supporting Nover & Williamson.

Holland et al.[5], investigated the binary SnO-SiO_2 system, with SnO contents of 20-70 mol%, by means of ^{119}Sn Mossbauer and ^{119}Sn , ^{29}Si NMR spectroscopy. They concluded from the ^{119}Sn Mossbauer spectroscopy that the chemical shift and quadrupolar splitting decreases with increasing SnO content with a discontinuity at around 30-35 mol%. ^{29}Si NMR spectroscopy showed that ^{29}Si chemical shift changes very slowly with composition. Their interpretation of this is that SnO does not depolymerize the silicate network to the same extent as Na_2O or even PbO. At low concentrations of SiO_2 there will still be silicate polyanions which implies separation is taking place with silica rich units in an SnO matrix. The second explanation could be that, due to identical electronegativity of Sn and Si, the Si nucleus sees only a slowly changing environment as the composition changes. Thus, the electron redistribution taking place from Si-O-Si linkages to the Si-O-Sn linkage produces very little change in the electron density seen by the Si nucleus [5]. They could not obtain useful information from the ^{119}Sn NMR due to the very broad peaks resulting from the large chemical shift range of Sn in a disordered environment.

Karim and Holland [6] looked at the density and thermal expansion of the same glasses and reported that the expansion coefficient increased, which indicates a decrease in the cross- linking and cation-oxygen bond strength, with tin content. They also reported a discontinuity in the changes of density and thermal expansion coefficient with tin content at 30-35 mol% SnO. They interpreted this data that, as the tin content increases, the Si-O-Sn linkages become more covalent and concluded that the tin suddenly becomes a network intermediate rather than a modifier.

Conversely Williams et al. [7] reported an increase in the ionicity of tin with increasing tin content and Karim et al. [6] concluded from the ^{119}Sn Mossbouer data that

the covalency of Sn-O bonds decreases with increasing tin content.

Bent et al. [8], investigated the structural role of tin in tin-silicate glasses by means of neutron diffraction. They concluded that Sn^{2+} is in a well defined environment in tin silicate glasses indicating that it takes the role of a conditional glass former for all compositions. They also found that the majority of tin atoms are three coordinated to oxygen and they are in a SnO_3 triangular pyramid, although a minority of Sn^{2+} are in a SnO_4 square pyramid environment, particularly for high silica compositions. Sn^{2+} ions with an average connectivity of three can only be incorporated into a tetrahedral Si-O network if some of the oxygens in the structure are three coordinated to three cations which conflicts with Zachariasen's rules for glass formation [9]. On the basis of this information they proposed a model for tin silicate glasses. Figure 7.1 and figure 7.2 show possible configurations for these models where there is Sn-O-Sn bonding [9].

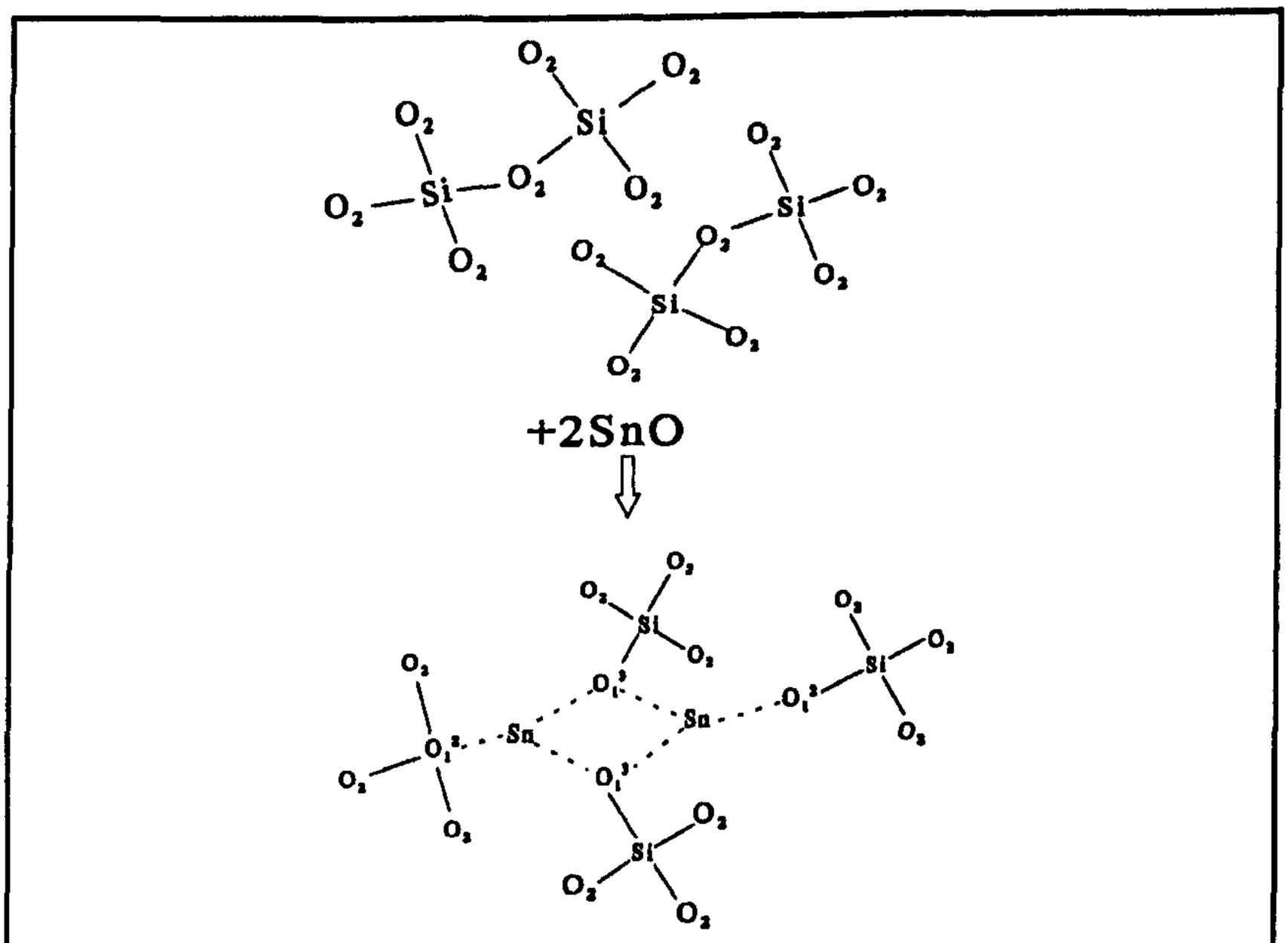

Figure 7.1 A possible configuration for the inclusion of the three coordinated tin in a silicate glass network [9]. The three coordinated oxygen are either bonded to one silicon, O_1^{3-} or bonded to two silicon , O_2^{2}, and two coordinated oxygen are bonded to one Si, Q_1^{2}, or two Si, Q_2^{2}.

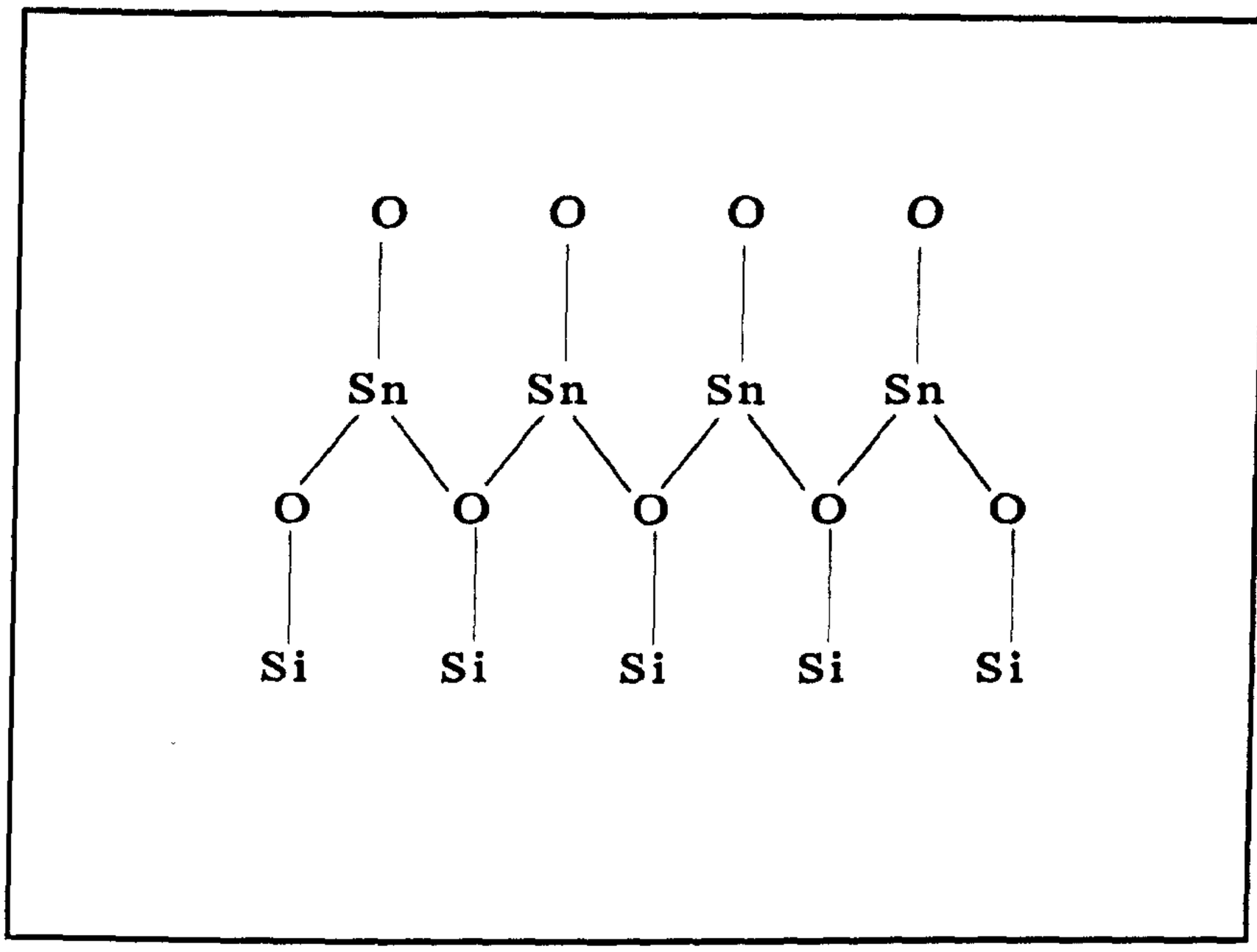

Figure 7.2 A possible configuration for the tin silicate glass structure which requires Sn-O-Sn-O chains [8].

We have investigated tin silicates by means of ^{17}O NMR spectroscopy as well as ^{29}Si, and ^{119}Sn spectroscopies in order to probe the SnO-SiO_2 glass structure and the metastable $SnSiO_3$ crystal phase structure.

7.2 Experimental Procedures

Tin silicate samples were prepared by Julian Bent. ^{17}O enrichment of the SiO_2 was carried out by the Geissberger method [10] as explained in chapter 4. Nominal glasses $(SnO)_x$-$(SiO_2)_{100-x}$ where x=35, 45, and 60 were prepared by the method first used by Keysselitz [1], but using silica crucibles. The stannous oxalate decomposed according to equation 7.1 to maintain the reducing atmosphere in the silica crucible which was covered with an alumina crucible. This restricted the decomposition and disproportionation of SnO, equation 7.2.

$$SnC_2O_4 \rightarrow SnO + CO_2 + CO \qquad (7.1)$$

$$2SnO \rightarrow Sn + SnO_2 \qquad (7.2)$$

Because the glass is formed between the metallic tin at the bottom of the crucible and a crust of SnO_2 at the surface, the crucible was removed from the furnace at the temperature, allowed to cool and the yellow-orange tin silicate glass was separated from the crucible, tin and SnO_2. Solid fragments of $60SnO\text{-}40Si^{17}O_2$ glass were heated at 570°C for 35 minutes under argon and then slowly cooled at one end of the tube furnace. The compositions of ^{17}O enriched samples were obtained [11] from their density and previous physical property studies by Karim [12] and Sears [13]. The densities and the compositions obtained are given in table 7.1. ^{17}O and ^{29}Si NMR experiments were carried out using the Chemagnetics 4mm probe at a spinning speed of about 15 kHz at a field of 14.4 T and ^{119}Sn NMR measurements were done using the Bruker 4 mm probe at a spinning speed of about 10-13 kHz at a field of 5.7 T.

The purpose of this study was to investigate the structural role of tin in tin silicates by means of mainly ^{17}O NMR spectroscopy and also ^{29}Si, ^{119}Sn NMR spectroscopy.

***Table 7.1** The measured density and deduced compositions of ^{17}O enriched $SnO\text{-}SiO_2$ glasses [11]*

nominal composition	density(gcm^{-3})	SnO Content (mol. %)	SiO_2 content (mol. %)
$60SnO\text{-}40SiO_2$	3.99±0.05	54±4	46±4
$45SnO\text{-}55SiO_2$	3.60±0.05	42±4	58±4
$35SnO\text{-}65SiO_2$	3.52±0.09	39±4	61±4

7.3 Results and Discussion

Figure 7.3 shows the ^{17}O NMR spectra of tin silicate glasses with tin contents of 39, 42 and 54 mol%. In all samples three distinct oxygen sites are visible. The peak

at the far right side of the spectrum, which is at about 33ppm is assigned to the Si-O-Si species. The middle peak at about 110ppm is assigned to the Si-O-Sn species and the third peak at the left hand side of the spectrum which is at about 207 ppm is assigned to the Sn-O-Sn species.

We have integrated the area of each peak to determine their relative intensities in each glass and the partially crystallized sample and the results are given in table 7.2. The Si-O-Sn peak intensity increases more sharply than the Sn-O-Sn peak from 28 to 44% with increasing tin content. For the glass with tin content of 54 mol.% the relative intensity of the Si-O-Sn peak is almost equal to the Si-O-Si peak. The relative intensity of the peak at 207 ppm (Sn-O-Sn) increases from 12.4 to 15% with increasing tin content from the 39% to 54%. However the change in the relative intensity of this peak is not as great as in the Si-O-Sn peak at 110ppm.

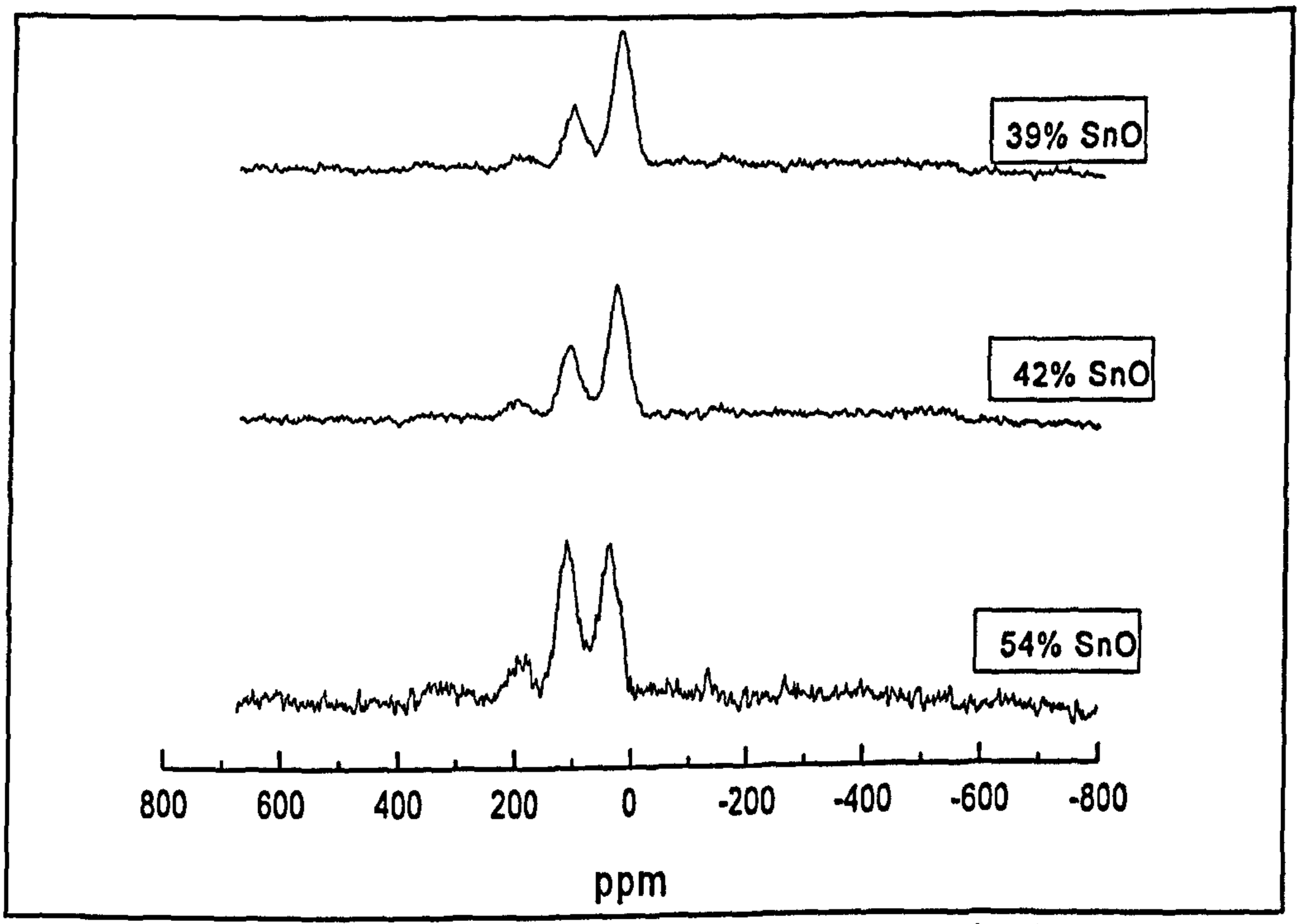

Figure 7.3 ^{17}O MAS NMR spectra of three tin silicate glasses with tin content of 39, 42, 54 mol.%..

Table 7.2 Relative peak intensities obtained from the ^{17}O NMR spectrums of SnO-SiO_2 glasses and calculated probabilities of each site.

Sample	Peak Position ±1ppm	Relative Int. %
39% SnO	207 110 33	12 28 60
42% SnO	207 110 33	13 33 54
54% SnO	207 110 33	15 44 41
partially crystallised 54% SnO	207 110 33	14 35 51

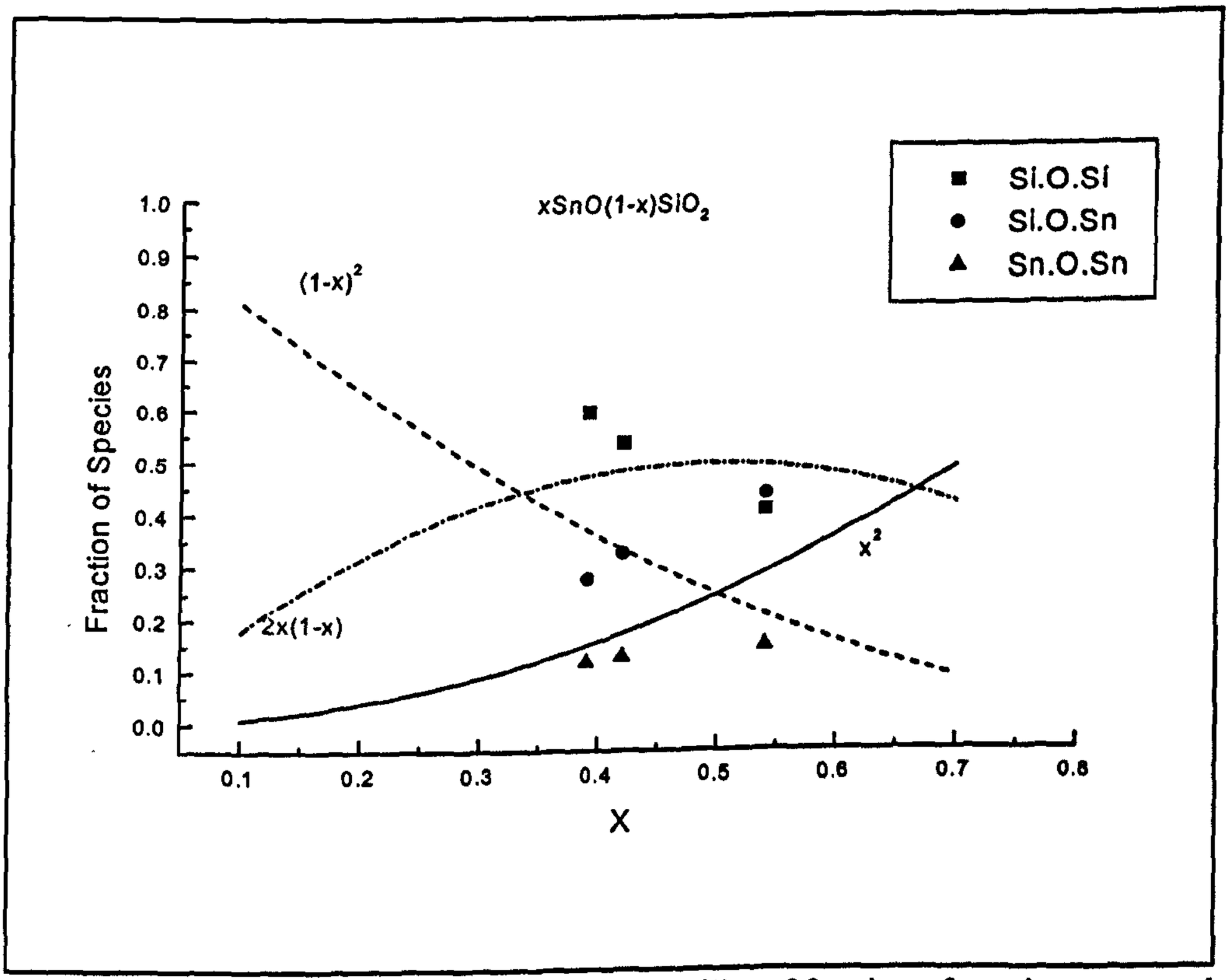

Figure 7.4 Simple statistical calculation of probability of fraction of species compared with ^{17}O NMR results

The relative intensity of the third peak, assigned to the Si-O-Si species, decreases as the tin content increases. The changes in the relative intensities of the peaks may be as a result of breaking of Si-O-Si linkages of SiO_4 tetrahedra, as the tin content increases, to form Si-O-Sn and Sn-O-Sn linkages.

There is no obvious evidence for three coordinated oxygen in these glasses from the ^{17}O NMR spectra (i.e., no characteristic C_Q). This conflicts with the proposition made by Bent at al [9] that these glasses have three coordinated Sn^{2+} which require three coordinated oxygen around them. Therefore we calculated the probability of Si-O-Si, Si-O-Sn, and Sn-O-Sn species occurring in the glass as a function of tin content. The simple formula for each species are given in table 7.3 and the plots of these functions as well as experimental values are displayed in figure 7.4. We assumed that Si and Sn have equal probability of occupying a given site. The simple statistical probability of finding each species in these glasses does not fit the experimental values. This may be due to the presence of some other oxygen environments as well as two coordinated oxygens.

Table 7.3 The equations for the probability of each species in xSnO(1-x)SiO,

Species	Probability
Si-O-Si	$(1-x)^2$
Si-O-Sn	$2(1-x)x$
Sn-O-Sn	x^2

Therefore a model based on the assumption of the presence of two and three coordinated oxygens in the glass was tried. If we assume the sample has general formula $xSnO\ (1-x)SiO_2$, the number of oxygens in the sample is given by, 2-x. Assuming x number of these oxygens are three coordinated, equivalent to the concentration of three

coordinated Sn atoms, 2-2x of the oxygens would be two coordinated oxygens. Ignoring the probability of Sn_3O and Si_3O, there are two configurations for three coordinated oxygen, Si_2-O-Sn, and Sn_2-O-Si. The relative probabilities of finding these two configurations in the sample is given by,

$$Si_2OSn \qquad px(1-x)^2$$

$$SiOSn_2 \qquad (1-p)x^2(1-x)$$

where p is the weighting function,

$$p=1 \qquad x\leq 0.5$$

$$p=0 \qquad x>0.5$$

i.e. all three coordinated oxygens in the glass (x) must be either in Si_2-O-Sn or Sn_2-O-Si species. The three ^{17}O peaks can then be assigned to as follows: 33ppm to $SiOSi+Si_2OSn$, 110ppm to $SiOSn+SiOSn_2$ and 207 ppm to SnOSn. Therefore it is possible to derive simple formula for the fractions of two and three coordinated oxygen present together in the sample:

fraction of oxygens in Si-O-Si+Si_2-O-Sn:

$$p\leq 0.5 \rightarrow \quad \frac{(1-x)^2(2-2x)+x}{(2-x)}$$

$$p>0.5 \rightarrow \quad \frac{(1-x)^2(2-2x)}{(2-x)}$$

fraction of oxygens in Si-O-Sn+Si-O-Sn_2

$$p\leq 0.5 \rightarrow \quad \frac{2x(1-x)(2-2x)}{(2-x)}$$

$$P>0.5 \rightarrow \quad \frac{2x(1-x)(2-2x)+x}{(2-x)}$$

the fraction of oxygens in Sn-O-Sn,

$$\frac{x^2(2-2x)}{(2-x)}$$

By using these formula we calculated the fractions of oxygens and plotted them as a function of tin content as shown in figure 7.5. As can be seen from the figure, under these assumptions the lines obtained from the statistical calculations follow fairly closly the behaviour of experimental values which may be an indirect evidence of presence of three coordinated oxygen in these glasses.

The ^{17}O NMR spectrum of the partially crystallized sample with tin content of 54 mol.%, given in figure 7.6, does not show much difference from the corresponding glass sample although the relative intensity of Sn-O-Sn and Si-O-Sn peaks increases while the relative intensity of the Si-O-Si peak decreases. The Si-O-Sn and Sn-O-Sn peaks in the crystallized sample are narrower than the corresponding peaks in glass and the Si-O-Sn peak shows some structure. The results of the simulation of these peaks is given in table 7.4. Although the Si-O-Si peak does not show the characteristic line shape observed for ^{17}O spectra of crystalline SiO_2, it gives a quadrupolar coupling constant C_Q=5.0 MHz which is characteristic for this site.

***Table 7.4** ^{17}O quadrupolar parameters of three sites in partially crystallised tin-silicate sample*

Site	C_Q (±0.3 MHz)	η (±0.1)	δ (±3 ppm)
Si-O-Si	5.0	0.5	50
Si-O-Sn	3.6	0.6	137
Sn-O-Sn	3.7	0.5	187

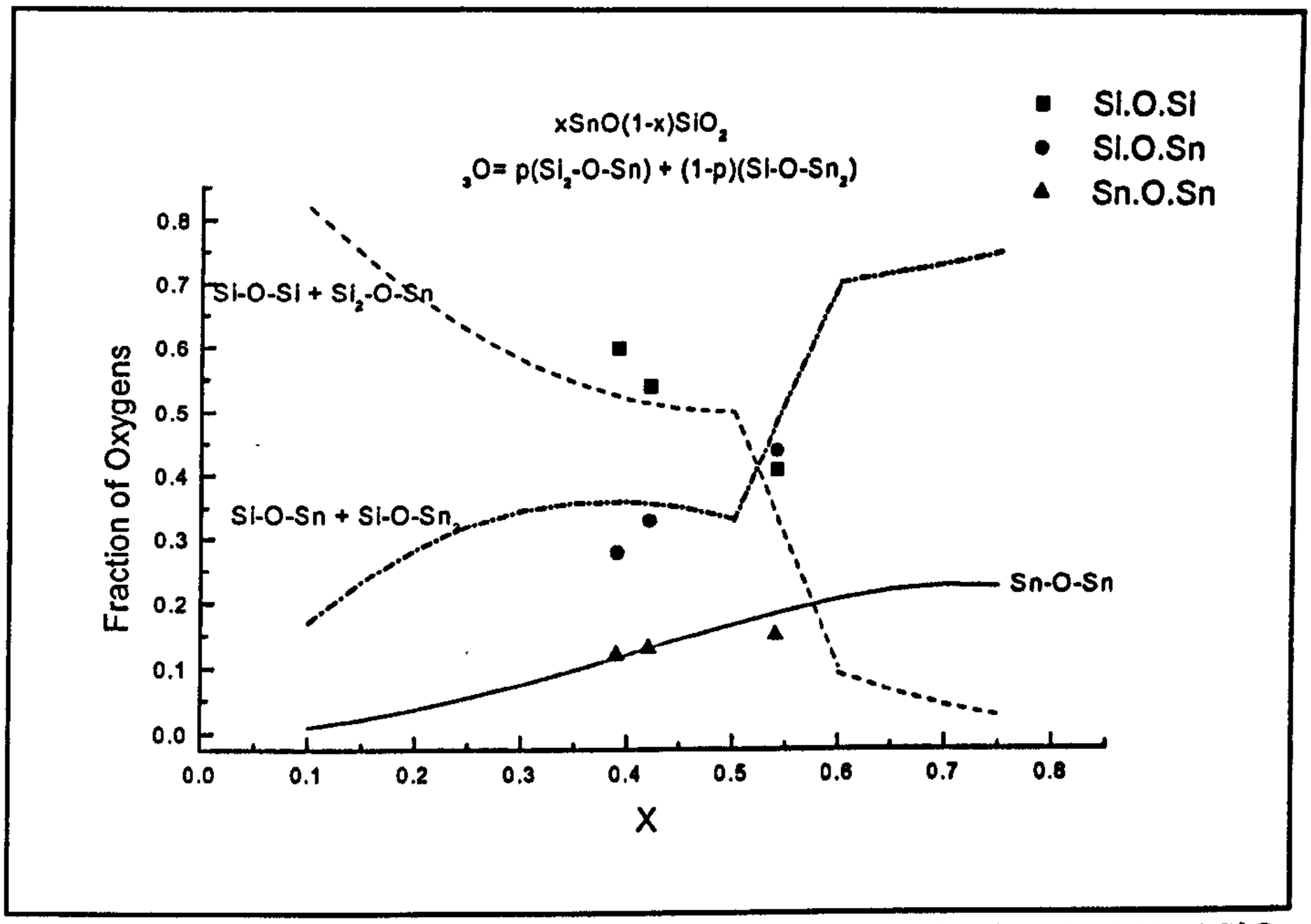

Figure 7.5 Statistical model for calculated oxygen species in $xSnO(1-x)SiO_2$ with ^{17}O NMR results.

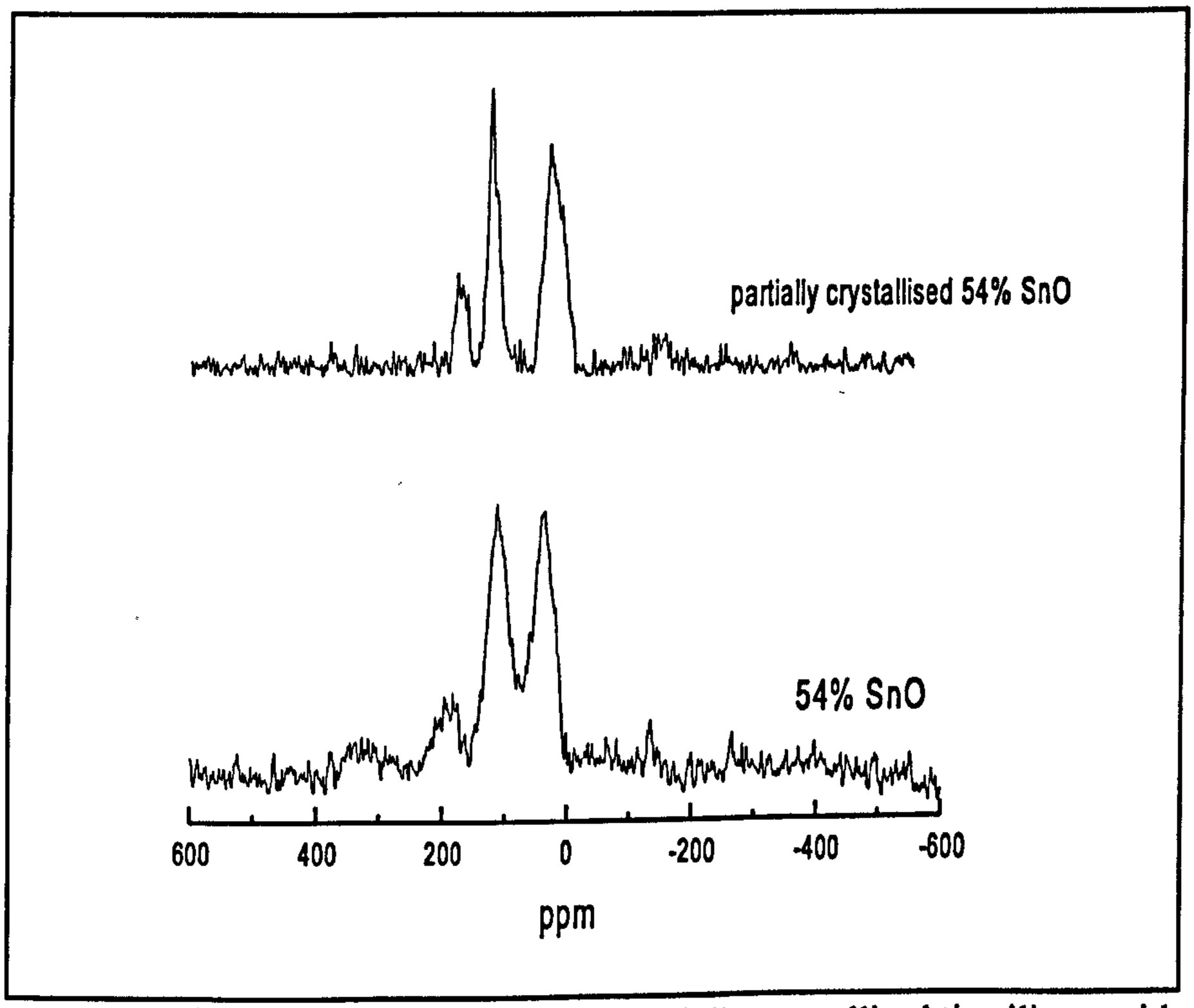

Figure 7.6 ^{17}O MAS NMR spectrum of partially crystallised tin silicate with tin content of 54 mol.% and corresponding glass sample.

Figure 7.7 shows the ^{29}Si NMR spectrum of this sample. The narrow peaks at -68 ppm and -74 ppm are due to silicon in the crystalline phase and the shifts are consistent with Q^0 and Q^1 species respectively. Therefore these species have to have Sn around which indicates the presence of Sn in the crystalline phase. The broad peak at about -110ppm, with a tail at the left hand side is presumably from the glass in the sample. In order to obtain more information we fitted this spectrum with four peaks shown in figure 7.8. The peak at -111ppm with width at half maximum 12 ppm can be attributed to Q^4, whereas the peak at -104 ppm may be attributed to that of Si site with one tin around (Q^3). This figure shows that a considerable amount of silicon is not in the crystalline phase since the ratio of total intensity of crystalline sites to the glass site is about 1:9. The ratio of crystalline peaks is 3:1(-68 ppm:-74ppm), whereas the ratio of glass peaks is 2:2.6 (-104:-111). The results of the simulation of the spectrum are given in table 7.5.

***Table7.5** The intensities of the peaks obtained from the simulation of ^{29}Si spectrum of partially crystallised sample.*

Peak at ±1 ppm	FWHM ±1ppm	Int. Intensity
-68	2	3
-74	2	1
-104	9	18
-111	12	23

As can be seen from the table 7.5 about 10% of the total signal is from the crystal while about 90% of the total signal is from glass. Q^4 and Q^3 species in the glass site shares about 50% and 40% of the total signal respectively. Q^4 site has all Si, whereas Q^3 site includes 0.5Sn/Si which gives the number of Sn in the Q^3 site as 20 unit. Therefore the remaining Sn (80 unit) has to be in the crystal site. The number of Si in

the crystal is 10 unit. As a result the approximate composition of the crystal can be given as $SiSn_8O_{10}$ which contradicts the finding of Nover et el.[3]. The crystal peaks Q^0 and Q^1 have 2Sn/Si and 1.5Sn/Si respectively. Since the intensity of the Q^0 is about three, it has 6Sn/si while the intensity of the Q^1 is about 1, it has 1.5Sn/Si. From this simple calculation it is possible to say 7.5Sn/Si which is very close to the composition $SiSn_8O_{10}$ found earlier.

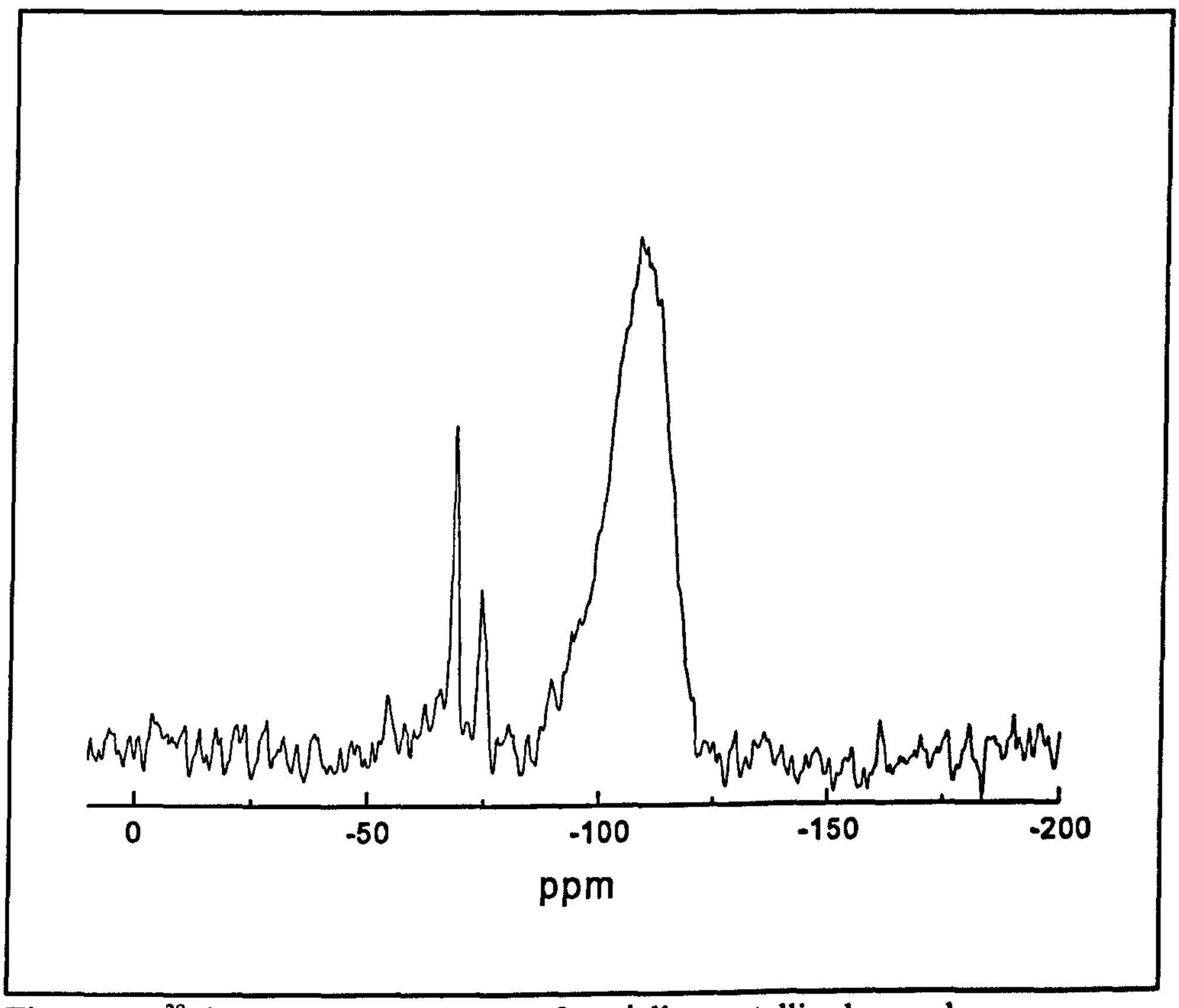

Figure 7.7 ^{29}Si MAS NMR spectrum of partially crystallised sample

The ^{119}Sn NMR spectra of the same sample at two different spinning speeds are given in figure 7.9. Although it is difficult to identify the crystalline peaks due to spinning side bands, two isotropic crystalline peaks appear at 555 ppm and 640 ppm.

Underneath these two crystalline peaks and the spinning side bands is a broad peak due to the glass which makes it very difficult to measure the ratio of crystalline tin species with respect to the glass present in the sample.

7.4 Conclusion

^{17}O NMR results reveal that addition of SnO into a SiO_2 network breaks up Si-O-Si linkages and forms Si-O-Sn as well as Sn-O-Sn linkages. The relative intensities of ^{17}O peaks from the Si-O-Sn and Sn-O-Sn linkages increase as the tin content increases while the intensity from the Si-O-Si linkage decreases as the tin content increases, as expected. Therefore SnO depolymerises the SiO_4 tetrahedra and forms a new structural network in the glass. The models for the new network are given in figure 7.1 and figure 7.2 which require three coordinated oxygen atoms to charge balance three coordinated Sn^{2+}. ^{17}O NMR spectra of glasses do not directly indicate the presence of any three coordinated oxygens. However the statistical model shown in figure 7.5 follows the experimental values and this may indicate that there are not only two coordinated oxygens but also three coordinated oxygens bonded to the three coordinated Sn^{2+} in these glasses.

The ^{17}O NMR spectrum of the partially crystallised sample shows narrower Si-O-Sn and Sn-O-Sn lines than the corresponding glass sample which may be an indication of more ordered Si-O-Sn and Sn-O-Sn sites in the sample. The simulation of Si-O-Si gives C_Q=5.0 MHz which is consistent for this site in silicates.

The ^{29}Si NMR spectrum of partially crystallised sample shows the presence of two crystalline sites and a complex glass site in the sample. The simulation of the glass spectrum gives two components at -111 ppm Q^4 and at -104 ppm Q^3. The spectrum also

shows that there is a considerable amount of Si in the glass site. The calculation done from the relative intensities of the peaks gives the possible composition of the crystal as $SiSn_8O_{10}$ which contradicts Nover et al. [3].

The ^{119}Sn NMR spectrum of the partially crystallized sample indicates the presence of two crystalline Sn sites in the sample as well as a broad glass peak underneath. Due to this broad peak it is not possible to obtain the relative intensities of these sites.

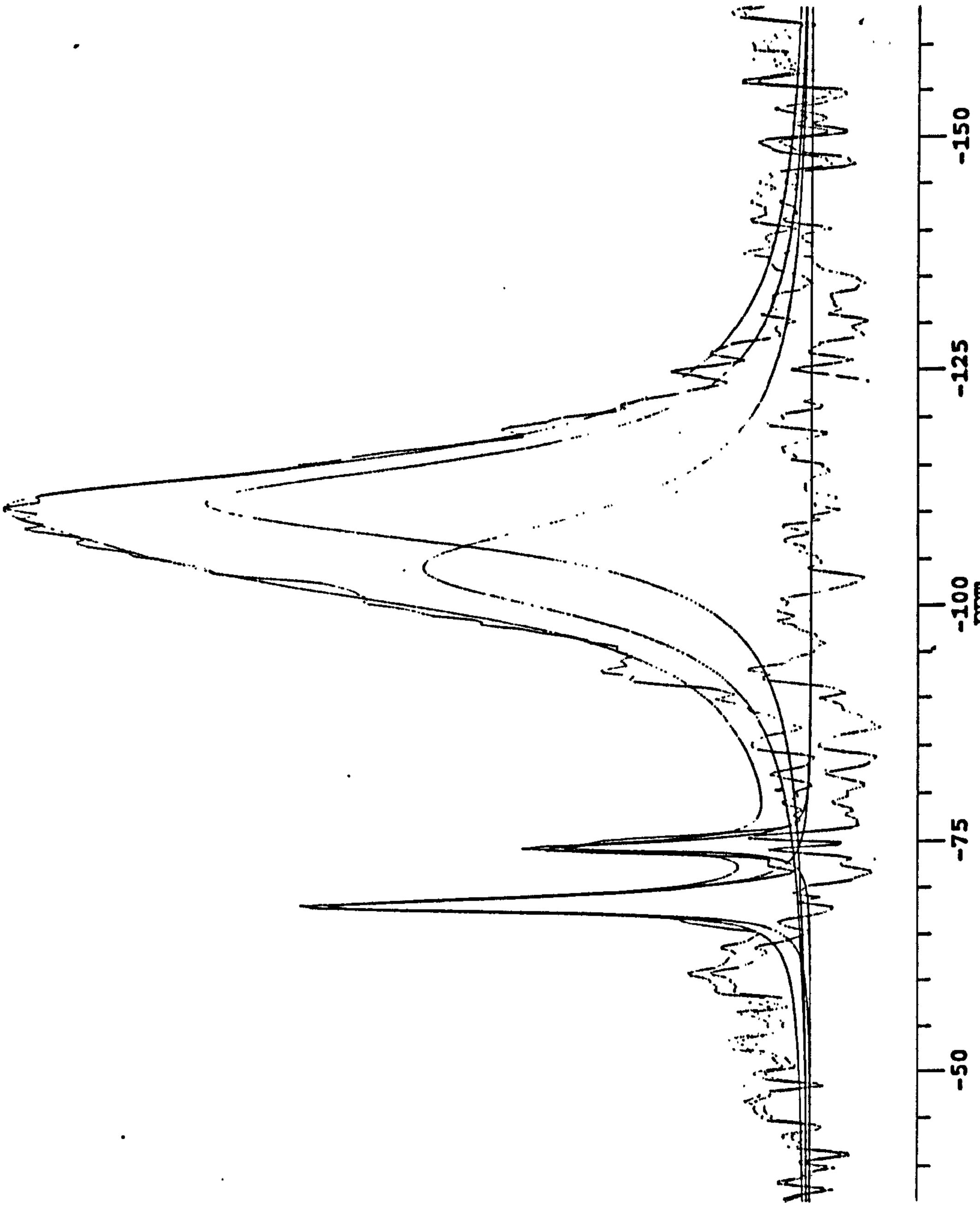

Figure 7.8 Simulation of ^{29}Si NMR spectra of partially crystallized sample.

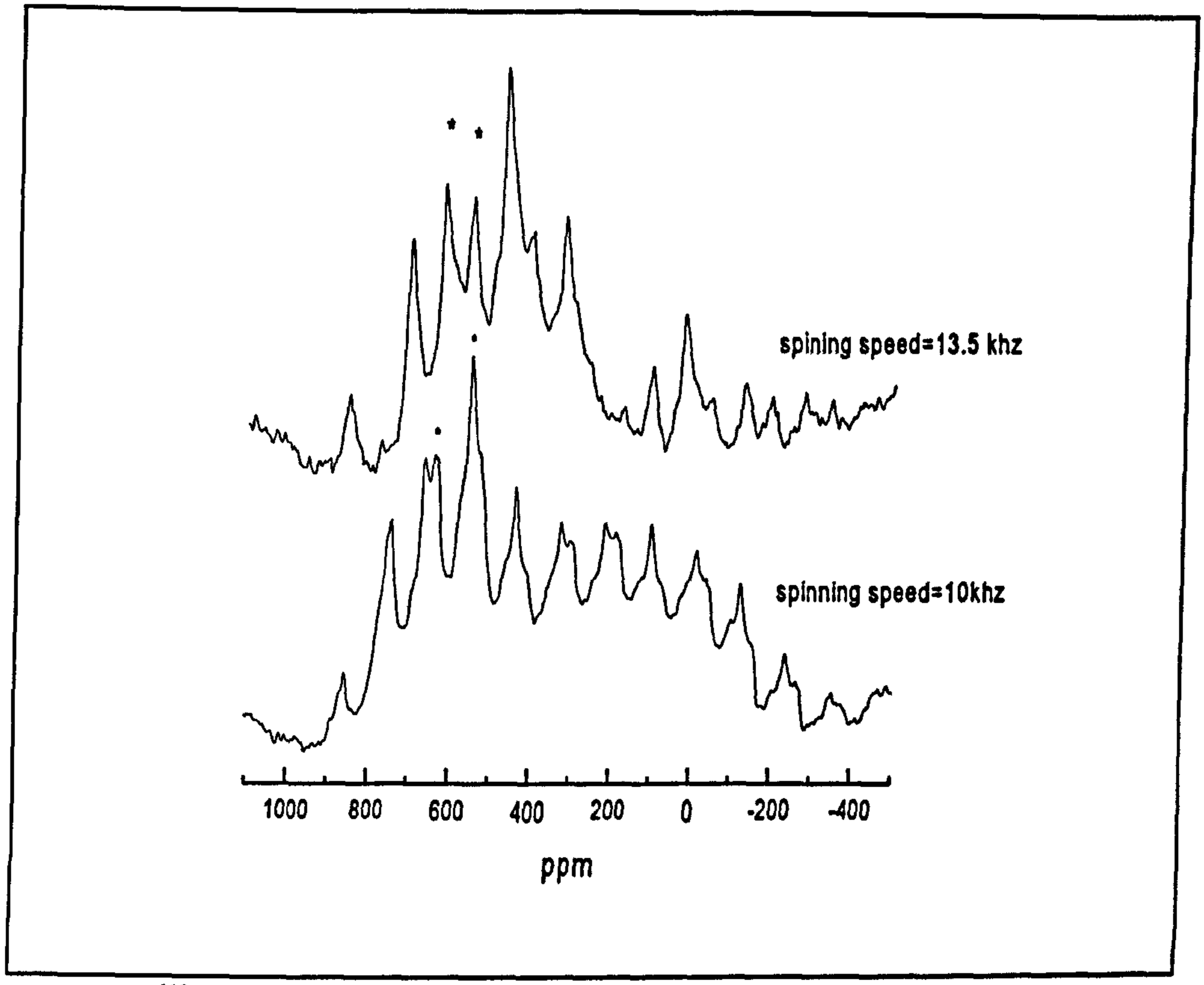

Figure 7.9 ^{119}Sn MAS NMR spectrum of partially crystallized sample at two different spinning speed.

References

[1] B. Keysselitz, E.J. Kohlmeyer, Metal Erz., 30(1930)172.

[2] B.I. Slonimskii, A.A. Teseidler, S.B. Trund. Gos. Non. Issled. Inst. Tsvet. Metal, Gorn Delo. 3(1959)82.

[3] J.C. Nover, J. Williamson, Phys. Chem. Glasses 8 (1967)164.

[4] T. Ishikawa, S. Akagi, Phys. Chem. Glasses, 19(1978)108.

[5] D. Holland, M.M. Karim, C.E. Johnson, K. Williams, J.A. Johnson, Fundamentals of Glass Science and Technology ESG, 1993, Venice.

[6] M.M. Karim, D. Holland, Phys. Chem. Glasses, 36(1995)206.

[7] K.F.E. Williams, C.E. Johnson, J.A. Johnson, D. Holland, M.M. Karim, J. Phys. Condensed matter, 7(1995)9485.

[8] J.F. Bent, A.C. Hannon, D. Holland, M.M. Karim, Journal of Non-Cryst. Solids, (1998)340.

[9] W.H. Zachariansen, J. Am. Ceram. Soc., 54(1932)3841.

[10] A.E. Geissberger, P.J. Bray, J. Non Crys. Solids, 54(1983)121-137.

[11] J.F. Bent, Ph.D. Thesis, Department of Physics, University of Warwick, 1999

[12] M.M.A. Karim, A Study of Tin Oxides in silicate Based Glasses, Ph.D. Thesis, Department of Physics, University of Warwick, March 1995.

[13] A. Sears, The Characterization of Stannosilicate Glasses, Ph.D. Thesis, Department of Physics, University of Warwick, December 1998.

Chapter 8
Conclusions

8.1 General Conclusion

We have investigated some glassy and crystalline silicates by means of mainly ^{17}O NMR. Since conclusions are given at the end of each experimental chapter, a generall summary of the results and possible future work will be outlined in this chapter.

NMR is one of the most suitable spectroscopic tools for the investigation of glasses and amorphous solids since diffraction techniques such as XRD can provide limited information on these materials due to lack of long range order in their structure. This study is particularly concentrated on ^{17}O NMR since it is the most common element in the materials studied. In addition because it is a quadrupolar nucleus, it is possible to obtain quadruoplar parameters from the spectra which can be used to obtain more structural information. As stated earlier ^{17}O NMR has become one of the most important tools to obtain structural information in glasses and amorphous solids. Therefore we investigated the relation between ^{17}O NMR quadupolar parameters (C_Q, and η) and the Si-O-Al bond angle in crystalline aluminosilicates. It was found that the relation between the ^{17}O quadrupole coupling constant C_Q and Si-O-Al bond angle is functionally similar to that found for the Si-O-Si symmetric bond angle. The C_{Q180} value is smaller than the corresponding value for the Si-O-Si bond angle as expected due to replacement of Si by Al. The dependence of the asymmetry parameter on the Si-O-Al bond angle also shows similarities to the case of Si-O-Si bond angle although the value of η increases more rapidly at smaller angles. The chemical shift also increases with decreasing Si-O-Al bond angle, but it is not monotonic. The results presented in chapter 5 confirm the correlation between C_Q of ^{17}O and Si-O-Al bond angle which can be used

for obtaining the bond angles and related structural parameters by simply simulating the ^{17}O NMR spectrum and obtaining the C_Q, and η. As a result ^{17}O NMR may be used as a structural tool to distinguish and identify multiple oxygen sites in materials whose structure is known or partially known.

One of the main drawbacks of ^{17}O NMR is the lack of high resolution due to the large quadrupolar interaction which prevents the observation of chemically different oxygen sites in the sample. Therefore Multiple Quantum MAS NMR has been employed for obtaining information on the structural role of Al^{3+} in aluminosilicate glasses with different Si/Al ratios. MQ MAS experiments showed that Si-O-Si species is present in the glasses with Si/Al ratio 3 and 1.5. Although this technique is not quantitative the intensity of the Si-O-Si peak decreases with decreasing Si/Al ratio. As the Si/Al ratio continues to decrease such that Si/Al=0.7 a new species appears on the MQ MAS spectrum of glass 4. The presence of Al-O-Al species may be OAl_3 or OAl_2Si triclusters.

The ^{27}Al and ^{29}Si MAS NMR spectra, which are broad and without any structure, do not give much information except that we were able to confirm the nominal compositions of the glass from the ^{29}Si spectra. In addition ^{27}Al spectra for glass 4 with Si/Al =0.7 shows the presence on small amount of six coordinated Al in the sample.

The structural role of Sn^{2+} in tin-silicates was investigated mainly by means of ^{17}O MAS NMR. The ^{17}O MAS NMR spectra of the tin-silicate glasses with SnO content of 39, 42, 54 mol.% have three distinct oxygen sites which are attributed to Si-O-Si, Si-O-Sn and Sn-O-Sn linkages in the samples. The increasing relative intensity of Si-O-Sn peak and the decreasing relative intensity of Si-O-Si peak with increasing SnO content indicates that the addition of Sn into the glass breaks up the Si-O-Si linkages and forms Si-O-Sn linkages as well as Sn-O-Sn linkages. Therefore tin depolymerises the SiO_4

tetrahedra and forms a new structural network in the glass. As explained in chapter 7, there is some evidence of three coordinated Sn^{2+} which requires three coordinated oxygen. However there is no indication of three coordinated oxygen in the ^{17}O NMR spectra of glasses studied. In order to investigate the possible presence of three coordinated oxygen in these glasses a model was developed which assumes the coexistance of three and two coordinated oxygens. The model closely follows the experimental values such that it may be an indication of indirect evidence for the presence of three coordinated oxygens in tin-silicates. A partially crystallized sample with 54 mol.% SnO content, gives narrower Si-O-Sn and Sn-O-Sn ^{17}O peaks than the corresponding glass.

Although ^{29}Si NMR spectra of the partially crystallized sample shows two crystalline and one glassy peak, the simulation of the spectrum shows that there are two components at -111ppm and -104ppm which may be attributed to Q^4 and Q^3 respectively, confirming that some of the tin is in the crystalline phase, and some of it is in the glassy site.

The ^{119}Sn NMR spectra of partially crystallised sample showed that there are two crystalline Sn sites as well as glass in the sample.

8.2 Suggestions for Further Work

Although we have obtained experimentally a correlation between the ^{17}O quadrupolar coupling constant and Si-O-Al bond angle, the dependence of the quadrupolar coupling constant on the Si-O-Al bond angle may be investigated theoretically. It would be interesting to test this functional dependence of ^{17}O quadrupolar coupling constant on the Si-O-Al bond angle in some other crystalline materials.

^{17}O NMR experiments should be performed by using thick walled rotor or sample should be packed into an insert which can be put into the rotor, in case of rotor crashing and losing the valuable sample.

In order to obtain more decisive information on the model for tin -silicate glasses two or three more glasses with tin content of smaller than 39 mol.% and greater than 54mol.% should be investigated so that it would be possible to cover a large compositional range.